University of Southampton

Faculty of Science, Mathematics and Engineering

School of Chemistry

Behaviour and improvement of screen printed reference electrodes. Application to a commercial glucose sensor.

by

Sergio Martinez Montequin

Submitted for the degree of

Doctor of Philosophy

July 2005

Highfield,

Southampton

SO17 1BJ

UNIVERSITY OF SOUTHAMPTON

ABSTRACT

FACULTY OF SCIENCE, MATHEMATICS AND ENGINEERING

SCHOOL OF CHEMISTRY

Doctor of Philosophy

BEHAVIOUR AND IMPROVEMENT OF SCREEN PRINTED REFERENCE ELECTRODES. APPLICATION TO A COMMERCIAL GLUCOSE SENSOR.

by Sergio Martinez Montequin

The factors that limit the performance of the counter-reference electrode in a commercial screen printed biosensor (SPE) for the quantification of glucose in whole blood have been investigated. The electrochemistry of this Ag/AgCl SPE is limited by the resistance of the track ($R \sim 125\ \Omega$). The open circuit potential at long times (equilibrium potential) depends on the activity of Cl^- in the solution following the Nernst equation, meanwhile at short times ($t < 100$ s) the potential transient recorded from the moment the electrode is immersed in the solution showed some anomalous and irreproducible behaviour, probably associated with some nucleation process occurring at the electrode. The cyclic voltammetry showed also a change of slope at low overpotentials (η = -80 mV) due to the different potentials needed to reduce two different kinds of AgCl particles; those in contact with Ag and those isolated.

We have proposed two different types of counter reference electrodes. One type is based in replacing the Ag from the ink with carbon, meanwhile the other one uses the same Ag/AgCl ink, but adding different amounts of KCl. SPEs employing the first approach show potentials more negative than those of the commercial SPEs due to the increase of the resistance of the track. Also these electrodes are unable to transfer the required charge predicted for the overall sensor in working conditions, so this formulation was discarded.

The SPEs loaded with KCl show shorter equilibration times than the commercial electrodes. The potential of the transient part of the curve is very reproducible. During the transient part of the chronopotentiometry, the potential is established by the gradient of Cl^- created by the dissolution of the Cl^- embedded in the ink.

Finally, SPEs treated with light and air show an anomalous behaviour compared with fresh SPEs. This negative effect consisted in a shift towards less negative values of the potential recorded in a cathodic galvanostatic experiment. This anomalous behaviour was similar to that produced by oxidising the Ag in the SPE to Ag_2O, but no mechanism that explains this similarity was found. Also SPEs partially oxidised and reduced in Cl^- solutions showed this shift of the potential to less negative values. Since this shift means that it is easier to reduce these oxidised and reduced electrodes we believe that the mechanism involve a facilitated nucleation process at the oxidised or reduced electrodes.

Index

Index ..... **II**

Author's declaration ..... **VI**

Acknowledgements ..... **VII**

Abbreviations and Symbols Used In This Thesis ..... **IX**

1 Introduction *1*

1.1. Overall aim of the project **2**

1.2. (Bio)Sensors, an introduction. **2**

1.3. Thick film and thin film technologies in the design of (bio)sensors **6**

1.4. Screen printed electrodes **8**

1.4.1. Components of the screen printed (bio)sensor 9

1.5. Glucose analysis and diabetes: past, present and future **13**

1.5.1. Diabetes 13

1.5.2. Glucose Biosensors: 14

1.5.3. And what about the future? 16

1.6. Reference electrodes **18**

1.6.1. Solid state reference electrodes. 22

1.6.2. MediSense's glucose biosensor strip 24

1.7. General overview of thesis **26**

2 Experimental *28*

2.1. Experimental procedures **29**

2.1.1. Electrochemical cell set-up 29

2.1.1.1. Trigger 29

2.1.2. Microscopy, X-ray analysis and contact angle measurements 31

2.1.2.1. Image analysis 32

2.1.3. Electrochemistry of solids 32

2.1.4. Sectioning of the SPEs 33

2.1.5. Rheology 33

2.1.6. Calculation of the activity of chloride 34

2.2. Electrodes **35**

2.2.1. Reference electrodes 35

2.2.1.1. Saturated calomel electrodes (SCE): 35

2.2.1.2. Saturated mercurous sulfate electrodes (SMSE): 36

2.2.1.3. Ag/AgCl bulk electrodes 36
2.2.2. Screen printed electrodes 37
2.2.3. Carbon paste electrodes 43
2.2.4. Other electrodes 44

2.3. Chemicals 44

3 Commercial Ag/AgCl screen printed electrode 46

3.1. Composition of the ink 47
3.1.1. Chloride contents of the ink 49
3.1.2. Ag/AgCl ratio 52
3.1.3. Solvents 56

3.2. Sectioning and X-ray mapping of screen printed electrodes. 56

3.3. Exchange current 58

3.4. Chronoamperometry of the whole electrode 63

3.5. Variation of the Open circuit potential (OCP) with chloride concentration 71

3.6. Variation of the OCP with the temperature 77

3.7. Variation of the potential vs. time at zero current (OCP). 79

3.8. Chronopotentiometry of the electrode 82

3.9. Cyclic Voltammetry 86
3.9.1. Nucleation model 89

3.10. Conclusions 93

4 Behaviour of Ag and AgCl electrodes in chloride solutions 94

4.1. Introduction 95
1. Presence of different equilibria: 97
2. Variation of the activities of chloride or silver (I) inside and outside the ink, dissolution of the AgCl in the SPE: 98
3. Double layer charging: 98
4. Wetting of the electrode, variation of the surface area of the electrode: 98
5. Parallel Faradaic process at the electrode: 98
6. Adsorption of Cl^- on the Ag or AgCl particles: 98

4.2. The literature 99

4.3. Trigger/Triggering circuit 100

4.4. Behaviour of different batches of SPEs 103

4.5. Behaviour of the SPE in Cl^- solutions with added electrolyte ... 104

4.6. Effect of saturating the solution with AgCl. 106

4.7. Adsorption of Cl⁻ on Ag/AgCl ink. 107

4.8. Effect of opening the SPE. 109

4.9. Effect of the temperature on the transients 110

4.10. Effect of surfactants on the transients 114

4.11. Effect of the covering mesh on the transient at OCP 116

4.12. Contact angle measurement 117

4.13. Wetting of the electrode 122

4.14. Double layer model 126

4.15. Nucleation 134

4.16. Conclusions 141

5 New formulations as pseudo-reference counter SPEs 143

5.1. Electrochemical behaviour of AgCl 145

5.1.1. Conductivity of AgCl 148

5.1.2. Electrochemistry of the AgCl particles 149

5.1.3. Glassy carbon electrodes 150

5.1.4. Carbon paste electrodes 152

5.2. Graphite-AgCl counter reference electrodes. Preliminary studies 154

5.3. Screen printed counter reference electrodes 163

5.4. Screen printed graphite loaded with AgCl 164

5.4.1. Preparation and composition of the electrodes. 165

5.4.1.1. Rheology 165

5.4.1.2. SEM images of the SPE 166

5.4.2. Behaviour of the carbon paste loaded with AgCl counter-reference electrodes. 167

5.4.3. Conclusions 171

5.5. Ag/AgCl pastes loaded with KCl as counter reference electrodes. 172

5.5.1. Preparation and composition of the electrodes. 173

5.5.1.1. Rheology 173

5.5.1.2. SEM images of the SPE 174

5.5.2. Behaviour of the Ag/AgCl electrodes loaded with KCl. 175

5.5.2.1. Chronopotentiometry at OCP 175

5.5.2.1.1. Modelling of the dissolution of chloride from the ink to the solution. 178

5.5.2.1.2. Assuming that the electrode is a 2D structure with no thickness, and hence the Cl^- is initially confined in a plane: ... 179
5.5.2.1.3. Assuming that the Cl^- is diffusing out of a layer of thickness h at the electrode: ... 180
5.5.2.1.4. Averaging the concentration in the whole layer of ink ... 183
5.5.2.2. Chronopotentiometry at various currents. ... 186
5.5.2.3. Chronoamperometry of a reversible redox couple using the screen printed electrode as reference-counter electrode. ... 195
5.5.3. Conclusions ... 205

5.6. Conclusions ... 205

6 Effect of aging and oxidation on the performance of the SPEs ... 207

6.1. Introduction ... 208

6.2. Silver oxides ... 209
6.2.1. Electrochemistry of silver - silver oxide ... 210
6.2.2. Silver oxide on the screen printed electrodes ... 216
6.2.3. Silver oxide at pH 7 ... 218

6.3. Incidence of silver oxide on the performance of the SPE ... 220

6.4. Effect of oxidation on the performance of the proposed Ag/AgCl electrodes loaded with KCl ... 229

6.5. Conclusions ... 236

7 Overall conclusions ... 238

8 Appendices ... 242

8.1. Penetration depth of electrons in the sample ... 243

8.2. GC-MS analysis of the solvents enclosed with the SPE in the package ... 244

9 References ... 253

Author´s declaration

I declare that the work in this dissertation was carried out in accordance with the regulations of the University of Southampton. The work is original except where indicated by special reference in the text and no part of the dissertation has been submitted for any other degree at this or other institution. All the work not entirely of the author has been properly referenced and acknowledged.

Any views expressed in this dissertation are those of the author only, and in no way represent those of the University of Southampton.

Acknowledgements

I would like to use this opportunity to thank all the people that has helped me out in the course of this Thesis, either academically in the lab, or in the daily routine since I got here in Southampton, already four years ago.

First of all, I would like to thank Prof. Phil Bartlett and MediSense for the opportunity and the funding. I have to thank my industrial advisors (Dr. Terry Reid, Dr. Neil Carpenter and Dr. Nigel Forrow) for the support, as well as Robin and the guys at the test printing facilities at MediSense for helping me out with the printing of the new formulations (actually, they were printing them...I was just providing the inks. Thanks lads for telling me that water does not go along very well with the aqueous-based screens: sorry about the mess!!)

Special thanks have to go to Phil Bartlett; as someone said, a man of inexhaustible patience and knowledge. I would like to add, a man of quick and sound science. He managed to impress me with the speed in which he would pinpoint loads of different information out of the simplest (or at least, simplest to me!!) experiment. I have enjoyed all the scientific talks and the scientific silences trying to find any plausible explanation of what is happening at the electrode. Thanks also for all the time and patience spent reading and correcting (three times) the science and the English in this Thesis, especially all the "on the solution" and "in the surface". I think that I got the "in" and the "on" now right. I would like to thank as well Dr. Guy Denuault for his different point of view as my advisor during my degree.

I also have to thank all the technical staff in the department, Alistair Clark, the clerical staff and all the staff at the stores and at the glassblowers'. All the work they are performing backstage is absolutely indispensable for any researcher. Also thanks go to Dr John Langley and Julie Herniman for the mass spec. analysis of one of my samples.

All the members of the Bartlett's and Denuault's group, past and present, for the encouragement and daily discussions mainly not scientifically related. Stuart & Stuart, Romaric (in which continent are you now?), David (*"la selva se lo llevo"*), Toru (thanks for praising my cuisine!), Rob (get ready, your *Viva Voce* will be soon), Jan (aka Sexy-Maxy), Shorab (the only Swedish I know that is not tall and blonde ☺), Mohammed, Mamdouh and Enass (the Egyptian connection), Alex (is nice to have someone around

sharing your Spanish point of view), Maciej (samero, Chihiro; and remember that *Alien* is far better than *Aliens* - no comparison between Ridley and James), Tim (stop going to job interviews and work harder on the bike; soon you will be too old to win Le Tour), Kirsty, Liz and Anna (for keeping the feminine balance right amongst all the blokes), Suzanne (the same applies, but also thanks for all the chatting in the lab, with you and Timmy), Ruth (the soon-to-be teacher), all the new comers (Henry, Jin, Sumeet and Veronica, you got here when I was almost finishing, but I have already to thank you), the lads on the 7th floor for all the footy and last but of course not least, Clélia, for keeping always an optimistic approach and a lovely smile (and for praising my cuisine as well)!!!

I also have to thank my other friends out of the department (specially Tania) and my house mates, for keeping me sane amongst all this chemistry. Thanks Leslie, Dong, PingPing, Lei, Yijuan, Daisuke and all at the Academicals Football society. Also I have to thank all my friends from my first degree in Oviedo; it seems like little by little we are all coming to England (Felipe, Miriam, Gregorio, Eva, Dani and the last two that are not in England yet, Miriam and Pedro José)

I would like to end this very long list thanking my family - my parents and my sisters - for almost 30 years of love and support, and Anna, for all the support during this last year, specially during the writing up (support on the phone is not ideal, but... I guess that I should thank Telediscount and Ryanair for offering such cheap fares to Spain)

All this support is very much appreciated. I could not have finished this thesis without it.

Abbreviations and Symbols Used In This Thesis

a.u.	Arbitrary units
BSE	Back Scattered Electron microscopy
CE	Counter Electrode
CPE	Carbon Paste Electrode
CP-GCE	Carbon Paste on Glassy Carbon Electrode
Cps	Counts per second
CRE	Counter-Reference Electrode
DE	Dummy Electrode
EDAX	Energy Dispersive X-ray Analysis
(E)SEM	(Enviromental) Scaning Electron Microscopy
GCE	Glassy Carbon Electrode
GC-MS	Gas Chromatography coupled with Mass Spectroscopy
GOx	Glucose Oxidase
GSE	Gas-phase Secondary Electron microscopy
OCP	Open Circuit Potential
PBS	Phosphate Buffer Solution
PIXE	Particle Induced X-ray Emission Spectrometry
PVC	Poly(vinyl chloride)
RE	Reference Electrode
RSD	Relative standard deviation
SCE	Saturated Calomel Electrode
SDS	Sodium dodecylsulfate
SHE	Standard Hydrogen Electrode
SMSE	Saturated Mercurous Sulfate Electrode
SPE	Screen Printed Electrode
TGA	ThermoGravimetric Analysis
TTL	Transistor-transistor logic
WE	Working Electrode
XPS	Photoelectron Spectroscopy
A	Area of the electrode
a_i	Activity of the species i
C	Capacitance of a condensator

c	Speed of light in *vacuo*, 2.99792458 x 10^8 m s^{-1}
$C_j(x,t)$	Conc. of the species j at time t and at distance x from the electrode
C_j^*	Original concentration of the species j in the solution
D	Diffusion coefficient
E	Potential
E_i^T	Potential of the electrode i at a temperature T
$E_{P/2}$	Half peak potential
F	Faraday's constant, 96484.56 C mol^{-1}
h	Planck's constant, 6.626176 x 10^{-34} J s
i	Current
i_m	Current of the *maxima*
I_M	Ionic strength on the molar scale (mol dm^{-3})
I_m	Ionic strength on the molal scale (mol kg^{-1})
K	Equilibrium constant
k	Rate constant
k_B	Boltzmann constant, 1.3806503 × 10^{-23} J K^{-1}
K_s	Solubility constant/product
m_i	Molal concentration of the species i (mol kg^{-1})
M_i	Molar concentration of the species i (mol dm^{-3})
n	Number of electrons transferred in a redox reaction per molecule oxidised or reduced
pa_{Cl^-}	$-\log_{10} a_{Cl^-}$
Q	Charge
R	Resistance
R	Molar gas constant, 8.31441 J mol^{-1} K^{-1}
R_{ct}	Charge transfer resistance
t	Time
t_m	Time of the *maxima*
T	Temperature
v	Scan rate
$\Delta G^{\ddagger}$	Standard Gibbs free energy of activation
α	Transfer coefficient
χ	Effective hydrodynamic radius
χ	Surface potential

ϕ	Galvani potential
γ_i^m	Activity coefficient of the species *i* on the molal scale
γ_j	Activity coefficient of the species j on the molar scale
η	Overpotential $(E - E^0)$
η	Viscosity of the solution
λ	Wavelength
ν	Frequency
σ	Standard deviation[1] $\sigma = \sqrt{\frac{\sum_{i=1}^{N}(x_i - \bar{x})^2}{N-1}}$
ψ	Volta potential

Subscripts

a	Anodic
c	Cathodic
o	Oxidised species
r	Reduced species
sat	Saturated solution

1 Introduction

1.1. Overall aim of the project

Commercial blood glucose sensors are manufactured in large numbers using screen printing technology. The finished device operates by measuring the current due to glucose oxidation catalysed by glucose oxidase and a ferrocene derivative at the working electrode in a two electrode electrochemical cell. To operate, the second electrode in the device should be able to pass the necessary current without a significant change in the applied potential. The electrode generally used for this application is a screen printed silver/silver chloride electrode. As the designs and performance of blood glucose electrodes have improved, the performance of the secondary electrode (the silver/silver chloride electrode) has not been enhanced to match improvements in the working electrode and it is now often a limiting factor in the design or performance of the overall sensor.

The aim of this project was to investigate the performance of screen printed silver/silver chloride electrodes using a range of techniques and to understand the factors which limit the electrode's performance. The work also involved studies of various ways to improve the performance of the electrode, and different alternatives for this application.

This work is based in the screen printed glucose sensors provided by MediSense® (Abbott Laboratories). These strips are used in a bipotentiostatic two electrode system, with a working, a counter-reference electrode and an additional working electrode without GOx, which is used to allow subtraction of the background used by interferent species.

1.2. (Bio)Sensors, an introduction.

Chemical sensors are devices capable of satisfying the increasing demand for precise analytical information at lower cost through devices that require relatively simple instrumentation[2]. A sensor is a self-contained integrated device having a selective sensing element either intimately connected to, or integrated within, a transducer[3]. IUPAC states that a sensor is a device capable of continually and reversibly transducing a chemical event into a measurable signal[4-6]. An explanation should be made at this point: according to this definition, disposable devices such as MediSense's

glucose sensor should not be called sensors, since these devices provide a discrete value of the monitored chemical event. In theory, MediSense's glucose strips could be used in solution to monitor continuously the concentration of glucose, but the overall device is engineered in such a way that it only gives a discrete reading per strip. It is important to note that this device will handle a biological fluid (blood), so it is paramount to dispose the sample and the strip to avoid the biological hazard of a possible cross-contamination.

In the literature there are several devices that although they are called sensors, a strict analysis shows that the requirements are not met, as for example, sensors based on immunological reactions, or devices based on a transient response. Immunological reactions involve the formation of complexes of high affinity, that are, consequently, irreversible. Devices based on transient responses do not provide a continuous output since the measurement is performed at predefined, discrete intervals.

The purpose of a sensor is to produce a measurable (electrical) signal proportional to the concentration of the species of interest. A schematic representation of a sensor that complies with this definition can be seen in Figure 1.

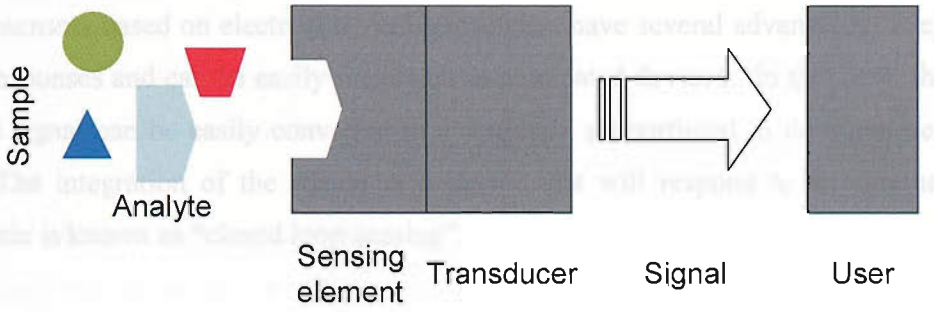

Figure 1 Schematic representation of a sensor, modified from Gerard *et al.*[3]

Ideally, since the sensing element is selective, a sensor-based system needs only little, if any, treatment of the sample. This is an important feature when an *in situ* application is required[2].

Several subdivisions of the term "sensor" can be made, according to the sensing element (ion selective, enzymatic, inmunological, *etc.*) and to the nature of the transducer (optical, electrochemical). Both classifications are complementary, thus, we can find, for example, electrochemical ion selective sensors, optical sensors based on a enzymatic reaction, or piezoelectric sensors based on a immunological reaction as the sensing element.

Biosensors are a subgroup of chemical sensors in which the sensing element is composed of a biological recognition element, typically an enzyme, antibody, nucleic acid (DNA or RNA probes) or micro organism[7], but not limited to this, since organelles, tissues, cell receptors or biomimetic molecules have also been employed[8, 9]. Biosensors are very specific sensors, due to the fact that biological reactions are highly selective. Thus, if designed properly, the improvement in the selectivity of the overall device will be remarkable.

During the last years, a significant increase in the number of articles relating to biosensors had occurred. Nevertheless only a small percentage of these articles consider the application of biosensors to real samples and real problems, and an even smaller number of these relate to biosensors which are commercially available[7]. Product engineering is normally not included as part of the development of a biosensor[10], so it is very difficult for most of the published biosensors to achieve the last step in their development and abandon the laboratory to become a device suitable for large-scale production[11]. Additionally, the market demand for such device should be enough to justify the large investment needed to go into production.

Biosensors based on electrochemical transducers have several advantages. They give fast responses and can be easily integrated in automated devices. In this case, the transduced signal can be easily converted to a response, proportional to the measured stimulus. The integration of the sensor in a device that will respond to an external characteristic is known as "closed loop sensing".

Electrochemical biosensors can be classified as conductimetric, amperometric, potentiometric or impedimetric according to the electrochemical technique used to monitor the analytical signal. Potentiometric and amperometric devices are the most common devices[3, 7, 12].

In the case of amperometric sensors, a predetermined potential difference is applied between two electrodes (called the working and reference electrode). This potential difference is selected so that it will reduce or oxidise species at the working electrode or at the vicinity of its surface. The flow of electrons generated or consumed at the electrode (and thus the extent of the reduction or oxidation) can be easily monitored. The current recorded will be proportional to the rate at which the species are

being reduced or oxidised, and, directly or indirectly, to the concentration of the species of interest.

Depending on which step is the step limiting the current (the diffusion of species to or from the electrode or the kinetics of the reaction), we could have two different situations. If the rate of the redox reaction is the limiting step, there is no mass transport limitation, and the current is proportional to the rate constant and the concentration of the analyte (kinetic control) through:

$$i = nFAkc \qquad \text{Equation 1}$$

where i is the current measured[i]; n, the number of electrons transferred per molecule oxidised or reduced; F, Faraday's constant; A, the area of electrode; k, the rate constant for the redox reaction, and c, the concentration of the redox species.

If the rate of the redox reaction is fast, there will be a depletion of the species at the electrode, so the diffusion of species to or from the electrode will be the limiting step. In this case (diffusion control), the current will be proportional to the diffusion coefficient (D), the concentration of the species (c) and will depend upon the geometry of the electrode and the geometry of the diffusion profile. For example, for a microdisc electrode under diffusion control, this relation is:

$$i = 4nFDcr \qquad \text{Equation 2}$$

where D is the diffusion coefficient and r is the radius of the electrode.

Potentiometric sensors are based on the opposite concept. A certain current is driven through the electrode (normally, zero current), and the potential of the system is measured. At zero current (open circuit potential), the potential at thermodynamic equilibrium will be related to the activity of species at the electrode through the Nernst equation:

$$E = E^0 - \frac{RT}{nF}\ln\left(\frac{a_{red}}{a_{ox}}\right) \qquad \text{Equation 3}$$

where E is the equilibrium potential for the reaction; E^0, the standard potential of the system; R, the gas constant; T, the temperature; and a_{red} and a_{ox}, are the activities of the reduced and oxidised species respectively.

[i] Although IUPAC recommends the use of capital i (I) as the symbol for the intensity of the electrical current, we adopted the traditional i due to its widespread amongst the published literature.

Amperometric sensors are preferred to potentiometric ones because they are more sensitive and respond faster since it is not necessary to wait until equilibrium is achieved as in potentiometric devices[12]. Also, potentiometric (bio) sensors depend largely in the stability of the reference electrode. The first amperometric biosensor was published in 1962 for glucose analysis[13]. That biosensor monitored the depletion of oxygen consumed when glucose (the analyte) was oxidised by the action of glucose oxidase inmobilizated behind a membrane covering a Clark oxygen electrode.

1.3. Thick film and thin film technologies in the design of (bio)sensors

Nowadays there is an increasing interest to perform multitude of analyses in the field, at any time and in any place, and there is also a need to obtain the value of interest almost immediately[2]; thus, the need for portable versions of analytical instrumentation increases[14].

This leads to a decentralization of the analysis, with analysis being performed by non specialized personnel, on-site, that is, in the place where the sample is located, away from a well established laboratory. For example, physicians need to monitor up to 30 parameters of a patient (blood gases, electrolytes, metabolites, enzymes, coagulation indices, haematology, immunochemistry) during the course of a disease, during the course of a treatment, or during a procedure[15]. The value of the result diminishes rapidly with time, and, as for blood gases, where the physiological chemical concentration rate of change can be fast, close to real time results are often mandatory.

These new analytical tools have to be rapid to respond, portable, easy to use by non expert personnel, robust, needing small, if any, pretreatment of the sample, and above all, precise. Additionally, these tools will be used frequently, so the cost per analysis should be minimized.

One of the most important factors that assures the prevalence and widespread use of electrochemical (and amongst these especially, amperometric) (bio)sensors is the possibility of building miniaturized electrodes in a massive, reproducible and economic

way[2, 10, 16], to produce a (bio)sensor that can be portable, easy to operate and disposable[3, 7, 17]. This in turn leads to improved reproducibility by avoiding operator error[8]. Most of these characteristics are possible due to the development of two fabrication techniques: thick film and thin film[12, 18, 19].

Thick film and thin film techniques comprise of depositing layers of metals, insulators, or semiconductor materials on insulating surfaces. Thin films are deposited using vacuum evaporation, sputtering or chemical vapour deposition, whereas thick films are deposited using screen printing or lamination technologies. Thin films can be as thin as a monolayer or have thicknesses as large as one micron. Thick films, on the other hand, have thicknesses of tens of microns.

The primary limitation of the thin-film microfabrication of sensors is that the design and capital equipment costs are very high, although per-unit costs may be relatively low[12]. By comparison, the thick-film technique is relatively inexpensive; however, the quality of the deposited film is lower. Thin-film processes give patterned films that are highly reproducible (line resolution < 1 μm), whereas thick-film processes yield structures with greater variability in both in-plane resolution and thickness.

Although most researchers are devoted to one or the other approach (thin or thick film), there are reports of sensors that combine both thin and thick technology in the same device. In some cases, metal basal tracks are deposited by sputtering. On top of these tracks, the thick film layer will be printed. This is done to enhance the conductivity of the electrode, due to the much lower electrical resistance of the underlying metal track and to enhance the electrochemical properties[15, 20, 21]. A publication by Slater *et al.* is a good (but rare) example of the opposite case[22]. In this publication, the electrodes are built using screen printed technology, and, over the working electrode, a thin layer of gold is deposited by sputtering. This layer of gold was used as a preconcentration layer for the quantification of lead in spiked water.

1.4. Screen printed electrodes

The best known examples of thick film technology are screen printed electrodes (SPE). The modest cost of SPEs has further enhanced their desirability because it allows the device to become disposable[19, 23]. Screen printing is a technique conventionally used in the graphics industry and for the deposition of solder pastes onto printed circuit boards. The fabrication process is achieved by sequential deposition of thick films on a substrate through patterned masks.

Several different methods for building SPEs are reported in the literature though they share the same basic steps. A schematic representation is shown in Figure 2.

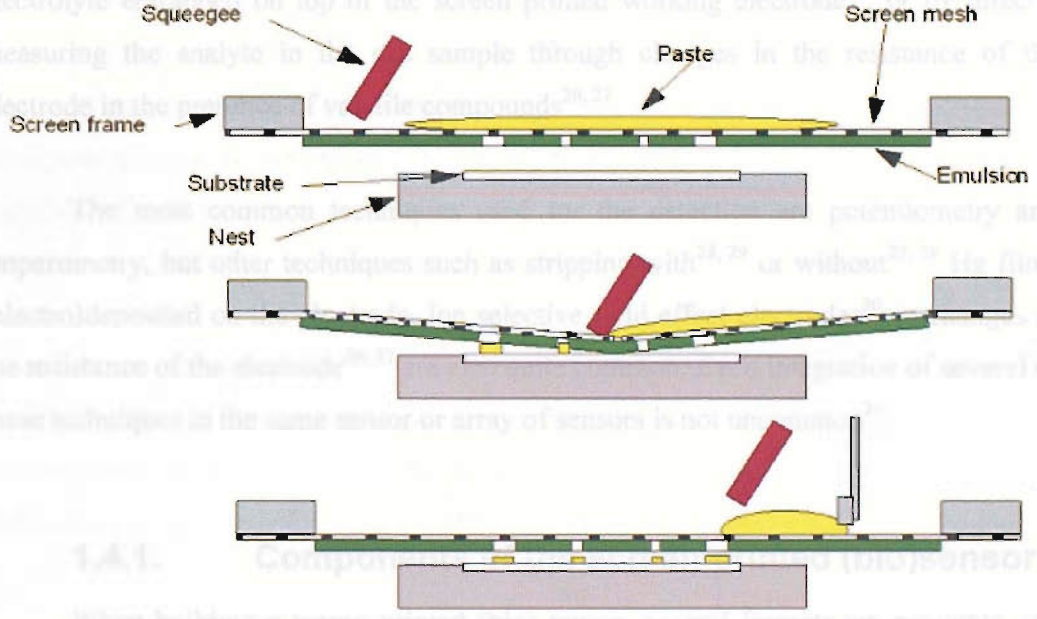

Figure 2 The basic screen print process[24]

A conductive or dielectric film is applied to a substrate through a mask (screen) placed on top of the substrate. The substrate is held in place in a "nest". A thin layer of slurry (commonly known as "ink" or "paste") is forced through the open regions of the screen by a squeegee. This technique forms a patterned film with the desired shape and thickness on the substrate. The slurry is a liquefied mixture of the powdered film material and a suitable binder. This slurry is applied using a squeegee whose velocity, force against the screen and inclination are carefully controlled so that a uniform layer of material is pressed through the mask onto the substrate. The resultant substrate with the patterned slurry is then dried (in a furnace or at room temperature) or (photo)cured

to evaporate solvents, polymerize components and/or sinter the particles into a continuous film[12]. Since different layers of materials (inks) are going to be printed, meticulous control of the raw materials is needed. The inks will be batch-prepared and then sequentially printed on the substrate. This control has to ensure that different batches of inks present the same behaviour.

Screen printed technology has been applied successfully to several fields[19], such as environmental monitoring[14], clinical and biomedical analysis[12], and food technology[7].

SPEs have been mostly designed for use with solutions, but they have been used also to monitor components in mixtures of gases, both by dissolving the gas in an electrolyte entrapped on top of the screen printed working electrode[25], or by directly measuring the analyte in the gas sample through changes in the resistance of the electrode in the presence of volatile compounds[26, 27].

The most common techniques used for the detection are potentiometry and amperometry, but other techniques such as stripping with[28, 29] or without[22, 28] Hg films (electro)deposited on the electrode, ion selective field effect electrodes[30] or changes in the resistance of the electrode[26, 27] are also quite common. Even integration of several of these techniques in the same sensor or array of sensors is not uncommon[31].

1.4.1. Components of the screen printed (bio)sensor

When building a screen printed (bio) sensor, several formats are available, the choice of which will depend on the sample, nature of the sensing layer, manufacturing constraints, etc. SPEs are constructed in layers, with the substrate being the first of them. On top of the substrate, a basal conducting layer can be deposited/printed; and on top of this layer, the electrodes will be printed. The (bio)sensing layer will be printed / deposited on top of the electrode (or forming part of it), followed, in some cases, by one or more finishing layers, that will act as junction bridges, pre-treatment layers, protective films or electrolyte reservoirs.

Each of these constitutive layers will be explain further.

We must mention that although most of the researchers print their own electrodes, there is an increasing number of authors that modify commercially available

SPEs, such as Costa *et al.* who use AndCare® SPEs[32, 33] or Kataky *et al.* who use Cambridge Life Sciences PLC electrodes[34] or SPEs developed by other groups[28].

The choice of the substrate materials is made depending on the subsequent steps, and can be divided in two groups, ceramic substrates or polymeric ones. Ceramic substrates are chosen mainly for thin film technologies or when any of the subsequent steps in the design of the sensor require high temperatures. The ceramic materials used are usually (oxidised) silicon wafers[21, 35-37] or alumina[38-42]. On the other hand, and when a cheap and disposable substrate is needed (especially for thick film technology), polymeric films will be employed, such as polyvinylchloride (PVC) [16, 25, 43-52], polyimide (Kapton)[53], polyester[23, 29, 54-58], polyethylene[59], epoxy films[60] or nitrocellulose[61].

In screen printed biosensors, after the selection of the substrate, the choice of configurations and printed materials should be made. Each of these electrodes has its particular functions and characteristics. The most important electrode is the working electrode. In addition, another electrode (called the blank electrode or secondary working electrode) can be printed for use in a bipotentiostatic set-up [41, 48-50, 52]. This secondary working electrode will have the same composition as the working electrode except that the specific sensing element is usually omitted. This allows an evaluation of the response due to interferences in the sample. The net signal due to the analyte is obtained by comparing the responses of both working electrodes.

Early SPEs were composed of only the working electrode[62-64], and an external reference (and counter electrode in three electrode set-ups) was employed. Researchers soon realised that it was an incongruence to miniaturise the working electrode and, at the same time, use a bulky reference and counter electrode, so reference electrodes and in some cases counter electrodes were incorporated in the sensor.

A conductive track is printed, in some cases, underneath the electrodes. This track will be responsible for the current flow from the electrode to the instrument. We have mentioned that some authors use specific methods to build these tracks (like photolithographic deposition[20] or placing thin layers of metals beneath the electrodes[53]). Although these alternatives yield a better result, they involve more fabrication steps; the

normal tendency is to print the conductive tracks (if any) for all the electrodes with the same composition as one of the electrodes.

A wide range of materials are available for the construction of the screen printed electrodes. The choice is made according to the characteristics needed in the final device. For the working, counter and blank electrodes the materials most widely used are carbon inks (graphite)[39, 59]. Gold[65] or platinum[38] are also used for the working electrode. Carbon inks have low price, present low capacitive currents, and a large potential window. Above all, carbon paste can be easily modified prior to the printing step, giving it particular characteristics[39, 50, 66].

For the reference electrode, silver/silver chloride is the one nearly everyone selects. Silver/silver chloride inks are commercially available from several suppliers, being easy to print with acceptable results. Most of the groups use one of the different choices of pastes commercially available and assume that it behaves well. Only when the ink is home made, do the authors investigate it further.

In the next section, and since the reference electrode is the topic of this work, a more detailed description will be given. The only other alternatives to Ag/AgCl found in the literature were Ag paste electrodes[40, 67], Ag/AgI paste[68]and platinum paste[38]. In the first case, the Ag electrode was not chloridized to form a film of AgCl. In the last case, Bilitewski *et al.* proposed a platinum screen printed electrode as the reference electrode for their sensor.

The last and most important layer of the (bio) sensor is the (bio)sensing element. Although the (bio)sensing element is not the subject of this project it is obviously a very important parameter when designing a (bio)sensor and so is thus briefly detailed. A review on the topic has been published elsewhere[69] where (bio)sensors are split into three groups based on the choice of the technique used to immobilise the (bio)sensing element (mostly enzymes). These three groups are explained below:

- Multiple layers formed by manual deposition of a solution containing the enzyme[16, 25, 34, 43-46, 49, 52, 55, 56, 60] or sensing element, *e.g.* an ion selective membrane[31]. This is the most widely used approach. The enzyme is deposited in a droplet thus maintaining intact all its properties. The major drawback of this deposition is that the enzyme will not be entrapped or strongly attached to the

electrode, so it will diffuse into the sample, unless a membrane is added on top of the sensor. Another drawback is that many steps will be necessary to fabricate the biosensor. Consequently, this deposition method is only of use in laboratory applications and is not suitable for mass production. Within this category we also include those techniques based on the (electro)polymerization of a mixture of monomer and the sensing element[31, 41, 58, 68, 70-72].

- Screen printing of inks or slurries in two or more steps: first, the electrode is printed, followed by the deposition by screen printing of a slurry or paste containing the sensing element[38, 50, 55, 72]. This technique is most often employed for mass construction of (bio)sensors since all the components of the working electrode will be screen printed in successive steps. The sensing element is physically entrapped in the electrode and this will normally overcome the use of an outer membrane. It is important to ensure that the enzyme will survive the printing step and that it remains active once it is entrapped.
- One step deposition of the sensing element in which it is mixed with the material of the electrode (normally graphite or conducting polymers) and this ink is then printed as the working electrode[3, 20, 53, 73]. In this case, the polymer will be conductive and will therefore act also as the conducting matrix. Some reports cite the direct electron transfer from the enzyme to the polymeric matrix[63, 74], in which case, even the use of mediators is overcome. This approach is the most attractive one for mass production due to the small number of steps required (only one), but it is also the technique that requires the most complex optimisation process[69].

In fact, the border between the last two techniques is quite thin, and often (bio)sensors that could be built in a "one step printing" process are printed in two steps; the paste containing the sensing element is often the most expensive one, and its application is restricted to the sensing area of the working electrode, meanwhile a similar paste without the sensing element is printed first as the working electrode. This is the case for MediSense® glucose sensors as we will see later (section 2.2.2, page 37).

1.5. Glucose analysis and diabetes: past, present and future

The biggest market for biosensors is currently clinical analysis, and amongst this field, glucose analysis is easily the largest market. This is hardly surprising, around 1.8 million people in the UK alone (approximately 3 % of the population) and 17 million in USA are diagnosed with diabetes. There is therefore great impetus for the development of effective and portable blood glucose sensors that do not hamper the daily life of their users.

1.5.1. Diabetes

Diabetes is characterized by the deficiency in the body of insulin, or by its low activity. Insulin is a hormone produced in the pancreas that regulates the concentration of glucose in the blood. If the concentration of glucose in the blood is high, insulin will trigger the storage of glucose in the muscle, fat and liver cells: if the concentration is low, glucose will be released from the liver and become available in the blood stream. Glucose is the main energy source of cells, and the only source of energy for neurons, so it is important that it is available in the blood stream in a certain concentration range. On the other hand, a low amount of glucose in the blood stream will cause cells to start burning fat as a source of energy, this will increase the amount of ketones in the blood (a by product of fat metabolism), and thus decrease slightly the pH of the blood (diabetic ketoacidosis)[75], that can cause several alterations in the organism.

There are three types of diabetes[76]:

- Type 1: Where the patient produces little or no insulin due to a malfunction of the pancreas. It is unclear why, but for some reason the insulin producing cells of the pancreas (islands or islets of Langerhans) are attacked by the immune system. The onset of type 1 diabetes is quite quick, with symptoms usually developing in childhood. Individuals with Type 1 diabetes are insulin dependant.
- Type 2: This type is far more common than type 1. In this case, the body becomes less sensitive to the insulin it produces or is unable to produce sufficient quantities. The symptoms of type 2 diabetes generally develop in later life. Most individuals do not even know of their condition. The symptoms are less severe and controlled diet is often sufficient; there is no need for extraneous insulin.

- Gestational diabetes is high blood glucose that develops at any time during pregnancy in a woman who does not have diabetes. This condition is transitory and in most cases, the patient returns to a normal condition after delivery.

Healthy fasting blood glucose levels range between 65 and 115 mg/dl (3.6 - 6.4 mM), but in a diabetic they are easily over 126 mg/dl (7 mM) and may reach as much as 540 mg/dl (30 mM) in cases of extreme hyperglycemia. If the condition is not managed properly the long term risks include, kidney, nerve, heart and artery damage, blindness, and in severe cases, diabetic coma and even death.

Diabetics need to monitor their blood glucose levels several times a day, so a way of doing this, in a fast, easy way compatible with a normal daily life is paramount. Precision and reliability are above all the most important features of a glucose blood sensor. The analysed glucose level will be used by the patient or physician to decide further action: if the level is too low, the subject will need to ingest glucose or if the level is too high, insulin should be taken (commonly injected, or more recently in aerosol format). In the latter case, it is necessary to know how much insulin is required. An erroneous glucose reading could have disastrous consequences.

1.5.2. Glucose Biosensors:

The use of a glucose oxidase modified electrode for the detection of glucose was first proposed by Clark and Lyons in 1962[13]. This first device was based on the entrapment of glucose oxidase (GOx) over an oxygen electrode via a semipermeable dialysis membrane. The enzyme oxidised glucose consuming oxygen and produces gluconic acid and hydrogen peroxide. The amount of glucose was evaluated by the decrease of the concentration of O_2 measured with a Clark electrode.

Some years later (in 1970), Clark filed a patent showing the possibility of using enzymes to convert electroinactive species into electroactive ones in order to analyze them.

As a variation on the detection system, in 1973 Guilbault and Lubrano proposed a glucose biosensor based on the detection of the H_2O_2 generated instead of the O_2 depleted[77].

The first commercial sensor available was the Yellow Spring Instruments, model 23YSI analyzer, first launched in 1973 and re-launched (successfully) later in 1975[78].

This biosensor monitors the H_2O_2 generated when glucose was oxidised by the action of glucose oxidase inmobilizated behind a membrane covering a Clark oxygen electrode.

Glucose sensors that use molecular O_2 as the electron acceptor in the reaction between glucose and GOx are referred to as first generation devices. The first biosensors of this generation rely on detecting the oxygen depletion to monitor the glucose concentration, and are subject to errors in measurement due to other blood species (such as ascorbic acid, aspirin, acetaminophen) which are electroactive in the same range. Often permselective membranes covered the sensor to exclude the interferents. These films will often also exclude surface active macromolecules leading to increased stability and sensor lifetime. In addition, detecting H_2O_2 instead of O_2 reduces the overpotential needed for the electrocatalytic detection, thus effectively reducing background reactions.

Another problem with first generation glucose sensors is their dependence on oxygen. Fluctuation of oxygen tension may cause errors in the measurement signal, and the reaction between GOx and glucose is restricted by the amount of O_2 available in solution (typically an order of magnitude less than that of glucose). Several strategies have been proposed to overcome this limitation[17].

To overcome the O_2 dependence of the sensor, alternative redox mediators were proposed. Glucose sensors which employ an artificial mediator are classified as second generation sensors. Many commercial blood glucose sensors use ferrocene or ferricyanide complexes as mediators while some use organic salts like tetrathiafulvalene-tetracyanoquinodimethane (TTF-TCNQ)[17]. A good mediator should operate at low overpotentials to help reduce the effects of interferents.

Third generation sensors try to obtain a direct transfer of the electrons from the redox site of the enzyme GOx to the electrode. Glucose oxidase does not directly transfer electrons to conventional electrodes because of the thick protein layer surrounding the flavin redox centre. Researchers try to "introduce" the electrode into the enzyme by using polymers that can facilitate the transfer. Several strategies can be found in the literature to achieve the direct transfer of electrons from the glucose oxidase to the electrode. An extensive review from Willner and Katz[79] covers the direct wiring of several enzymes to the electrode. Since the transference occurs directly

between the enzyme and the electrode, further minimization of the interfering background can be achieved.

In 1987, MediSense® was the first company to exploit screen printing technology and biosensing for the construction of a personal glucose meter. The electrode consisted of a carbon working electrode, constituted of GOx and a ferrocene mediator, and a silver/silver chloride reference electrode. A drop of blood is placed on the strip. A small portable meter (such as those shown in Figure 3) applies a potential between the working and reference electrode and calculates the blood glucose concentration from the resulting current transient. Nowadays, MediSense produces over 100 million of these strips a month.

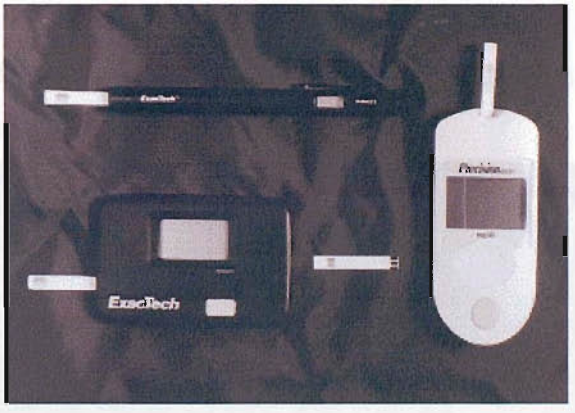

Figure 3 A range of electrochemical glucose biosensors commercialised under the MediSense® brand by Abbott Laboratories. The picture shows three generations of meters and their respective measuring strips (elongated white electrodes)[8]

Although the most usual way of measuring glucose is by electrochemical means, other alternatives such as optical spectroscopy, scattering or fluorescence are not uncommon and commercial instruments are also available.

1.5.3. And what about the future?

Research nowadays goes in three different directions; miniaturization of the device, with smaller sample volumes required, non invasive measurement and continuous monitoring of the glucose in the blood stream.

A great deal of effort has gone into producing sensors which require smaller and smaller blood droplets for measurement (*e.g.* Therasense's®[ii] FreeStyle Flash blood glucose meter can obtain readings from droplets as small as 0.3 μl[80]). The usual way of obtaining the droplet of blood is by a lancet piercing the skin (usually fingertips, but forearms or other regions can also be used with accurate results). Smaller droplets mean less pain for the user. Another very important line of research has been devoted to obtain faster analysis times.

One of the biggest inconveniences of glucose monitoring is that traditional meters require a drop of blood, great stress is being put in developing sensors that will not need a drop of blood (non invasive). Non invasive glucose sensors are now commercially available (like Diasensor® 2000, from Biocontrol Technology), that uses the fact that near infrared light can penetrate the skin several centimetres. Optical non invasive glucose sensors currently lack sufficient precision within the relevant clinical range over prolonged periods of time[81]. Additionally, in Figure 4, it can be seen that the Diasensor 2000® is anything but portable.

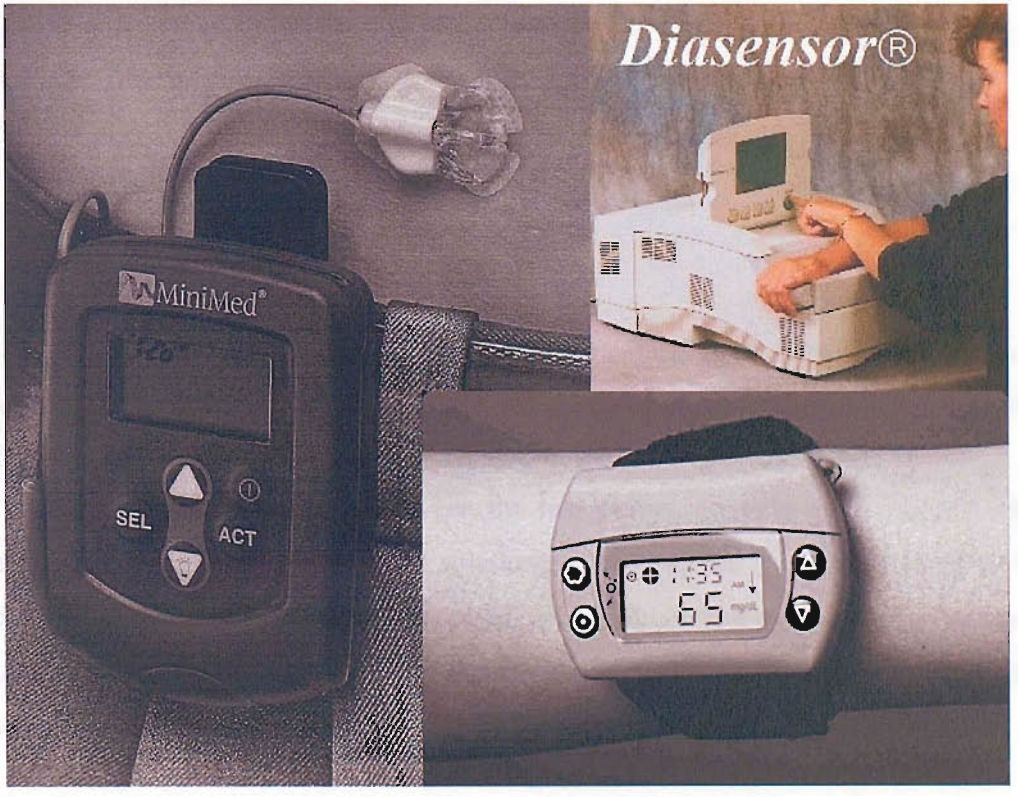

Figure 4 Photographs showing Minimed®'s CGMS[82] the Diasensor® 2000[83] and the Glucowatch® Biographer[84].

[ii] Therasense® is another subsidiary of Abbot Laboratories®

However the future would seem to be in sensors that could provide continuous blood glucose monitoring, such as commercially available devices like the Gluco-watch® [84] and Minimed's CGMS[iii] ® [82, 85].

GlucoWatch® biographer[84] applies a low current to the skin in order to drag ions (and glucose) through the skin (reverse iontopheresis) and cannot be considered as a non invasive device. Following a three hour warming period, it can provide up to 3 readings per hour for 12 hours: this approach has a considerable time lag due to the time needed for the transfer of interstitial fluid across the skin.

Minimed's CGMS[82, 85] uses a subcutaneous glucose electrode and can measure glucose levels every 10 seconds (storing the average value every 5 min) for up to 3 days. This sensor does not provide the patient with the actual result of the glucose measurement; it can only be inspected retrospectively and discussed with the physician.

If such a continuous sensor could be combined in a closed-loop system with a means of automatic insulin delivery it could offer very tight glyceamic control; acting as an artificial pancreas; unfortunately, such a panacea has still to be developed.

1.6. Reference electrodes

The first problem we have to address before talking about reference electrodes is to define what a cell potential is: in simple words, it is the sum of the electrical potential differences across all the interfaces of the system under study[86].

The potential difference between the two phases, (usually a solid phase - the electrode - and a liquid phase - the solution), is represented by $\Delta\phi$ and is given by $\Delta\phi = \phi_A - \phi_B$, where ϕ_A and ϕ_B are called the inner, or Galvani, potentials of each phase. Each of these systems reaches equilibrium by the transfer of charge across the interface between the two phases[87].

The Galvani potential or inner potential has two distinct components. One is the Volta potential (ψ) which is the potential determined by long range coulombic forces near the electrode, and the surface potential (χ) which is determined by short range

[iii] CGMS stands for "Continuous Glucose Measuring System"

effects of adsorbed ions and oriented water molecules. Thus, the Galvani potential is expressed as the sum of both potentials.

The Galvani potential ($\Delta\phi$) is the electric potential difference between points within the two bulk phases. On the contrary, the Volta potential is the electric potential difference between two charges. The Volta potential can be measured directly or calculated by classical electrostatics from the charge distribution[88], but the surface potential cannot; potentials can only be measured between two points in the same phase. Thus the Galvani potential can only be measured relative to a reference electrode.

The overall chemical reaction taking place in a cell is made up of two independent half-reactions, which describe the real chemical change at the two electrodes. Each half reaction responds to the interfacial potential difference at the corresponding electrode[89].

Normally, only one of these half reactions is interesting from an experimental point of view, and the electrode at which it occurs is commonly called the *working electrode*. To focus on it, the other half cell is usually standardised by the use of an electrode/electrolyte of known behaviour: *i.e.* the reference electrode.

Most electrochemical methods start from an equilibrium situation at the electrode. This equilibrium is displaced by means of altering the potential, as can be seen in:

$$\Delta G = -nF\Delta E = -RT\ln K \qquad \text{Equation 4}$$

where ΔG is the Gibbs free energy of the reaction, and K the equilibrium constant.

Considering that the potential of any electrochemical cell is the sum of the potentials of the reactions involved in both half cells, and assuming that the potential of the reference electrode is known and constant, one can easily infer that, at equilibrium, any changes in the potential of the cell are due to changes in the interfacial potential difference at the working electrode. This condition (that the potential of the reference electrode is known and constant), is crucial in any electrochemical method.

In practice, the absolute value of the potential of any given system is not be obtained; instead, relative values are used, and these values are referred against the potential of the standard hydrogen electrode ($Pt|H^+/H_2$), that is considered as the zero

(0.000 V) value by convention. In this sense, the potential of an electrode should be referred as "*more positive than*" or "*more negative than*".

The role of a reference electrode in an electrochemical system is to provide a stable potential with respect to which the potential of the working electrode will be established. In potentiostatic experiments, the potential between the reference and the working electrode will be controlled by a potentiostat. The reference electrode serves the purpose of providing a thermodynamic reference[90]. The potential of the reference electrode system should be stable over the operating range of temperatures (or at least, its variation known), needing short equilibration times, constant and invariant performance with solution composition and with low susceptibility to junction contamination or leaking that could contaminate the sample[86].

There are several different reference electrodes available, but three families of electrodes are mostly used. These are: the hydrogen electrode, the mercury-mercurous salt electrodes and silver – silver halide electrodes.

The most important reference electrode is the standard hydrogen electrode (SHE). It is the electrode universally adopted as the primary standard[86, 91], the one to which all the other reference electrodes and standard potentials are referred[iv]. Its intrinsic properties make it a complicated electrode in terms of construction, and its miniaturization is hardly achievable. Although a miniaturized/miniaturizable SHE has been reported[92], its use has not taken root in the scientific community. This electrode is based on the entrapment of an H_2 bubble in a capillary in contact with a Pt wire. Since the bubble is not isolated from the sample, other species can diffuse inside the capillary, as well as the diffusion of H_2 into the electrolyte, thus altering the reference electrode. Additionally, the electrode has to be prepared under high vacuum, and the H_2 bubble has to be electrogenerated in the electrolyte prior to its usage.

The mercury-mercurous salt electrodes (with chloride or sulfate salts) are probably the most widely used reference electrodes, especially the saturated calomel electrode (SCE)[90]. Silver halide electrodes are also widely used, particularly the silver –

[iv] The potential of any given electrode or reaction cannot be expressed in absolute values, but referred to the potential of other system. SHE electrode is adopted as the ZERO value, and the rest of the systems are referred to it.

silver chloride electrode. Ag/AgCl electrodes present very stable potentials and they are being used more frequently in place of calomel electrodes due to its lower toxicity and easily miniaturizable compact size[86]. The feasibility of miniaturization and the fact that the silver/silver chloride electrode is an all-solid electrode (since the solubility of silver chloride is very low, K_s = 1.77 x 10^{-10} M^2)[93] make it almost the only choice for the development of miniaturized sensors in general and screen printed electrodes in particular.

The Ag/AgCl electrode is, as is the mercurous salt electrode, a reference electrode of the second kind. The potential is established, not by the system M/M^{n+} (where M is a metal) as in electrodes of the first kind, but by the co-precipitation of a sparingly soluble salt, AgCl.

$$AgCl + 1e^- \rightarrow Ag + Cl^-$$

The potential of the electrode is dependant on the concentration of the redox species, following the Nernst equation (Equation 3):

$$E = E^0 + \frac{RT}{nF}\ln\left(\frac{a_{ox}}{a_{red}}\right) = E^0_{Ag/Ag^+} + \frac{RT}{nF}\ln\left(\frac{a_{Ag^+}}{a_{Ag}}\right)$$
$$= 0.7991 + \frac{8.31441 \times 29815}{1 \times 96485}\ln\gamma_{Ag^+}[Ag^+] \qquad \text{Equation 5}$$

where E is the equilibrium potential for the reaction; E^0, is the standard potential for the system, 0.7991 V (*vs.* SHE)[93]; R, the molar gas constant; T, the temperature; n, the number of electrons; F, Faraday's constant; a_{red} and a_{ox}, the activities of the reduced and oxidised species respectively (the activities of solids is 1 M); γ is the activity coefficient of each species.

Since the activities of Ag^+ and Cl^- are related to each other through the solubility product (K_s = 1.77x10^{-10} M^2 = $a_{Ag^+} \cdot a_{Cl^-}$)[93], the previous equation can be rewritten as follows (Equation 6):

$$E = E^0_{Ag/Ag^+} + \frac{RT}{nF}\ln\left(\frac{K_s}{a_{Cl^-}}\right) = 0.7991 + \frac{RT}{nF}\ln(K_s) - \frac{RT}{nF}\ln\gamma_{Cl^-}[Cl^-] =$$
$$= 0.2223 - \frac{RT}{nF}\ln\gamma_{Cl^-}[Cl^-] \qquad \text{Equation 6}$$

Written in this way, we can see that the potential of the Ag/Ag^+ couple in chloride solutions depends on the activity of Cl^- ions in the solution.

The value +0.2223 V is the reversible standard potential of the Ag/AgCl redox couple (*vs.* SHE)[93].

Since the potential of the reference electrode will depend on the activity of Cl^-, a constant concentration of chloride is needed. Usually, a saturated solution of potassium chloride is used. In this case the potential of the reference electrode will be 0.197 V *vs.* SHE[89].

1.6.1. Solid state reference electrodes.

In most screen printed (bio)sensors, the reference electrode is constructed using the Ag/AgCl couple. One of the first publications on screen printed Ag/AgCl electrodes was published by Burns and Nylander in 1986[51].

A report from Bilitewsky *et al.*[38] shows a screen printed reference electrode built from platinum paste, but such innovation is quite unusual. In this work, they proposed a reference electrode constructed with platinum paste for use in an amperometric sensor as part of a FIA system. The system was employed to analyze the stability of printed enzymes (oxidases and peroxidases) by the reduction of the H_2O_2 generated enzymatically at +0.6 V (*vs.* Pt) or the oxidation of *p*-benzoquinone from the regeneration of the peroxidase at -0.31 V. The potential of the reference electrode (Pt) in this system is believed to be unstable, and easily alterable with changes in composition of the sample (mainly changes in pH). The pH was fixed at pH 8 with a buffered solution through all the experiments.

Another report that did not use the Ag/AgCl couple[68], used Ag/AgI instead. This article is quite confusing since it does not mention why they chose Ag/AgI electrode instead of the usual Ag/AgCl. The quantification of pesticides was carried out by monitoring the decrease of activity of the cholinesterase in the presence of the pesticides. As a substrate for the cholinesterase, they used acetylthiocoline iodide (10^{-3} M); that was also used to fix the potential of the reference electrode. For this application, acetylthiocoline chloride is also commercially available, and in combination with the use of the Ag/AgCl reference pair could have been a more obvious choice for the reference electrode.

As the designs and performance of biosensors has improved, the performance of the secondary, silver/silver chloride, electrode has not been improved to match

improvements in the working electrode. One of the serious problems that has restricted the use of miniature electrochemical sensors in industrial or biomedical applications has been the lack of a reliable and durable reference electrode[94]. Hundreds of references can be found relating new applications or new designs for screen printed (bio)sensors, but there are very few references that pay any attention to the performance of the reference electrode. In most cases, the authors simply use one of the commercially available inks, using it "as it is", or they will use bulk reference and counter electrodes.

The use of Ag/AgCl reference electrodes in thick and thin film biosensors can be split into two groups, depending on how the reference electrode is constructed.

a. The first and most usual group for thick film devices are based on printing a conductive ink with particles of silver and silver chloride in defined proportions. This ink will be printed as the reference electrode on the (bio)sensor substrate. The ink can be made *in situ*[42, 46, 52, 95-97] or, most likely, a commercially available ink will be printed[22, 23, 25, 29, 35-37, 44, 47, 49, 50, 52, 54, 55, 57, 58, 61, 71, 97, 98].

b. Depositing only a silver track, that will later be oxidised to AgCl in a chloride medium, either electrochemically[20, 51, 71, 94, 99-104], or chemically[15, 31, 45, 56, 59, 105-107] (usually using $FeCl_3$). This is the most likely case for thin film device.

The previous two models are solid state electrodes with no internal electrolyte solution. As we stated before, the potential of the reference electrode will depend upon the concentration of chloride, thus, these reference electrodes will require a constant chloride concentration in the solution under test to function properly. To avoid this, the use of liquid reservoirs entrapped within membranes[99] or more often, solid electrolytes formed with a chlorinated salt and polymers such as PVC[35], polyvinylalcohol[107], agarose[102, 103] or agar agar[36, 37] (with an additional layer of PVC and Nafion or cellulose nitrate on top) have been reported. The main purpose of both approaches is to have a known activity of Cl^- in contact with the electrode that will not diffuse/leak into the sample, thus altering the potential of the Ag/AgCl electrode.

One of the most important advances in screen printed reference electrodes has been developed by Suzuki *et al* [94, 99, 100]. Their goal was the development of a solid state reference electrode with enhanced performance. Their novel silver design has an

improved stability by means of avoiding the contact of silver with the solution. In their case, a layer of silver was sputter-deposited on a substrate. This layer was covered with a non conductive membrane (polyimide), leaving a small slit on its surface. Through this slit, the silver was oxidised to silver chloride. The electrode prepared in this way showed a long term stability of over 40 hours depending on the fabrication procedure and the amount of silver deposited, and was employed successfully in the development of a Clark type oxygen electrode, acting in this case, both as reference and counter electrode[100]. The best improvement was achieved when the stability was measured in saturated KCl solution.

Although Suzuki's approach gives interesting results, its applicability to a commercial mass produced sensor is very difficult and expensive. The sensor was made with thin film technology, sputtering silver with a supporting layer of gold underneath it. Apart from this, each electrode must be electrochemically treated to form the silver chloride layer. These two steps are difficult to achieve on a mass production scale.

Suzuki based the improvement in stability of their reference electrode on the fact that the Ag layer is isolated from the solution. Most of the Ag/AgCl electrodes reported for screen printed applications do not avoid contact of Ag with the solution, but are based on a layer of Ag and AgCl ink, where the Ag and AgCl are homogeneously distributed throughout. In this sense and according to the reasoning of Suzuki *et al.* electrodes where the Ag and AgCl are not separated should exhibit stable potentials over shorter times than electrodes where the Ag is kept away from the solution.

Simmonis *et al.*[36, 37] used an approach based on depositing agar doped with KCl on an Ag/AgCl screen printed electrode. The electrode was later covered with a layer of PVC and another of cellulose nitrate. In this way, they managed to obtain screen printed electrodes that showed stable potentials for 500 hours (with a final drift of the potential of less than 10 mV). Such electrodes could be used discontinuously for 10 hours every day for up to 70 days, with less than 10 mV drift overall and less than 2 mV drift per measuring session.

1.6.2. MediSense's glucose biosensor strip

The screen printed electrode which is the object of this study is a screen printed electrode for monitoring glucose levels in diabetics. In simple terms, it consists of two electrodes, a working electrode and a counter-reference electrode (CRE), made of silver

and silver chloride particles. This counter-reference electrode acts both as the counter and reference electrode, so it should be capable of passing the necessary amount of current without significant change of the potential. This criterion will be satisfied if the exchange current density is large. This can be achieved if the electrochemical reaction is fast and we have a good supply of reactant. Improvements on the limiting step of the reaction (kinetics or mass transport) will enhance the current density and hence the performance of the CRE.

On the working electrode in the glucose sensor, oxidation is taking place. In the sensor, this oxidation is compensated with the reduction of the AgCl at the Ag/AgCl electrode. A schematic representation can be seen in Figure 5.

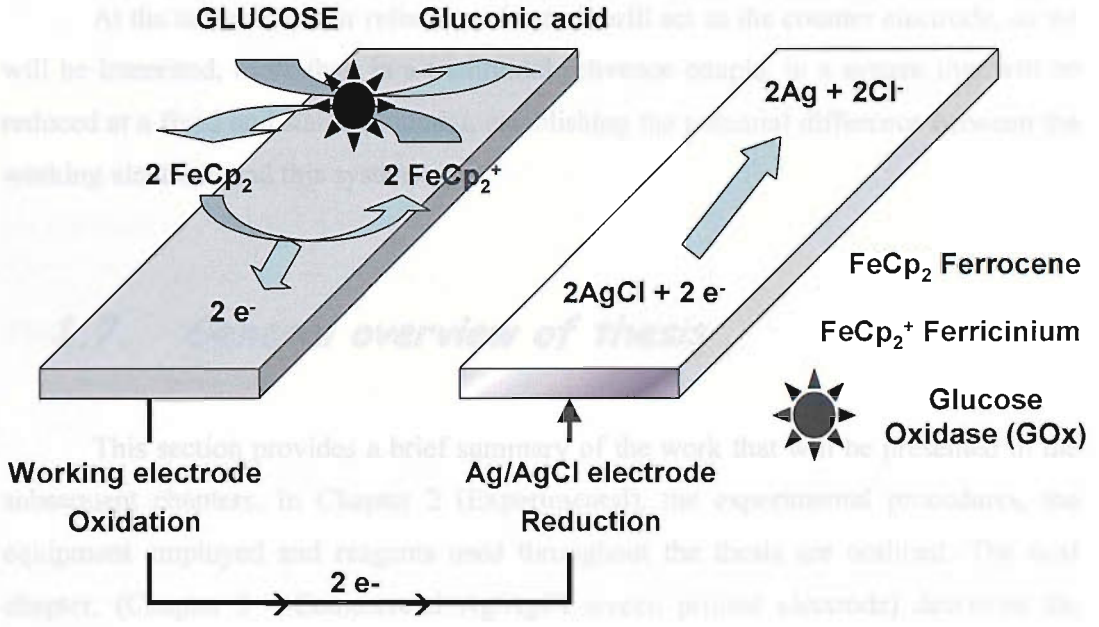

Figure 5 Schematic representation of the reactions occurring on the glucose sensor. At the working electrode, glucose is oxidised by GOx to yield gluconic acid and the reduced form of the mediator, ferrocene. The generated ferrocene will be oxidised back to ferricinium at the electrode. The two electrons obtained will be used at the pseudo-reference electrode in the reduction of AgCl to Ag and chloride.

It is important to note that the main goal of the work published on miniaturized reference electrodes was to produce a universal reference electrode, but our goal is to build a reference electrode for our particular application, with sample and operating parameters known in advance.

The sample (blood) is well know and well defined with minimum variations of the concentration of chloride. The presence of an internal electrode solution is not needed since the sample provides the reference electrode with a predefined

concentration of chloride. Also the time scale of the experiment is different in our case to those for the miniaturized reference electrodes published previously. In the later case, the goal was to produce a reference electrode with as long life times as possible (days); in our case the measurement will take less than one minute, with the aim of reducing the measurement time to 3 seconds. What is even more important in our case, compared with cited references, is that the electrode must perform as expected from the very first moment the electrode comes into contact with the solution, even though it is stored in a dry form and will be wetted with the sample. Faster wetting times will yield shorter times needed for the analysis.

At the same time, our reference electrode will act as the counter electrode, so we will be interested, more than in a traditional reference couple, in a system that will be reduced at a fixed and stable potential, establishing the potential difference between the working electrode and this system.

1.7. General overview of thesis

This section provides a brief summary of the work that will be presented in the subsequent chapters. In Chapter 2 (Experimental), the experimental procedures, the equipment employed and reagents used throughout the thesis are outlined. The next chapter, (Chapter 3 - Commercial Ag/AgCl screen printed electrode) describes the composition and the electro-chemical performance of the commercial screen printed electrodes tested, focussing both on short and long times after the electrode is placed in the solution. We have found that the electrochemistry of the SPE is limited by the resistance of the track. We have also found evidence for nucleation of Ag on AgCl occurring at the SPE.

Chapter 4 (Behaviour of Ag and AgCl electrodes in chloride solutions) tries to explain the shape of the potential transients of the SPE immediately after the electrodes are immersed in the solution. Several models are proposed, and the experimental conditions were altered in order to try to predict the variations found with those expected from the proposed model.

Chapter 5 (New formulations as pseudo-reference counter SPEs) deals with new formulations proposed as alternative counter-reference electrode. This chapter has been divided in two sections, each with a different counter reference approach; the first one

describes the use of carbon electrodes loaded with AgCl and the second one proposes Ag/AgCl SPE loaded with KCl. Better results (faster equilibration and stability of the potentials at all currents tested) were obtained with Ag/AgCl SPEs loaded with KCl. These SPEs were tested as counter reference electrodes in a model system with a glassy carbon electrode as the working electrode for the electrochemical analysis of ferrocene derivatives.

The following chapter (6 - Effect of aging and oxidation on the performance of the SPEs) describes how the storage conditions affect both the commercial and the proposed electrodes. It was found that light and air had an adverse incidence on the performance of the SPE electrodes, and we have proposed a mechanism that could explain this behaviour.

Overall conclusions are described in Chapter 7, meanwhile Chapter 8 (Appendices) shows the mass spectra recorded for the solvents employed in the commercial ink, along with the calculation of the penetration depth of electrons inside the commercial Ag/AgCl layer.

The last chapter of the thesis (Chapter 9) gathers the bibliographic references cited through the Thesis.

2 Experimental

2.1. Experimental procedures

2.1.1. Electrochemical cell set-up

An Autolab PGSTAT 30 (ECO Chemie, Utrecht, Netherlands) connected to a personal computer was employed for the electrochemical measurements. All electrochemical measurements were performed in a thermostated cell. The temperature inside the cell was kept constant using a water bath (Grant, model WFP, UK).

A conventional three electrode system was used, with a platinum mesh electrode as the counter electrode (CE). All potential measurements are referred against the reference electrode used for each experiment, a saturated mercurous sulfate reference electrode (SMSE) or a saturated calomel reference electrode (SCE).

To study the behaviour of the Ag/AgCl screen printed electrode (SPE), this electrode was connected as the working electrode. Adaptors to connect the SPE to the potentiostat were provided by MediSense's electrical workshop.

Since in the overall sensor the solution (blood) is oxygenated, none of the solutions used in the experiments shown in this thesis were desoxygenated. Gases in the solutions were equilibrated with air.

2.1.1.1. Trigger

We noticed that, even at open circuit potentials, the potential of the electrode changes from the moment the electrode is immersed in the solution. We found that it was very difficult to record the initial seconds of the wetting of the electrode, since the synchronization of the start of the measurement with the moment the electrode is immersed in the solution was difficult to achieve.

In order to overcome this limitation, a simple trigger was designed. This circuit sends a TTL signal (+5 V) to the potentiostat once the electrode is immersed in the solution. This +5 V signal will immediately trigger the start of the measurement.

This triggering circuit was built on a stripboard according to the scheme shown in Figure 6.

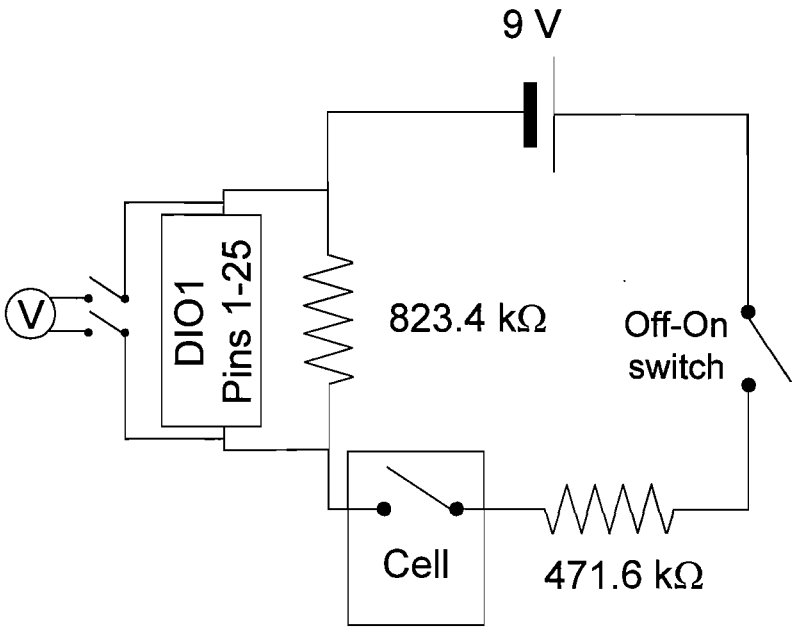

Figure 6 Scheme of the triggering circuit. The circuit comprises two resistors and one switch. The switch marked as "Cell" represents the electrical contacts mounted on the cell (*vide infra*).

When the circuit is closed, the circuit will send a +5.7 V signal to the potentiostat. The potentiostat will receive that signal through any of its DIO ports.

To detect when the electrodes are placed in solution, two electrical contacts were set on the cell: one placed on the holder of the electrodes and the other one on the exterior of the cell, as can be seen in Figure 7. These contacts were made from adhesive copper tape (3M, UK). When the electrode holder (and so the screen printed electrode) is lowered, the two ends of the trigger circuit make contact and close the circuit, starting the measurement. This methodology proved to be adequate for measuring the first moments of the electrode's wetting.

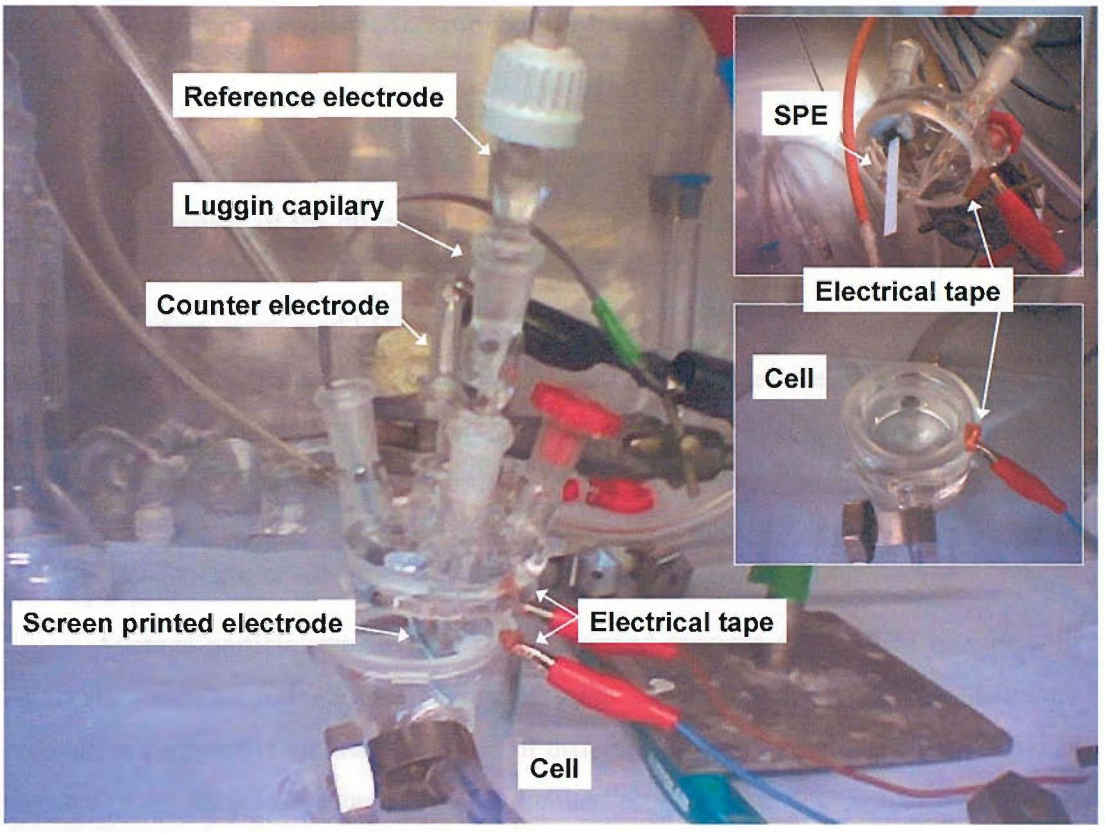

Figure 7 Electrochemical cell used. The insets show detail of the two electrical tape contacts that trigger the measurement.

2.1.2. Microscopy, X-ray analysis and contact angle measurements

During these investigations, an electron microscope was used, employing several detection techniques, Gas-phase secondary electron microscopy (GSE), Back Scattered Electron microscopy (BSE) and Energy dispersion X-ray analysis (EDAX) [108, 109].

Scanning electron microscopy (SEM) and energy dispersive X-ray analysis (EDAX) were performed on a Phillips XL30 ESEM TMP Scanning Electron Microscope (Phillips, The Netherlands), equipped with EDAX Genesis software (EDAX Inc, USA).

Unless otherwise stated, microscopy was performed using the ESEM (Environmental Scanning Electron Microscopy) mode. This mode allows scanning of non-conductive samples without previous sputtering[109].

Contact Angle measurements were performed on a Drop Shape Analyzer (DSA 100) from Krüss (Germany). This instrument is controlled via a PC, with automatic

drop size dosification and specific software for the analysis of the shape of the drop on the substrate.

2.1.2.1. Image analysis

The analysis of the microscope images was done using three different pieces of software:

The afore mentioned EDAX Genesis software for the EDAX mapping.

Analysis of feature sizes and distances was done over the SEM saved images with UTHSCA Image Tool version 3.0[110] (Freeware available on the Internet at http://ddsdx.uthscsa.edu/dig/itdesc.html). This software allows the measurement of 2D lengths from the number of pixels in an image, after the calibration of the image in pixels per μm.

Average particle size analysis was performed over the saved SEM images with AnalySIS version 5.0 (Soft Imaging System GmbH, Germany). This software recognizes particles in an image as areas of different color/brightness. It then calculates the area of the particle in square pixels. A calibration of the image using the information about the image allows the conversion of the areas to μm^2.

2.1.3. Electrochemistry of solids

In some of the experiments, electrochemistry of solid particles attached to an electrode was performed. Physical attachment of the particles was achieved by means of rubbing the electrode onto a Whatman filter paper loaded with the particles[111]. Although this technique was easy to use, the stability of the attachment was very poor and the particles fell off very easily during the electrochemical measurement, yielding a very noisy and irreproducible scan.

To enhance the attachment carbon pastes were used[111]. In this case, one gram of spectroscopic grade graphite (Ultra Carbon, USA) was mixed with 0.36 ml of Uvasol (spectroscopic paraffin; Merck, Germany) to prepare the blank paste. The graphite powder acts as the electrical matrix, as well as a diluent for the solids tested. The paraffin oil was used in order to give the paste a sticky texture. Since this oil is immiscible in water, the paste will remain fixed to the electrode. We also prepared pastes loaded with the particles under study [AgCl, provided by MediSense, (code M15103, batch 0561) and/or Ag_2O (99%, Aldrich, UK)], maintaining the same solids to paraffin ratio.

2.1.4. Sectioning of the SPEs

Sectioning of the SPE could not be performed directly due to the soft character of the Ag/AgCl printed ink. Two ways of shearing the electrode were employed:

- The electrodes were embedded prior to cutting in an impregnation epoxy resin (Epofix Kit, Struers) and left to cure overnight. To allow a better impregnation and avoid the formation of bubbles, the resin was heated to 40 °C, thus reducing the viscosity. Once the resin was cured, the samples were extracted from the cast and sectioned. A precision saw (Buehler Isomet 4000) was used for sectioning the samples.
- Another way of sectioning the SPEs avoiding deformation was by freezing[112, 113] the SPEs with liquid N_2. A pre-cut was previously performed in the back of the electrode with a guillotine. Once the SPE is frozen, the PVC basecard (section 2.2.2, see below) will become fragile and can be easily and cleanly fractured.

2.1.5. Rheology

The viscosity of the screen printable inks is an important parameter that indicates the suitability of the ink for the screen printing process. These inks are non-Newtonian fluids, and the viscosity depends on the stress (the viscosity of Newtonian fluids is constant with the applied stress). Due to this characteristic, measuring the viscosity with standard procedures (with ascending bubbles, descending balls, or by letting the matter flow freely down a slope) causes changes in the properties of the ink. Additionally, these inks show a thixotropic behaviour, where the ink shows a time dependant decrease of the viscosity the longer the fluid undergoes shear.

Instead of viscosity, it is more accurate to talk about rheology. Rheology describes the visco-elastic deformation of a fluid (a solid, a liquid or a gas) in terms of stress, strain, temperature, and time. In our case, it describes the variation of the viscosity of inks with the applied stress.

Rheology measurements are performed by immersing a disk in the sample and rotating it at a measured speed. The friction between the ink and the disk will create a torsion that can be measured with a torque. This torsion is directly related with the viscosity and with the capacity of the matter to flow. Low viscosity inks or fluids will flow easily, and will slow the measuring disk less; on the contrary, high viscosity inks or fluids will hamper more the rotation of the disk.

Rheology was measured at MediSense facilities in Witney. The rheometer was a TA Instruments AR 500 (West Sussex, UK) equipped with a peltier plate that thermostats the sample.

2.1.6. Calculation of the activity of chloride

As we have shown in the introduction, the equilibrium potential of a redox system is related with the activities of the species in solution through the Nernst equation (Equation 6, page 21).

The activity is defined as the effective concentration of a species in solution, and it is calculated as[113]:

$$a_i = \gamma_i^m m_i \qquad \text{Equation 7}$$

where γ_i^m is the activity coefficient of the species i on the molal scale (m), and m_i is the molal concentration of the species (mol kg^{-1}).

These activity coefficients can be found tabulated in the literature (*e.g.* Lobo[114]), and there are several empirical equations that can predict their values. In "Handbook of Electrolyte Solutions"[115], Horvath reviews several of these empirical equations.

Mean-ion activity coefficients can be obtained from electromotive forces, or from freezing point data. In all cases, the activity coefficient of each ion depends on all the electrolytes in the solution, so the activity coefficient of a specific ion cannot be calculated, and several assumptions have to be made to evaluate the activity coefficient of each ion. For a 1:1 electrolyte, a good approximation is that the activities of each ion of the pair are equal. In this case, $\gamma_\pm = \sqrt{\gamma_- \gamma_+}$. For other electrolytes (M_nX_y), the mean-ion activity coefficient will be equal to $\gamma_\pm = \left((\gamma_+)^n (\gamma_-)^y\right)^{1/(n+y)}$

In our case, we have used molar concentrations throughout this Thesis, but most of the activity literature is tabulated and calculated in molal activity coefficients; Equation 8[115] permits conversion between the scales:

$$\gamma_\pm^M = \left(\frac{m}{M} d_0\right) \gamma_\pm^m \qquad \text{Equation 8}$$

where $\gamma_\pm^M$ is the mean-ion activity coefficient on the molar scale, m is the molality of the solution, M the molarity and d_0 the density of the pure solvent. To simplify we will be using $\gamma_\pm$ as the mean-ion activity coefficient in the molar scale ($\gamma_\pm^M \equiv \gamma_\pm$)

The activity coefficients are one at infinite dilution, and can be approximated by Debye-Hückel expression for very diluted solutions[87], if the ionic strength (I_m) is lower[115] than 0.005 mol kg^{-1}.

The Debye-Hückel limiting law is the starting point for several more precise calculations. The general approach is to add terms with experimental parameters that produce a much better agreement with tabulated data. The equation that we used to evaluate the activity coefficients was the Bromley equation[116]:

$$\log_{10}\gamma_{\pm}^{m} = \frac{-A_m|z_+z_-|\sqrt{I_m}}{1+a_i\sqrt{I_m}} + \frac{(0.06+0.6B_m)|z_+z_-|I_m}{\left[1+\left(1.5I_m/|z_+z_-|\right)\right]^2} + B_m I_m \qquad \text{Equation 9}$$

where A_m is the Debye-Hückel parameter (0.5108 kg^{½} mol$^{-½}$), a_i and B_m are empirical parameters (a_i is 1 for 1:1 electrolytes; B_m is 0.240 kg mol^{-1} for KCl solutions); z is the charge of the ion and I_m, is the ionic strength, calculated as $I_m = \sum_i m_i z_i^2$

2.2. Electrodes

2.2.1. Reference electrodes

2.2.1.1. Saturated calomel electrodes (SCE):

These electrodes were constructed according to the inverted type described in the following recipe[117]. A small amount of triply distilled mercury (99.999%, Alfa Aesar, UK) was placed in a sealed tube (inner tube) provided with a platinum electrical contact. On top of the mercury, a layer of calomel paste was placed. The calomel paste was obtained by grinding together with a ceramic mortar and pestle, KCl (Analar grade, BDH, UK), Hg_2Cl_2 (Analar, Hopkins and Williams, UK), few drops of mercury and few drops of saturated KCl (Analar grade, Merck, UK) solution. The resulting greyish paste was then carefully packed on top of the mercury ensuring that no air bubbles were left. The rest of the glass tube was then filled with glass or cotton wool. This inner tube was placed, inverted, into another glass tube with a sinter on the bottom. The outer tube was filled with saturated KCl prior to the final assembly.

When not in use, the SCE electrodes were stored in saturated KCl solution. The potential of the electrodes was found to be stable and with negligible drift over the time scale of the experiments (potential was stable within 0.1 mV during working sessions).

The potential of the electrode built in this manner was checked frequently with a digital voltmeter (Keithley, UK) against a commercial SCE electrode (Cole Palmer, Illinois, USA). Any significant deviation observed against this commercial SCE was corrected (if it was less than 5 mV) or the electrode replaced (if the deviation was more than 5 mV).

2.2.1.2. Saturated mercurous sulfate electrodes (SMSE):

These electrodes were constructed following a similar procedure as for the SCE, *mutans mutantis* (K_2SO_4 and Hg_2SO_4 instead of KCl and Hg_2Cl_2).

When not in use, these electrodes were stored in saturated K_2SO_4. The potential of the electrodes was found to be stable with negligible drift over the time scale of experiments. The potential of the electrode built in this manner was checked frequently with a digital voltmeter (Keithley, UK) against a commercial SCE electrode (Cole Palmer, Illinois, USA). Any significant deviation observed from the expected value (400 mV) was corrected (if it was less than 5 mV) or the electrode replaced (if the deviation was more than 5 mV).

2.2.1.3. Ag/AgCl bulk electrodes

These electrodes were constructed using a self made assembly and the electrochemical treatment described by Suzuki *et al*[94]. A silver wire of approximately 4 cm length (Goodfellow (UK), purity 99.99% and 0.5 mm in diameter) was soldered to a nickel wire (RS, UK). This assembly was then inserted inside a 1 ml micropipette tip, with the soldered connection inside the tip, and the Ag wire protruding from the narrow end. To avoid any contact of the Ni wire and the soldered union with the solution, the tip was filled with epoxy resin (RS, UK) and cured at room temperature. The silver wire was cleaned with acetone to eliminate any grease, followed by a short immersion in 6 M HNO_3. A film of AgCl was electrodeposited on the silver wire by applying a constant potential of +0.45 V *vs.* SCE for 30 min in a saturated KCl solution. Before the oxidation, a negative potential (-0.55 V *vs.* SCE) was applied 30 s to dissolve superficial impurities and activate the surface. The anodised wire was then assembled inside a glass tube (10 cm long) with a porous frit. This tube was filled with saturated KCl.

Although silver chloride is substantially insoluble in aqueous solutions (K_s = 1.77 x 10^{-10} M^2), its solubility in saturated chloride solutions is two orders of magnitude higher, and silver is redissolved in the form of $[AgCl_n]^{(n-1)-}$ [99, 117, 118]. The major

drawback of this redissolution is that some areas of the silver chloride film can be dissolved, leaving the Ag wire exposed to the solution. This redissolution can be prevented by adding crystals of AgCl so the solution is saturated with Ag^+,[94, 99, 100] enhancing the durability of the electrode.

When not in use, these electrodes were stored in saturated KCl solution. The potential of the electrodes was found to be stable with negligible drift over the time scale of experiments. The potential of the electrode built in this manner was checked frequently with a digital voltmeter (Keithley, UK) against a commercial SCE electrode (Cole Palmer, Illinois, USA). Any significant deviation observed from the expected value of 45 mV was corrected (if it was less than 5 mV) or the electrode replaced (if the deviation was more than 5 mV).

2.2.2. Screen printed electrodes

Commercial screen printed electrodes were supplied by MediSense (Abbott Laboratories, UK), under the commercial designation of G2b. The size of the whole screen printed electrode is 4 cm x 0.5 cm, and the Ag/AgCl electrode is approximately a square of 2 mm x 2 mm. The structure of the electrode is shown in Figure 8.

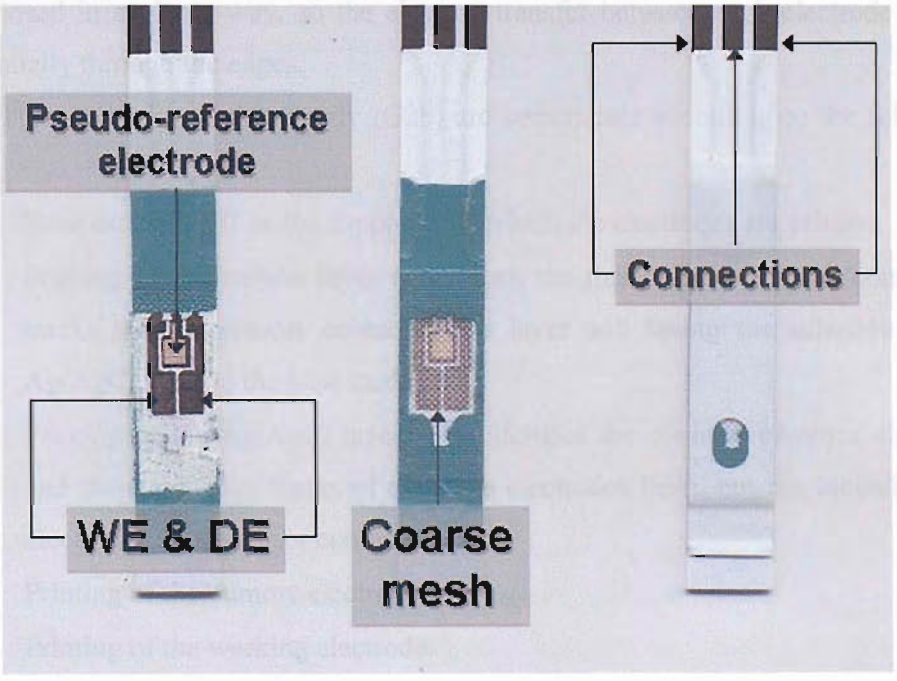

Figure 8 Scheme of a MediSense's G2b SPE. Right, complete sensor; centre, sensor without the lidding tape; left, sensor without the lidding tape and without the coarse mesh (*vide infra*). WE and DE represent working and dummy electrodes.

The sensor consists on three different electrodes. Two of them (WE and DE) are carbon-based electrodes, and act as the working and dummy electrode respectively. Both electrodes are constructed with Gwent carbon ink. Additionally, the WE contains glucose oxidase (GOx) and ferrocene. The net analytical signal is obtained by subtracting the current from the working electrode (oxidation of glucose plus interferences) from the signal from the dummy electrode (oxidation of interferences in the sample).

The third electrode is an Ag/AgCl pseudo-reference electrode[v]. The Ag/AgCl electrode is made using a commercial ink from DuPont. DuPont states that the ink contains 78% of solids, made up of Ag particles (51.04% w/w) and AgCl particles (27.48% w/w). These particles are embedded on a polymeric resin. The thickness of the Ag/AgCl track is approximately 30 μm, and the exposed area of the Ag/AgCl electrode is 2.69 mm^2. The composition of the ink will be discussed later (chapter 3.1, page 47).

Five additional layers of different composition are placed on top of the electrodes; two nylon meshes, two insulating layers and a lidding layer. These layers will define a reproducible volume of the electrochemical cell and facilitate a fast and reproducible wetting of the electrodes. As can be seen in the figure, the three electrodes are disposed in a planar way, so the electron transfer between each electrode occurs preferentially through the edges.

The electrodes of this family (G2b) are constructed according to the following steps:

- Base card of PVC as the support onto which the electrodes are printed.
- Printing of the carbon layer underneath the three electrodes, the connection tracks and the sensors contacts. This layer will favour the adhesion of the Ag/AgCl layer to the base card.
- Printing of the Ag/AgCl layer. This includes the counter-reference electrode and the conductive tracks of the three electrodes from, but not including, the electrodes to the sensor contacts.
- Printing of the dummy electrode.
- Printing of the working electrode.
- Fine mesh: weave with spaces of 60 x 60 μm. This mesh ensures a proper wetting of the electrode

[v] It is called a pseudo-reference electrode because its potential is not invariant; the potential depends on the composition of the test solution, in this case, the potential depends on the activity of Cl^-.

- First insulating layer
- Coarse mesh: weave with spaces of 2 mm x 2 mm, with a thickness of 2 mm. This layer will draw the sample from the application point towards the electrochemical cell.
- Second insulation
- Lidding tape. This tape covers the electrodes, leaving a small application point where the drop of sample will be placed.

In the next scanning electron microscopy (SEM) images, we can see a cross section of SPE, showing the layers of different composition. Figure 9 shows the cross section of the SPE, meanwhile a close up to the Ag/AgCl track is shown in figures 10 and 11.

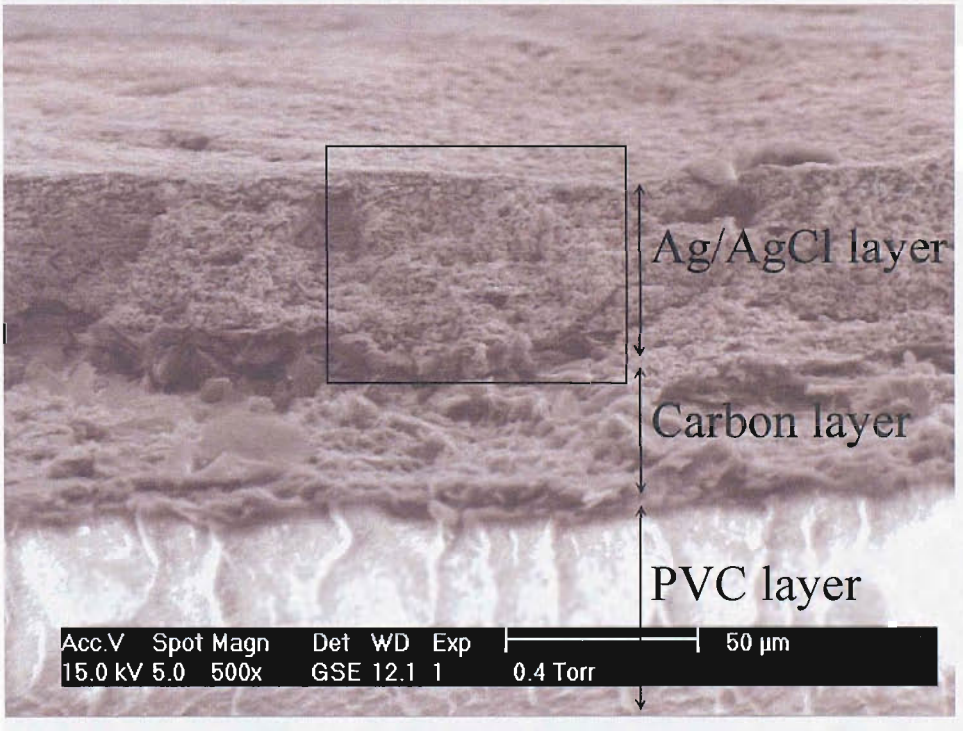

Figure 9 Cross section of a SPE across the Ag/AgCl electrode using the gas-phase secondary electron (GSE) detector. The mesh layers and the lidding tape were removed before sectioning. The sectioning was made after freezing the SPE with liquid nitrogen. The boxed area has been enlarged in next SEM pictures.

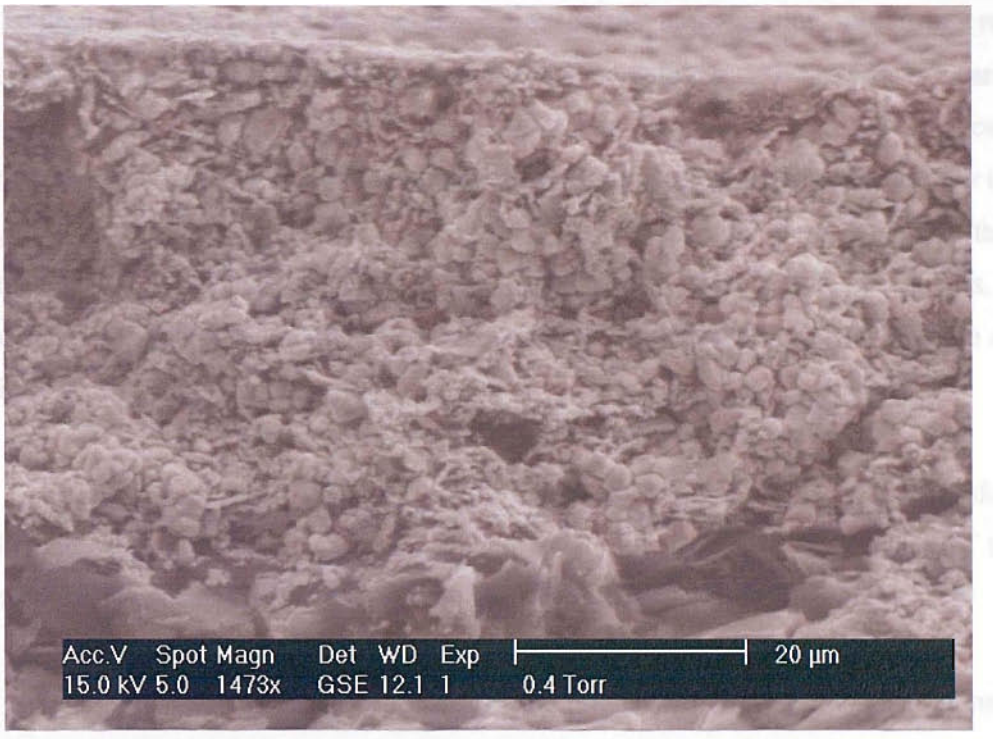

Figure 10 Close up of the SPE shown in Figure 9.

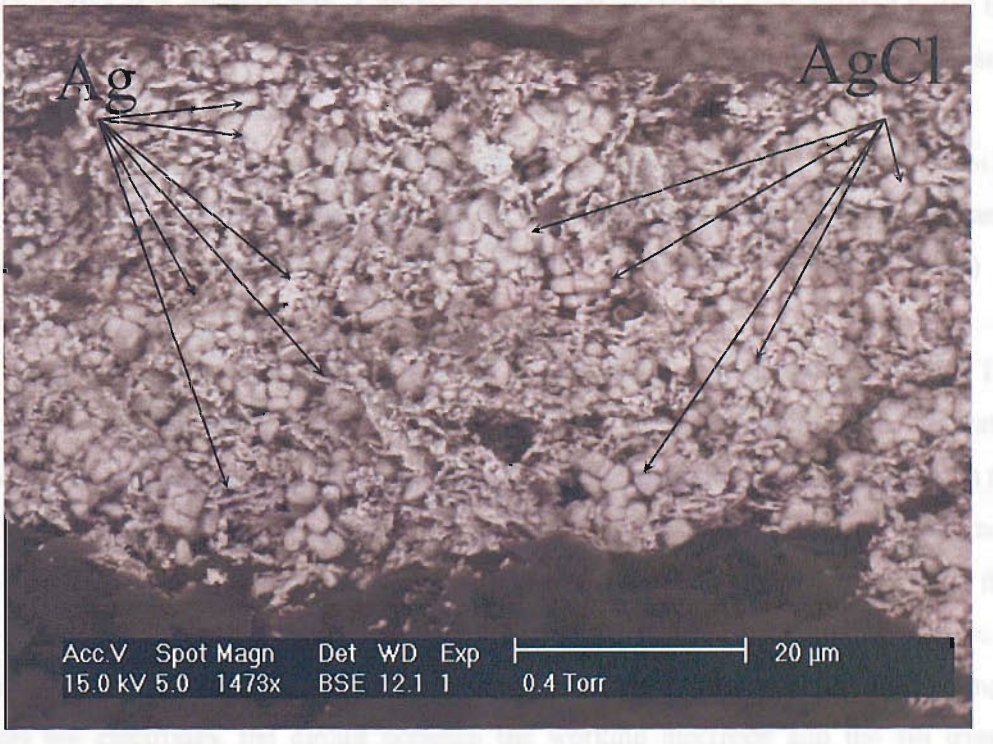

Figure 11 Close up of the SPE shown in Figure 9, using the back scattered detector. AgCl particles are the smooth, round, greyish particles; meanwhile Ag particles are the angular, brighter flakes.

Figures 10 and 11 show the same area of the cross section, but using two different detectors. We can see that the image obtained with the GSE detector is clearer, sharper and with much more 3D depth than the picture obtained with the BSE detector. On the other hand, the picture obtained with the BSE gives chemical information for the sample, due to the fact that heavy atoms (*e.g.* Ag) back-scatter more electrons than lighter ones (*e.g.* Cl), thus the brighter areas in the picture represent heavier atoms. In Figure 11, AgCl particles are the smooth, rounded, greyish particles; meanwhile the Ag particles are the angular, flaky, brighter ones.

Unless otherwise stated, the lidding tape was removed from the SPE before performing any electrochemical measurement, in order to expose the surface of the electrode. The coarse and fine meshes were left untouched.

In addition, screen printed electrodes were printed with different compositions at MediSense's printing facilities in Witney. These facilities comprise an industrial screen printer (Thieme 3000s) directly connected to a Natgraph continuous oven operating at 55 °C. (After each printing step, a drying step was intercalated). Each printed board has 5 rows of 50 electrodes (250 electrodes per board). We printed approximately 20 boards of each composition tested.

Different ink compositions were prepared by mixing different components with commercial inks. Solids were ground with an Ikamill A10 (Janke & Kunkel, Germany) grinding mill and dispersed in the ink using a Dispermat (BYK-Gardner) at approximately 1000 rpm.

All electrodes were printed on PVC boards, using a different mask (G3). The change from G2b (used in the commercial SPE tested) to G3 electrodes was motivated by MediSense's decision to withdraw G2b meters and electrodes from the market, in the near future. Several characteristics differentiate G2b and G3 electrodes. The most significant difference, apart from the disposition of the electrodes (Figure 12[vi]), is that G3 has got no dummy electrode. The G3 electrodes have a working electrode, a counter-reference electrode, and a fill trigger contact. At the moment when the sample covers the electrodes, the circuit between the working electrode and the fill trigger contact is closed, triggering the measurement.

[vi] In the G3 electrodes, the CRE surrounds three out of four sides of the WE, meanwhile in G2b electrodes, it is the WE that surrounds the CRE

Another difference is that G3 electrodes are printed on Mylar basecards, meanwhile G2bs are printed on PVC boards. In our trials, we chose PVC boards because they produce cleaner cross section cuts.

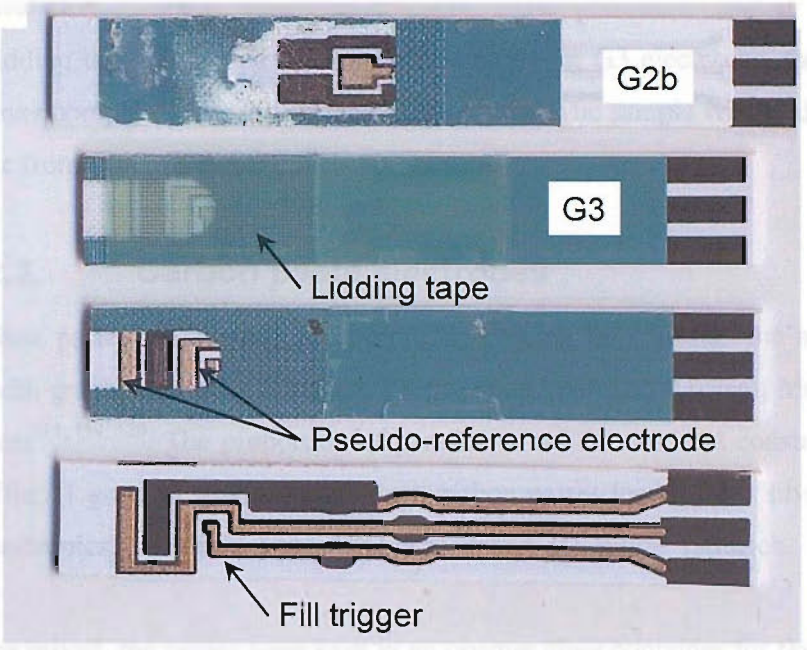

Figure 12 Scheme of a MediSense's G2b (top) and G3 (bottom) SPEs. G2b sensor is shown here without the lidding tape and the coarse mesh. From top to bottom, complete G3 sensor; G3 sensor without the lidding tape or the coarse mesh; G3 sensor without the lidding tape, coarse mesh and without the insulation. Also this last sensor does not have the enzymatic layer on top of the working electrode.

The electrodes of this family (G3) are constructed according to the following steps:

- Base card of Mylar as the support where the electrodes are printed.
- Printing of the carbon layer underneath the three electrodes, the connection tracks and the sensors contacts. This layer will favour the adhesion of the Ag/AgCl layer to the base card.
- Printing of the Ag/AgCl layer. This includes the whole CRE and trigger electrode, and the conductive track of the working electrode from, but not including, the working electrode itself. Ag/AgCl ink is not deposited on the sensor contacts.
- Printing of the working electrode.

- Coarse mesh: weave with spaces of 2 mm x 2 mm, with a thickness of 2 mm. This layer will draw the sample from the application point towards the electrochemical cell.
- Insulation
- Lidding tape. This tape covers the electrodes. In G3 electrodes, the tape will cover completely the top surface of the sensor. The sample will be drawn from the front side of the electrode.

2.2.3. Carbon paste electrodes

Carbon pastes were made by thoroughly mixing in a mortar the solids (fine powders) with graphite powder (Carbone Lorraine) and paraffin (Uvasol, Merck) as an binding agent[111, 119, 120]. The proportion of paraffin to solids was kept constant, at 0.36 ml of paraffin / 1 gram of solids. In this way, carbon pastes loaded with silver chloride (Gwent Electronics Materials Ltd., UK) and silver (I) oxide (Aldrich, UK) were prepared.

Once mixed, the pastes were kept in an opaque glass container for no more than 3 months.

The carbon paste electrodes (CPE) where built employing two different methods:

- Spreading carbon paste over a glassy carbon electrode (GCE, 4 mm in diameter) with a spatula.
- Making a carbon paste cylinder on top of a stainless steel rod. A hollow PTFE electrode with a stainless steel rod was constructed in such a way that it will leave a cavity in one end. The size of this cavity was approximately a cylinder of 3.1 mm in diameter. The depth of the cavity, and hence the volume of the carbon paste, can be controlled by means of a screw holding the stainless steel rod. The paste was packed inside the cavity, and the excess of paste was eliminated by rubbing the electrode against a clean sheet of paper. The depth of the cavity was typically between 0.1 and 0.3 mm.

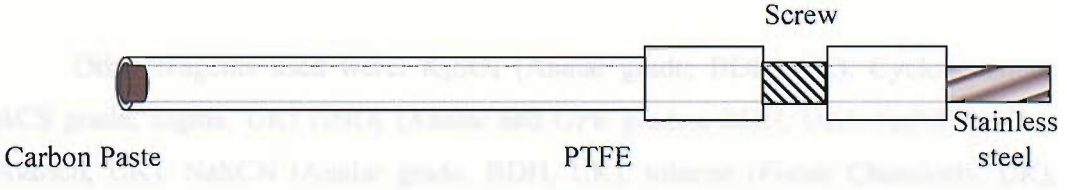

Figure 13 Schematic representation of the Carbon Paste electrode

After every measurement, the remaining paste was removed with acetone and the electrode gently rinsed and, in the case of the GCE, polished.

2.2.4. Other electrodes

Silver, platinum and glassy carbon (GCE) disk electrodes were also built. These electrodes were made by encapsulating the metal or the glassy carbon and an electrical contact (usually a Ni wire) in epoxy resin. The casting was done at room temperature inside a 1 ml micropipette tip, with the electrical connection inside the tip, and the metal wire or glassy carbon protruding from the wider end. Once the epoxy was cured, the micropipette tip was removed and the electrode was polished, subsequently with sand paper (320, 800 and 1200) followed by polishing with 1 and 0.3 μm alumina (Al_2O_3; Buehler GmbH, Germany).

A homemade silver bulk electrode was also employed. This electrode was circular with a diameter of about 3.1 mm. The electrode was mounted in a polytetrafluoroethylene cylinder. The electrode was thoroughly polished as stated before.

2.3. Chemicals

All reagents were commercially available and were employed without any further purification, unless otherwise mentioned. All solutions were prepared using deionised water (18 MΩ cm^{-1}) from a "Still Plus" system coupled to a "RO 50", both from Whatman, UK.

Most of the experiments were carried out in KCl (Analar grade, BDH, UK), with or without supporting electrolyte *i.e.* KNO_3 (Analar grade, BDH, UK) or phosphate buffer solution (PBS). PBS was prepared using potassium dihydrogenphosphate (Analar grade, BDH, UK) and orthophosphoric acid (Aldrich, UK) in variable amounts.

Other reagents used were: K_2SO_4 (Analar grade, BDH, UK). Cyclohexanone (ACS grade, Sigma, UK) HNO_3 (Analar and GPR grades, BDH, UK), $Fe(NH_4)(SO_4)_2$ (Aldrich, UK), NaSCN (Analar grade, BDH, UK), toluene (Fisher Chemicals, UK), acetone, Brij56 [$C_{16}H_{33}(OCH_2CH_2)_nOH$, where n ~10] (Aldrich, UK), sodium dodecylsulfate (SDS) (Fluka, UK). 1,1'-ferrocenedicarboxylic acid [$Fe(C_5H_4\text{-}COOH)_2$],

(Aldrich, UK), Na_2SO_4 (Aldrich, UK), $NaNO_3$ (Aldrich, UK), $MgCl_2$ (Aldrich, UK), $FeCl_3$ (Aldrich, UK), $CaCl_2$ (Aldrich, UK).

To make inks and/or carbon paste electrodes, the following reagents were used: AgCl particles (Gwent Electronic Materials Ltd., Newport, UK). Silver / silver chloride screen printable ink (DuPont plc. (UK), Carbon screen printable ink (Gwent Electronic Materials Ltd., Newport, UK), Graphite in powder (Carbone of America, USA), Uvasol, spectroscopic liquid paraffin (Merck, Germany).

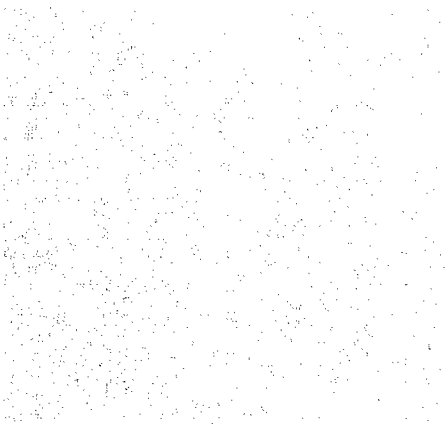

3 Commercial Ag/AgCl screen printed electrode

3.1. Composition of the ink

The counter reference screen printed electrodes (CR SPEs) used in this work were manufactured using DuPont's commercial ink. This Ag/AgCl ink is used by MediSense without any treatment, apart from a jog or shake to homogenise its contents.

DuPont's ink is a heterogeneous dispersion of Ag and AgCl particles and a polymeric matrix in organic solvents. X-ray analysis (EDAX, Energy Dispersive X-ray Analysis) of the ink was performed to evaluate the dispersion of Ag and AgCl in the ink. A thin layer of ink was applied onto a carbon disc, and analysed on the ESEM after drying.

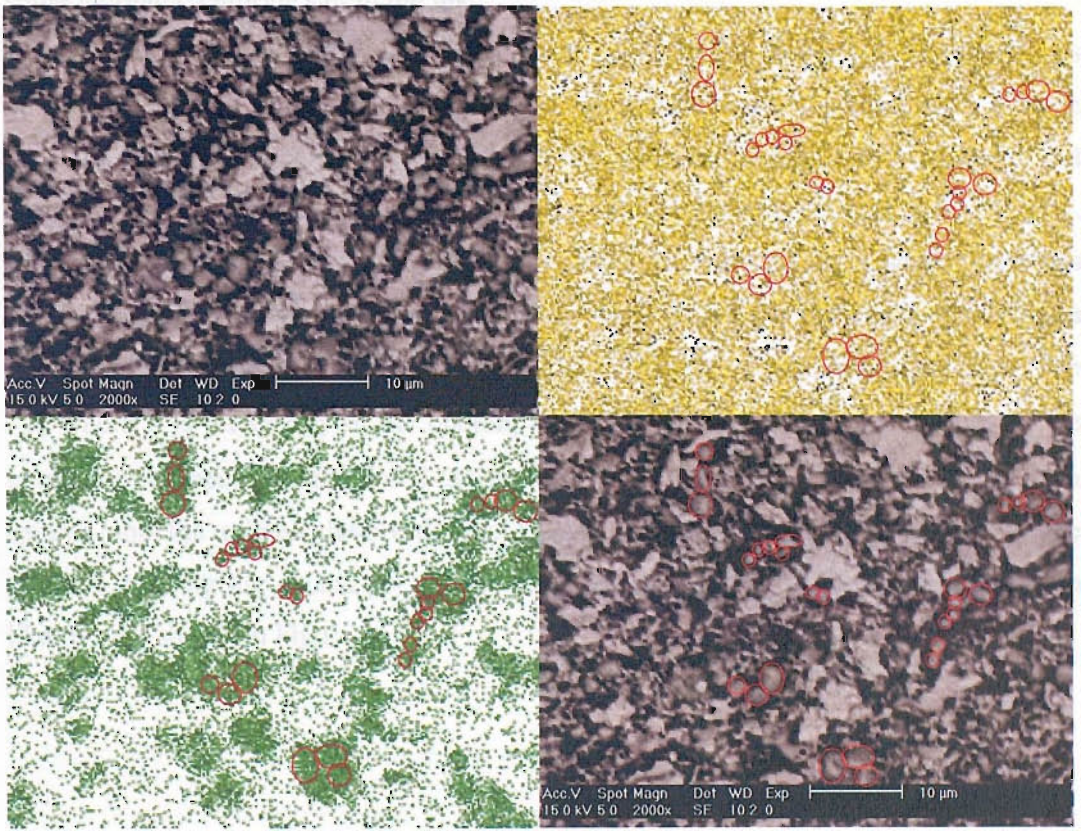

Figure 14: X-ray analysis of a thin layer of Ag/AgCl ink dried on a carbon disk. Top left and bottom right, micrograph of the area analysed. Top right and bottom left are EDAX figures showing the distribution of silver (yellow dots) and the distribution of chlorine (green dots) in the same area. For clarity, the same areas in the micrographs and in the EDAX figures are marked with red circles.

This micrograph (Figure 14) shows the distribution of silver and silver chloride in the ink. Those areas rich in chlorine in the EDAX are believed to be AgCl particles. Several of this particles were rounded with red circles, and this lay-out of circles has

been superimposed in the micrograph and in the EDAX figure for the distribution of silver, where we can see that these areas show a lower concentration of Ag. Comparing both pictures, AgCl particles are the greyish, rounded particles in the micrograph, meanwhile Ag particles appears as angular brighter particles.

The EDAX analysis of the ink showed that there are in average 4 atoms of silver for every atom of chlorine in the area analysed. Considering that all of the chlorine detected appears in the form of AgCl, there are 3 atoms of Ag for every molecule of AgCl. Apart from the chlorine present as AgCl particles, we have detected chlorine in the background. This background could be due to three different possibilities: instrumental noise, presence of any form of chlorinated organic polymer or presence of some inorganic chloride salt in the ink.

In the first case, this instrumental noise could be due to the way the analysis is performed. The sample is being irradiated with electrons accelerated with a large potential (15 kV). Once these electrons interact with the sample, they will knock out electrons of the inner shell of the atoms in the sample, creating an electronic vacancy. Electrons from outer shells (large energy orbitals) drop into the inner shells vacancies (low energy orbitals), and the energy difference between the two orbitals is released as a photon, with an energy (or wavelength considering Planck's equation $E = h\nu$, or $E = h\,c\,/\,\lambda$, where E is the energy of the photon; h, Planck's constant; ν, the frequency of the photon; c the speed of light, and λ the wavelength of the radiation) specific to the atom excited and the orbitals involved. The EDAX detector measures the energy of the photons, plotting the counts per second (cps) registered at each energy in a spectrum like the one shown in Figure 15.

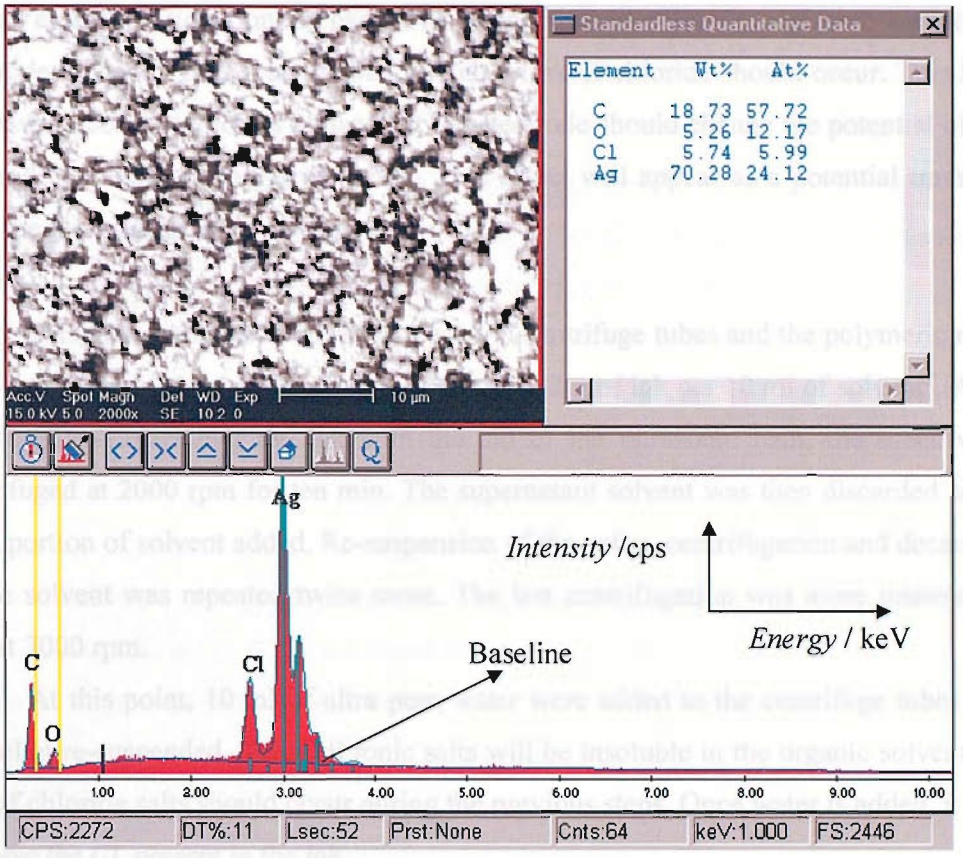

Figure 15: X-ray analysis of a thin layer of Ag/AgCl ink. From left to right and top to bottom: 1.-micrograph of the zone scanned (magnification 2000x, approximate size 58 x 46 µm); 2.-quantitative analysis of the area scanned; 3.- X-ray spectrum of the same area.

The X-ray mapping is performed by exciting a part of the sample and analysing the energy of the photons emitted from that area. If the energy of these photons is between certain pre-assigned values for every element, the software concludes that an atom of that particular element is present at that spot. In the spectrum we can see that there is a background in addition to the expected peaks. Since in the mapping mode, the instrument does not correct for this baseline, we can expect a background in the X-ray mapping.

3.1.1. Chloride contents of the ink

Determining if the ink contains any form of soluble chloride is important to understand the performance of the Ag/AgCl electrode. In the case that the ink contains soluble chloride, once the electrode is dipped in the solution, the sample solution will dissolve this chloride, increasing locally the concentration of chloride at the electrode, thus altering the potential of the reference electrode to more negative values through the

Nernst equation (Equation 6, page 21). Since the concentration of chloride at the electrode will be higher than the bulk value, a flux of chloride should occur. This later decrease of concentration of chloride at the electrode should change the potential of the electrode towards less negative values. This effect will appear as a potential transient once the electrode is placed in solution.

Weighed amounts of ink were placed in centrifuge tubes and the polymeric resin dissolved with toluene or acetone (approximately 2 g of ink per 10 ml of solvent). After dissolving/re-suspending the ink with the aid of the ultrasonic bath, the tubes were centrifuged at 2000 rpm for ten min. The supernatant solvent was then discarded and a fresh portion of solvent added. Re-suspension of the pellet, centrifugation and decanting of the solvent was repeated twice more. The last centrifugation was more intense, 15 min at 3000 rpm.

At this point, 10 ml of ultra pure water were added to the centrifuge tubes and the pellet re-suspended. Since all ionic salts will be insoluble in the organic solvent, no loss of chloride salts should occur during the previous steps. Once water is added, it will dissolve the Cl^- present in the ink.

The aqueous supernatant was then transferred to an electrochemical cell and the open circuit potential of a MediSense's SPE against SMSE was recorded. This open circuit potential can be related to the activity of chloride through the Nernst equation (Equation 6, page 21) as simplified in Equation 10[vii]:

$$E = 0.2223 - 0.0592 \log a_{Cl^-} \qquad \text{Equation 10}$$

The potential is proportional to the activity of chloride, until it reaches a plateau at low a_{Cl^-} characterised by the re-dissolution of AgCl to $Ag^+ + Cl^-$.

[vii] In this experiment, MediSense's Ag/AgCl SPE has been used as an ion selective electrode. We have to assume that the behaviour of the SPE follows the Nernst equation. This statement was previously demonstrated and will be presented in section 3.5, page 71. In addition, soluble Cl^- from the ink of this electrode could interfere with the analysis of the Cl^- of the ink. To avoid this, the SPE was dipped in a 0.03 M KCl solution for one hour to attain full equilibration of the electrode, and also to dissolve any soluble Cl^- in the electrode. The SPE was rinsed with ultra pure water before the analysis.

In the extreme case when the concentration of chloride tends to zero, some AgCl should be dissolved in order to maintain the solubility product equilibrium. In this case, the activity of Cl^- and Ag^+ will be the same and equal to the square root of the solubility product (K_s = 1.77 x 10^{-10} M^2)[93], so the activity of Cl^- will be 13.3 μM. The theoretical potential of the plateau will be 510 mV *vs.* SHE (-129.2 mV *vs.* SMSE); this value is adopted as the theoretical detection limit for the quantification of Cl^- using a Ag/AgCl electrode[121].

At low concentrations of Cl^-, the potential of the ion selective electrode will depend on the activity of the total Cl^- present in solution, *i.e.* the chloride present in the sample and that dissolved from the Ag/AgCl electrode to comply with the solubility product.

Considering that at very low concentrations of chloride, the activity coefficient equals 1, and thus a_{Cl^-},= [Cl^-], we found that the response obtained when a commercial SPE was dipped in the aqueous supernatant (-155 ± 5 mV *vs.* SMSE for n = 4) represents a net concentration of Cl^- in the solution between 24 and 40 μM. This calculation was made taking into account the amount of Cl^- redissolved from AgCl in the SPE (for a more complete explanation of this calculation, see section 3.5, page 71). In other words, this amount means that there is between 24 and 40 μM extra soluble Cl^- over and above that coming from AgCl dissolution. This concentration of chloride in the supernatant represents an amount of chloride ions dissolved from the ink equivalent to 5.5 ± 1.0[viii] μg Cl^- per gram of ink (n = 4).

Additional experiments were performed adding ink to a solution of known Cl^- concentration, monitoring the variation of the concentration of Cl^- through the variation of the potential (section 4.6, page 106). These additional experiments showed that the ink adsorbs a small amount of chloride (38 μg Cl^- per gram of ink).

Putting these values in perspective, the amount of Cl^- released by the ink is negligible, and represents less than 0.00055 % of the SPE, or considering an average of 0.3 mg of ink per electrode, it represents 46 pmol of soluble Cl^- per SPE.

This experiment shows that the ink does not contain any significant form of soluble Cl^-, so the chloride detected in the X-ray mapping comes either from AgCl particles, from a chlorinated polymer or from instrumental background.

[viii] $\bar{x} \pm \sigma_{n-1}$

3.1.2. Ag/AgCl ratio

Data with a large scatter appear in MediSense's reports for the ratio of Ag to AgCl, as well as for the total contents of both species in the commercial ink. Table 1 shows the data obtained by MediSense using different techniques[122].

Values are percentages in weight	Information from DuPont plc.	PIXE elemental analysis of wet ink	SEM/EDAX of final SPE	XPS of final SPE	TGA of wet ink
Ag	51.04[ix]	69	79.7	45.8	-
Cl	6.08[x]	3.6	2	4.7	-
AgCl	27.48	14.54[xi]	8.08[xi]	18.98[xi]	-
Solids (Ag+AgCl)	78.5	72.6	81.7	50.5	78
Ratio Ag/AgCl	1.85 / 1	3.99 / 1	9.12 / 1	1.66 / 1	-
Molar ratio Ag/AgCl	2.46 / 1	5.31 / 1	12.11 / 1	2.21 / 1	

Table 1 Contents of Ag and AgCl in DuPont's ink reported by MediSense[122], using different techniques. Underlined, values not measured, but extrapolated from other data.

None of the three techniques is capable of giving an approximate ratio similar to that stated by DuPont plc. The only good agreement is the total contents of solids obtained from TGA (remaining weight after evaporation of solvents, and calcination of organics). This large scattering of the data with respect to DuPont's values could be summarised as follows:

- PIXE gives a large proportion of Ag in the sample (58.1%, without considering the Ag from AgCl particles), and a very low content of Cl. This yields a very large Ag to AgCl ratio. PIXE (Particle Induced X-ray Emission) is a technique similar to EDAX in the sense that it detects the X-rays formed when the sample is bombarded with high energy particles; in PIXE this bombardment is done with charged particles (usually protons)[123], meanwhile

[ix] This value is the value of the content of Ag, without considering that Ag forming part of AgCl. The total content of Ag is calculated as 51.04 + 27.48 - 6.08 = 72.44 % wt

[x] The amount of Cl has been directly calculated from the contents of AgCl

[xi] The amount of AgCl has been calculated assuming that all Cl detected comes from AgCl

in EDAX, these particles are electrons. PIXE shows a better sensitivity than EDAX due to the fact that the background is smaller. Since the particles used in PIXE are larger than electrons, they penetrate less deeply into the sample, generating less Bremsstrahlung background (when electrons collide with a target and suffer very large decelerations, the X-rays emitted constitute the continuous X-ray Bremsstrahlung background). Since the charged particles are bigger than in EDAX, the particles cannot penetrate more than a few nanometers inside the sample, thus this technique gives only information of the surface of the sample. In this case, the value obtained by PIXE could be representative only of the very superficial layer of the sample. Considering that PIXE is a surface technique, it is not well understood why MediSense performed such an analysis on a raw material.

- SEM/EDAX gives a very low content of Cl. The content of Ag (73.6 %, without considering the Ag atoms from AgCl) is very large compared to that given by DuPont. We have to consider that since the analysis has been made on cured ink, the solvents have been evaporated; hence the amount of solids has been concentrated. This concentration of the solids should not have affected the Ag to AgCl ratio, but it can be seen in the table that this ratio increased from 1.85 to almost 9.12 to 1. The values are not consistent with what we know from the manufacturer. The only possible explanation (apart from an analytical error) is that there could be an uneven redistribution of the particles in the ink at the moment of the printing or during the curing. The SEM electrons do not penetrate the whole 30 μm of the ink, but only the topmost 1μm[xii], so it is possible that the ink is richer in Ag than in AgCl in the topmost part of the Ag / AgCl layer, and consequently, richer in AgCl in the bottom part.

  Our SEM analysis of cured ink (Figure 15, page 49) yielded a Ag / AgCl molar ratio of ~ 3, that is a weight ratio of 2.26, more similar to DuPont's values, possibly indicating that the distribution of Ag and AgCl is more even in the layer analysed. That analysis was made by spreading a thin layer of ink (thinner than the layer in the SPE; 30 μm) on a carbon substrate, so the

[xii] This calculation has been made considering several data obtained in different sections of this thesis, and appears compiled in the appendix 8.1.

X-rays comes from a more representative layer of sample, with potentially less segregation of Ag/AgCl particles within the analysed layer.

- XPS data showed a very low amount of solids, 50.5 %. XPS analyses the very top layer of the printed and cured ink (typically from a few atom layers to 3 nm[123]). In this case, the analysed layer is rich in polymer, and poor in solids. The proportion of Ag to AgCl is similar to that on the wet ink, with slightly more AgCl than in the wet ink. The amount of material analysed with XPS (0.5 to 3 nm) is very small compared with the size of the Ag or AgCl particles (~5 μm), so inferring spatial distribution of Ag or AgCl particles from this data is quite adventurous. XPS differs from EDAX and PIXE in the way the information is extracted. In this case, XPS, photons are used to ionise the sample (usually low energy X-rays), and the energy of the ejected electron is analysed. The X-rays knock out electrons from the inner shell of the atoms of the sample. These electrons leave the sample with an energy $E = h\nu - E_1 - \phi$, where $h\nu$ is the energy of the incident photon, E_1 the electron binding energy and ϕ the work function of the specimen. Measuring this energy, and knowing the energy of the incident photoelectron, the electron binding energy can be obtained[123]. This energy is specific of the atom analysed and its chemical state. Since only the electrons from atoms in the very topmost layer can effectively leave the sample, the information obtained with this technique comes from a very thin layer of sample (a few nanometers).

None of the three analyses of the ink (PIXE, EDAX or XPS) gives plausible evidence of the composition of the ink. The biggest drawback of the three techniques is their spatial sensitivity, analysing very discrete amounts of sample, probably not representative of the whole sample. Furthermore, there is no certainty of how deep into the sample these techniques analyse. The reference layer of the SPE is around 30 μm thick; EDAX analyses only the topmost 1 μm, meanwhile XPS and PIXE analyse only a few nm of its surface.

Another point is that PIXE requires high vacuum, so analysing the "wet ink" present additional drawbacks. Under evacuation, the decrease in pressure in the chamber will increase the volatility of the solvents, thus altering the sample. The structure and distribution of this sample could hardly be similar to that of the SPE, since the curing of the ink took place in a very different way.

In all three cases, the contents of the ink are not well defined, so we carried out our own analysis. Four aliquots of around 1 gram of DuPont's Ag / AgCl ink were placed in a centrifuge tube. This ink was dispersed in 10 ml of cyclohexanone with the help of an ultrasonic bath. The solids of the ink were then precipitated by gravity in a centrifuge (15 min at 3000 rpm), and the supernatant (solvents and polymers of the ink), discarded. This washing and centrifuging was repeated three more times, twice with cyclohexanone and the last one with pure water, to dissolve any possible salts in the ink.

At this moment, we had isolated the silver and silver chloride particles of the ink. Adding 6 N HNO_3 to the centrifuge tubes will dissolve the Ag as Ag^+, leaving the AgCl particles intact[xiii]. This AgCl suspension in $AgNO_3$ was filtered (on a pre-weighted Whatman N°1 filter paper), washed with H_2O, and the solids (AgCl) weighed after dissication (overnight at 80 °C plus 3 h at 140 °C)[124].

The quantification of Ag from the acidic Ag^+ NO_3^- solution was made using the Volhard method[124]. The titration was made adding 1 ml of a ferric indicator - $Fe(NH_4)(SO_4)_{2\ sat}$ in diluted nitric acid – and titrated with previously standarised NaSCN.

Under these conditions, the SCN^- precipitates the Ag^+ in the solution. Once a little excess of SCN^- is added, the thiocyanate will complex the Fe(III) changing the colour of the solution from milky white to reddish-brown, and thus indicating the end point of the titration.

From these two methods (volumetric titration of Ag^+ from the Ag particles, and gravimetric analysis of the AgCl not dissolved) repeated for four different samples of Ag/AgCl ink of the same batch, we found that the ink contains:

Ag 49.6 ± 1.8 % in weight

AgCl 25.6 ± 0.8 % in weight

These values give a ratio Ag / AgCl of 1.94 / 1 in weight and an atomic ratio of 2.58 / 1. These values of AgCl and Ag contents are slightly smaller than those reported by DuPont, but they are in good agreement. The ratio Ag to AgCl is slightly larger than that reported.

[xiii] This acidic solution was left overnight (in the dark) to remove any NO_2 in solution that could interfere with the following quantification of Ag^+.

3.1.3. Solvents

IR and Mass Spectroscopy performed by MediSense[125] showed that the polymeric matrix is acrylic, comprising a dual solvent, dual polymer system. The solvents consist of petroleum distillates and dipropylene glycol methyl ethers, and the polymer is a copolymer of methyl methacrylate and butyl acrylate. No evidence of any chlorinated polymers was found, so the chloride background present in the EDAX pictures (figures 14 and 15) probably comes from background noise in the detector.

3.2. Sectioning and X-ray mapping of screen printed electrodes.

As a result of the manufacturing process, it is possible that the Ag and AgCl particles are unevenly distributed throughout the layer of ink. In the process of drying the ink, smaller particles could settle (AgCl particles are smaller than Ag ones). This process is known as the "Brazilian nut effect". Particles of different shapes immersed in a liquid could, under shaking, segregate; larger particles rise to the top even if there is no density difference with the other components. Size segregation is linked to convective flow inside shaken grain containers; during shaking small particles may occasionally fill the voids generated below the larger particles producing the net effect of their upward motion[126].

In our case, we have to consider that the Ag and AgCl particles are of very different shape as we have already seen in figures 10 and 11. The particles are not shaken, but instead, they are squeezed through the printing mesh, and this mechanical stress could segregate the particles.

If this is the case, then there could be a larger ratio of Ag on the surface and a larger ratio of AgCl on the interior of the printed ink. This uneven distribution of the particles in the screen printed electrode will affect the performance of the electrode, especially when we consider that the position of the electrode-solution interface will change during the wetting of the electrode.

Due to the soft character of the Ag/AgCl printed ink, sectioning of the sample (for the commercial screen printed electrode) could not be performed directly. Prior to sectioning, the SPE were embedded in an impregnation epoxy resin (Epofix Kit, Struers) and left to cure overnight. To achieve good impregnation and avoid the formation of

bubbles, the resin was heated at 40 °C, to reduce its viscosity. Once the resin was cured, the samples were extracted from the mould and sectioned using a Buhler precision saw. The sections were then placed vertically in the microscope chamber, with the surface perpendicular to the electron beam. X-ray mapping of the section was performed to record the distribution of carbon, silver and chloride. This technique shows, first of all, the distribution of the layers that compose the screen printed Ag/AgCl electrode.

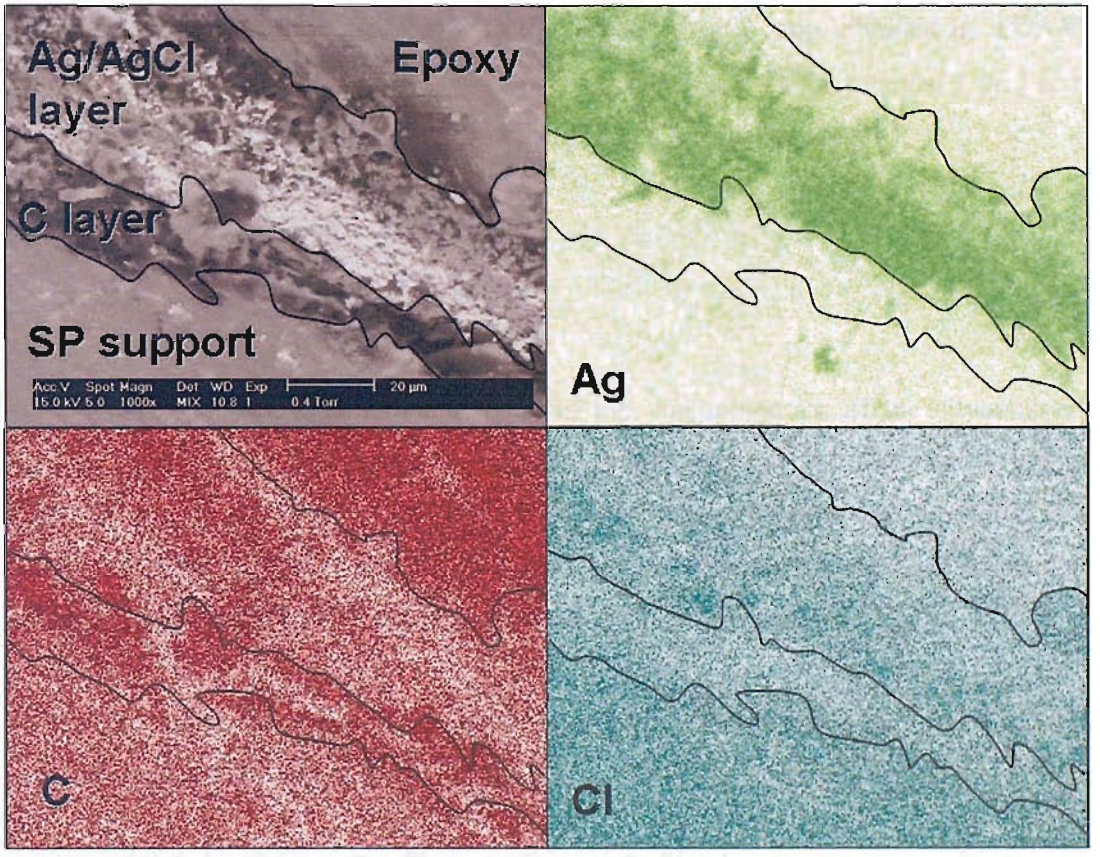

Figure 16 X-ray mapping of a cross section of a Ag/AgCl SPE embedded in epoxy resin.

From these images, we can draw several conclusions:

1. The white layer that supports the electrode has a large concentration of chloride suggesting that this support consists on a chlorinated polymer, i.e. PVC (polyvinylchloride). This layer has a lower density of carbon atoms than the epoxy layer, signifying that the epoxy is denser than the PVC.
2. Between the PVC tab and the epoxy layer, two different zones can be seen. The bottom one is rich in carbon and low in chlorine. This layer is the graphite track printed under the Ag/AgCl layer to promote the

adhesion of the Ag/AgCl layer to the PVC support. The Ag/AgCl electrode is printed over it and shows up as rich in silver and chlorine.

3. In the Ag/AgCl ink part, the chlorine appears more concentrated in the bottom of the layer. This suggests that Ag and AgCl particles are not evenly distributed, but rather that the AgCl particles tend to accumulate in the bottom of the printed layer. In this case, the outer part of the electrode will be richer than the interior in Ag.

These results are consistent with the large Ag/AgCl ratio obtained by EDAX analysis of dried electrodes. EDAX gives only information from the topmost 1 μm, and from the X-ray mapping, it is evident that there is less AgCl in this part.

3.3. Exchange current

One of the most important regions of the voltammogram of the silver/silver chloride couple is the region around the open circuit potential. We have said that the silver/silver chloride electrode should be capable of passing current with the minimum possible change in the potential, that is, the electrode should have a large exchange current. The electrode should be ideally reversible and non polarizable[86].

The electrochemistry of the reference couple should be fast, and current should increase sharply with a small overpotential.

$$i = i_0 \left[\frac{c_R(0,t)}{c_R^*} e^{\frac{(1-\alpha)nF\eta}{RT}} - \frac{c_O(0,t)}{c_O^*} e^{\frac{-\alpha nF\eta}{RT}} \right] \qquad \text{Equation 11}$$

The relationship between i and E is shown in Equation 11, and it is known as the *current-overpotential* equation[89] or the Butler-Volmer equation. Where i_0 is the exchange current, c_O^* and c_R^* are the original concentration of the oxidised and reduced species in the bulk solution respectively, $C_O(0,t)$ and $C_R(0,t)$ are the concentration of the oxidised and reduced species at time t and at a distance 0 from the electrode (*i.e.* at the electrode surface), α is the transfer coefficient, that is a symmetry coefficient between 0 and 1 that gives an indication of how sensitive the reduction reaction is to changes in the overpotential. A coefficient of 0.5 indicates that both reactions (oxidation and reduction) are equally sensitive.

The two terms inside the brackets in Equation 11 account for the forward and backward reactions. The first exponential is the current obtained from the oxidation reaction; meanwhile, the second term is the current of the reduction reaction. In this equation it can be seen that the larger the exchange current (i_0), the larger the current a system will be able to pass at the same overpotential. i_0 is related with the kinetics of the electrochemical reaction and the area of the electrode through:

$$i_0 = nFAk^0 c_O^{*(1-\alpha)} c_R^{*\alpha} \qquad \text{Equation 12}$$

where k^0 is the standard rate constant and A, the area of the electrode.

A very useful way of analysing η - i data is by plotting the logarithm of the current against the overpotential under certain experimental conditions (a Tafel plot), ensuring that the experiment is done under conditions where the current is not mass transfer controlled. In this case, the concentrations of species at the electrode will be the same as in the bulk, so the equation can be reduced to:

$$i/i_0 = e^{\frac{(1-\alpha)nF\eta}{RT}} - e^{\frac{-\alpha nF\eta}{RT}} \qquad \text{Equation 13}$$

In addition, at large overpotentials, one or the other of the exponential terms will be significantly bigger than the other one, showing that only one part of the reaction (the oxidation or the reduction) is responsible for the current passing. Equation 13 can then be reduced even further to give:

$$|i| = i_0 \, e^{\frac{-\alpha nF\eta}{RT}} \quad \text{reduction}(\eta << 0)$$
$$|i| = i_0 \, e^{\frac{(1-\alpha)nF\eta}{RT}} \quad \text{oxidation}(\eta >> 0) \qquad \text{Equation 14}$$

A representation of the log $|i|$ *vs.* η at larger overpotentials will be linear with a slope proportional to $-\alpha nF/2.3RT$ or $(1-\alpha)nF/2.3RT$ depending [xiv] whether the overpotential is large and negative (reduction) or large and positive (oxidation). The extrapolation of these lines to zero overpotential gives the logarithm of the exchange current (i_0). The Tafel plot allows us to evaluate the exchange current and transfer coefficient from simple i - η data, provided that the experiment is done without the complication of mass transfer limitations.

[xiv] 2.3 accounts for the change of the logarithm from base e to base 10 ($\log_e 10$).

To ensure that our experiments are done under conditions where mass transfer is not rate limiting, the concentration of species in the bulk (Cl^-) was very large, 2 M. This ensures that there is no significant depletion of Cl^- at the electrode surface. Additionally, the scan was performed at very low scan rate, thus ensuring that the transport of species towards the electrode is larger than the consumption.

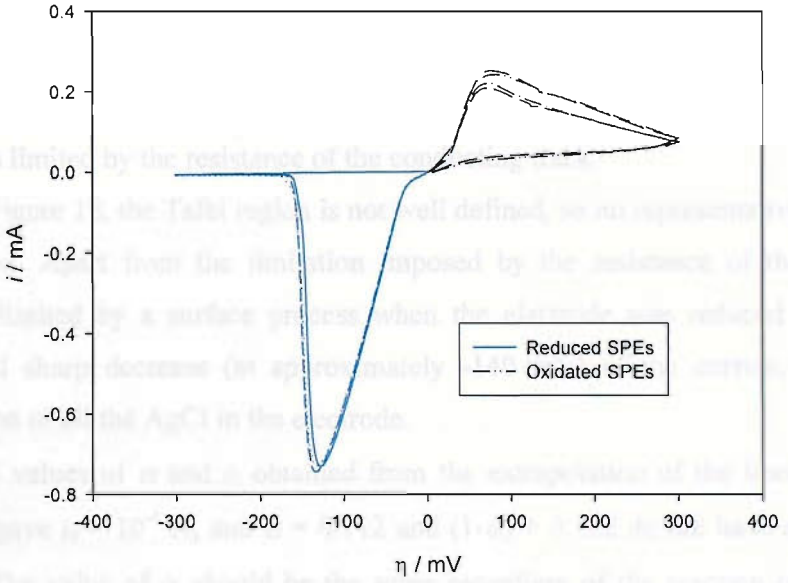

Figure 17 Cyclic voltammetry of several new SPEs. Scan started from open circuit potential. The scan was performed in 2 M KCl, scanning, with different electrodes, only to oxidation or reduction, at 1 mV/s.

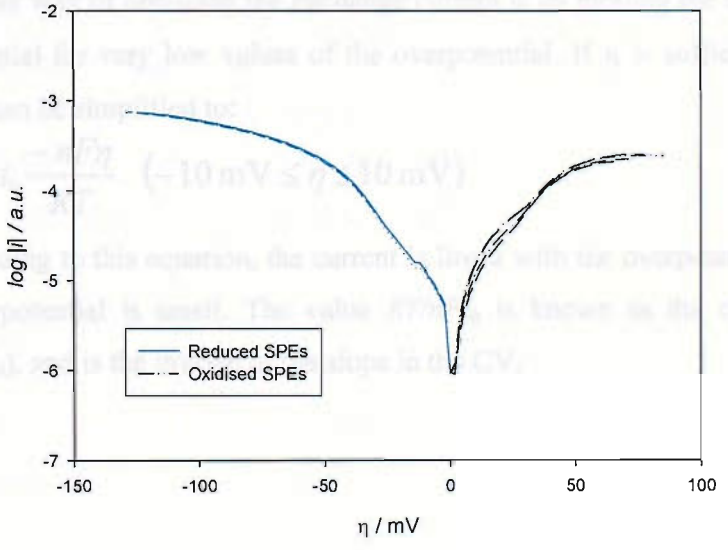

Figure 18 Tafel plots for the oxidation and reduction curves in Figure 17, the CV of several SPEs in 2 M KCl at 1 mV / s. Blue reduction; black, oxidation ones.

From these two figures (17 and 18), we can see that the data is quite reproducible between different electrodes. The rising part of both oxidation and reduction waves in Figure 17 is linear, thus indicative of a resistance limitation. What is more, the slopes are similar for both oxidation and reduction. The value of the slope (7.4 10^{-3} A V^{-1}) suggest that there is a resistance of approximately 135 Ω. The resistance measured for the conducting track of the electrode (the longest length between the connection pad and the edge of the exposed AgCl electrode) was measured with a DVM obtaining similar values - 150 Ω. This means that the electrochemistry of the Ag/AgCl electrode is limited by the resistance of the conducting track

In Figure 18, the Tafel region is not well defined, so no representative data could be extracted. Apart from the limitation imposed by the resistance of the track, the current is limited by a surface process when the electrode was reduced. There is a sudden and sharp decrease (at approximately -140 mV) of the current, due to the consumption of all the AgCl in the electrode.

The values of α and i_0 obtained from the extrapolation of the linear ranges in Figure 18 gave $i_0 \sim 10^{-4}$ A, and $\alpha = 0.112$ and $(1-\alpha) = 0.122$ do not have any physical meaning. The value of α should be the same regardless of the reaction (oxidation or reduction) chosen. What is more, α ranges normally between 0.3 and 0.7[89]. Since both reactions are equally impeded, we can consider that there is some resistance hindering the results.

Another way of obtaining the exchange current is by plotting the current against the overpotential for very low values of the overpotential. If η is sufficiently small[xv], Equation 13 can be simplified to:

$$i = i_0 \frac{-nF\eta}{RT} \quad (-10\,\text{mV} \le \eta \le 10\,\text{mV}) \qquad \text{Equation 15}$$

According to this equation, the current is linear with the overpotential, provided that the overpotential is small. The value RT/nFi_0 is known as the charge transfer resistance (R_{ct}), and is the inverse of the slope in the CV.

[xv] Euler's equation states that, for very low values of x, $e^x = 1 + x$

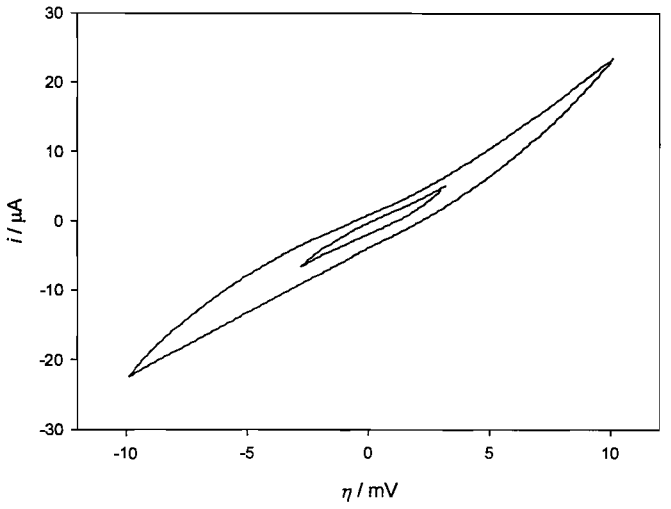

Figure 19 Cyclic voltammetry of a SPE at low scan rates (0.5 mV/s) in 2 M KCl. The scans shown are the third of a series of three scans.

From this figure, the resistance has been calculated to be 554 Ω. This resistance accounts both for the resistance of the track (135 Ω, as we have mentioned before) and the R_{ct}, so the value of the R_{ct} is 419 Ω. In this case, i_0 = 61.4 μA.

In the case of miniaturized reference electrodes, we prefer to talk about superficial exchange current density instead of exchange current density. The former is the exchange current divided by the superficial area of the electrode, meanwhile the second is the exchange current divided by the real area. The superficial current density is directly related with the amount of charge that can be transferred per superficial unit of area, and the larger this number, the smaller the electrode can be constructed that is able to pass a certain current, thus the smaller the overall device and the smaller the sample volume. Considering the superficial area of the electrode (2.69 mm^2) the superficial exchange current density is 2.28 mA cm^{-2}. This value compares unfavourably with other miniaturized reference electrodes found in the literature[127], where Lowy *et al.* report a Ag/AgCl miniaturized reference electrode with an superficial exchange current density of 4.8 mA cm^{-2}. This publication describes the use of a silver/silver chloride wire (0.25 mm in diameter) immersed in an acrylic hydrogel containing KCl inside a 10 μl micropipette tip as a reference electrode. Exchange current (density) values for screen printed electrodes were not found in the literature.

In Figure 19 we can see the small degree of irreversibility shown by the SPE. Scanning the electrode at low overpotentials gives an idea of how non-polarizable the

electrode is[90]. A perfectly non-polarizable reference electrode should exhibit the same current on the backward and forward scan, meanwhile an imperfectly non-polarizable electrode shows a small degree of hysteresis, as is the case for the SPE. This hysteresis is related with the charging of the double layer and represents the amount of charge needed to charge the double layer. The charge, as the area between the forward and backward scan, measured from Figure 19 is 0.33 mC. This charge represents a capacitance of the electrode of $C = Q/2\Delta E$ = 8.4 mF (the charge accounts both for the forward and backward scan, that is a complete charge discharge cycle, so we should divide the obtained charge by two).

This capacitance of the electrode is very large, and it is believed to be due to the high porosity of the electrode (which increases the surface area of the printed Ag/AgCl), and because of the high surface area of the carbon layer printed underneath the Ag/AgCl layer. The exact formulation of MediSense's carbon ink is proprietary, but it is composed of a 2:1 mixture of carbon black (with typical surface areas of 200 m^2/g) and graphite (10 m^2/g).

3.4. Chronoamperometry of the whole electrode

We have obtained the physical proportion of Ag and AgCl in the ink, but we are more interested in the amount that is electrochemically available. To evaluate this, fresh new Ag/AgCl screen printed electrodes were held at a fixed overpotential against a reference electrode (SCE) and the variation of the current with time was recorded. The charge passed was also recorded, and from the charge and using Faraday's law, the amounts of Ag and AgCl oxidised or reduced respectively were determined. For these experiments we used a concentrated chloride solution (2 M) to minimise the effect that the electrochemical reaction could have on the bulk concentration (the reduction of AgCl will release Cl^- to the bulk, whereas the oxidation of Ag will decrease the amount of Cl^- in the bulk through formation of AgCl).

Every experiment was carried with five electrodes taken from three different batches. Typical results are shown in Figure 20. The electrodes were previously stabilized at open circuit potential until the open circuit potential was stable within 0.1 mV for more than 30 s (typically, 3 min).

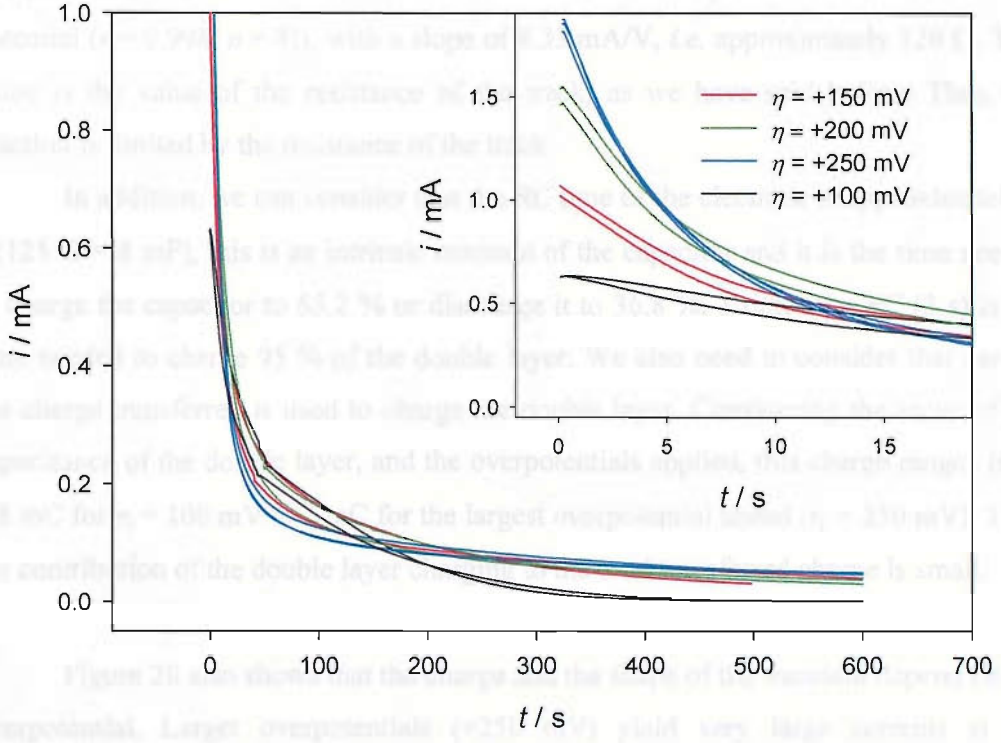

Figure 20 Chronoamperometry of several Ag / AgCl SPE in 2 M KCl at different overpotentials.

We can see in Figure 20 that a good reproducibility was achieved, with similar curves and charges for each overpotential studied. The average values of charge and RSD[1,xvi] appear in Table 2:

Overpotential / mV	Charge / mC	RSD / %	*n*
η = +100 mV	43.66	4.0	5
η = +150 mV	62.45	3.6	5
η = +200 mV	64.30	4.7	5
η = +250 mV	62.28	4.3	5

Table 2 Charges transferred when new Ag/AgCl screen printed electrodes were oxidised at several overpotentials for 600 s in 2 M KCl solution.

Several details have to be noticed in Figure 20. The first one is that once the potential is stepped, the current at the electrode rises, and this current is larger the larger the overpotential (insert in Figure 20). Plotting the initial value of the current against the

[xvi] RSD Relative standard deviation: Standard deviation divided by the average ($\sigma / \bar{x}$), given as a percentage.

overpotential, we found that there is a linear relationship of the current with the potential (r = 0.998, n = 8)), with a slope of 8.33 mA/V, *i.e.* approximately 120 Ω. This value is the value of the resistance of the track, as we have said before. Thus, the reaction is limited by the resistance of the track.

In addition, we can consider that the *RC* time of the electrode is approximately 1 s (125 Ω × 8 mF), this is an intrinsic constant of the capacitor and it is the time needed to charge the capacitor to 63.2 % or discharge it to 36.8 %. 3 times the *RC* (3 s) is the time needed to charge 95 % of the double layer. We also need to consider that part of the charge transferred is used to charge the double layer. Considering the value of the capacitance of the double layer, and the overpotentials applied, this charge ranges from 0.8 mC for η = 100 mV to 2 mC for the largest overpotential tested (η = 250 mV). Thus the contribution of the double layer charging to the total transferred charge is small.

Figure 20 also shows that the charge and the shape of the transient depend on the overpotential. Larger overpotentials (+250 mV) yield very large currents at the beginning of the experiment, but these currents decrease rapidly, even at a faster rate than transients recorded at lower overpotentials (+100 mV).

For low overpotentials (+100 mV), the current drops to zero in the time scale of the experiment (10 min), but there is a significant current passing at that time when the oxidation has been performed at larger overpotentials. For larger overpotentials, the oxidation could be carried out over longer times, obtaining larger charges. The charge passed for large overpotentials (η > 100 mV) is quite reproducible, suggesting that there is some difference when the oxidation is performed at η = 100 mV and at larger overpotentials.

The current against time plot shows an inverse potential dependence of the current with the time ($i \propto t^{-m}$), similar to the Cotrell decay (Equation 16)[89].

$$i(t) = \frac{nFAc_o^* \sqrt{D}}{\sqrt{\pi t}}$$ Equation 16

The best way of demonstrating this dependence, is by plotting the current against the $t^{-½}$, or by rearranging Equation 16:

$$\log i(t) = \log\left(\frac{nFAc_o^* \sqrt{D}}{\sqrt{\pi t}}\right) = \log\left(\frac{nFAc_o^* \sqrt{D}}{\sqrt{\pi}}\right) - \tfrac{1}{2}\log t$$

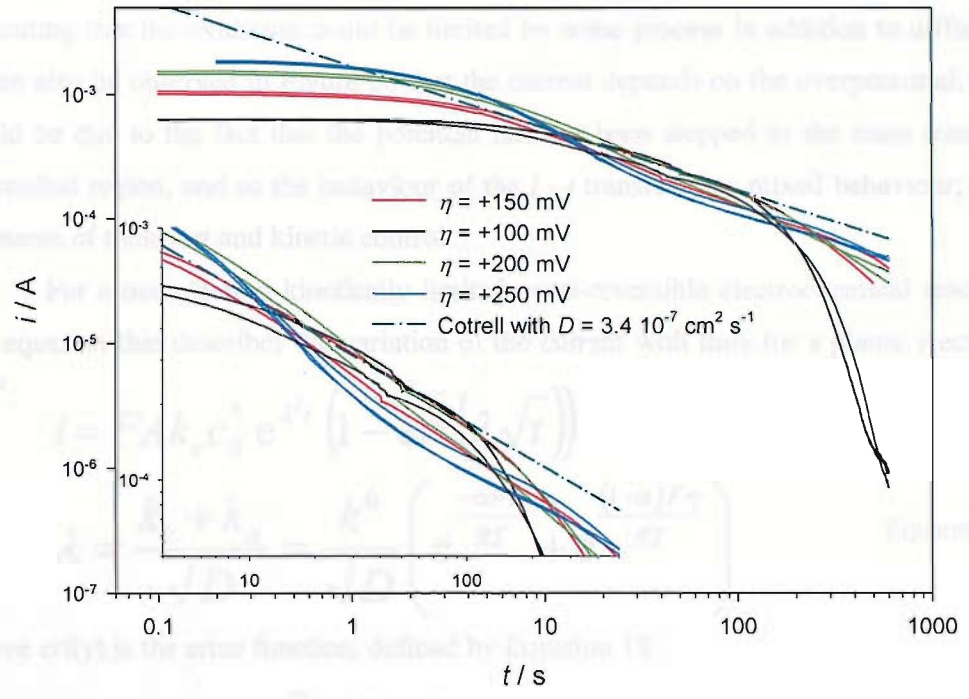

Figure 21 Chronoamperometry of several Ag / AgCl SPE in 2 M KCl at different overpotentials, plotted on a logarithmic scale. For comparison, we have included the expected behaviour of the transient of a diffusion controlled process (D = 3.4 10^{-7} cm^2 s^{-1}, A = 2.69 10^{-2} cm^2, c_0^* = 2 M).

Figure 21 shows some interesting features. The first is that at short times (t < 3-4 s), the current varies slightly with time. We have already mentioned that at these short times, the current is limited by the resistance of the track (120 Ω).

We have included in Figure 21 the expected behaviour of the transient of a diffusion controlled process. For this calculation we have used the superficial area of the electrode, the concentration of Cl^- in the solution, and we have approximated a value for the diffusion coefficient from the figure (D = 3.4 10^{-7} cm^2 s^{-1}). For small overpotentials (η = 100), the transient does not follow a Cotrell decay. The current decreases with time faster than the expected from the Cotrell equation. For the largest overpotentials tested, 250 mV, the variation of the log i with the log t is not linear. We can see that the transient features a shoulder at approximately t = 40-50 s.

For the other two overpotentials tested (150 and 200 mV), we can see that there seems to be a linear relationship between log i and log t, between 10 and 300 seconds. In this case, the slope is larger than the expected -1/2 from the Cotrell equation, indicating that the current drops faster than expected for a diffusion controlled process. The Cotrell equation can only be applied when the rate limiting step of the

electrochemical reaction is the diffusion of the redox species towards the electrode, indicating that the oxidation could be limited by some process in addition to diffusion. It can also be observed in Figure 20 that the current depends on the overpotential. This could be due to the fact that the potential has not been stepped to the mass transfer-controlled region, and so the behaviour of the *i* - *t* transient has mixed behaviour; with elements of transport and kinetic control.

For a one electron kinetically limited quasi-reversible electrochemical reaction, the equation that describes the variation of the current with time for a planar electrode is[128]:

$$i = FAk_c c_0^* \, e^{\lambda^2 t} \left(1 - \mathrm{erf}\left(\lambda\sqrt{t}\right)\right)$$

$$\lambda = \frac{k_c + k_a}{\sqrt{D}} = \frac{k^0}{\sqrt{D}}\left(e^{\frac{-\alpha F\eta}{RT}} + e^{\frac{(1-\alpha)F\eta}{RT}}\right) \qquad \text{Equation 17}$$

where erf(*y*) is the error function, defined by Equation 18:

$$\mathrm{erf}(y) = \frac{2}{\sqrt{\pi}} \int_0^y e^{-x^2} dx \qquad \text{Equation 18}$$

We can see that λ in Equation 17 depends on the overpotential applied. Considering room temperature (T = 298 K) and usual values of α (0.5), there is an increase of approximately 250% of the value of λ for every 50 mV increase in the overpotential. This in turn implies that there is a significant increase of the current expected from Equation 17 at different overpotentials. The current transients recorded in our case (figures 20 and 21) are very similar for all overpotentials over 150 mV, in opposition to what we could expect for a one electron kinetically limited quasi-reversible electrochemical reaction (Equation 17).

Therefore we can conclude that the Ag oxidation in a Cl^- medium is not limited by the kinetics of the electron transfer. At very short times (t < 3-4 s), the current is limited by the resistance of the electrode, meanwhile at longer times, the current could be limited by a diffusion process. The slope of the Cotrell plot is slightly more positive than -1/2. The current transients recorded suggest a diffusion coefficient of 3.4×10^{-7} $cm^2\ s^{-1}$. Since this diffusion coefficient is much smaller that that of Cl^- in a 2 M KCl solution (D = 1.9 10^{-5} $cm^2\ s^{-1}$)[114], we can consider that the limiting step is not the diffusion of Cl^- from the bulk solution towards the electrode, but the diffusion of chloride through the resin or through the growing AgCl layer.

It is also interesting to mention that when the SPE is oxidised at η = +100 mV, the current drops to zero on the time scale of the experiment. The charge transferred (Table 2) suggests that not all the Ag available is oxidised, but that the formation of the AgCl layer passivates the electrode. When the electrodes were oxidised at larger overpotentials, for the same amount of charge, they could still pass current.

An additional experiment was performed where the SPEs were stepped at different overpotentials, as shown in Figure 22:

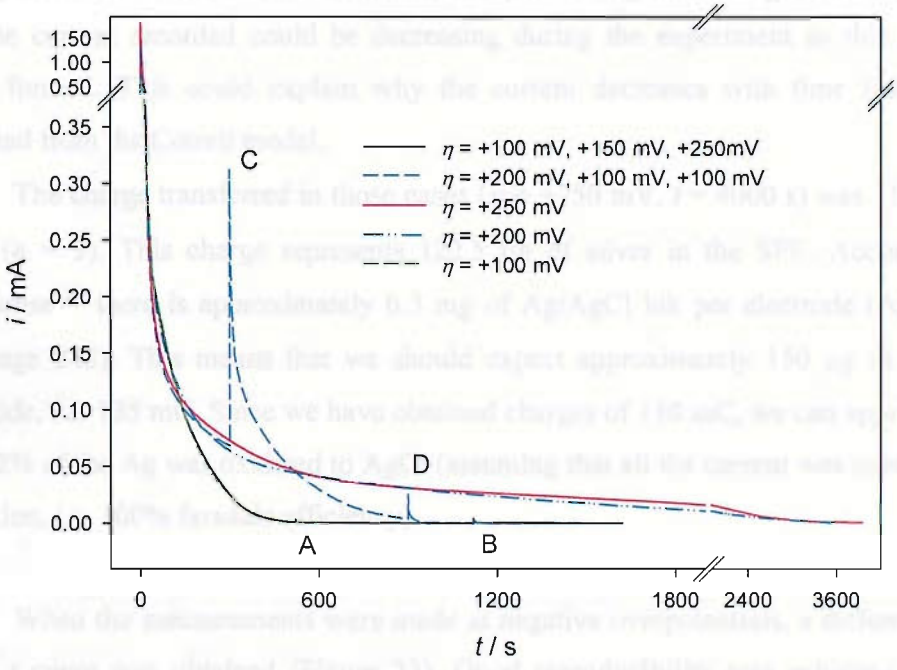

Figure 22 Current transient of several SPE in 2 M KCl poised at different η, as shown in the legend. The letters show the moment where the overpotential was changed. For clarity, the scale at long times and large currents has been shortened.

A SPE was oxidised at +100 mV until the current dropped to zero (black line). At this moment (marked with A in the figure), the overpotential was increased to +150 mV, and later (B) to +250 mV, but no further charge could be transferred, even at the larger overpotentials. In the opposite experiment (dashed blue line), an electrode was poised at an overpotential of +200 mV, until 45 mC were transferred (this is the total average charge transferred when a SPE is poised at η = +100 mV, Table 2). At this moment (C), the electrode was poised at η = +100 mV, verifying the formation of a passivation layer. This passivation layer blocked any further oxidation of the electrode, even if the overpotential was increased again to +250 mV (D).

Several authors[20, 51, 94, 99, 100] suggest that if high currents are driven through the electrode for the oxidation of Ag to AgCl, the result is a porous AgCl layer, whereas at lower current densities, a more compact film is obtained. It is evident from our experiments (Figure 20 and Figure 22), that a porous film is formed if the electrode is poised at overpotentials equal to or larger than +150 mV. At these larger overpotentials, the oxidation of the electrode gave larger oxidation charges, indicating that the oxidation could be carried on for longer times before the growing AgCl film passivates the Ag surface. In this case, the formation of a passivating film of AgCl could be slow, and the current recorded could be decreasing during the experiment as this layer is being formed. This could explain why the current decreases with time faster than expected from the Cotrell model.

The charge transferred in those cases (η = +250 mV, t = 4000 s) was 110 mC ± 4.3% (n = 3). This charge represents 122.5 μg of silver in the SPE. According to Medisense[129] there is approximately 0.3 mg of Ag/AgCl ink per electrode (Appendix 8.1, page 243). This means that we should expect approximately 150 μg of Ag per electrode, *i.e.* 135 mC. Since we have obtained charges of 110 mC, we can approximate that 82% of the Ag was oxidised to AgCl (assuming that all the current was used for the oxidation, *i.e.* 100% faradaic efficiency).

When the measurements were made at negative overpotentials, a different form of i - t curve was obtained (Figure 23). Good reproducibility was achieved for the reduction when all charges were considered. The charges transferred were similar regardless of the overpotential. The mean charge for the reductions shown here (Figure 23) was 53.6 mC, with a RSD of 3.1 % (n = 6). The value of the charge was similar to those obtained by other techniques (CV at slow scan rate) as shown in Figure 17.

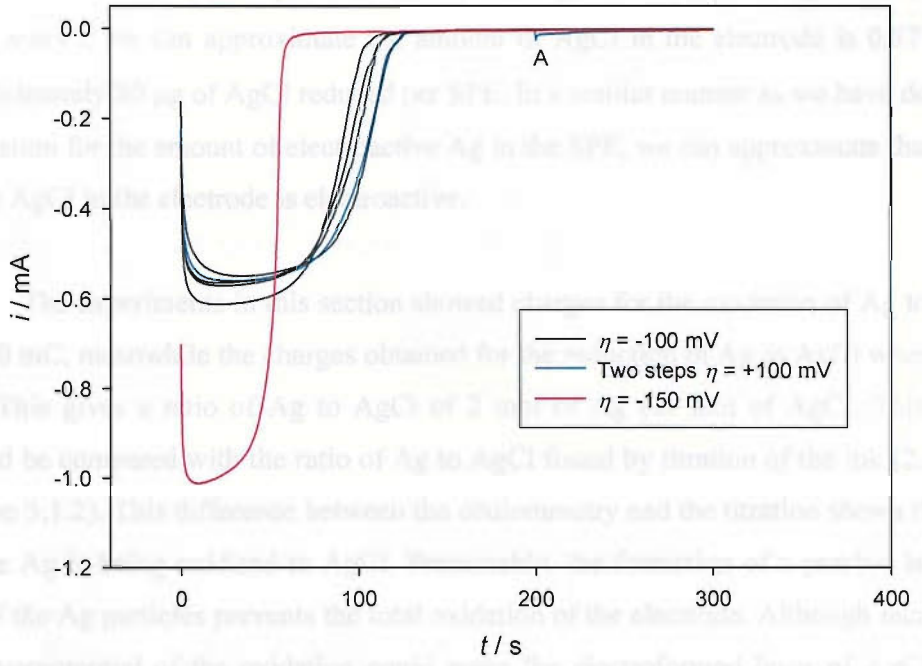

Figure 23 Chronoamperometry of six Ag / AgCl SPE in 2 M KCl at different overpotentials. The electrodes were previously stabilized at open circuit potential for 3 min. The SPE marked in blue was poised at $\eta = +100$ mV in two steps.

We can see that after 2 ~ 3 seconds following the initial transient, the current reaches a plateau, and remains at this plateau until an abrupt decrease of the current to zero. The current in this plateau is limited by the resistance of the track, as the ratio η/i is approximately constant for all the SPE tested. The value of the R ranges between 150 and 180 Ω, that is slightly larger than the resistance of the track (125 Ω, as we have obtained before).

According to this data, the reduction of AgCl is not mass transfer-controlled, so that diffusion of Cl^- from the electrode to the bulk solution is not the limiting step. Therefore we conclude that the reduction is limited by the kinetics of the reaction and the track resistance.

The sharp decrease of the current at the end of the plateau indicates that all the electroactive oxidised species (AgCl) has been reduced to Ag. The total amount of AgCl contents of the electrode could be approximated by the area under the curve in Figure 23. It is shown in the figure (blue line) that if the chronoamperometry was stopped (marked with an A in the graph), and another reduction step was performed, minute charges were recorded (usually in the range of 1 mC). These minute charges are related with the double layer charging, since $Q = C \times \eta = 0.8$ mC.

To reduce completely the electrode, we require 53.6 mC. Using Faraday's law ($Q = n \cdot m \cdot F$), we can approximate the amount of AgCl in the electrode is 0.57 μmol, approximately 80 μg of AgCl reduced per SPE. In a similar manner as we have done the estimation for the amount of electroactive Ag in the SPE, we can approximate that 98 % of the AgCl in the electrode is electroactive.

The experiments in this section showed charges for the oxidation of Ag to AgCl of 110 mC, meanwhile the charges obtained for the reduction of Ag to AgCl where 53.6 mC. This gives a ratio of Ag to AgCl of 2 mol of Ag per mol of AgCl. This value should be compared with the ratio of Ag to AgCl found by titration of the ink (2.58 : 1, section 3.1.2). This difference between the coulommetry and the titration shows that not all the Ag is being oxidised to AgCl. Presumably, the formation of a passive layer on top of the Ag particles prevents the total oxidation of the electrode. Although increasing the overpotential of the oxidation could make the electroformed layer of AgCl more porous (and thus allow more Ag to be oxidised), these pores will eventually be blocked as well, blocking any further oxidation. Since not all the Ag is being oxidised (approximately 82%), the ratio Ag to AgCl will be smaller than expected.

In the case of the Ag / AgCl electrode in operation in the glucose biosensor, we are more interested in the reduction peak, as we have already mentioned in the introduction (Figure 5). The measurement of glucose in the sensor takes less than 45 seconds. During this time, a current of between -5 and -50 μA (for normal glucose levels) will pass through the pseudo-reference electrode, so between 0.225 and 2.25 mC will be required during the measurement of glucose. This charge represents less than 5% of the amount of silver chloride available for electrochemical reduction. In contrast, the oxidation of the electrode has little importance on the overall performance of the glucose sensor.

3.5. Variation of the Open circuit potential (OCP) with chloride concentration

The open circuit potential, or equilibrium potential of the cell, is established by the two independent half-reactions (backward and forward reaction), which describe the

real chemical changes occurring at the electrode. This equilibrium potential, or open circuit potential, is the potential at which both reactions (oxidation and reduction) occur at the same rate, i.e. they have the same intensity, so the net current is zero, and hence there is no net change at the electrode. The open circuit potential of any electrode is intrinsic to the reactions occurring at the electrode, and thus gives a measure of the thermodynamics of the reactions occurring at the electrodes.

One of the most important parameters that establishes the potential of a redox electrode is the concentration (actually, the activities) of the different redox species involved in the electrode reaction. As stated earlier, the relationship between the concentration and the equilibrium potential *vs.* SHE (standard hydrogen electrode) is described by the Nernst equation (Equation 6).

Adding all the constants and considering that $T = 298$ K, Equation 6 is simplified to Equation 19.

$$E = 0.2223 - 0.0592 \log \gamma_{Cl^-} [Cl^-] \qquad \text{Equation 19}$$

From Equation 19 we can see that the potential decreases approximately 59.2 mV every 10 fold increase of the activity of chloride at 25 °C. This variation of the potential with the activity of chloride means that the Ag/AgCl reference electrode should be held in a solution with a known and stable concentration of chloride. This is done normally by keeping the reference electrode in a separate solution of a known and stable concentration (normally a saturated solution), separated from the sample with a frit or ceramic plug. In MediSense's screen printed Ag / AgCl electrode, the reference electrode is not separated from the solution, and since it is not held in a solution with a fixed concentration of chloride, its potential will depend on the activity of Cl^- in the sample (blood in this case). Values published for the concentration of Cl^- in human blood appear scattered in the literature between 98 and 130 mmol dm^{-3} [91, 104, 130]. These values give a theoretical equilibrium potential for the screen printed Ag/AgCl electrode between 285 to 278 mV *vs.* SHE (assuming that the SPE shows a Nernstian response in this range of Cl^- concentration).

To demonstrate that the equilibrium potential of the Ag / AgCl screen printed electrode follows the Nernst equation, the open circuit potential of five SPEs was recorded in solutions with increasing concentrations of potassium chloride. Potassium chloride can be used as a primary standard[1, 124]. To avoid any irreproducibility due to the hygroscopic character of the KCl, it was dried at 140 °C overnight, and kept in a dissicator. This ensures that the potassium chloride used in the solution does not contain any superficial moisture, so the solution will have an accurate concentration of chloride.

For comparison purposes, a Ag / AgCl wire was also tested. This wire is the interior part of a Ag / AgCl reference electrode, and will give a reasonable indication of the response of the Ag/AgCl system in these conditions.

To minimise any contamination effects when the electrodes were taken from one solution to the next, the following procedure was adopted:

- First, the five electrodes were stabilised in a beaker containing the solution with the lower concentration for 15 min.
- From this solution, the SPE was transferred to the electrochemical cell, were the open circuit potential of the electrode was recorded 5 min after the electrode was immersed.
- After this, the electrode was dried with tissue paper and transferred to the next, more concentrated solution.
- Another electrode was then transferred from the diluted solution to the electrochemical cell, the potential recorded, and the electrode was also dried and transferred to the more concentrated solution.
- Once all the five electrodes and the Ag / AgCl wire had been measured, the solution in the cell was changed for the next more concentrated solution, and the whole process repeated.

This procedure also ensures that each electrode is thoroughly equilibrated before measuring the potential.

In Figure 24 we have plotted the open circuit potential against the a_{Cl^-}. The activities were calculated using the procedure described in section 2.1.6. This procedure requires that the Cl^- solutions are prepared of a specific molality. To simplify the preparation of the solutions, we used molarity instead, and the molarity (mol per litre of solution) was converted to molarity (mol per kg of solvent) using the density[131] and the fact that the weight of the solution equals the weight of the solvent plus the weight of the KCl. After obtaining the molality of the solution, the activity coefficient was obtained using the Bromley equation[116]. The mean-ion activity coefficient in this molal scale was converted to the molar scale, multiplied by the molar concentration and plotted against the open circuit potential.

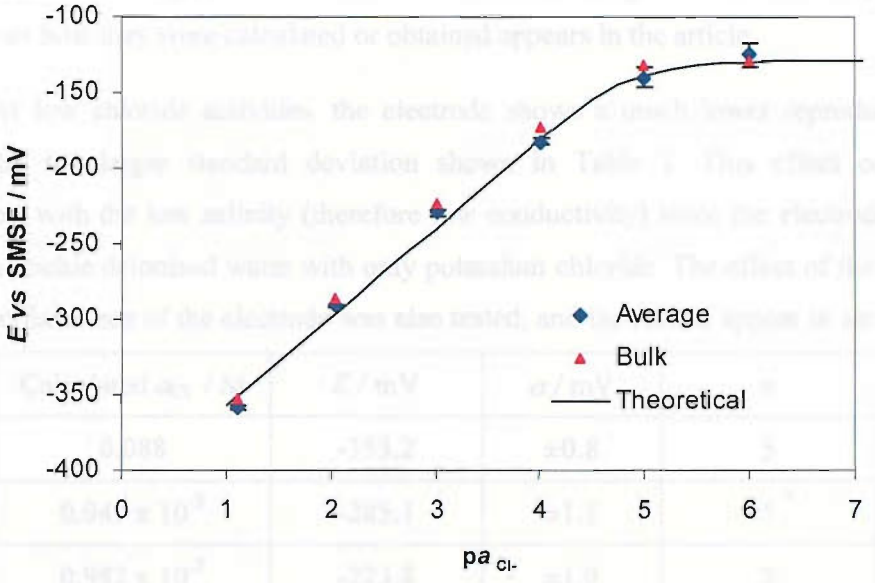

Figure 24 OCP of SPEs with different concentrations of chloride. Each concentration was tested with 5 different SPEs, and the average and the standard deviation is plotted. For comparison, the response of a bulk Ag / AgCl electrode (without internal electrolyte) was also plotted. In black, the expected values from the Nernst equation considering the redissolution of AgCl (*vide infra*).

First of all, the open circuit potential (OCP, equilibrium potential) shows a good agreement with the Nernst equation, with an increase in open circuit potential of approximately 61.6 mV per decade change of the activity of Cl^-. The equilibrium potential is linear with the logarithm of the activity of chloride from 0.1 M to 50 μM ($5x10^{-5}$ M) (E / mV = -416.3 - 61.6 log a_{Cl^-}; $r^2 = 0.995$; $n = 19$). The extrapolation to the y intercept of this line (-416.3 mV) is the open circuit potential for the system when pa_{Cl^-} equals zero, so a_{Cl^-} will be 1 M, that is, by definition, the standard potential E^0 of the Ag/AgCl redox couple. $E^0_{Ag/AgCl}$ is -417.7 mV *vs.* SMSE[93] (0.2223 V - 0.640 V, for the change of reference electrode), so our estimation from the intercept is 1.4 mV more negative than the expected value.

Our results show a similar linear range to previous results published by Lowy *et al*[91] (linear between $8x10^{-2}$ M and 10^{-5} M) for a miniaturized silver/silver chloride electrode, Alegret *et al*[20] (between 10^{-1} M and 10^{-4} M) for a screen printed Ag/AgCl electrode, but shorter than Desmond *et al.*[35] (between 1 M and 10^{-5} M) for a screen printed electrode on a Si substrate. In these three cases, the methods used to calculate the linearity were different. Lowy *et al*[91] used calculated Cl^- activities, meanwhile

Desmond used, wrongly, Cl^- molar concentrations. Alegret used activities, but no mention of how they were calculated or obtained appears in the article.

At low chloride activities, the electrode shows a much lower reproducibility, shown by the larger standard deviation shown in Table 3. This effect could be associated with the low salinity (therefore low conductivity) since the electrodes were tested in double deionised water with only potassium chloride. The effect of the salinity on the performance of the electrode was also tested, and the results appear in section 4.5.

Calculated a_{Cl^-} / M	E / mV	σ / mV	n
0.088	-353.2	±0.8	5
0.949×10^{-2}	-285.1	±1.1	5
0.982×10^{-3}	-223.8	±1.9	5
0.994×10^{-4}	-177.4	±2.2	4
0.998×10^{-5}	-134.1	±6.0	5
0.999×10^{-6}	-119.5	±7.8	3

Table 3 Standard deviation (σ) at different concentrations of chloride

For chloride activities lower than 10^{-5} M, the electrode shows non Nernstian behaviour, achieving a plateau (no change of potential with the variation of chloride concentration) at around 1 μM. The presence of a plateau for lower activities of chloride can be explained in terms of the redissolution of AgCl. The activities of Ag^+ and Cl^- are related with each other via the solubility product, ($K_S = a_{Cl^-} a_{Ag^+} = 1.77 \times 10^{-10}$ M^2)[93]. At any given activity of Cl^-, there is going to be a redissolution of AgCl to comply with this solubility product. Hence the activity of Cl^- in any given solution will be the sum of the activity of the bulk plus the amount redissolved (β). The effect that this redissolution will have on the overall activity of the Cl^- will be larger the smaller the concentration of Cl^- in the solution.

At equilibrium we can write that the activity of Cl^- will be $a^i_{Cl^-} + \beta / V$, and that the activity of Ag^+ will be β / V, where $a^i_{Cl^-}$ is the initial activity of chloride in the solution and V is the volume of the solution. As we have said, these two activities are related with each other through the solubility product, hence:

$$K_s = a_{Cl^-} \times a_{Ag^+} = \left(a^i_{Cl^-} + \frac{\beta}{V} \right) \times \frac{\beta}{V} \qquad \text{Equation 20}$$

Substituting $\beta' = \beta / V$ in Equation 20, and solving, we conclude that[xvii]:

$$\beta' = \frac{-a^{i}_{Cl^-} + \sqrt{\left(a^{i}_{Cl^-}\right)^2 + 4K_s}}{2} \qquad \text{Equation 21}$$

Substituting $a^{i}_{Cl^-} + \beta'$, the new effective concentration of Cl^- in Equation 6 we obtain the theoretical response of the open circuit potential of the Ag / AgCl electrode with respect to the $a^{i}_{Cl^-}$.

$$E = E^0 - \frac{RT}{nF}\ln\left(a^{i}_{Cl^-} + \frac{-a^{i}_{Cl^-} + \sqrt{\left(a^{i}_{Cl^-}\right)^2 + 4K_s}}{2}\right) =$$

$$= E^0 - \frac{RT}{nF}\ln\left(\frac{a^{i}_{Cl^-} + \sqrt{\left(a^{i}_{Cl^-}\right)^2 + 4K_s}}{2}\right) \qquad \text{Equation 22}$$

Equation 22 describes the potential of the electrode, and it has been plotted in Figure 24 as the theoretical response.

For values of $a^{i}_{Cl^-}$ where $a^{i}_{Cl^-} >> 4K_s$, the logarithm in the equation is simplified to ln ($a^{i}_{Cl^-}$), indicating that there is no significative contribution of Cl^- in the solution from the redissolution of AgCl. At those $a^{i}_{Cl^-}$ where ($4K_s$) is significantly bigger than $(a^{i}_{Cl^-})^2$, the equation shows that the potential becomes independent of the concentration of Cl^-.

In the extreme case when the activity of chloride tends to zero, some AgCl must dissolve in order to maintain the equilibrium. In this case, the activity of Cl^- and Ag^+ will be the same and equal to the square root of the solubility product (K_s = 1.77 x 10^{-10} M^2)[93]. Considering these activities for Ag^+ and Cl^-, we can use the Nernst equation to predict the value of the potential of the plateau. This calculated value (E = 510 mV *vs.* SHE, E = -129.2 mV *vs.* SMSE) is within the error of the measurement at low a_{Cl^-} shown in Figure 24.

[xvii] The negative root has been eliminated because it does not have any real meaning.

3.6. Variation of the OCP with the temperature

Another important factor that could affect the performance of the reference electrode is the temperature. A reference electrode uses a redox pair that is at equilibrium. The position of this equilibrium is determined by the thermodynamics of the system, and can be related to the Gibbs free energy for the reaction through[89]:

$$\Delta G^0 = -RT\ln K = -nFE^0 = \Delta H - T\Delta S \qquad \text{Equation 23}$$

From Equation 23, we can see that the equilibrium for any redox couple will change with temperature, and the potential will change with temperature.

In our case, we have to consider that at the moment of the glucose measurement, the sensor is at room temperature, while the sample (a drop of blood) is at a higher temperature, usually 36.5 °C, but will cool down quickly once placed over the SPE .In such case, there should be a variation of the temperature of the reference electrode, first an increase when the sample is placed on the electrode, followed by a decrease as both sample and electrode cools down to room temperature. The equilibrium potential will fluctuate accordingly. The variation of the potential of standard reference electrodes is well known and can be found tabulated in the bibliography. Data was also found in the literature for a screen printed electrode[98]. In that publication, they report a decrease of 0.260 mV per °C.

The effect of the temperature on the open circuit potential (*vs.* SMSE) was evaluated for four different solutions (0.5 M KNO_3 with different concentrations of chloride: 10 mM, 30 mM, 100 mM, and 0.3 M), in the range between 25 and 40 °C. The average OCP of at least four new fresh electrodes has been plotted against the temperature in Figure 25.

To improve the reproducibility, the potential was recorded 2 min after immersing the electrode in the solution, and the electrodes were kept sealed at the temperature tested before the measurement. Between measurements, the reference electrode (SMSE) assembled in the Luggin capillary was kept in a test tube inside the thermostatic bath. For the measurement, the assembled SMSE was mounted on the electrochemical cell and covered with a damped cloth at that temperature.

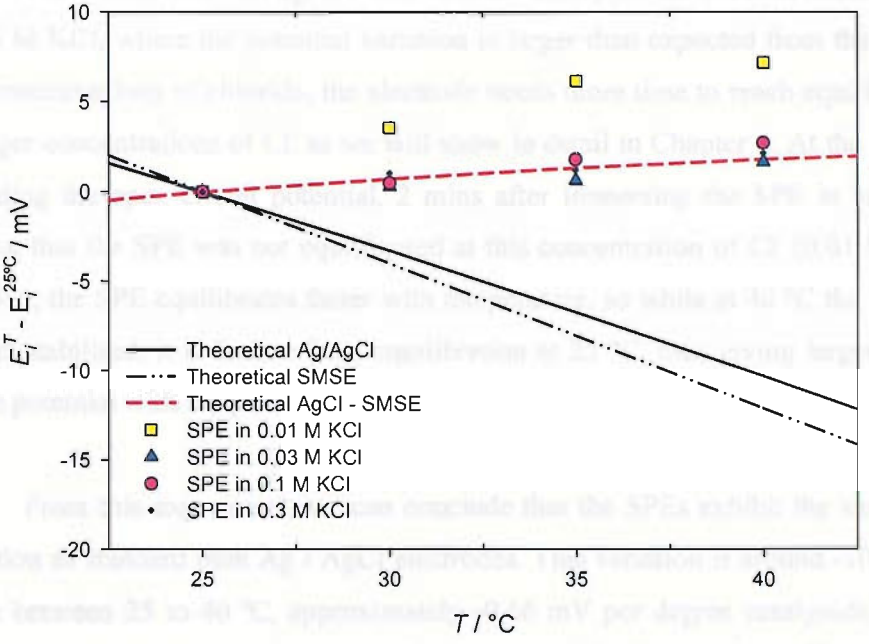

Figure 25 Variation of the OCP of Ag/AgCl screen printed electrodes with the temperature. Each measurement is the average of the OCP of at least four new, fresh screen printed electrodes in 0.5 M KNO_3 with different concentrations of KCl, at different temperatures. For comparison purposes, the potentials were normalised calculating the difference of the potential at each temperature minus the potential obtained at 25° C in each of the solutions tested.

The standard potential of a Ag/AgCl electrode varies with the temperature (in °C) as shown in Equation 24[86]

$$E^0_{Ag/AgCl} / V = 0.23659 - 485.64x10^{-6}\,T - 342.05x10^{-9}\,T^2 \quad \text{Equation 24}$$

In our case, and since the reference electrode (SMSE) is also immersed in the same solution, not thermally isolated from the cell, the potential of the SMSE will vary according to Equation 25[86].

$$E^0_{Hg/Hg_2SO_4} / V = 0.63495 - 781.44x10^{-6}\,T - 426.89x10^{-9}\,T^2 \quad \text{Equation 25}$$

For our experiment, we should expect a variation of the potential due to the thermal variation of both electrodes, the working and the reference electrode. Combining both equations, the potential measured (ΔE between the reference and the working electrode) will be:

$$E^0_{Ag/AgCl\ vs\ SMSE} / V = -0.397.60 + 243.61x10^{-6}\,T + 189.61x10^{-9}\,T^2 \quad \text{Equation 26}$$

The results obtained agreed well with the theory for all concentrations except for 0.010 M KCl, where the potential variation is larger than expected from the theory. At low concentrations of chloride, the electrode needs more time to reach equilibrium than at larger concentrations of Cl^- as we will show in detail in Chapter 4. At the moment of recording the open circuit potential, 2 mins after immersing the SPE in solution, we believe that the SPE was not equilibrated at this concentration of Cl^- (0.01 M KCl). In addition, the SPE equilibrates faster with temperature, so while at 40 °C the potential is almost stabilised, it is further from equilibration at 25 °C, thus giving larger variations of the potential with temperature.

From this experiment, we can conclude that the SPEs exhibit the same thermal variation as standard bulk Ag / AgCl electrodes. This variation is around -10 mV in the range between 25 to 40 °C, approximately -0.66 mV per degree centigrade, well over the 0.260 mV decrease per degree centigrade reported by Desmond *et al*[98].

3.7. Variation of the potential vs. time at zero current (OCP).

All the experiments that we have shown so far are based on the behaviour of the electrode at long times, once the SPE has achieved equilibrium. We have verified that this behaviour is similar to that of bulk electrodes (Nernst response of the SPE in solutions with different activity of Cl^-, variation of the potential with T).

In the case of the MediSense glucose sensor, we need to remember that the commercial screen printed counter reference electrode is packed and stored in a dry state. At the moment of use this counter reference electrode will be dipped in the sample, the electrode will be wetted, and the interface equilibrium between the electrode and the sample solution will be established. Ideally, in the biosensor, this equilibration should be as fast as possible, and once the counter-reference electrode is equilibrated, its potential should be stable, without any drift or variation during the electrochemical measurement.

The time needed to reach equilibrium is a limiting factor in the development of the glucose sensor. On one hand, we would like to perform the glucose analysis at very

short times after the drop of sample is applied on the sensor, but at the same time short analysis times mean that the sensor is not at equilibrium, so the analysis may be irreproducible. In this case, we have to find a compromise solution; the analysis is carried over at short times using a transient response, when the electrode may not yet be equilibrated.

To study the behaviour of the SPE immediately after the electrode has been placed in solution, we have monitored the open circuit potential of the screen printed Ag/AgCl electrodes from the moment the electrode is dipped in a 2 M KCl solution. This high concentration of KCl was chosen so to avoid any possible variation of the activity of Cl^- in the solution caused to the immersion of the SPE. The open circuit potential is directly related to the equilibrium potential of the Ag/AgCl system. According to the Nernst equation (Equation 27), the equilibrium potential of the Ag/AgCl system in 2 M KCl at 298 K should be:

$$E = E^0 - \frac{RT}{nF}\ln\left(\frac{a_R}{a_O}\right) = 0.2223 - \frac{8.31441 \text{ x } 298.15}{1 \text{ x } 96485}\ln\frac{\gamma_{Cl^-}[Cl^-][Ag]}{[AgCl]} \quad \text{Equation 27}$$

$$E = 0.2223 - 0.05916 \text{ x } \log(0.6617 \text{ x } 2) = 0.2151 \text{ V } vs \text{ NHE} = -26.1 \text{ mV } vs \text{ SCE}$$

where E is the potential of the cell; E^0, the standard potential of the system, in this case 0.2223 mV (*vs.* SHE)[93]; R, the gas constant; T, the temperature (298.15 K); n, number of electrons transferred; F, Faraday's constant; a_R and a_O, activities of the reduced and oxidised species respectively. These activities are equal to 1 for solids and to the molar concentration in very dilute solutions. For concentrated solutions, the molar concentration should be multiplied by the activity coefficient (γ). The mean-ion activity coefficient of a 2 M KCl solution is 0.6617. This calculation has been made in a similar way as the calculations in section 3.5 (using Equation 9, page 35).

The open circuit potential of several SPEs is shown in Figure 26. It can be seen in the figure that, at long times, a good stability and reproducibility is achieved in all cases, with variations of potential between electrodes of less than 0.2 mV.

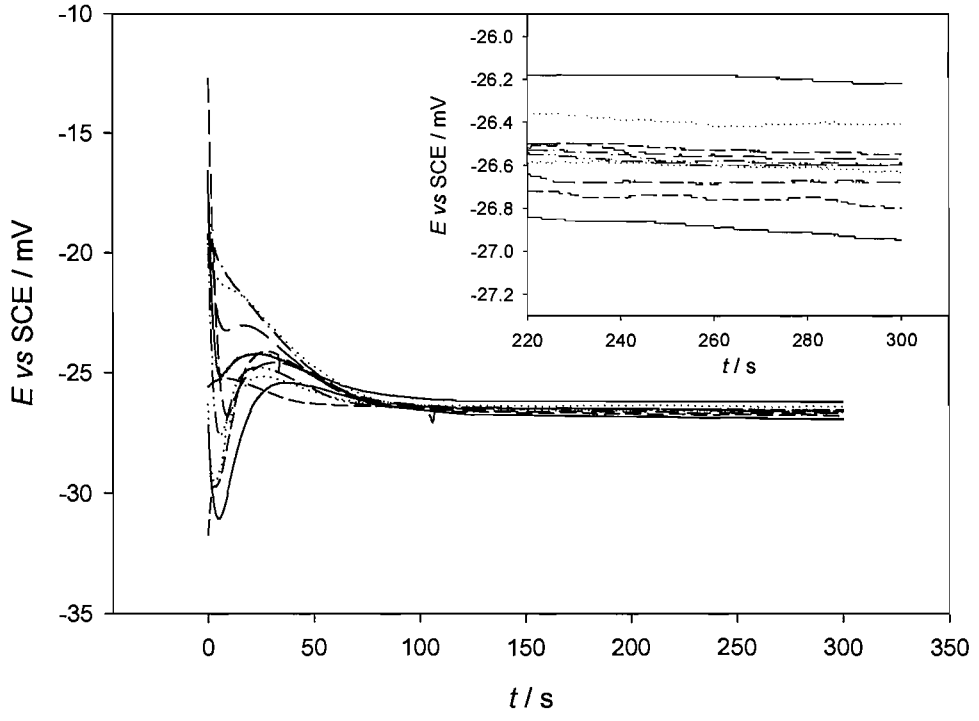

Figure 26 Variation of the open circuit potential of ten new Ag/AgCl screen printed electrodes from the moment the SPE was dipped in a 2 M KCl solution.

Notice that the electrodes behave in a very reproducible manner at long times (more than 60 s), but an important variation is recorded for shorter times. The standard deviation (σ) after the first 30 s is 0.9 mV (average -24.4 mV, n=10), meanwhile at 60 s, the σ is 0.3 mV (average -25.8 mV) and only 0.2 mV (average -26.6 mV) at the end of the experiment (after 5 min). The equilibrium potential, -26.6 mV, is 0.5 mV more negative than the expected value obtained from the Nernst equation (Equation 27). During the experiment, the potential of the electrode shifts from around -15 mV at the beginning of the experiment to -26.6 mV at the end of the measurement.

The structure of the electrode is complex. It contains silver and silver chloride particles embedded in a polymeric resin. Once the resin its cured, it presents pores, which will be filled with solution once the electrode is immersed in the solution. At the beginning of the experiment, the amount of chloride inside the pores and in the resin could be low, so less negative potentials than the values expected from the Nernst equation for the system Ag/AgCl in 2 M KCl (-26.6 mV *vs.* SCE) are recorded.

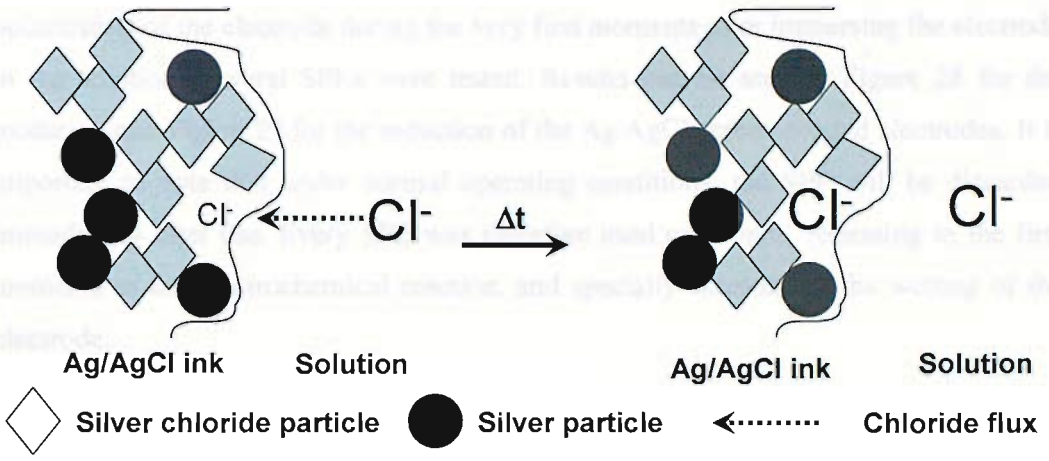

Figure 27 Schematic representation of the possible diffusion occurring once the SPE is dipped in the solution.

As soon as more chloride reaches the silver/silver chloride particles, a decrease in the potential is recorded. According to this model shown in Figure 27, the first part of the curve is controlled by the equilibration of the chloride both in the pores (at the electrode), and in the bulk; meanwhile, when these concentrations are equal, the potential of the electrode shows a stable value. The same reasoning could be proposed considering the Ag^+ in the solution. At the beginning, once the electrode is placed in the solution, some AgCl will dissolve to comply with the solubility product (K_s), so a larger concentration of Ag^+ will be present at the electrode, giving more positive overpotentials (Equation 5, page 21). The amount of Ag^+ at the electrode will decrease to match that of the bulk, shifting the potential to less positive values.

This process was studied in more detail in Chapter 4.

3.8. Chronopotentiometry of the electrode

In a similar way to the previous experiment, chronopotentiometry monitors the potential between the reference electrode (a saturated calomel electrode) and the working electrode (the SP Ag / AgCl electrode) as a function of time. In this case, a fixed current was driven through the system.

In our experiments, we placed an SPE in a 2 M KCl solution and then imposed a small oxidative or reductive current of 150 nA. This current was chosen in order to study the behaviour of the electrode near open circuit potential, and to check the

polarization of the electrode during the very first moments after immersing the electrode in the solution. Several SPEs were tested. Results can be seen in Figure 28 for the oxidation and Figure 29 for the reduction of the Ag/AgCl screen printed electrodes. It is important to note that under normal operating conditions, the SPE will be discarded immediately after use. Every SPE was therefore used only once, focussing in the first moments of the electrochemical reaction, and specially considering the wetting of the electrode.

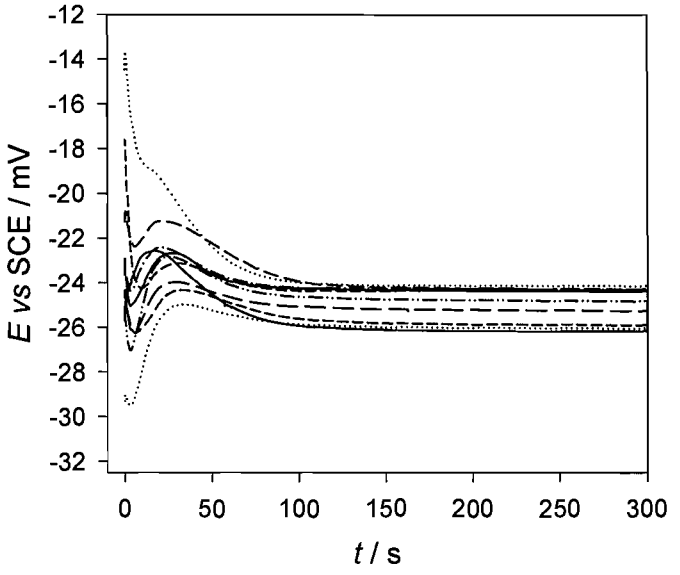

Figure 28 Chronopotentiometry of eleven screen printed electrodes at +150 nA in 2 M KCl.

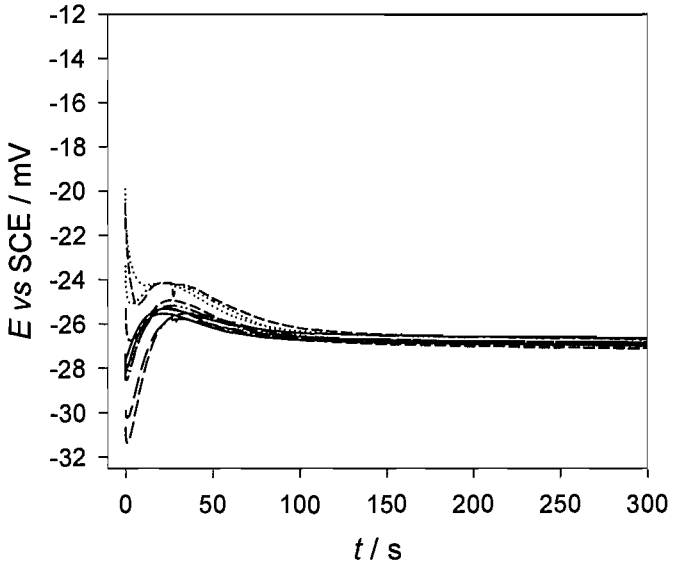

Figure 29 Chronopotentiometry of ten SPE at -150 nA in 2 M KCl.

Again, the behaviour of the SPE is very stable in both cases, and very reproducible, especially when imposing a reduction current. Once the electrodes reach steady state (after 150 s), the potential variation was lower than 0.1 mV without any appreciable drift on the time scale of the experiment. For the reduction, the σ of the final potential (at 5 min) was around 0.2 mV (n = 10), with an average value of -26.9 mV. The standard deviation of the potential value for shorter equilibration times (at 30 seconds) was 0.6 mV (n = 10 and an average of -25.1 mV).

In the case of the oxidation, the behaviour has poorer reproducibility. The average value was -24.9 mV with a standard deviation (σ) of the final potential (at 5 min) of around 0.8 mV (n = 11). The RSD of the potential value for shorter equilibration times (at 30 seconds) was 1.3 mV (n = 11, average -23.0 mV).

For the practical application of the sensor, it is important to note the reactions that are taking place in the glucose sensor (Figure 5). The screen printed Ag / AgCl acts as the reference and the counter electrode, operating as the cathode in the cell. In this case, a reduction will occur at the Ag / AgCl electrode. Hence the oxidation process is less important to us in the analytical performance of the blood glucose sensor.

We also need to consider the reproducibility at both short and long times. The behaviour of the screen printed Ag/AgCl electrodes is quite reproducible at longer times, once the system is in steady state. Much poorer reproducibility can be seen at short times. The overall device (the glucose sensor) has to work at as short a time as possible, to minimise the assay time for the patient. MediSense told us that these sensors lack reproducibility for very short times, less than 15 seconds. This is consistent with our finding here.

For the oxidation and reduction currents, the electrodes give potentials close to the equilibrium potential for Ag/AgCl vs. SCE in 2M KCl[xviii], as expected from, and demonstrated in Figure 26 (-26.6 mV *vs.* SCE). According to Equation 11, when a current is flowing through the system, a proportional increase of the overpotential should be expected. Since we are passing a current, we are away from equilibrium, and so the potential of the system will differ from the equilibration potential. The new potential should now take into account the resistance of the track and the fact that the

[xviii] Since the concentration of chloride in the bulk is very high compared to the consumption at the electrode (at +150 nA, the consumption of chloride is around 3.88 x 10^{-11} mol s^{-1} cm^{-2}) we can disregard the diffusion of chloride from the bulk, since the concentration gradient will be minute.

concentrations of species at the electrode are not the same as in the bulk. The resistance of the track means that when some current passes through the system, a proportional variation of the potential should be expected. Both effects are very weak; the variation of the potential due to the resistance of the track is negligible ($\Delta E = iR$ = 150 nA 120 Ω = 0.018 mV), meanwhile the consumption of species at the electrode is minute compared with the concentration of the bulk. It can be noted that the difference between oxidation and reduction is minimal, only about 2 mV.

In a typical blood sample, the concentration of Cl^- is much lower, between 98 and 130 mmol/L[91, 104]. The same experiment was therefore repeated at a lower Cl^- concentration (0.125 M KCl). In this case, and because the concentration of chloride in the bulk is smaller than that of previous experiment, a larger difference in the potential for the oxidation and reduction is expected. The open circuit potential was also recorded.

In a 0.125 M KCl solution, the theoretical equilibrium potential is 277.9 mV *vs.* SHE, 36.7 mV *vs.* SCE.

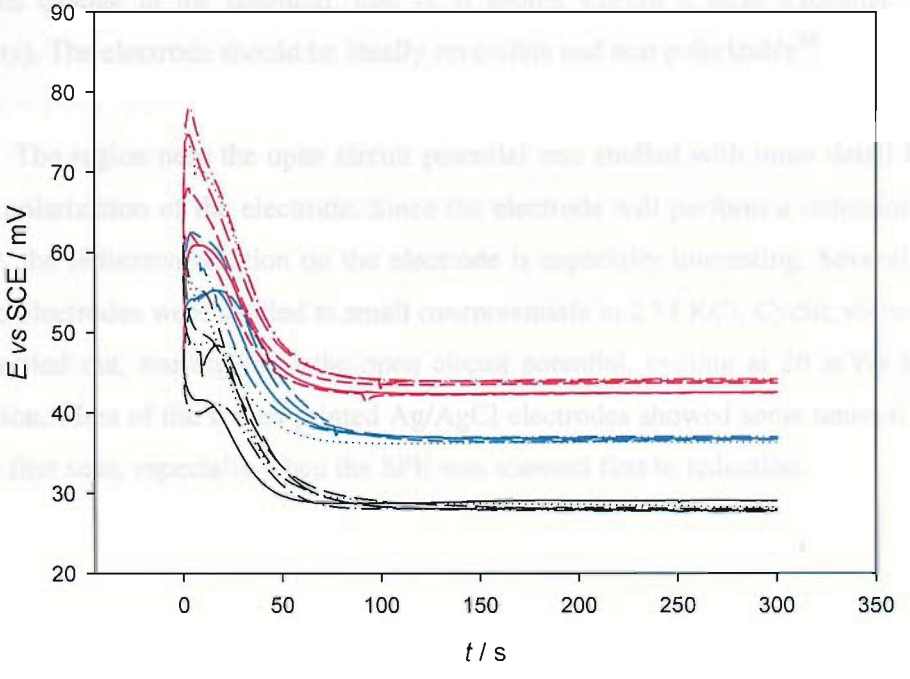

Figure 30 Chronopotentiometry of several SPEs. In red, 6 electrodes poised at +150 nA; open circuit measurement in blue (5 electrodes) and 6 electrodes poised at -150 nA, in black. All measurements were performed with new electrodes in 0.125 M KCl.

Comparing the results in 0.125 M KCl (Figure 30) with the previous ones in 2 M KCl (Figure 26, Figure 28 and Figure 29) we can see that the behaviour shows some

differences. The feature observed at the beginning of the experiment (within the first 10-15 seconds) is less evident at the former Cl^- concentration; only the electrodes reduced show the characteristic curve. On the other hand, and due to the absence or diminution of the first effect, the tendency of the potential is clearer. In addition, the potential drift is much larger in this solution (0.125 M KCl) that that recorded for the more concentrated solution (2 M KCl). As we have proposed earlier, this effect could be due to the difference in Ag^+ and Cl^- activities between the interior of the electrode and the solution (Figure 27).

3.9. Cyclic Voltammetry

One of the most important regions of the voltammogram of the silver/silver chloride couple is the region around the open circuit potential. We have said that the silver/silver chloride electrode should be capable of passing current with the minimum possible change in the potential, that is, it should exhibit a large exchange current (density). The electrode should be ideally reversible and non polarizable[86].

The region near the open circuit potential was studied with more detail looking at the polarization of the electrode. Since the electrode will perform a reduction in the sensor, the reduction reaction on the electrode is especially interesting. Several screen printed electrodes were studied at small overpotentials in 2 M KCl. Cyclic voltammetry was carried out, starting from the open circuit potential, cycling at 20 mV/s towards reduction. Most of the screen printed Ag/AgCl electrodes showed some unusual effects on the first scan, especially when the SPE was scanned first to reduction.

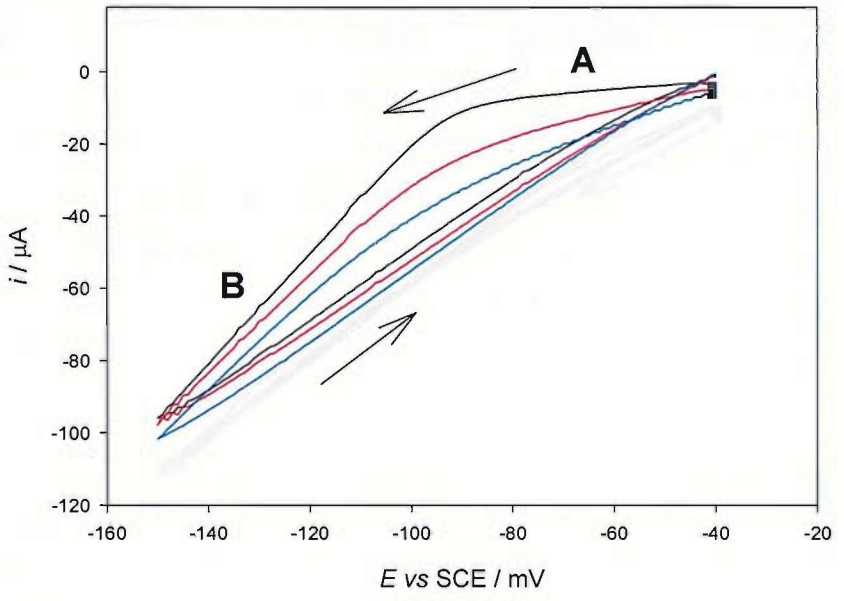

Figure 31 Typical first cyclic voltammetric scan of three different screen printed Ag/AgCl electrodes near the open circuit potential. The scans were performed at room temperature in 2 M KCl, starting at open circuit potential and scanning at 20 mV/s.

We can see in Figure 31, the electrodes exhibit two different slopes with the inflexion point appearing at approximately -0.1 V (*vs.* SCE). This effect was only seen on the first scan, and disappeared if the electrode was immersed in the solution for more than 2 min before the scan started. Different electrodes showed different CV, and typical scans are shown in Figure 31, where we can see that the region A is more pronounced in some electrodes than in others. Typical second scans are shown in Figure 32, where we can see that the effect is not present for two of the electrodes tested, meanwhile for the other one (black curve), it is less pronounced that in the first scan.

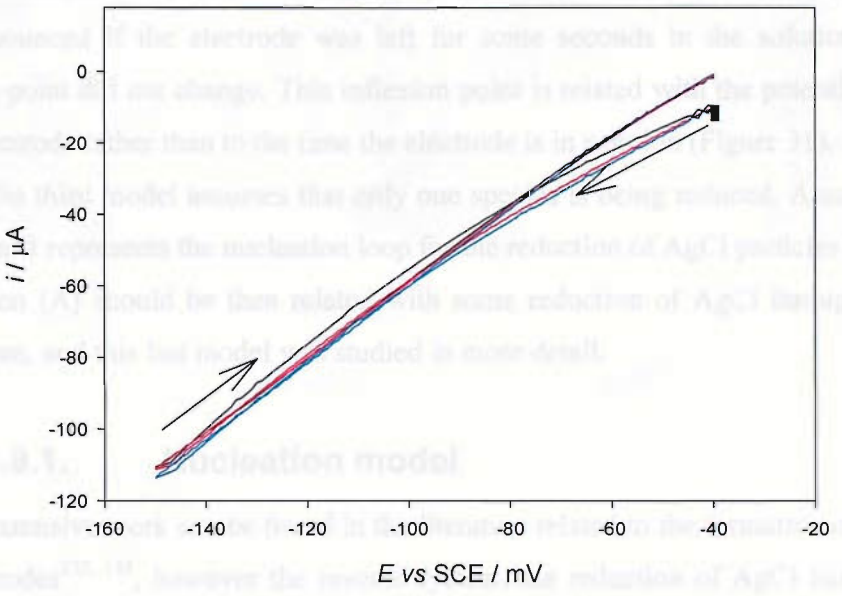

Figure 32 Second scans of the three Ag/AgCl SPEs shown in Figure 31. The scans were performed at room temperature in 2 M KCl, starting at OCP and scanning at 20 mV/s.

The nucleation loop shown in Figure 31 disappeared if the electrode was immersed in the solution for more than 2 min before the scan started. This effect could suggest that the SPE evolves in solution even without applying any potential or passing any current.

These results suggest that two different processes take place, with the second one (represented by region B in Figure 31) responsible for more current passed than the first one. Second and subsequent scans exhibit a slope slightly smaller than the slope in region B, as shown in Figure 32. Three different models were considered to explain this behaviour

The first model assumes that two different processes are taking place. These two processes can be due to two different species with similar potentials being reduced at the electrode. In this case, some species is being reduced over the interval of potentials marked in region A, meanwhile at more negative potentials, another species starts to reduce. In this case, the current obtained in region B will be the result of adding the contributions for the reduction of both species.

Another possibility is that there is a change in the area of the electrode with the wetting. In this case, and considering that the current density is constant, an increase of the area (through wetting of the electrode) will increase the current that the system can pass at any given overpotential. In this case, the inflexion point should depend on the

time the electrode has been immersed in the solution. We have seen that the inflexion is less pronounced if the electrode was left for some seconds in the solution, but the inflexion point did not change. This inflexion point is related with the potential applied to the electrode rather than to the time the electrode is in solution (Figure 31).

The third model assumes that only one species is being reduced. Assuming that the region B represents the nucleation loop for the reduction of AgCl particles to Ag, the first region (A) should be then related with some reduction of AgCl through another mechanism, and this last model was studied in more detail.

3.9.1. Nucleation model

Extensive work can be found in the literature related to the formation of AgCl on Ag electrodes[132, 133], however the reverse system, the reduction of AgCl has not been studied.

The theory of nucleation states that in order to form the first nuclei, an overpotential should be applied to the system in order to create the new interface. This overpotential required for the formation of the first nuclei, will shift the potential of the reaction to a larger value. If we reverse the scan once these nuclei have been formed, since we are applying a larger overpotential, the electrochemical reaction will occur vigorously[90], and the currents recorded on the backward scan will be larger than those on the forward scan, creating a "loop". Once we have created these nuclei, and since no additional energy is required to form the interface, no nucleation loop will be seen in subsequent scans. The model we have proposed assumes that some AgCl particles are touching some Ag particles. Since at those particles the Ag/AgCl interface is already present, they will not require any extra nucleation overpotential, consequently these particles will be reduced at lower overpotentials. On the other hand, those AgCl particles that are not in contact with Ag, will require a larger overpotential to reduce. This behaviour can explain the second part of the curve (region B) as well as its absence on subsequent scans. A scheme for this situation is represented in Figure 33.

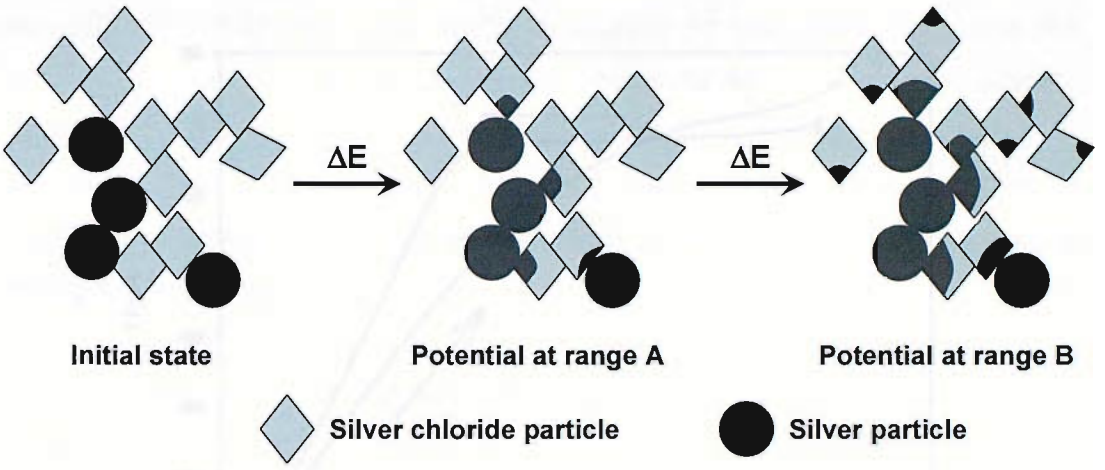

Figure 33 Schematic representation of the non nucleation (A) and nucleation (B) reduction processes.

In Figure 33 we have differentiated between two types of particles. AgCl particles in direct contact with Ag particles, and AgCl particles that are not in direct contact with silver particles. When the electrode is scanned to reduction, at potentials below the nucleation potential, contacted AgCl particles can undergo reduction (potential at region A). Once there has been a sufficient increase of the potential, AgCl particles not in direct contact with Ag will have enough energy to create the new interface (AgCl / Ag interface) needed to perform the reduction.

Considering the relative slope of the two regions (A and B), the current for the first process is smaller than the net current for the second process (current of B minus the extrapolation for the current of range A). In this case, we can assume that there are more non-touching than touching particles.

In order to separate the two processes occurring in the nucleation loop, we applied an intermediate potential until the first reaction was complete (the current dropped to zero). A fixed potential of -80 mV was applied to five electrodes. In Figure 34 we can see a typical voltammogram showing how the nucleation loop changes after applying this intermediate potential. For the five electrodes, the charge needed to exhaust the first process ranged between 89% and 93% of the total reduction charge of the electrode as stated in section 3.4, page 63.

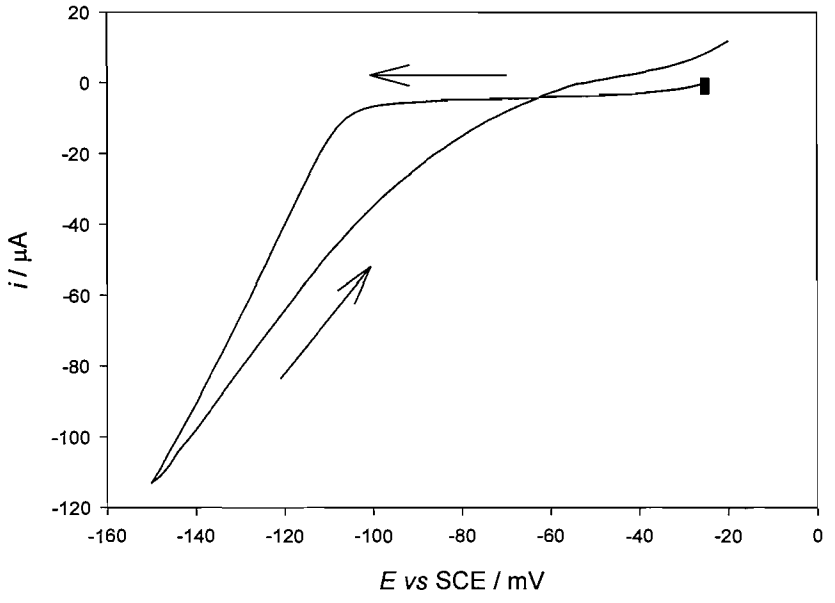

Figure 34 Typical voltammetric scan of a Ag/AgCl screen printed electrode after applying -80 mV until the current dropped to zero (Q = 50 mC). The scan was performed at room temperature in 2 M KCl, between -26 and -150 mV (*vs.* SCE) at 20 mV/s.

The first process (region A) disappears completely, and a typical nucleation loop is found. Intermediate reduction of the electrode gave intermediate results, with the first part of the curve less pronounced after the pre-reduction step. This result proves that the two processes are separate. We can deplete the first process and still see the second one. This experiment rules out the wetting effect since the current in zone A before the inflexion point does not depend in the amount of time the electrode is hold in solution, but in the amount of charge transferred.

Considering the charges involved, it seems as if the first process (region A) is responsible of approximately 91% of the reduction of the electrode. At the beginning, we can consider that few AgCl particles are touching with Ag particles, so the most important (largest current) process is the second one (range B). Once the first touching particles have been reduced, these particles will help to reduce adjacent AgCl particles in a chain reaction. Although there are few touching particles at the beginning, the amount of particles that are communicated with Ag particles directly or via another AgCl particle is very high. In the scheme in Figure 33, a representation of this phenomenon can be seen. For example, the silver chloride particle at the top of the scheme is not connected with any silver particle at the beginning of the experiment, but it will be connected once the silver chloride particle right under it has been reduced. The

data of 89-93% of the total charge needed to complete the first process gives us an idea of how the particles are interconnected. The rest of the AgCl that is not in direct or indirect contact with Ag is then the AgCl responsible of passing the current the remaining 7-11% of the total charge. This AgCl could be in electrical contact with the electrode (*i.e.* through contact with the underlying graphite layer) and therefore need an extra potential to reduce.

In chapter 5, we will discuss further the electrochemical behaviour of AgCl particles and demonstrate that AgCl particles embedded in a graphite matrix show similar behaviour as that shown here for the SPE. AgCl particles deposited on a graphite electrode (carbon paste or glassy carbon) shown a cathodic nucleation loop at the same overpotentials showed here for the SPE (section 5.1). In this case, we also found that on subsequent scans, since there are nuclei already present, the overpotential needed is smaller on the second scan than for the first one.

3.10. Conclusions

In this chapter, we have taken a deep look into the behaviour of the commercially available electrode, focussing mainly on the behaviour of the electrode once it is dipped in the solution (*i.e.* at long times). Several parameters were studied, and were compared with the behaviour of standard, bulk silver, silver chloride electrodes found in the literature. The SPE exhibits a Nernstian behaviour of the open circuit potential with the activity of chloride. The temperature dependence of the open circuit potential of the electrode also followed the behaviour of bulk Ag/AgCl published in the literature.

Other parameters such as the exchange current were also evaluated. We found that the commercial solid state SPE used in this thesis showed a smaller superficial current density than miniaturized, solution equilibrated, reference electrodes found in the literature. We have obtained through volumetric and gravimetric analysis similar values of the composition of the ink as those stated by DuPont. We have also found that the resistance of the track (approximately 125 Ω) adds a significant distortion to the potential at any given current, following Ohm's law. Also it was found that the high capacitance of the electrode distorts the behaviour of the electrode, especially at very short times after a certain potential is applied.

One effect that was also seen when the SPE was scanned near open circuit potential was a nucleation of Ag on AgCl particles. This nucleation appeared as a change of the slope of the *i vs. E* curve. This nucleation could not be seen in electrodes left in solution for a certain time before the scan, suggesting that the electrode evolves once in solution, even without applying any potential or current through the electrode.

Once equilibrated, the SPE shows a good behaviour, similar to that of bulk, equilibrated reference electrodes. The main drawback of this SPE is that the potential is not stable within the measuring time of the device. The measurement of glucose in the overall sensor takes place within 30-40 seconds, with MediSense's future sensors aiming at 3-5 seconds. Within this time-span the screen printed reference electrode is not stable, and this conditions the performance of the sensor.

4 Behaviour of Ag and AgCl electrodes in chloride solutions

4.1. Introduction

We have stated that the screen printed Ag/AgCl is stored dried, sealed in an aluminium foil package. In operation, the reference electrode should achieve its equilibrium potential as soon as possible upon immersion in the sample. In addition, the potential of the reference electrode should be stable and remain fixed throughout the measurement. Because of these two requirements, we have mentioned that the variation of the potential of the SPE after it is placed in the solution should be minimal. In an earlier section (3.7), we observed that the potential changes during the first 30-60 seconds, after immersion in the solution.

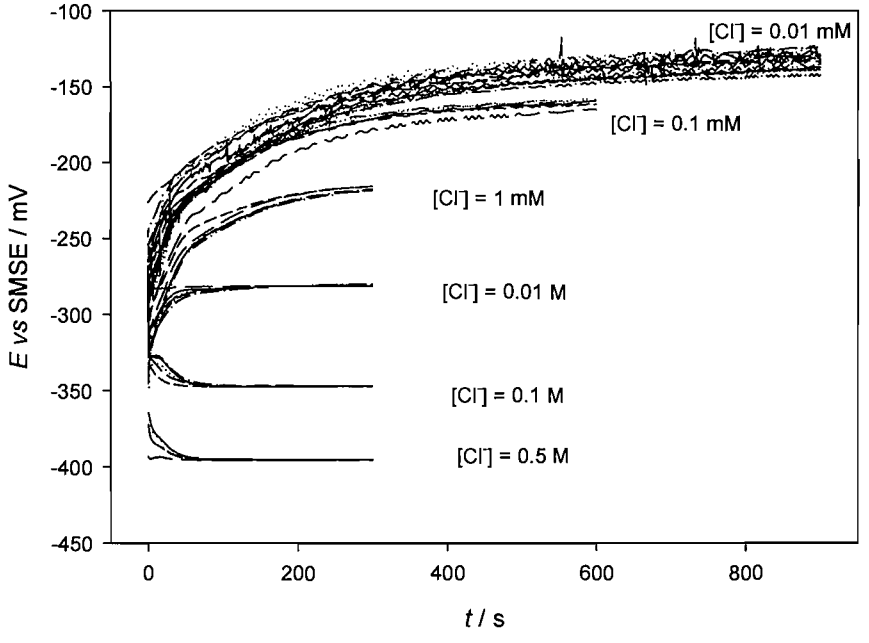

Figure 35 Open circuit potential of screen printed electrodes with different concentrations of chloride. Each concentration was tested with five different, fresh electrodes (taken directly from the package). Each electrode was discarded after use.

In Figure 35, the variation of the OCP with time of several fresh electrodes is shown for solutions with different concentrations of Cl^-. The variation of the equilibrium potential with Cl^- has already been discussed in section 3.5, where we showed that the screen printed Ag/AgCl electrodes obey the Nernst equation. The behaviour of the electrode in solution is very reproducible in concentrated solutions, and this reproducibility decreases as the concentration of Cl^- decreases (see Table 4). The stability of the OCP also decreases as the concentration of Cl^- decreases, and the time

required to attain a stable potential increases as Cl^- decreases. The low reproducibility present at low concentration of Cl^- could be due to the large noise present in the transients in Figure 35.

	Standard deviation (σ) after *t* seconds / mV			
$[Cl^-]$ / M	*t* = 60 s	*t* = 300 s	*t* = 900 s	*n*
0.5	0.65	0.22	-	5
0.1	1.0	0.31	-	8
0.01	1.99	0.49	-	6
10^{-3}	5.05	1.33		5
10^{-4}	6.13	3.60		5
10^{-5}	8.28	3.89	5.80	12

Table 4 Variation, at different times, of the standard deviation of the open circuit potential of the data shown in Figure 35.

The large noise and lower reproducibility seen for the more diluted solutions can be associated with the low amount of Cl^- in the solution, the lower conductivity of the solution and/or the lower ionic strength of the dilute solutions. The same experiments were repeated adding a supporting electrolyte (*vide infra*, Figure 39 and Figure 40), obtaining a significant reduction of the noise, and a better reproducibility of the open circuit potential between electrodes. In this sense, increasing the ionic strength and the conductivity of the solution increases the reproducibility of the potential at long times, even at lower concentrations of chloride.

The most important feature in Figure 35 is the different way the electrode potentials evolve depending on the concentration of Cl^-. It can be seen in the figure that the electrodes exhibit a potential of around -320 mV at the very first moment the electrode is placed in solution. This potential evolves rapidly in two differentiated trends. Electrodes in solutions with Cl^- concentration above 30 mM evolve to more negative potentials, meanwhile, SPEs in solutions with concentrations less than 30 mM evolve to less negative potentials.

In the results shown in Figure 35, it should be noticed that the screen printed Ag/AgCl electrodes reach the equilibrium potential faster the larger the concentration of

chloride in the solution. This equilibration time is approximately 60 s for chloride concentrations around the physiological value (0.1 M).

Overlapped with the mentioned drift of the open circuit potential, we can see another feature at short times after the immersion of the SPE in the solution (first 30 seconds). This additional feature is not evident in Figure 35, mainly due to the large amount of data in the figure, but it can be seen more clearly in Figure 26, included here again as Figure 36 for clarity. We will refer to these effects as *"long time"*, and *"short time"* transients respectively.

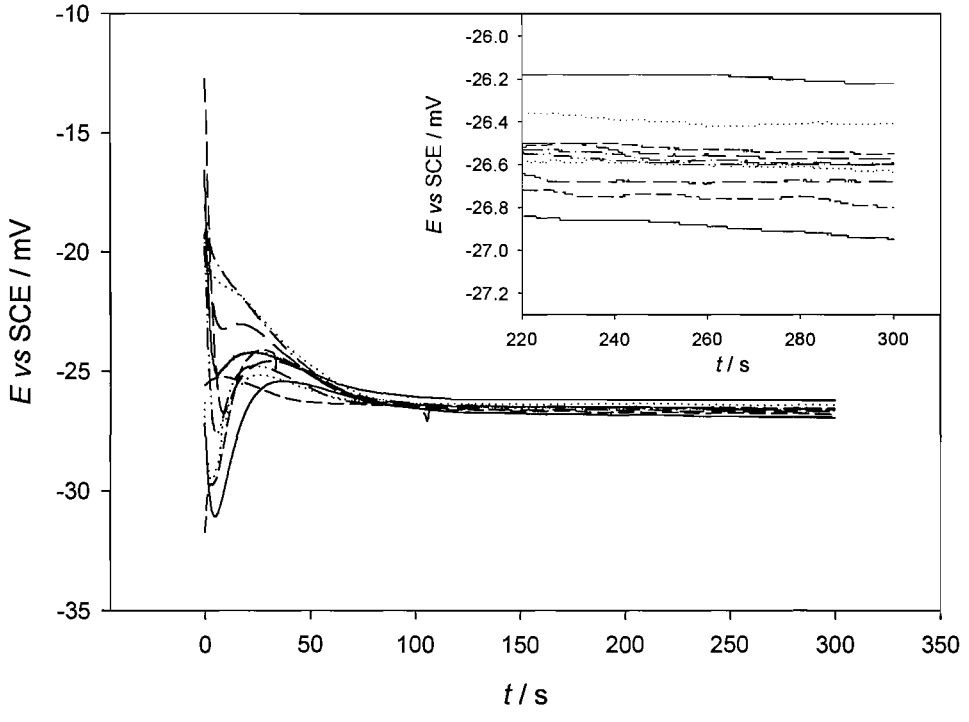

Figure 36 Variation of the open circuit potential of ten new Ag/AgCl screen printed electrodes from the moment the SPE was dipped in a 2 M KCl solution.

We have considered several theories to explain this behaviour. These theories are introduced here. They will be developed in the following subsections:

1. *Presence of different equilibria:*

The dried electrode exhibits a potential characteristic of the interfaces of the system, Ag/AgCl electrode and air. Once the electrode is placed in solution, the OCP will evolve to the expected value given by the Nernst equation.

2. *Variation of the activities of chloride or silver (I) inside and outside the ink, dissolution of the AgCl in the SPE:*

The initial potential could also be explained considering that there is some variation of the activity of Ag^+ and/or Cl^- when the electrode is dipped in the solution. This variation of activities could be due to dissolution of AgCl to comply with the solubility product, or any other variation of Cl^- or Ag^+ activity at the electrode surface. For any solution of any given concentration of Cl^-, the concentration of Ag^+ and Cl^- is fixed through K_s. This will force the dissolution of AgCl to equilibrate the expression $K_s = [Ag^+]\,[Cl^-]$. During this dissolution, the concentrations of Ag^+ and Cl^- at the electrode change, hence changes in the open circuit potential should be expected.

3. *Double layer charging:*

In this case, we have to consider that once an electrode is placed in a solution, there will be a distribution of charges across the interface. The magnitude of this double layer charge will depend on the concentration of ions in the solution. Charging this capacitor will affect the transient open circuit potential.

4. *Wetting of the electrode, variation of the surface area of the electrode:*

The effective surface area of the electrode could change during the wetting process. The solution will wet only the outmost layer of the SPE at first, and progress through the ink with time. In addition, the wetting could cause the screen printed electrodes to swell or contract, presenting larger or smaller area.

5. *Parallel Faradaic process at the electrode:*

Reduction or oxidation of some other species present in the ink or in the solution (*e.g.* O_2).

6. *Adsorption of Cl^- on the Ag or AgCl particles:*

This will have an effect on the potential of the screen printed electrode in the sense that the adsorption of Cl^- will deplete locally the $[Cl^-]$ at the electrode. Different concentrations of Cl^- will give different amounts of adsorbed Cl^-, so the SPE will behave differently according to the solution. Additionally, the charge build up of this double layer (capacitor) will have an effect in the potential across the electrode-solution interface.

All of these possibilities were evaluated by changing the experimental conditions and looking to see if the changes were consistent with the predictions of the different models in each case.

4.2. The literature

We have searched in the literature for similar transient studies, and a few articles were found that show similar experiments. There are very few articles that deal with the behaviour of the Ag/AgCl electrode from the first moment it is dipped in the solution, probably due to the fact that most of the researchers are interested in the system Ag / AgCl already equilibrated in Cl^- solutions as a reference electrode. Classically, many of the procedures for constructing Ag / AgCl reference electrodes involve the thermal decomposition of silver oxide to Ag on Pt, and the subsequent electrodeposition of AgCl on the Ag from a Cl^- solution[134] (thermal electrolytic process). Using this procedure, the electrode will already be wetted and equilibrated with the solution during the electrodeposition of AgCl. The other two most common procedures are the thermal process (thermal decomposition of silver oxide and silver chlorate to form a deposit of Ag and AgCl) and the electrolytic process (electrodeposition of Ag and subsequent electrodeposition of AgCl from Cl^- solution).

In a classic paper by Taniguchi and Janz[135] (later expanded in Janz's chapter in "Reference electrodes"[86]), they show how the ratio Ag/AgCl affects the equilibration transients of fresh thermal-electrolytic electrodes (aging effect). The porosity of the Ag particles and also the difference in concentration between the electrolytic and the testing solution affected the equilibration. They suggested that the reason for the transients was a concentration-polarization effect during the electrolytic chloridation. In the latter stages of this process, the electrode reaction may occur beneath a porous deposit of silver chloride of increasing thickness. Within the pores of this deposit, concentration polarization may cause the solution to become largely depleted of electrolyte, and this depletion may persist when the electrode is transferred to the measuring solution. When the electrode is placed in the testing solution the equilibration of the inner and outer solutions occurs, and this leads to a fluctuation of the potential. This fluctuation is more marked (and the equilibration takes more time) the more porous the electrode. It is important to note that the time scales of Taniguchi and Janz's experiments were in the range of hours (10 to 30 hours). In contrast, in our experiments we are equilibrating the

electrodes in seconds (usually 100 – 500 seconds, depending on the testing solution). In addition, the potential drift is not comparable; they report drifts of, at most, 0.80 mV compared to our experiments where the drift is as large as 120 mV for 0.01 mM Cl^- solutions. We also need to consider that, in contrast with our Ag/AgCl SPE, Taniguchi and Janz's electrodes were not dried before the measurement, but they monitor the changes in the OCP when the electrode was moved between two solutions with different concentration of Cl^-, *i.e.* the electrolytic and the testing solutions.

Another reference from Djokić and Burrell[136] includes a study of the behaviour of different forms of silver once it is placed in a solution containing 0.85% NaCl (~ 0.145 M). In this case, they found decreasing potential transients when sputtered Ag samples where dipped in the solution, and they relate the decrease of the open circuit potential with the presence of Ag_2O in the sputtered samples. They conclude that the potential variation is due to the dissolution of Ag^+. At the beginning of the experiment, they suggest that the potential is established by the Ag_2O / Ag system (E^0 = 0.342 *vs.* SHE)[93], and after the dissolution of this layer of Ag_2O, the potential shifts to that of the AgCl / Ag system. In this case, the variation of potential was around 100 mV in the first 60 seconds, similar to the results shown in this Thesis.

Tensamani and Lu Cheng[137, 138] have reported a potential variation of ~15 mV when AgCl either on Ag or graphite electrodes are immersed in a Cl^- solution (the concentration of the solution was not stated). In their paper, they claim that the potential drift comes from a chemical capacitor in the surface of the electrode, due to the adsorption of Cl^- on the electrode. The experimental set-up used in this paper (reference electrode in a separate cell, linked to the working cell by a Pt wire instead of the saline bridge) makes it very difficult to extrapolate any information to our system.

4.3. Trigger/Triggering circuit

Previous experiments (sections 3.1.2 and 3.7) presented a remarkable irreproducibility at very short times. We have noticed under open circuit conditions, the potential of the electrode changes from the very moment the electrode is immersed in the solution. We have found that it was very difficult to record the very first part of this

transient, because the time at which the electrode is immersed in the solution was not well synchronized with the start of the measurement.

In order to overcome this limitation, a simple trigger was designed. This circuit sends a TTL signal (+5 V) to the potentiostat once the electrode is immersed in the solution. This +5 V signal automatically starts the measurement.

This triggering circuit was built on a stripboard according to the scheme shown previously in Figure 6, page 30.

When the circuit is closed, the circuit sends a +5.7 V signal to the potentiostat. The potentiostat (Autolab PGSTAT, Eco Chemie) can receive this signal through any of its DIO ports.

Several ideas were tested to detect when the electrode is immersed in the solution:

- The first approach used the other two electrodes on the glucose screen printed sensor; the working and the dummy electrodes (WE and DE). The sensor has three electrodes: the Ag/AgCl counter-reference electrode and two carbon-based electrodes (WE and DE) situated at both sides of the Ag/AgCl electrode. Both electrodes were wired to the circuit so that when the electrode was in the solution, current could flow between them, closing the circuit. This approach, although practical and very reproducible, interfered with the measurement of the potential. Since there was a +5.7 V potential across the carbon-based electrodes, particularly over the Ag/AgCl electrode, this adversely affected the measurement of the potential. In Figure 37, we can see how switching the triggering circuit on and off affected the measured potential.

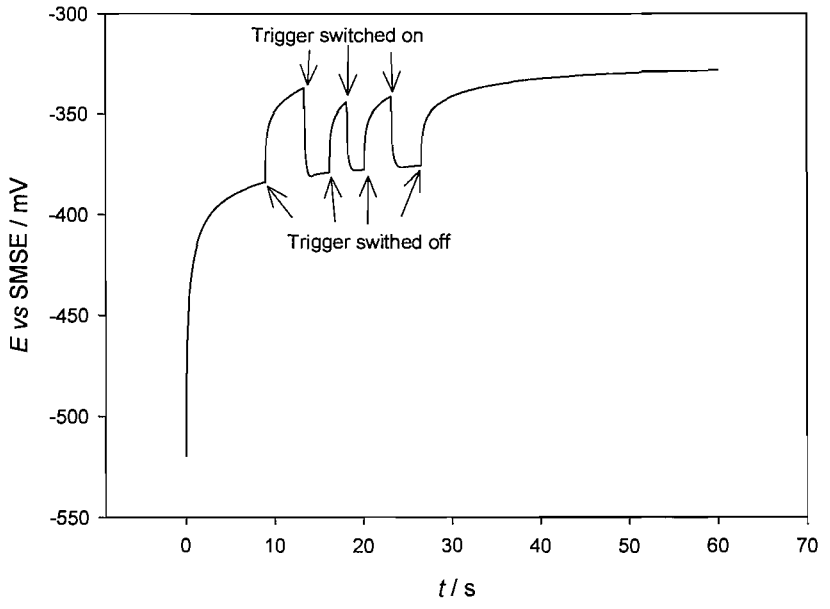

Figure 37 Effect of the +5 V triggering potential. Chronopotentiometry at open circuit potential of the Ag/AgCl reference electrode in a solution containing 0.5 M KNO_3 and 30 mM KCl. The arrows show when the triggering circuit was switched on and off. The trigger was on at the beginning of the measurement.

- Another approach used only one of the carbon-based electrodes and an additional electrode (a stainless steel or platinum wire) in the solution. The idea was to move the +5 V triggering potential away from the Ag/AgCl electrode, but no improvement was achieved.
- Finally, both ends of the triggering sensor were set outside of the cell and placed one in the holder of the electrodes and the other one attached on the exterior of the cell, as shown in Figure 7. These contacts were made from copper adhesive tape (electrical tape from 3M, UK). When the electrode holder (and so the screen printed electrode) is lowered, both ends of the triggering circuit came into contact and close the circuit, starting the measurement. In this case, the moment at which the measurement starts is not perfectly synchronised with the dipping of the electrode, but since the triggering circuit is completely outside the cell, it does not interfere with the measurement.

This methodology proved to be adequate to record the initial part of the transient.

4.4. Behaviour of different batches of SPEs

We found that the different batches of SPEs used showed different behaviours when the electrodes were immersed in Cl^- solutions. In Figure 38, we illustrate these differences.

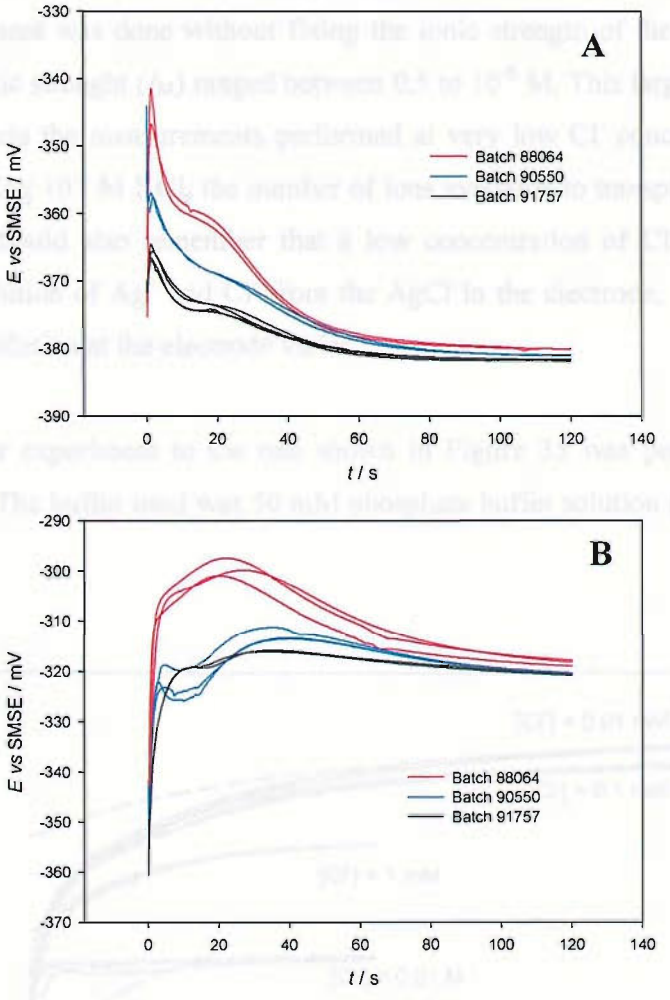

Figure 38 Typical chronopotentiometry at open circuit of different batches of sealed Ag/AgCl SPEs in 0.5 M KNO_3 and 0.3 M KCl (A) or 0.03 M KCl (B) at 25 °C.

In the figure, the behaviour of the electrode is remarkably different at the two KCl concentrations shown. We have contacted MediSense about this matter, and there were no manufacturing differences between the two batches. The only difference between the two batches was the batch of Ag/AgCl ink used for manufacturing these electrodes.

4.5. Behaviour of the SPE in Cl^- solutions with added electrolyte

The experiments shown in the introduction of this section (Figure 35) describe the behaviour of the SPE when it is submerged in KCl solutions. It is important to note that this experiment was done without fixing the ionic strength of the solution, so the values of the ionic strenght (I_M) ranged between 0.5 to 10^{-5} M. This large variation in I_M particularly affects the measurements performed at very low Cl^- concentration. In the solution containing 10^{-5} M KCl, the number of ions available to transport any charge is very low. We should also remember that a low concentration of Cl^- in the solution forces the dissolution of Ag^+ and Cl^- from the AgCl in the electrode, so that the ionic strength of the solution at the electrode varies.

A similar experiment to the one shown in Figure 35 was performed using a buffer solution. The buffer used was 50 mM phosphate buffer solution (PBS) at pH 7[139, 140].

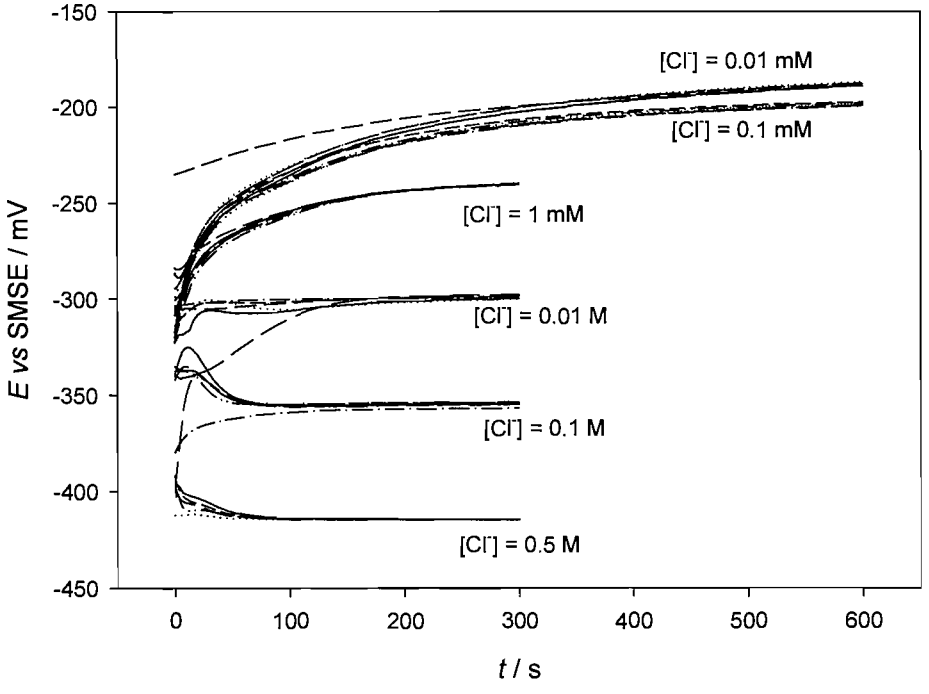

Figure 39 Open circuit potential of SPEs in phosphate buffer solution (PBS) (50 mM, pH=7) with different concentrations of chloride. Each concentration was tested with five different, fresh electrodes (taken directly from the package). Each SPE was discarded after use.

In this case, improved reproducibility was obtained in the presence of the buffer. The variation of the final potential (t = 300s) was linear with the concentration of Cl^-, with a slope of 57.8 mV per pCl^- unit (E = -420.29 – 57.9 log [Cl^-]; r = 0.998; n=27), with linear range within 0.5 M to 10^{-4} M. It is evident from Figure 39, that the addition of supporting electrolyte (even at low concentration) eliminates the fluctuation of the potential transients at very low Cl^- concentrations as compared with Figure 35. We believe that the increase in the conductivity of the solution is responsible for the reduction of the noise.

Since the reproducibility of the behaviour of the electrodes at short times in Figure 35 is not very good, and in order to rule out any contribution from the PBS buffer (specially from side reactions such as the formation of Ag_3PO_4), new measurement were performed with a different supporting electrolyte, 0.5 M KNO_3.

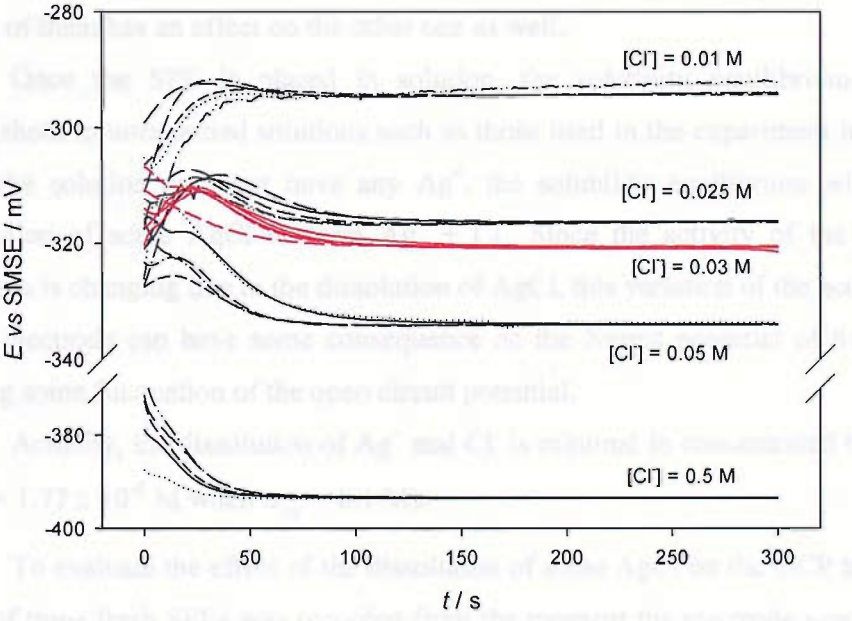

Figure 40 OCP of SPEs in 0.5 M KNO_3 with different concentrations of chloride. Each concentration was tested with at least five different, fresh electrodes, discarding the SPE after use. (For comparison purposes, the area between -340 and -370 mV has been cut out).

In this case, the correlation between the potential at long times (t = 300 s) and the logarithm of the concentration of chloride showed a slope of 0.0590 mV with a very good correlation coefficient (r = 0.99990, n = 26). The intercept was -411.0 mV.

Three of the five electrodes measured in a 30 mM KCl solution (red lines) showed the same potential at the beginning of the experiment (t = 0) and after equilibration. This concentration of Cl^- minimises the *"long time"* transient of the electrode's open circuit potential, so the *"short time"* features can be seen with more detail.

4.6. Effect of saturating the solution with AgCl.

As we have said in the introduction of this chapter (section 4.1, page 95), once the electrode is placed in solution, there are several equilibria that have to be established. One of them is the electrochemical equilibrium described by the Nernst equation. Another one is the equilibrium of a sparingly soluble salt and its ions, described by the solubility product (K_s). Both equilibria are related with each other, and the displacement of one of them has an effect on the other one as well.

Once the SPE is placed in solution, the solubility equilibrium has to be established. In unsaturated solutions such as those used in the experiment in Figure 35, since the solution does not have any Ag^+, the solubility equilibrium will force the dissolution of some AgCl to form $Ag^+ + Cl^-$. Since the activity of the ions at the electrode is changing due to the dissolution of AgCl, this variation of the activity of Ag^+ at the electrode can have some consequence on the Nernst potential of the electrode, causing some fluctuation of the open circuit potential.

Actually, the dissolution of Ag^+ and Cl^- is minimal in concentrated Cl^- solutions ($a_{Ag^+} = 1.77 \times 10^{-9}$ M when $a_{Cl^-} = 0.1$ M).

To evaluate the effect of the dissolution of some AgCl on the OCP transient, the OCP of three fresh SPEs was recorded from the moment the electrode was dipped in a solution containing 0.5 M KNO_3 and 0.3 M KCl. After saturating the solution with AgCl (by the dropwise addition of $AgNO_3$), the OCP of another three fresh SPE was also recorded. Characteristic transients are shown in Figure 41.

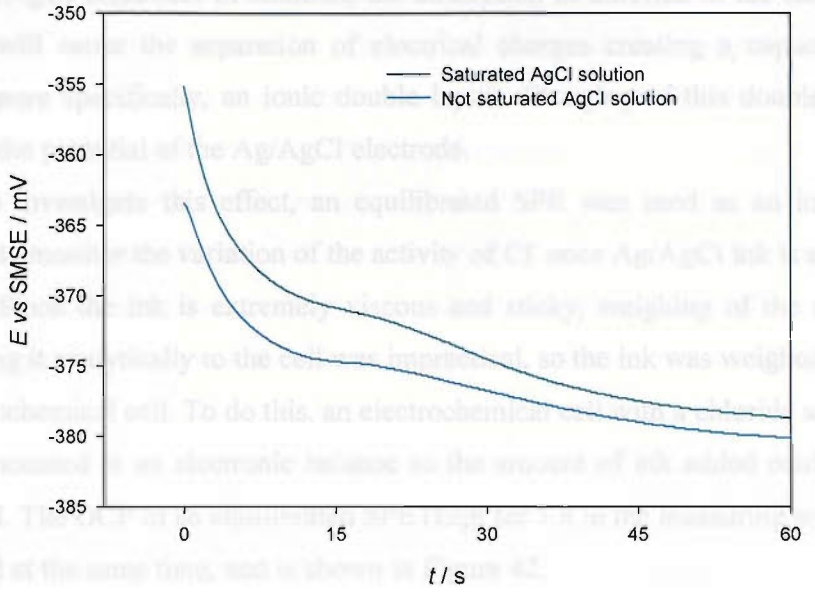

Figure 41 Effect of saturating the solution with AgCl on the OCP transient of fresh SPE recorded in 0.5 M KNO_3 and 0.3 M KCl. The solution was saturated by adding several drops of $AgNO_3$ directly in the electrochemical cell.

We can see in Figure 41 that both transients show similar behaviour. The only difference seen is that the transient of the SPE recorded in the AgCl saturated solution shows a less negative potential than that of the SPE in the solution not saturated with AgCl. The saturation of the solution was done by the addition of $AgNO_3$ and this procedure forms a "mist" of solid AgCl in solution that reduces slightly the Cl^- in solution, thus displacing the potentials to less negative values.

Both *"short time" and "long time"* features are similar in both cases shown in Figure 41, so the features are not believed to be related with the dissolution of Ag^+ from the electrode.

4.7. Adsorption of Cl^- on Ag/AgCl ink.

One effect that we have proposed as an explanation of the open circuit transients is the adsorption of Cl^- on the silver and silver chloride particles. Indeed, it has been found in the literature that silver particles adsorb anions on their surface [141-145].

In this case, the ink could adsorb Cl^- from the sample solution and therefore locally deplete the amount of chloride at the electrode surface, in turn altering the OCP

of the Ag/AgCl electrode. In addition, the adsorption of chloride in the surface of the particles will cause the separation of electrical charges creating a capacitor on the surface (more specifically, an ionic double layer). Charging of this double layer will also alter the potential of the Ag/AgCl electrode.

To investigate this effect, an equilibrated SPE was used as an ion selective electrode to monitor the variation of the activity of Cl^- once Ag/AgCl ink is added to the solution. Since the ink is extremely viscous and sticky, weighing of the sample and transferring it analytically to the cell was impractical, so the ink was weighed directly in the electrochemical cell. To do this, an electrochemical cell with a chloride solution was directly mounted in an electronic balance so the amount of ink added could be easily monitored. The OCP of an equilibrated SPE (kept for 1 h in the measuring solution) was monitored at the same time, and is shown in Figure 42.

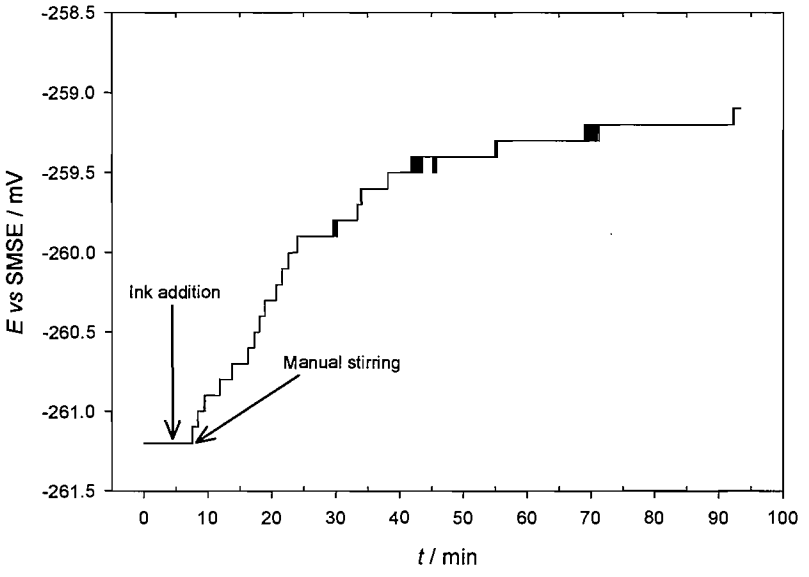

Figure 42 Potential transient of an equilibrated SPE when 2.451 g of ink were added to 15 ml of a solution with 0.5 M KNO_3, saturated AgCl and 3 mM KCl at 25 °C. Marked with arrows is the moment when the ink was added (~5 min) and when the solution was stirred (~8 min).

In Figure 42 there is a variation of the potential from -261.2 to -259.1 mV; this represents a variation of the concentration of Cl^- in the sample of 0.17 mM. Taking into account the volume of the cell, and the amount of ink added, we conclude that DuPont's ink adsorbs approximately 38 μg of Cl^- per gram of ink.

In the graph it can be seen that the variation of the potential is minimal, even at very long times. This indicates that the ink is adsorbing some Cl^-, but in a very small amount and at a very slow rate. The quantities of ink tested here are typically one

thousand times larger than those present in the SPE, so we should expect that the amount of Cl^- adsorbed on a screen printed Ag/AgCl would be proportionally smaller, and thus negligible in terms of depletion of Cl^- at the electrode surface.

Also, in this graph we can see that there is no leaking of Cl^- from the ink, since a shift of the potential towards more negative values was not observed. In section3.1.1 (page 49), we suggested that the ink may contain some Cl^- source apart from the AgCl[xix], but these results indicate that the ink is not releasing any chloride into the solution.

In more precise terms, the release of Cl^- to the solution and the adsorption of Cl^- in the ink have opposite effects, and our experiment demonstrates that the adsorption of chloride here is slightly more important than the leaking of Cl^- from the ink.

These two results (ink does adsorb more Cl^- than it releases, but in a minimal scale) indicate that the ink does not alter significantly the concentration of Cl^- in the solution, and that a different explanation should be found to explain the open circuit transients recorded when a SPE is immersed in the solution.

The effect that the adsorption of Cl^- at the Ag particles will have in the double layer charging and thus in the open circuit potential will be studied in detail later.

4.8. Effect of opening the SPE.

The SPE is distributed sealed in a package. Upon use, the package will be removed and the SPE will immediately be used. We have found that there is a strong smell of organic solvent when the electrode is opened. Gas Chromatography coupled with Mass Spectroscopy (GC-MS) was used to analyse the volatile fraction in the package and identify the species responsible for the odour. To perform this analysis, a sealed screen printed electrode was opened and the package washed with H_2CCl_2 and a fraction of this washing was injected in the GC-MS.

The spectra are shown in the appendix. They show evidence for cyclohexanone, diethylene glycol butyl ether and several *o, p* and *m* ethyl or methyl substituted toluenes.

[xix] The ink releases 5.5 ± 1.0 μg Cl^- per gram of ink.

It is possible that these solvents could have some adverse effect on the electrochemistry and/or wetting of the electrode. To evaluate this effect, several SPEs were taken from the sealed packages, the lidding tape removed, and the electrodes were kept in the dark at room temperature so that these volatile compounds could evaporate from the electrode. The transient at OCP of three of these opened electrodes was compared with another three electrodes from the same batch, but kept in the sealed packages until the moment of performing the analysis. The comparison of characteristic transients is shown in Figure 43.

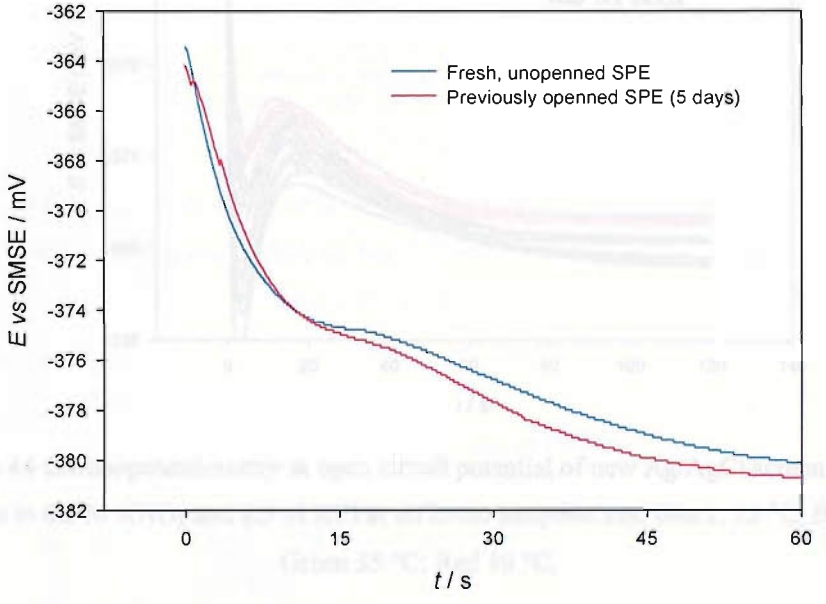

Figure 43 Comparison of the transient at OCP right after immersing the electrode in a solution with 0.5 M KNO_3 and 0.3 M KCl of two SPEs from the same batch. The transient in red is the characteristic signal (n = 3) of a SPE kept unsealed in the dark for 5 days to evaporate the solvents, meanwhile the transient in blue is from an electrode unsealed till the last moment before the analysis.

We can see in Figure 43 that there is no significant difference between the two sets of experiments, so we believe that the volatile solvents included in the package with the SPE are not responsible of the features present in the transient.

4.9. Effect of the temperature on the transients

In order to see if the transients recorded for the OCP of the SPE do have a surface wetting component, two experiments were performed; measurement of the

variation of the open circuit potential of the SPE at different temperatures, and measurement of the effect of adding surfactants on the open circuit potential (section 4.10). In the first experiment, the effect of temperature for different chloride concentrations was evaluated. In the next figures (Figure 44 to Figure 47) the effect of the temperature on the transients can be seen.

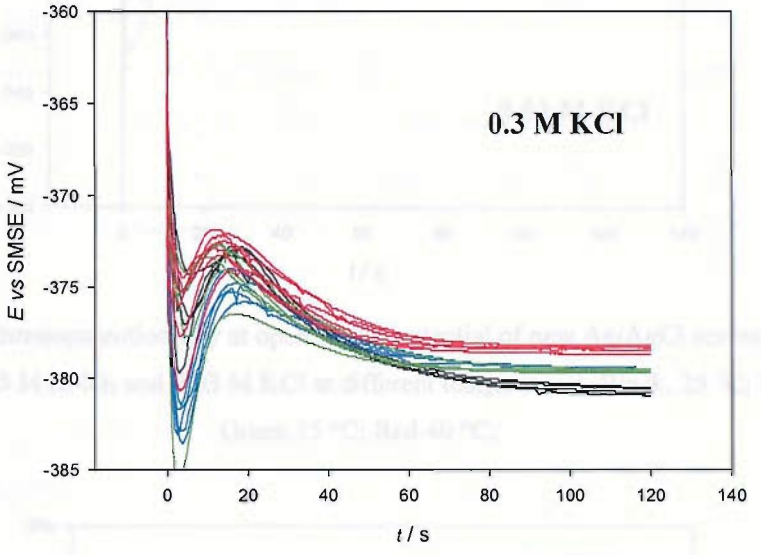

Figure 44 Chronopotentiometry at open circuit potential of new Ag/AgCl screen printed electrodes in 0.5 M KNO_3 and 0.3 M KCl at different temperatures. Black, 25 °C; Blue 30 °C; Green 35 °C; Red 40 °C.

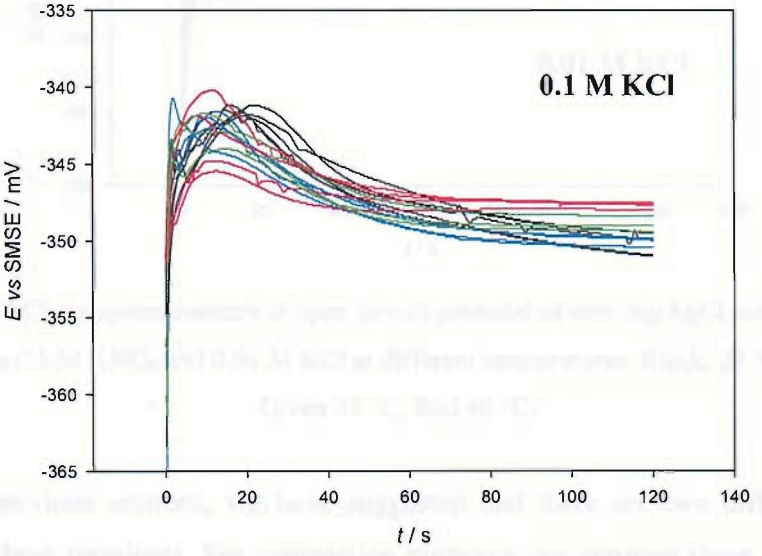

Figure 45 Chronopotentiometry at open circuit potential of new Ag/AgCl screen printed electrodes in 0.5 M KNO_3 and 0.1 M KCl at different temperatures. Black, 25 °C; Blue 30 °C; Green 35 °C; Red 40 °C.

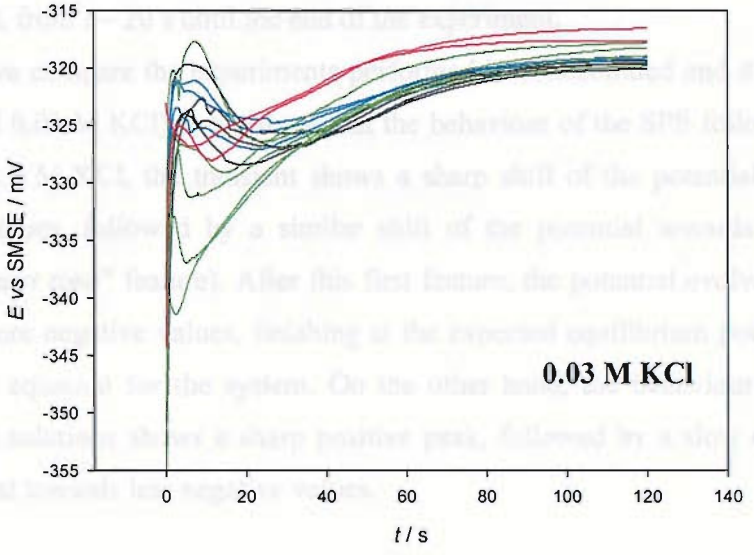

Figure 46 Chronopotentiometry at open circuit potential of new Ag/AgCl screen printed electrodes in 0.5 M KNO_3 and 0.03 M KCl at different temperatures. Black, 25 °C; Blue 30 °C; Green 35 °C; Red 40 °C.

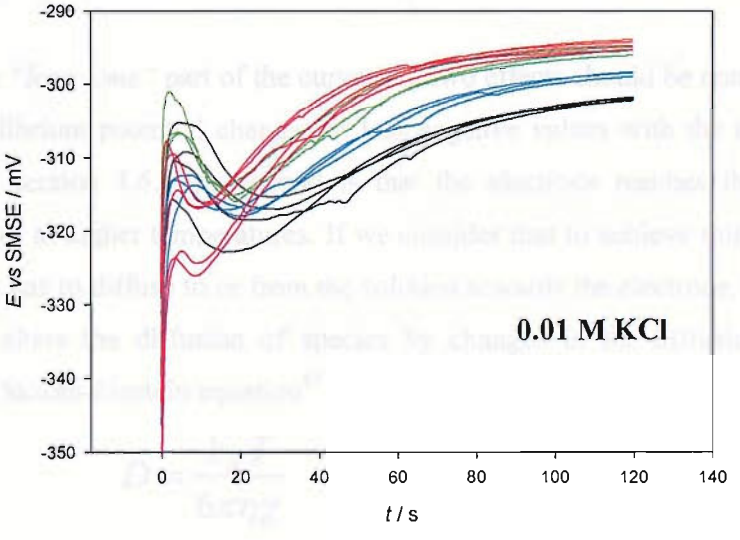

Figure 47 Chronopotentiometry at open circuit potential of new Ag/AgCl screen printed electrodes in 0.5 M KNO_3 and 0.01 M KCl at different temperatures. Black, 25 °C; Blue 30 °C; Green 35 °C; Red 40 °C.

In previous sections, we have suggested that there are two different features present in these transients. For comparison purposes, we separate these transients into two effects (*"short time"* and *"long time"*). The *"Short time"* zone comprises the first moments from placing the electrode in solution until the first peak appears

(approximately the first 20 seconds). The *"Long time"* zone covers the rest of the experiment, from $t \sim 20$ s until the end of the experiment.

If we compare the experiments performed in concentrated and diluted solutions (0.3 M and 0.01 M KCl), we can see that the behaviour of the SPE follows an opposite trend. In 0.3 M KCl, the transient shows a sharp shift of the potential towards more negative values, followed by a similar shift of the potential towards more positive values ("*short time*" feature). After this first feature, the potential evolves more slowly towards more negative values, finishing at the expected equilibrium potential given by the Nernst equation for the system. On the other hand, the behaviour of the SPE in dilute KCl solutions shows a sharp positive peak, followed by a slow equilibration of the potential towards less negative values.

From the data it can be seen that the *"short time"* zone of the transient is not affected by changes in the temperature. The behaviour of the electrode is very irreproducible at short times after immersing the electrode in the solution, but no discernible tendency or variation with temperature was found in this part of the transients.

In the *"long time"* part of the curve (B), two effects should be noted. The first is that the equilibrium potential changes to less negative values with the temperature as explained in section 3.6. The second is that the electrode reaches the equilibrium potential faster at higher temperatures. If we consider that to achieve this equilibration, some species has to diffuse to or from the solution towards the electrode, increasing the temperature alters the diffusion of species by changes in the diffusion coefficient, according to Stokes-Einstein equation[87].

$$D = \frac{k_B T}{6\pi\eta\chi} \qquad \text{Equation 28}$$

where k_B is the Boltzmann constant, η the viscosity of the solution and χ the effective hydrodynamic radius of the diffusing species (assumed to be spherical particles). The variation of D with the temperature is about[89] $1-2$ % per °C, a change of 16 to 34 % in the range of temperatures studied here (from 25 to 40 °C).

A change in the diffusion coefficient is not the only possible cause for the variation of the potential transients with the temperature. If we consider that to achieve equilibrium a chemical reaction is taking place, increasing the temperature will increase the rate of the reaction according to Arrhenius equation:

$$\Delta G^{\ddagger} = A - RT \log k \qquad \text{Equation 29}$$

where $\Delta G^{\ddagger}$ is the standard Gibbs free energy of activation, A is a constant and k is the rate constant of the reaction. We could consider that any chemical reaction is activated by increasing the temperature through the increase in the mobility of the molecules and hence an increase of the effective collisions or the energy of those collisions.

Actually, diffusion is also an activated process, so equations 28 and 29 come to the same result, which is speeding up the process with the temperature.

4.10. Effect of surfactants on the transients

It is possible that the solution wets the SPE slowly throughout the resin (the Ag/AgCl is made by mixing Ag and AgCl with a resin, this resin leaves pores and voids) and this alters the area of the electrode. A possible mechanism is that, after immersing the electrode in the solution, the solution initially only touches the outermost part of the electrode, and then percolates slowly inside the resin. In this case, the effective area of the electrode would increase with time. The equilibrium potential of the electrode is independent of the area of the electrode, so the final point after the equilibration should be constant (only determined by the thermodynamics). However, the path followed to reach this equilibrium, and hence the intermediate states, could vary with the wetting of the electrode.

In addition, we have to consider that the Ag/AgCl screen printed electrode contains a dispersion of silver and silver chloride particles. These particles may be non-uniformly distributed, so the interface between the electrode and the solution could have a different composition as the wetting of the SPE proceeds through the ink layer. One way to investigate whether the transients have a wetting component is by adding some surfactant to the solution and thus improving the wettability.

These experiments were done with two different kinds of surfactants, Brij 56 ($(C_{16}H_{33}(OCH_2CH_2)_nOH$, n ~10), a non ionic surfactant and SDS (sodium dodecylsulfate) an ionic surfactant. For these experiments, we saturated the solution with AgCl to avoid any possible effect from the dissolution of Ag^+ from the electrode into solution.

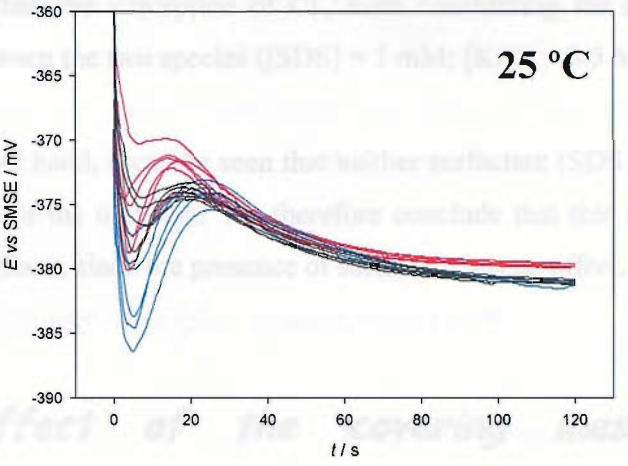

Figure 48 Chronopotentiometry at OCP of new SPE in 0.5 M KNO_3, saturated AgCl and 0.3 M KCl with different surfactants. Black, 1 mM Brij56; Blue, 1 mM SDS; Red, no surfactant

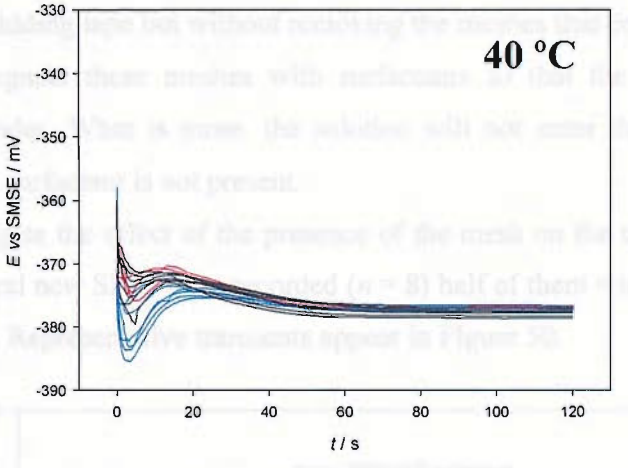

Figure 49 Chronopotentiometry at OCP of new SPE in 0.5 M KNO_3, saturated AgCl and 0.3 M KCl with different surfactants. Black, 1 mM Brij56; Blue, 1 mM SDS; Red, no surfactant.

The main effect that we can see in figures 48 and 49 is that the *"short time"* zone presents a larger first minimum when there is 1 mM SDS in the solution. In the presence of SDS, the first peak is more intense, but it is important to notice that the presence of SDS does not speed up the process; it only enhances its intensity. This indicates that the process responsible of the first part of the transient may not be related with the wettability of the electrode.

We should consider that SDS is an ionic molecule (DS^- + Na^+), and as that, it could adsorb on the surface, building up charge in the electrode interface. If this is the case, this experiment shows that the adsorption of DS^- has a bigger effect on the open

circuit potential than the adsorption of Cl^-, even considering the huge difference in concentration between the two species ([SDS] = 1 mM; [KCl] = 0.3 M).

On the other hand, it can be seen that neither surfactant (SDS or Brij) affects the *"long time"* zone of the transient. We therefore conclude that this zone is not related with wettability effects, since the presence of surfactant has no effect.

4.11. Effect of the covering mesh on the transient at OCP.

The OCP transients shown in previous section (*e.g.* Figure 40) were done after stripping out the lidding tape but without removing the meshes that cover the electrodes. MediSense impregnate these meshes with surfactants so that the solution properly covers the electrodes. What is more, the solution will not enter the space under the lidding tape if the surfactant is not present.

To investigate the effect of the presence of the mesh on the transients, the OCP transients of several new SPEs were recorded (n = 8) half of them with and half of them without the mesh. Representative transients appear in Figure 50.

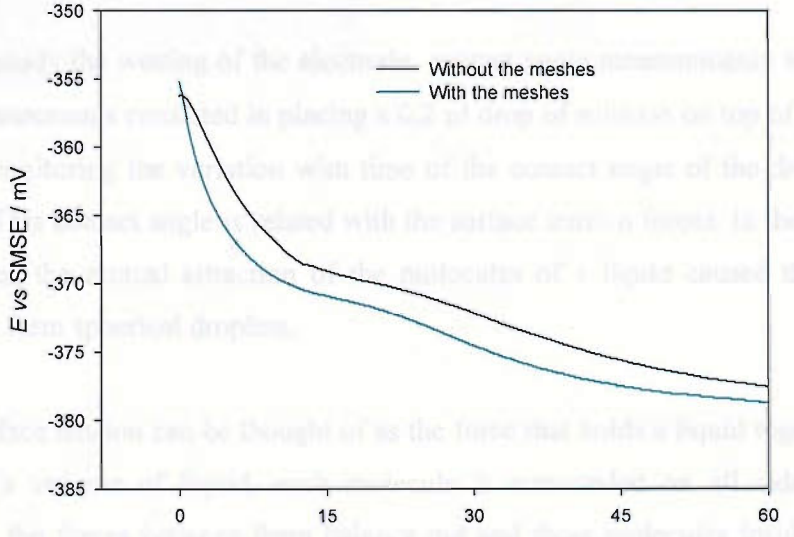

Figure 50 Effect of the removal of the meshes on the SPE in the transient at open circuit potential of fresh SPEs in 0.5 M KNO_3, 0.3 M KCl and saturated AgCl. 4 transients of each kind were recorded, and a representative transient of each kind is shown here.

We can see in Figure 50 that there is no difference if the scan is performed with or without the meshes. A slight difference in the potential is recorded, but the two features (at *"short times"* and at *"long times"* are present in both cases. This supports our statement that both features are not related with the way the Ag/AgCl SPE is wetted.

4.12. Contact angle measurement

In the previous section, we have seen that the addition of surfactants to the solution does not modify the OCP transient, and so we tentatively concluded that the wetting of the electrode is not a limiting step in the performance of the electrode. Actually, the OCP represents the potential of the system when no current is flowing externally; that is the potential in which both oxidation and reduction reactions are taking place at the electrode at the same rate. Considering this, the OCP is not strongly related with the area of the electrode, but with the relative activities of the electrochemical species. In this sense, the wetting of the electrode should have a small effect on the open circuit transient, explaining why we have not seen any difference between in the OCP with the addition of surfactant, and hence, based on the experiments shown, we cannot conclude that the wetting of the electrode is not a limiting step in the performance of the electrode when there is a current flowing.

To study the wetting of the electrode, contact angle measurements where made. These measurements consisted in placing a 0.2 μl drop of solution on top of a fresh, dry SPE and monitoring the variation with time of the contact angle of the drop with the electrode. This contact angle is related with the surface tension forces. In the absence of other forces, the mutual attraction of the molecules of a liquid caused the liquid to coalesce to form spherical droplets.

Surface tension can be thought of as the force that holds a liquid together. In the depths of a volume of liquid, each molecule is surrounded on all sides by other molecules; the forces between them balance out and these molecules inside the liquid are in equilibrium. The situation is different at the surface of the liquid, as can be seen in Figure 51. At the liquid-air interface for example, the molecules at the surface are being attracted by the surrounding liquid but far less from the surrounding molecules of air, so the forces are not balanced, and there is a net effect that pulls the molecule

towards the interior of the liquid. In this case, the molecules of the liquid tend to minimise the surface in contact with the air, forming a sphere, since the sphere has the largest volume/surface ratio.

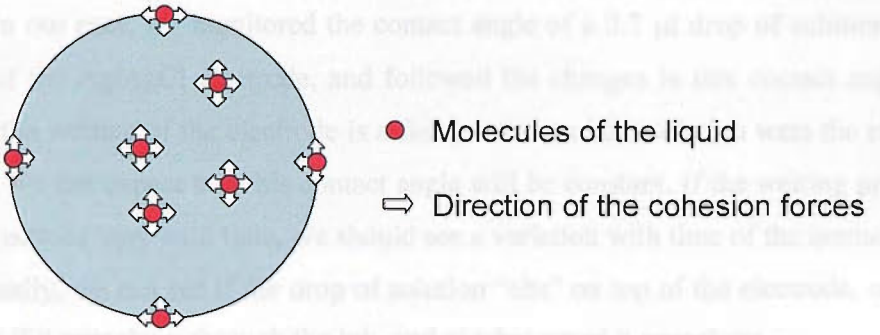

Figure 51 Schematic representation of the cohesion forces that keep a liquid together.

The case is different when the drop of liquid is on top of a surface. In this case there will be three different interfaces (and three different energies), the liquid / solid interface (surface-liquid energy), the liquid / air interface (surface tension energy) and the solid / air interface (surface energy). Depending on the magnitude of these forces we can have two situations, as shown in Figure 52.

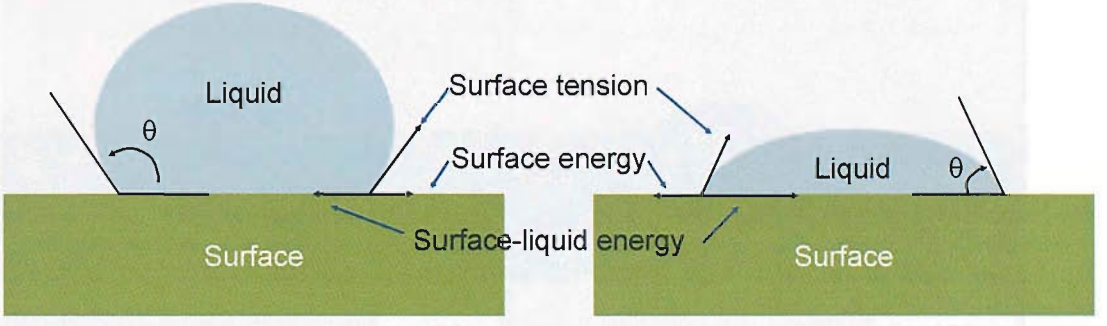

Figure 52 Balance of forces that establish the shape of a drop of liquid on a surface in contact with air. Left, hydrophobic; right hydrophilic.

In Figure 52 we can see the different forces that define the shape of a drop of liquid on a surface. For a constant surface energy, if the surface-liquid energy is larger than the surface tension, the drop will try to maximise the liquid / surface interface; hence the liquid will spread on the surface. In this case, the contact angle (θ, the angle between the surface / liquid interface and the liquid / air interface) will be smaller than 90°, and it is said that the liquid wets the surface (and that the surface is hydrophilic, if the liquid is water or an aqueous solution). In the opposite case, if the surface tension is larger than the surface-liquid energy, the drop will try to minimise the liquid / surface interface, and will not spread on the surface, but "sit" on top of it. In this case, the

contact angle will be larger than 90° and it is said that the liquid does not wet the surface (and that the surface is hydrophobic, if the liquid is water or an aqueous solution).

In our case, we monitored the contact angle of a 0.2 µl drop of solution placed on top of the Ag/AgCl electrode, and followed the changes in this contact angle with time. If the wetting of the electrode is a fast process and the solution wets the electrode quickly, we can expect that this contact angle will be constant. If the wetting properties of the electrode vary with time, we should see a variation with time of the contact angle. Additionally, we can see if the drop of solution "sits" on top of the electrode, or on the contrary if it percolates through the ink, and at what speed it percolates.

For this experiment, apart from removing the lidding tape on top of the SPE, the two meshes were also removed. The main purpose of these meshes is to define a cell volume and to spread the drop of sample on top of the electrode by capillarity, so the presence of these mashes would alter the results of this experiment.

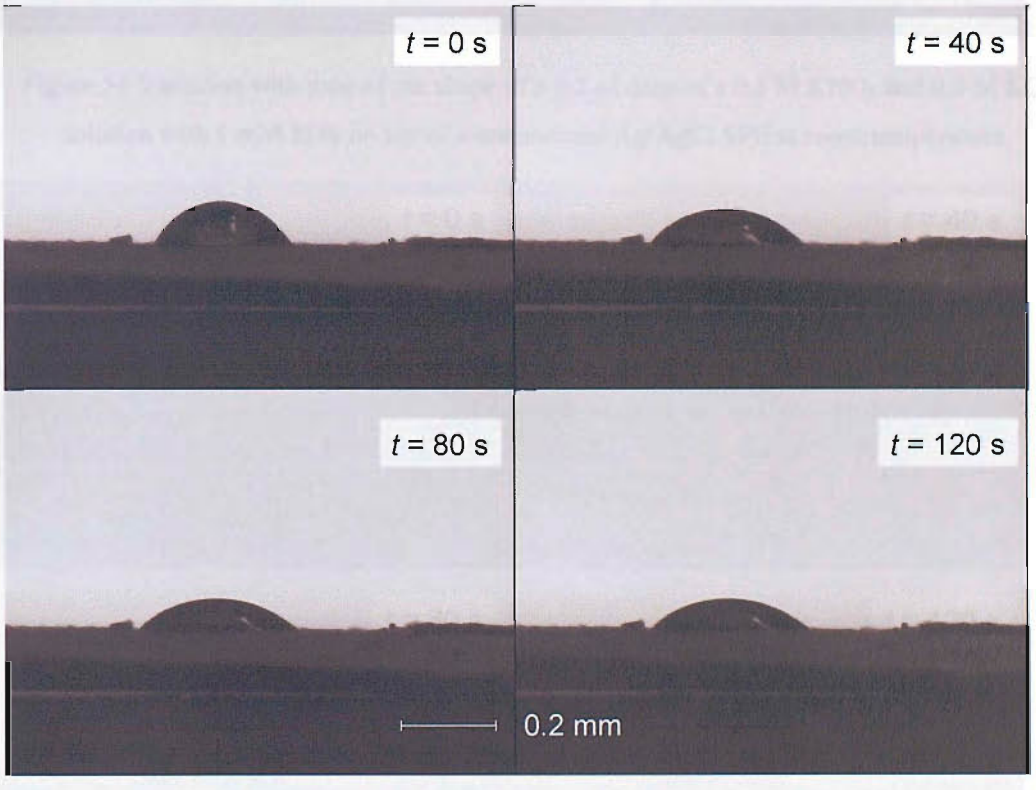

Figure 53 Variation with time of the shape of a 0.2 µl drop of a 0.5 M KNO_3 and 0.3 M KCl solution on top of a commercial Ag/AgCl SPE at room temperature.

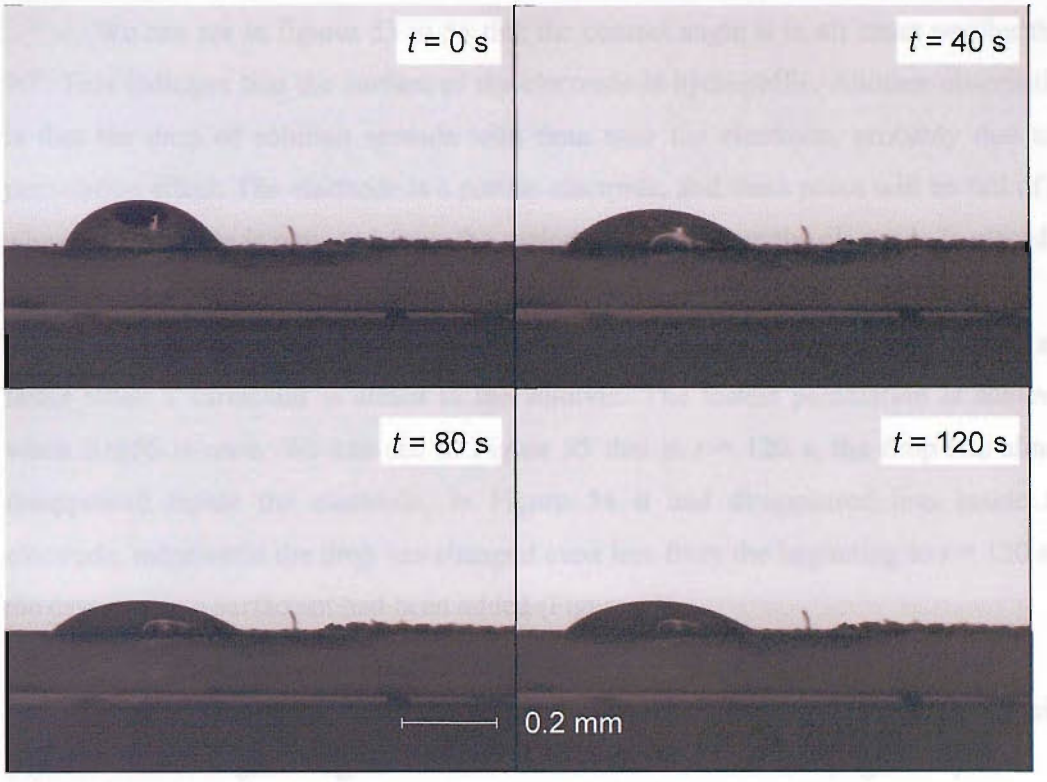

Figure 54 Variation with time of the shape of a 0.2 µl drop of a 0.5 M KNO_3 and 0.3 M KCl solution with 1 mM SDS on top of a commercial Ag/AgCl SPE at room temperature.

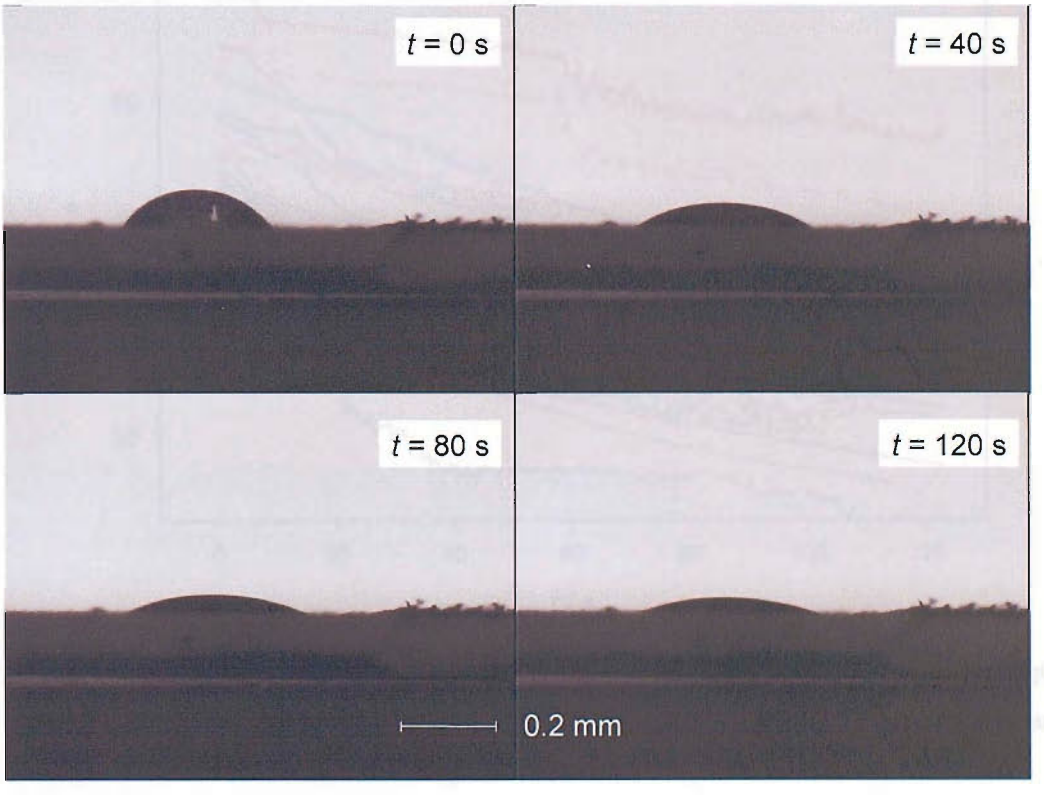

Figure 55 Variation with time of the shape of a 0.2 µl drop of a 0.5 M KNO_3 and 0.3 M KCl solution with 1 mM Brij 56 on top of a commercial Ag/AgCl SPE at room temperature.

We can see in figures 53 to 55 that the contact angle is in all cases smaller than 90°. This indicates that the surface of the electrode is hydrophilic. Another observation is that the drop of solution spreads with time over the electrode, probably due to a percolation effect. The electrode is a porous electrode, and these pores will be full of air when the electrode is removed from the sealed package. Once the electrode is placed in solution, these pores will be filled up with the solution (percolation).

We can see in the previous figures that the drop of solution spreads further and faster when a surfactant is added to the solution. The fastest percolation is achieved when Brij56 is used. We can see in Figure 55 that at t = 120 s, the drop has almost disappeared inside the electrode, in Figure 54 it had disappeared less inside the electrode, meanwhile the drop has changed even less from the beginning to t = 120 s in the case were no surfactant had been added (Figure 53).

We can also study this variation of the wetting of the electrode by comparing how the contact angle changes with time for the different solutions (Figure 56).

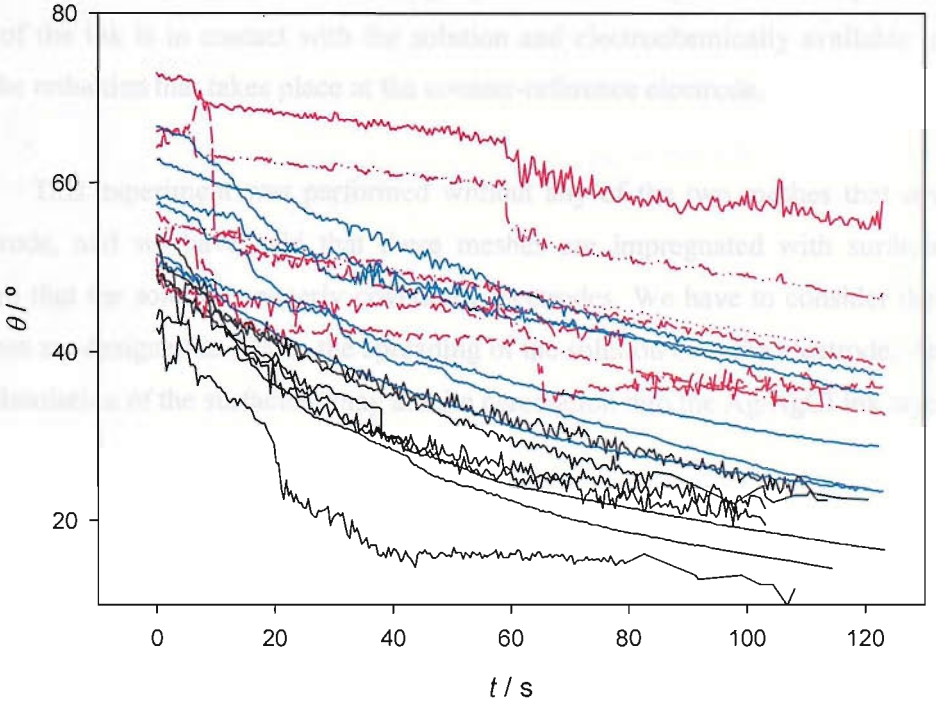

Figure 56 Variation of the contact angle (θ) of a 0.2 µl drop placed on top of a fresh Ag/AgCl SPE with time. The solutions used were 0.5 M KNO_3 plus 0.3 M KCl with different surfactants added. Black, 1 mM Brij56; blue, 1 mM SDS; red, no surfactant.

Figure 56 shows how the contact angle changes with time. We can see that the change is faster for the solution contained Brij56 (black lines), and that lower values of

the contact angle (as small as 20°) are recorded in this case on the time scale of the experiment. These low contact angle values show that the drop is extensively spread on the surface of the electrode, and that the wetting is faster and more effective in the presence of surfactants, and especially in the presence of Brij56, a non ionic surfactant.

Although MediSense claims that the wetting of the electrode occurs within the first seconds after the electrode is placed in solution[146], we can see here that the wetting of the electrode is an important issue. A drop of solution on top of the electrode takes 2-3 minutes to percolate inside the pores and throughout the structure of the electrode. This time compares unfavourably with the time scale of the measurement of glucose in the overall sensor, since the measurement takes place within the first 30 seconds after the drop of sample has been placed on top of the sample. Considering this time scale, when the measurement is taking place, only a fraction of the Ag/AgCl will be wetted with the solution, and electrochemically available. What is more, the goal of the project is to obtain a glucose sensor that could work within 3 seconds of placing the drop in solution. In that case, with the actual Ag/AgCl SPE, it is expected that only the topmost part of the ink is in contact with the solution and electrochemically available to carry out the reduction that takes place at the counter-reference electrode.

This experiment was performed without any of the two meshes that cover the electrode, and we have said that these meshes are impregnated with surfactants to ensure that the solution properly covers the electrodes. We have to consider that these meshes are designed to favour the spreading of the solution over the electrode. Anyway, the dissolution of the surfactant may aid the percolation into the Ag/AgCl ink layer.

4.13. Wetting of the electrode

The experiments shown in previous section suggest that it takes a certain time for the solution to percolate through the ink, and hence the area of the electrode in contact with the solution changes with time. We have also suggested that the OCP is not a suitable electrochemical tool to study how the electrode wets, as the potential depends on the activity of the different species in solution, but not in the area of the electrode

The case is different if some current is passing through the electrode, where the current is proportional to the area of the electrode as we have already mentioned (current over-potential equation, Equation 11). In this sense, right after the SPE is dipped in solution, there should be a small amount of Ag/AgCl available to carry out the reduction. As more solution percolates inside the electrode, more area will be available, and the reduction current can be passed with less overpotential required (it is easier - smaller overpotential- the larger the area of the electrode, as it is shown in Equation 11).

To identify how the wetting of the electrode affects the chronopotentiometry, several fresh electrodes were placed in a solution containing 0.5 M KNO_3, 0.3 M KCl and saturated AgCl, and the chronopotentiometry at -5 μA was recorded at different times after immersing the electrode in solution. The transients obtained are shown in Figure 57.

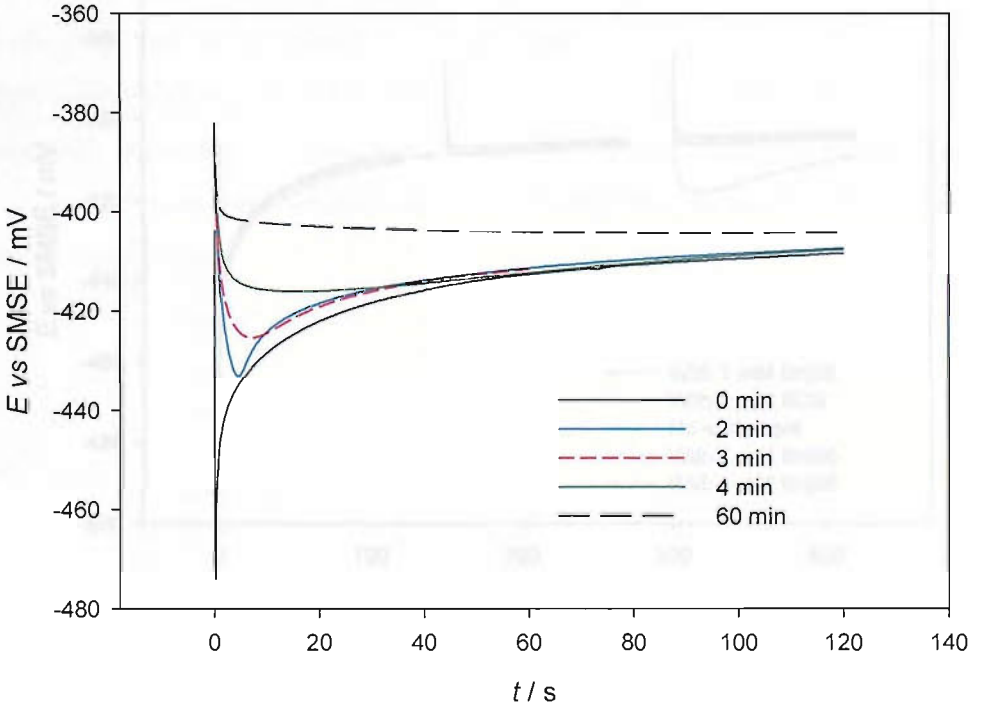

Figure 57 Effect of the time elapsed between a fresh SPE is placed in solution and the start of the chronopotentiometry at -5 μA in 0.5 M KNO_3, 0.3 M KCl and saturated AgCl. Each measurement was done with a different SPE.

We can see in Figure 57 that there is a change in the shape of the transient to less negative potentials, the longer the time the electrode is left in solution. This change affected only the potentials at short times, but all the electrodes behaved identically after

approximately 30 seconds. Even the SPE left in the solution for a very long time (1 hour) shows similar potentials as the control electrode (electrode measured right after immersing it in the solution).

Actually this experiment contradicts our statement that there is a wetting effect. It is evident that there is a change in the transients, but if the potential was only related with the time the electrode has been in solution, we should expect that the potential at beginning of the transient recorded after the electrode has been 2 mins in solution (beginning of blue line in Figure 57) should be the same as the potential after two minutes of the electrode that was scanned right after it was placed in solution (end of black solid line); but this is not the case. To corroborate this, we have run a similar set of experiments, but adding 1 mM of surfactant to the solution (Brij56 in one case, and SDS in the other).

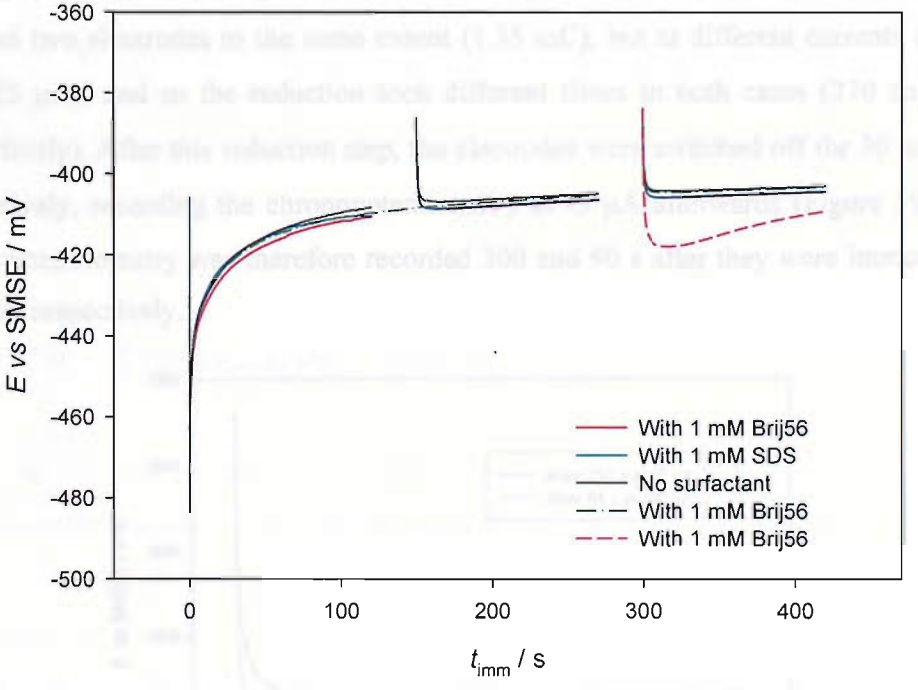

Figure 58 Chronopotentiometry at -5 μA of several SPE in 0.5 M KNO_3 and 0.3 M KCl, with or without surfactant. The potential is plotted against the time elapsed since the electrode has been placed in solution (t_{imm}). The black, red and blue solid lines were recorded with three different electrodes, stopping the chronopotentiometry for 30 seconds every 2 minutes. Dashed-dotted green line was recorded for 4.5 min, then stopping for ½ minute, and starting again. Dashed red line represents the transient of a fresh SPE 5 min after immersing it in the solution.

Several important features have to be addressed in Figure 58. First of all, the transients are very similar with (red and blue solid lines) and without (solid black line)

surfactant. This means that the current is not limited by the wetting of the electrode. In addition, we can see comparing the green dashed-dotted line with any of the solid lines that the electrode evolves during the *"cell off"* periods (between 120 and 150 s). We could expect that the potential was the same before and after switching the cell off (t = 120 s and t = 150 s), but we can see that the potential is slightly less negative after the *"off"* period, following the same tendency as the electrode we have not switched off. This means that the electrode is evolving even though we are not passing any current. Actually, we can see that the electrode does evolves faster to less negative potentials when we are passing some current than when the electrode is just immersed in the solution, as we can see comparing the dashed red line and the solid red line at t > 300 s.

Instead of comparing electrodes that have been in the solution the same periods of time but with different charges transferred, we can compare electrodes that are equally reduced but that have been in solution for different times. In this case, we have reduced two electrodes to the same extent (1.35 mC), but at different currents (-5 μA and -25 μA), and so the reduction took different times in both cases (270 and 54 s respectively). After this reduction step, the electrodes were switched off for 30 and 36 s respectively, recording the chronopotentiometry at -5 μA afterwards (Figure 59). The chronopotentiometry was therefore recorded 300 and 90 s after they were immersed in solution respectively.

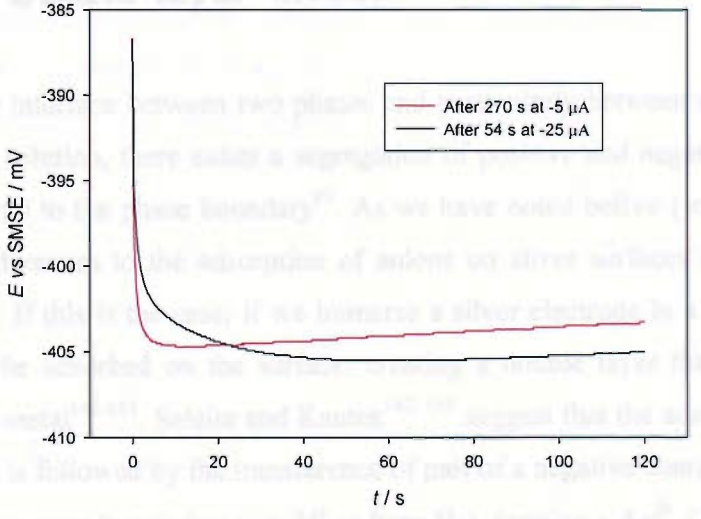

Figure 59 Chronopotentiometry at -5 μA in 0.5 M KNO_3, 0.3 M KCl and 1 mM of Brij56 of two SPEs after a reduction step performed in the same solution at -5 μA for 270 s and at -25 μA for 54 s (red and black lines respectively).

We can see in Figure 59 that the transients are different, thus suggesting that not only the reduction charge but also the period of time the electrode is kept in the solution are important. This set of experiments proves that the electrode evolves in solution even though there is no current passing. We can also say that the wetting of the SPE does not limit the chronopotentiometry, and thus the shift of the potential with time to less negative values when the electrode is poised cathodically cannot be explained by means of an increase of the available area to carry the reduction as the solution wets the Ag/AgCl layer.

At this moment we have to clarify how the glucose blood analysis takes place in the overall sensor. First of all, the sensor strip is extracted from the sealed package and inserted in the meter, so the meter gets to a *"stand by"* hold. Then the drop of blood is applied to the strip and it is driven from the application point to the electrode area. As soon as the sample touches the reference electrode, there will be an electrical connection between the working and the counter-reference electrode, triggering the analysis. Operating in this way, the analysis is performed exactly every time under the same circumstances (*i.e.* the SPE has been wetted for the same length of time).

4.14. Double layer model

At any interface between two phases and particularly between an electrode and an electrolyte solution, there exists a segregation of positive and negative charges in a direction normal to the phase boundary[90]. As we have noted before (section 4.6), there are several references to the adsorption of anions on silver surfaces in the literature, especially Cl^-. If this is the case, if we immerse a silver electrode in a Cl^- solution, the chloride will be adsorbed on the surface, creating a double layer that has a positive charge on the metal[141-145]. Salaita and Kautek[142, 145] suggest that the adsorption of Cl^- on Ag electrodes is followed by the transference of part of a negative charge from an Ag to any electron acceptor in solution (*e.g.* H^+ to form H_2), forming a $Ag^{\delta+}$ Cl^- species.

In this case, the solution near the silver will have an opposite charge to compensate the charge of the Ag particle. Actually, the charge at the silver will depend on the value of the potential and the value of the PZC (potential of zero charge). The PZC is the value of the potential where the excess charge at the electrode is zero.

This segregation of charged particles at the interface between the particles and the solution creates a capacitor at any electrode/electrolyte interface; the adsorption of ions on the surface of the electrode charges this capacitor up. Charging this capacitor (establishing the double layer) will require a variation of the potential through:

$$V_C = V\left(1 - e^{\frac{-t}{RC}}\right) \qquad \text{Equation 30}$$

where V_C is the potential across the capacitor, V the applied potential, R the resistance and C the capacitance. The charge on the capacitor will increase with time, and as a result so will the potential V_C. We can see from Equation 30 that the potential difference across the capacitor changes as the charging of the double layer progresses. It could be possible then, that once the Ag/AgCl electrode is placed in solution, the OCP varies as the double layer is charged.

In this case, there should be a Galvani potential drop across the inner layer and diffuse layer. If specific adsorption is weak, the positive electrode charge is only partially shielded by the adsorbed inner layer of anions, and consequently a diffuse layer of solvated anions is established. In the case of a strong specific adsorption, the specifically adsorbed charge may exceed the positive charge on the electrode, causing a charge reversal at the outer Helmholtz plane, so in this case a diffuse layer of cations will be established, reversing the overall potential of the double layer. A schematic representation of this effect is shown in "Instrumental Methods in Electrochemistry"[90], pages 163-165, and it is shown in Figure 60.

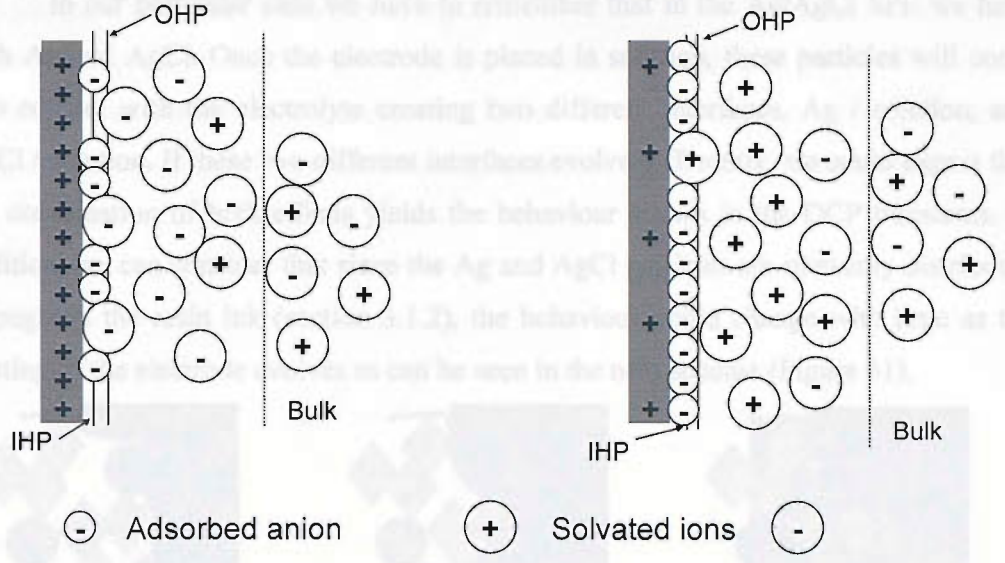

Figure 60 Schematic model of the ion distribution across the metal-electrolyte interface for weak specific adsorption (left) and strong specific adsorption (right). IHP is the inner Helmholtz plane, OHP is the outer Helmholtz plane. Small circles are unsolvated species, large circles are solvated species.

This change in potential between strong and weak adsorption of anions (specifically, Cl^-) could be an explanation of the reversal of the drift seen when comparing the transients for higher and lower concentrations of chloride. In this sense, if we are to explain the different shapes of the OCP transients performed with different [Cl^-] (*e.g.* figures 44 and 46), we can consider that the double layer charge is zero at the beginning of the experiment (when the electrode is not placed in solution), and that this double layer charges up once the electrode is placed in solution, to positive potentials if the [Cl^-] is low, and to more negative potentials for large [Cl^-].

This model also predicts that at lower concentrations, there will not be enough anions in the vicinity of the electrode to counterbalance the superficial charge of the electrode, so more Cl^- should diffuse from the bulk towards the electrode. On the other hand, at larger concentrations of Cl^-, the build up of the double layer will be faster, since there is more Cl^- available near the electrode. Consequently we could expect that the equilibration of the electrode will take more time in diluted solutions than in concentrated solutions. An implication of this model is that the Cl^- is more strongly specifically adsorbed at the electrode than the ions from the supporting electrolyte (KNO_3 or PBS).

In our particular case we have to remember that in the Ag/AgCl SPE we have both Ag and AgCl. Once the electrode is placed in solution, these particles will come into contact with the electrolyte creating two different interfaces, Ag / solution, and AgCl / solution. If these two different interfaces evolve differently, we could expect that the combination of both effects yields the behaviour shown in the OCP transients. In addition, we can consider that since the Ag and AgCl particles are unevenly distributed throughout the resin ink (section 3.1.2), the behaviour could change with time as the wetting of the electrode evolves as can be seen in the next scheme (Figure 61).

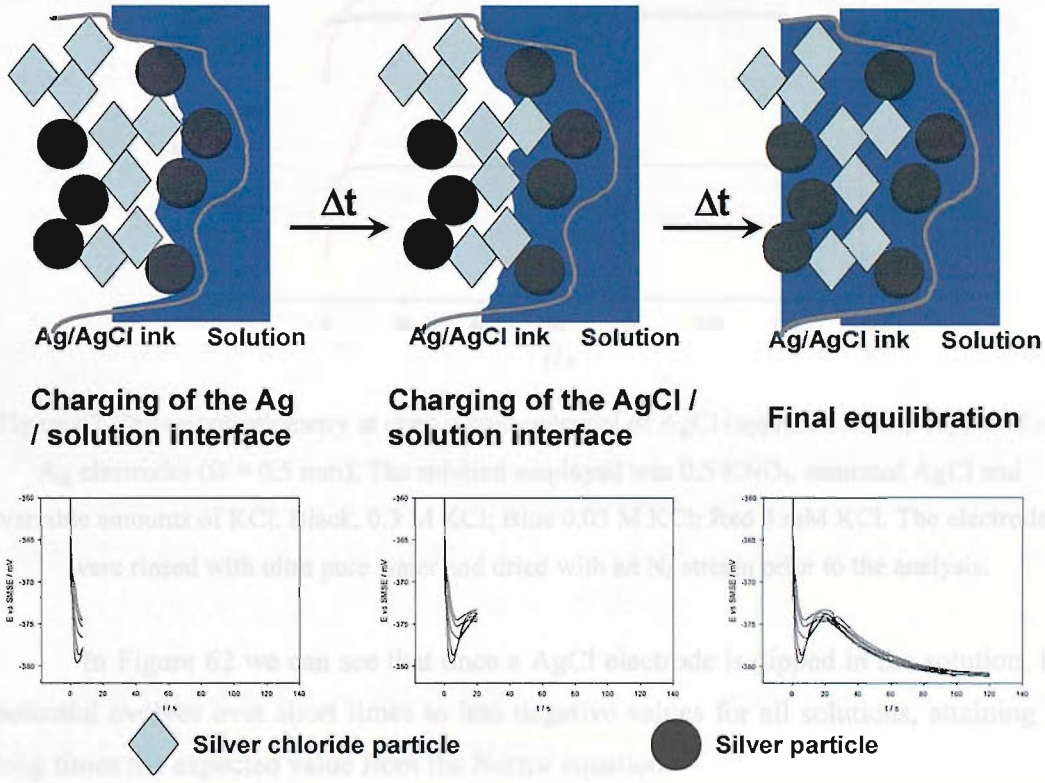

Figure 61 Schematic representation of the different stages of the wetting of the electrode, as well as the expected potential transients. The potential transient is the same transient show in Figure 44, at 25 °C.

To test this model we investigated the effect of immersing dry Ag and AgCl on Ag electrodes in solutions containing different concentrations of Cl^-, and recording the OCP of the electrodes from the moment the electrode is placed in solution. These Ag and AgCl on Ag electrodes were constructed using a Ag wire (with a diameter of 0.5 mm), embedded in epoxy resin. For some of the Ag electrodes a layer of AgCl was electrodeposited from saturated KCl and AgCl solution at +950 mV *vs.* SMSE. Considering the charge transferred (Q = 3.503 mC, 1.8 C cm^{-2}), the thickness of the AgCl layer was approximately 2.5 μm (assuming that the deposit is completely uniform

and compact, and that the density of AgCl is 5.56 g/cm^3)[147]. Prior to the measurement, these electrodes were rinsed with purified water and dried with a N_2 stream. Finally, the electrode was earthed to discharge any charge on its surface and the open circuit potential was recorded from the moment the electrode was dipped in the solution.

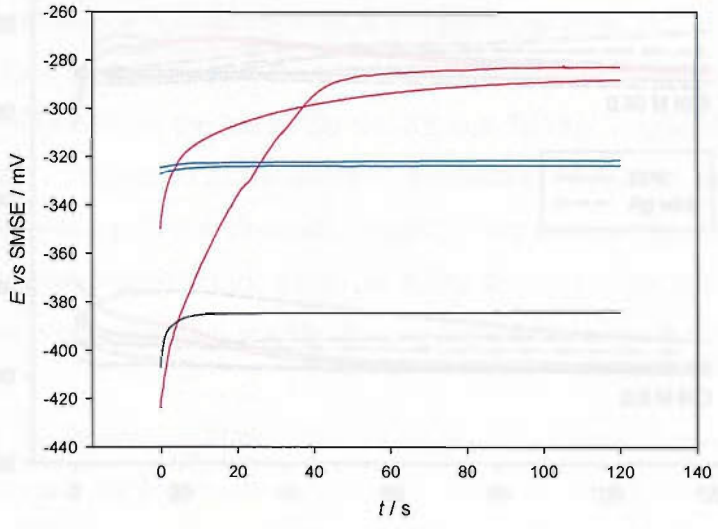

Figure 62 Chronopotentiometry at open circuit potential of AgCl (approx. 2.5 μm) deposited on Ag electrodes (Ø = 0.5 mm). The solution employed was 0.5 KNO_3, saturated AgCl and variable amounts of KCl. Black, 0.3 M KCl; Blue 0.03 M KCl; Red 3 mM KCl. The electrodes were rinsed with ultra pure water and dried with an N_2 stream prior to the analysis.

In Figure 62 we can see that once a AgCl electrode is dipped in the solution, its potential evolves over short times to less negative values for all solutions, attaining at long times the expected value from the Nernst equation.

In the case of the silver electrodes, these electrodes were polished with alumina (1 and 0.3 μm). The electrodes were then rinsed with water, dried with a N_2 stream and the chronopotentiometry at OCP was recorded from the moment the electrode is placed in solution. Afterwards, the electrodes were dipped in a solution containing 40 mM of $Na_2S_2O_3$ for at least 5 mins to dissolve any AgCl formed at the surface of the Ag wire[xx]. The electrodes were then rinsed with purified water and dipped in 6 M HNO_3 for 1 minute, followed by a wash with purified water and dried with a N_2 stream before scanning them again. We have employed this procedure between scans instead of just

[xx] Solutions of thiosulfate are usually employed in photography to dissolve the AgCl in the exposed film.

polishing the electrodes because we have found that with the polishing the transients are far less reproducible. We believe that the polishing step is not effective to remove impurities from the surface of the silver electrode.

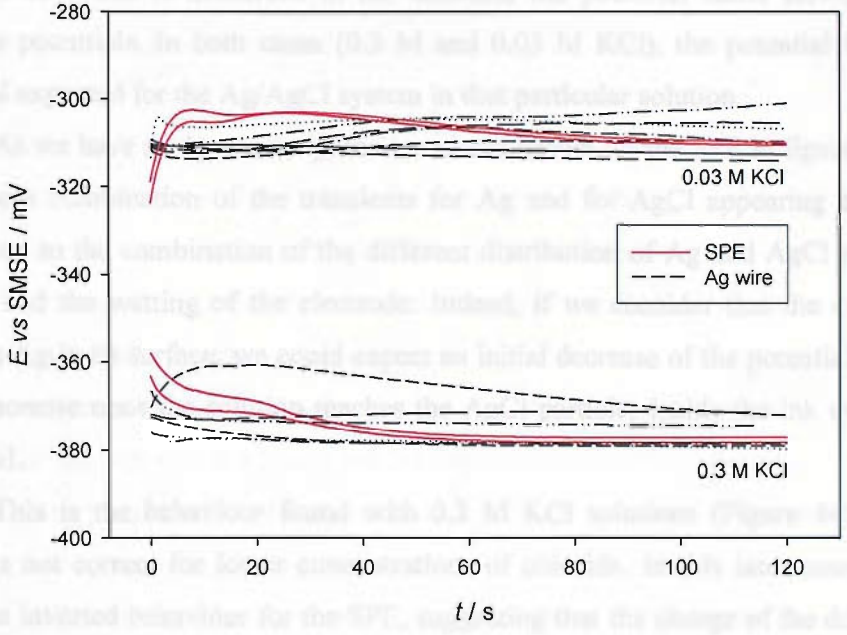

Figure 63 Chronopotentiometry at open circuit potential of Ag electrodes (Ø = 0.5 mm, black lines) compared to the transients of SPEs in the same solution (redlines). The solution used was 0.5 M KNO_3 with approx. 0.3 M or 0.03 M KCl. The solution was saturated with AgCl by the addition of $AgNO_3$.

The final potential in both solutions tends to the equilibrium potential of the system Ag/AgCl considering the concentration of Cl^-. Figure 63 also shows that the potential of the Ag wire is less stable and less reproducible than that of the SPE or that of the AgCl electrode show previously in Figure 62.

A crucial parameter in this case (Ag electrode) was how the solution was saturated with AgCl. If the solution was saturated with solid AgCl, the OCP were far more negative than those expected (around -450 mV *vs.* SMSE). These large potentials are believed to be due to the lack of enough Ag^+ in the solution to establish the Ag/AgCl equilibrium, so that the potential is established by another redox couple (probably $2Ag + ½\ O_2 \rightarrow Ag_2O$). For the transients recorded in Figure 63, the solution was saturated by adding $AgNO_3$ to the electrochemical cell. We have to consider that in this case, some Cl^- will precipitate with the excess Ag^+, reducing the concentration of Cl^- in the solution and thus shifting the potentials to less negative values.

There are some interesting features present here similar to those already shown for the SPE in Figure 35. The reproducibility and stability of the OCP decreases with the concentration of Cl^-. For the more concentrated Cl^- solution (0.3 M) we can see that once the electrode is immersed in the solution, the potential shifts slowly to more negative potentials. In both cases (0.3 M and 0.03 M KCl), the potential is near the potential expected for the Ag/AgCl system in that particular solution.

As we have said previously, the transients shown for the SPE in figures 44 to 47 could be a combination of the transients for Ag and for AgCl appearing at different times, due to the combination of the different distribution of Ag and AgCl particles in the ink and the wetting of the electrode. Indeed, if we consider that the electrode is richer in Ag in its surface, we could expect an initial decrease of the potential, followed by an increase once the solution reaches the AgCl particles inside the ink as shown in Figure 61.

This is the behaviour found with 0.3 M KCl solutions (Figure 44). But this model is not correct for lower concentrations of chloride. In this later case, we have found an inverted behaviour for the SPE, suggesting that the charge of the double layer is inverted, but that inversion was not found for the AgCl electrode. For AgCl on Ag electrodes (Figure 62) the potential shifted to less negative potentials for all chloride concentrations tested.

In addition we have to mention that some of the experiments done with Ag electrodes in 0.3 M and 0.03 M KCl showed a "wobble" in the OCP transient as show in Figure 64.

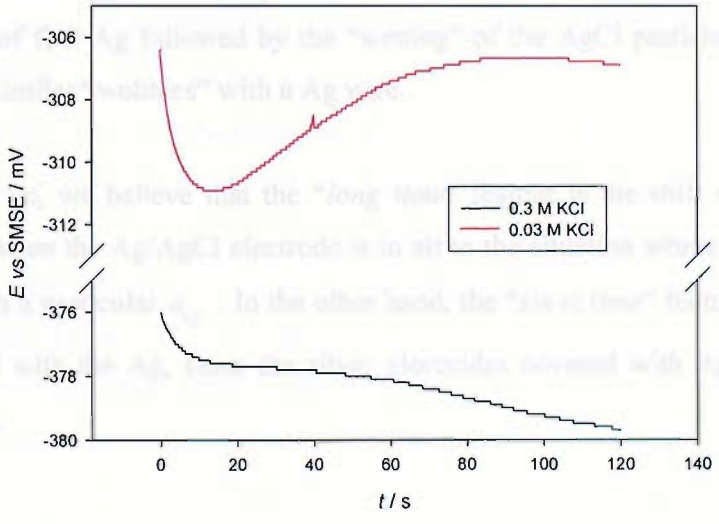

Figure 64 Detail of two OCP transients recorded with Ag wires after polishing and drying. The transient was recorded in 0.3 M KNO_3, saturated AgCl and variable amounts of KCl.

These transients are similar to those recorded for the SPE and this fact makes us believe that the transients recorded when the SPE is placed in solution are due to some reaction occurring on the Ag particles. Unfortunately, these transients recorded for the Ag electrodes appeared randomly and they could not be reproduced at will with the current procedure (mechanical polishing or dissolving slightly the Ag wire with 6 M HNO_3).

We believe that these "wobbles" are related with some process occurring on the Ag, and due to the time scale at which they appear; we believe that they are the same as the "*short time*" feature showed for the SPE. In addition, this feature is not related with the AgCl since we have never found any evidence of them in the experiments performed with AgCl on Ag electrodes.

It is interesting to note that in the two transients shown in Figure 64, the potential at the end of the experiment was approximately the same potential as at the beginning, right after the electrode was dipped in solution. We think that these "wobbles" are present in all the experiments performed with Ag electrodes, but they are too faint and could not be separated from the drift of the potential shown from the moment the electrode is placed in solution (potential ill defined by, probably, the interface between the electrode and the surrounding air) until it achieves equilibration (in this case, the potential is defined by the Nernst equation, as determined by the Ag/Ag^+ redox couple at this particular chloride activity). This long time shift is present here for Ag electrodes and we believe that it is the same as that seen previously for the SPE and called the "*long time*" feature.

Figure 64 also suggest that the potential transients seen for the SPEs are not due to the "wetting" of first Ag followed by the "wetting" of the AgCl particles, since we could reproduce similar "wobbles" with a Ag wire.

Summing up, we believe that the "*long time*" feature is the shift of the open circuit potential when the Ag/AgCl electrode is in air to the situation where it is wetted by a solution with a particular a_{Cl^-}. In the other hand, the "*short time*" feature is due to a process related with the Ag, since the silver electrodes covered with AgCl did not show this feature.

4.15. Nucleation

Another factor that could explain the "*short time*" feature is the presence of some additional Faradaic process at the electrode. In this case, we have to note that the electrode is held at open circuit potential, so no current passes externally through the external circuit.

In the previous section (section 3.9.1) we have shown that AgCl nucleates on the Ag particles at potentials slightly lower than the reversible Ag/AgCl redox potential. What is more, the characteristic nucleation loop disappeared if the electrode was placed in solution for a short time (usually 1-2 mins) before the potential sweep. This leads us to think that the nucleation can occur at the electrode without external current; thus it could also occur spontaneously in our setup under open circuit conditions, once the electrode is placed in solution. If this is the case, we should expect some drift of the potential, and this drift could be the potential drift that we can see at short times after the SPE is placed in solution.

As we have noted previously, the potential transients are due to two distinctive processes. The first one (at "*long times*") is probably due to the drift of the open circuit potential from a situation where the Ag/AgCl SPE is in air to the situation where it is wetted by a solution with a particular a_{Cl^-}.

Since this potential variation is positive (towards less negative potentials) for low concentrations of chloride, and *vice versa* for larger Cl^- concentrations, we assumed that there should be an intermediate Cl^-, and hence an associated value of the open circuit potential where the open circuit potential is the same right after the electrode is placed in solution and after the electrode has achieved its equilibration. From the data plotted in Figure 40, this Cl^- concentration was found to be 30 mM.

The models for nucleation normally describe the current *vs.* time transients while keeping the potential fixed. In our experiments so far, we have shown plots of potential against time, so additional experiments were carried out, and the measured potentiostatic transients were compared with different nucleation models.

The main problem that we found in our case is that in standard nucleation experiments, the potential is stepped from an equilibrium situation to an overpotential where the redox reaction takes place. In our case, the system evolves even at open

circuit potential once the SPE is placed in solution, so a careful selection of the potential at which we will perform the nucleation is needed.

Several electrodes (n = 4) were placed in a 0.5 M KNO_3 solution containing 30 mM KCl, and the final equilibration potential was recorded (average -319.8 mV *vs.* SMSE, with a σ = 0.9 mV). This potential was later used for the nucleation experiments, where the *i-t* transients were recorded from the moment the electrode was dipped in the solution.

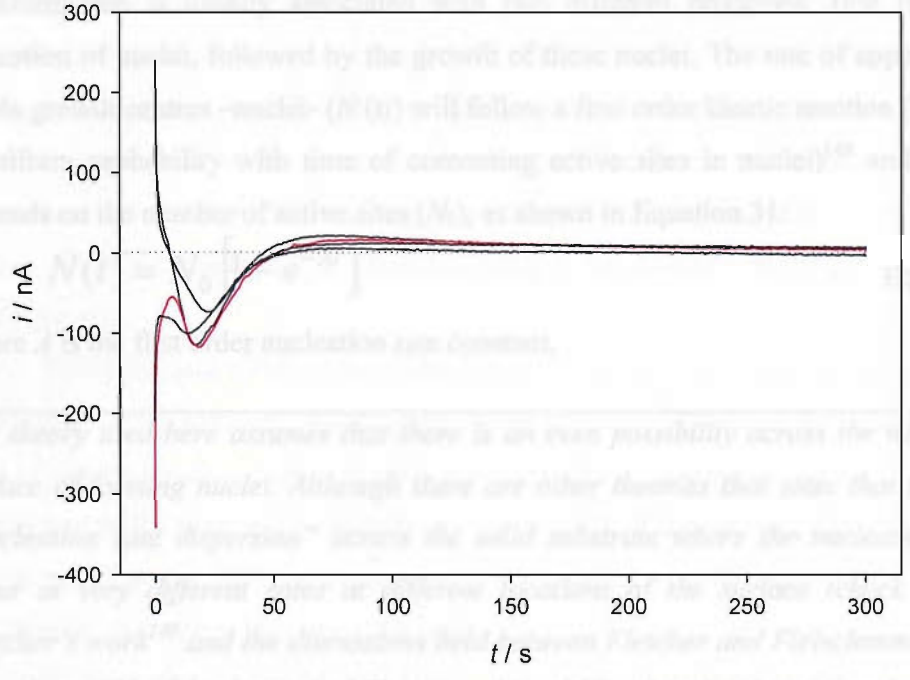

Figure 65 Nucleation transients recorded for four fresh screen printed electrodes held at -320 mV (red line) and -319 mV (black line) in 0.5 M KNO_3 + 30 mM KCl.

The resolution of the potentiostat does not allow control of the potential to tenths of millivolt, so -319.8 mV (average value of the equilibrium potential of the SPE in this solution) could not be achieved. In such a case, -320 mV (slightly reductive) or -319 mV (slightly oxidant) was applied.

First of all, we will discuss the limitations posed by the methodology that we are using. The potential chosen to perform the experiment (-319.8 mV) was an average value for four SPEs tested. Although the equilibrium potential is quite reproducible, we have to consider that there is a small variation between electrodes, so that the potential that we are applying could be slightly oxidising or reducing, but not precisely that of the equilibrium. This is probably the reason that explains why, after the peak in Figure 65,

the current does not drop back to zero in all the transients shown, but overshoots slightly, and the electrode changes from a situation where a reduction is taking place to one where an oxidation occurs. Also, we have to consider that the potential of the electrode after it is placed in solution is quite irreproducible, so the large difference between the curves seen in Figure 65 could be due to this irreproducibility.

The nucleation and growth mechanism of a system depends on several parameters. When an over-potential is applied to a system, the electrochemical phase transformation is usually associated with two different processes; first there is a formation of nuclei, followed by the growth of these nuclei. The rate of appearance of stable growth centres –nuclei- ($N(t)$) will follow a first order kinetic reaction (if there is a uniform probability with time of converting active sites in nuclei)[148] and this rate depends on the number of active sites (N_0), as shown in Equation 31:

$$N(t) = N_0\left[1 - e^{-At}\right] \qquad \text{Equation 31}$$

where A is the first order nucleation rate constant.

The theory used here assumes that there is an even possibility across the whole solid surface of forming nuclei. Although there are other theories that state that there is a "nucleation rate dispersion" across the solid substrate where the nucleation events occur at very different rates at different locations of the surface (check specially Fletcher's work[149] and the discussions held between Fletcher and Fleischmann[150-156] in the volume 530 of the Journal of Electroanalytical Chemistry), it is not the object of this Thesis to discuss these two approaches, but to provide a plausible explanation of the events occurring at the SPE when it is immersed in solution.

Then, we can have two extreme situations, depending on the value of At. If $At \gg 1$, $N(t)$ will be the same as N_0, so all possible active sites will become active nuclei (an instantaneous nucleation). Whereas if At is small, $N(t) = N_0At$ and the nuclei will be formed from active sites at a time dependant rate (progressive nucleation). An implication of this is that in an instantaneous nucleation process, all the nuclei are formed at the same stage, and hence they all grow at the same rate and they will all be of the same age. On the other hand, in a progressive nucleation process, active nuclei appear not only at early stage in the transients, but also when other nuclei are already growing, so the nuclei are of different sizes and different ages[157].

Once the nuclei are formed, and they start to grow, it is very important to note that the growth of each nucleus is not independent of each other, but that the growth of the nuclei will overlap with each other. This overlap means that the surface area available for the incorporation of materials into the lattice will initially increase with time until a maximum is achieved (a maximum of surface area), and from there on, the surface area decreases since the nuclei coalesce with each other, until we achieve a minimum of surface area were all the nuclei are aggregated in a unique continuous surface of minimal possible length.

Apart from the division mentioned before (instantaneous and progressive nucleation) the electrocrystalization can be divided according to the limiting step in the growth of the nuclei. In this case, we can have kinetic control, where the growth is limited by the lattice incorporation of adatoms to the periphery of a growing nucleus or diffusion control, where the limiting step is the diffusion of species to the growing nuclei. Another division can be made according to the direction of the growth (1D, 2D or 3D growth).

By investigating the shape of the current transient, and applying models of how the current varies with time found in the literature[148, 158-162], we can determinate which kind of nucleation and growth occurs. Normally, these models are function of several parameters as the number of available nuclei, density of the deposited species, the rate formation of nuclei, the rate constant of the formation of the deposit or the diffusion coefficient, parameters that are unavailable, *a priori*. Thus, it is usual to represent the transient in an adimensional form, where the ratio of the current to the current of the maximum is represented against the ratio of the time divided by the time at which the maximum appears [(i/i_m) *vs.* (t/t_m)], provided that there is a maximum. We will see that this is not always the case.

When the growth of the nucleus is limited by the diffusion of the species to the nuclei, the shape of the potentiostatic transient is characterised by a decrease of the current after the peak proportional to the $t^{-1/2}$ (Scharifker *et al*)[157], that is not our case. In addition, our experiments were performed at open circuit potential, so we should expect kinetic, rather than diffusion control.

In the case of 3D growth, where the current is limited by lattice incorporation, the current does not show a maximum[90]; at long times, the growth is limited to the direction perpendicular to the electrode, since the lateral growth is limited by the geometry of the electrode.

A similar case is the growth of the nuclei in only one direction (1D), under kinetic control. In the case of the instantaneous nucleation, it can be easily noted that the current will be independent of time. The current, and hence the charge deposited will be only a function of the number of growing nuclei and the rate of the deposition. In the case of progressive nucleation, the current will rise until all the available nucleation sites are already growing. In addition, 1D growth excludes any possibility of nuclei overlapping.

The last possibility that we have is 2D growth controlled by lattice incorporation. In this case, the theoretical models that describe the current transient[90, 158] appear in the following equations; equations 32 and 33 for instantaneous and progressive nucleation respectively.

$$\frac{i}{i_m} = \frac{t}{t_m}\exp\left(-\frac{1}{2}\frac{(t^2 - t_m{}^2)}{t_m{}^2}\right) \qquad \text{Equation 32}$$

$$\frac{i}{i_m} = \left(\frac{t}{t_m}\right)^2 \exp\left(-\frac{2}{3}\frac{(t^3 - t_m{}^3)}{t_m{}^3}\right) \qquad \text{Equation 33}$$

Figure 66 shows the dimensionless plot of the experimental data shown in Figure 65 compared with the last two models (equations 32 and 33).

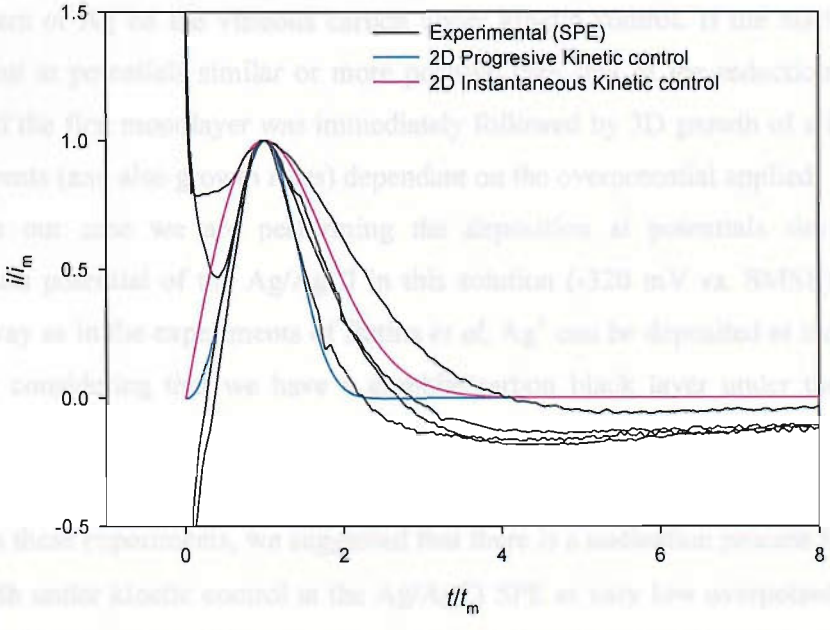

Figure 66 Comparison between experimental nucleation loops and theoretical ones. The experimental data is the same previously presented in Figure 65. The theoretical curves for the 2D nucleation under kinetic control were obtained from equations 32 and 33.

We can see in Figure 66 that our experimental data behaves similarly to the theory for a 2D nucleation under kinetic control. We can also see that the largest deviation between the theoretical model and our experimental data occurs at the beginning and at the end of the transient. As we have mentioned earlier, the initial part of the transients once the electrode is dipped in solution is very irreproducible. The last part of the curve depends on an adequate selection of the deposition potential.

Before the maximum, our experimental data fits better the progressive model, meanwhile after the maximum, the experimental data falls between the curves for instantaneous and progressive nucleation. We have to remember that "*instantaneous*" and "*progressive*" are the extreme situations of the same feature.

Since the nucleation shows a reduction process, we believe that the process involved could be the reduction of silver chloride to silver, or the reduction of Ag^+ to Ag. In the literature we have found that the formation of Ag from Ag(I) in $(NH_4)OH$ on a vitreous carbon electrode follows a similar pattern to the experimental results showed here. In this article[163], they carried out the deposition of several (2) layers of Ag at potentials 250 mV more positive than that obtained for the reduction wave of a cyclic voltammogram under the same conditions. With this experiment Batina *et al.* prove that if the nucleation and growth is carried out at potentials less negative than that of the reduction wave, they obtain a transient that accounts for the deposition of two monolayers of Ag on the vitreous carbon under kinetic control. If the nucleation was carried out at potentials similar or more positive than that of the reduction wave, the growth of the first monolayer was immediately followed by 3D growth of a layer of Ag with currents (and also growth rates) dependant on the overpotential applied.

In our case we are performing the deposition at potentials similar to the equilibrium potential of the Ag/AgCl in this solution (-320 mV *vs.* SMSE), and, in a similar way as in the experiments of Batina *et al*, Ag^+ can be deposited at the electrode, specially considering that we have a graphite/carbon black layer under the Ag/AgCl layer.

In these experiments, we suggested that there is a nucleation process followed by 2D growth under kinetic control at the Ag/AgCl SPE at very low overpotentials ($\eta \sim 0$ V). In a similar way, we can expect that this nucleation and growth occurs also at the SPE when the SPE is placed in solution and we monitor the OCP.

Before concluding that the "*short time*" feature present in the OCP transients (*e.g.* Figure 35 and figures between 44 and 47) is the nucleation and formation of AgCl, there are several factors that we have to address. Since the nucleation is occurring under kinetic control, the diffusion of Cl^- from the bulk towards the electrode should not affect the nucleation. Increasing the diffusion rate of Cl^- (i.e. by changing the temperature) should not affect the process. This is in agreement with our previous experiments, where the temperature does not affect the "*short time*" feature (figures between 44 and 47), but on the other hand, increasing the temperature should accelerate the rate of the nucleation, but no change in this direction was recorded.

This effect explains the positive (towards less negative potential) transients, but not the negative ones, present in the OCP transients of concentrated solutions (0.3 M KCl) as shown in 44. Also, this model does not explain the change of the "short time" transient with SDS.

4.16. Conclusions

The open circuit potential of the SPEs shows a transient potential, with equilibration times dependant on the concentration of chloride in the solutions. Several models were proposed to explain the behaviour of the electrode in these conditions. These models were tested by changing experimental parameters, but the response of these tests invalidated the models. A review of these experiments has been summarized in Table 5

Experiment	Results	Comments
Chloride concentration	Complete change of transients. Both at short and long times	Low concentration: The ΔE occurs towards less negative values
		Large concentration: The ΔE occurs towards more negative values
Ionic strength	Reduces the noise and the irreproducibility	No change in shape of transient
Temperature	Change of the "*long time*" feature	Shift of the equilibrium potential to less negative values. Faster equilibration of "*long time*" zone with increasing *T*.
Surfactants	More intense "*short time*" feature with SDS	Non ionic surfactant: No effect
		Ionic surfactant: More intense "short time" feature. Same time scale
Adsorption of Cl^-/ Release of Cl^-	Minimal variation of Cl^- in sample solution when the Ag/AgCl is placed in solution	Ink adsorbs 38 μg of Cl^- per gram of ink.
		Ink releases 5.5 μg of Cl^- per gram of ink.
Double layer	Not similar results	Experiments performed in Ag and AgCl on Ag in Cl^- solutions with diff concentration. Not comparable results as the SPE
Saturation of the solution with AgCl		No change
Removal of the meshes		
Leaving the electrode open		

Table 5 Experiments performed on the OCP transient of the SPE once it has been dipped in solution.

When the SPE is removed from the package it will have an OCP ill defined by, probably the interface between the Ag and AgCl particles and the surrounding air. Once the electrode is placed in solution, its OCP will evolve to that of the Ag/AgCl system in a saturated Ag^+ solution with a defined chloride activity (the Nernst equilibrium potential). This potential variation is probably the cause of the "*long time*" drift of the potential.

With the experiments shown here, we could not determine which mechanism describes the "*short time*" feature on the OCP transients recorded when the electrode is immersed in the solution. The experiments shown in this chapter, compared with others found in the bibliography, suggest that this part of the transient is related with a nucleation process on the electrode. We have also presented cyclic voltammetry scans featuring nucleation loops in section 3.9.1, and we have mentioned that these loops disappear if the electrode was left in solution for a certain time, suggesting that these two processes could be related and that it is likely that they are the same process.

Another explanation proposed was the adsorption of Cl^- anions on the electrode, and the building of a capacitor. In this case, the behaviour of a test model (Ag bulk electrode and AgCl deposited on an Ag electrode) matched the behaviour of the SPE at large Cl^- concentrations but could not explain the behaviour at lower Cl^-.

Another important feature shown in this chapter is that contact angle measurements showed that it takes some time for the solution to percolate thought the screen printed layer. We have also shown that neither the OCP transient nor the chronopotentiometry at -5 μA are affected by the wetting of the electrode since the addition of surfactant does not have any effect in the process.

At this time, we cannot propose a robust model that explains the features shown in the OCP transient of an SPE immediately after it is placed in solution.

5 New formulations as pseudo-reference counter SPEs

In this Thesis, we have tried to propose a reference electrode with good electrochemical properties, matching the requirements of the sensor and its constraints. In the introduction we mentioned that these requirements were:

- The potential of the reference electrode system should be maintained over a wide range of conditions (*e.g.* temperature), constant and invariant performance with solution composition and with low susceptibility to junction contamination or leaking that could contaminate the sample.[91, 164]
- The counter – reference electrode will be reduced during the measurement.
- The electrode will operate in a known solution (blood) with buffered pH and ionic strength. The composition of the sample could vary within certain pre-determined values.
- The electrode will be stored in a dried state, and it will be wetted with the sample at the moment of performing the measurement.
- The targeted time for measuring is 3 seconds from the moment the electrode touches the sample till the moment the measurement is made. The electrode must be equilibrated or behave reproducibly within that time span of the measurement.
- The electrode should be capable of being mass produced by screen printing technology, disposable, economic and robust.
- And last, but most important of all, the modification of the reference electrode should not force a change in the existing glucose meters. The electrochemical parameters (potential applied between counter – reference and working electrode) and the way the measurement is being performed must remain unchanged. If this last requirement is not met, a new medical approval (US FDA[xxi] and European Union validation) would be mandatory, with the subsequent cost of new clinical trials and investment in meters.

All these constraints seek the same goal: improvement of the reliability, speed and overall performance of the counter – reference electrode for the measurement of glucose in blood without changing the glucose sensor device.

[xxi] Food and Drug Administration

For this purpose, we tried two different approaches:

1. Silver chloride only counter reference electrodes. In this case, the system $AgCl + e^- \rightarrow Ag + Cl^-$ will be responsible for the electrochemical reaction occurring at the counter-reference electrode. The main advantage of this approach is that the system is greatly simplified; there is no Ag – AgCl interface initially present. The main drawback of this approach is that AgCl is poorly conductive (the conductivity of Gwent's AgCl powder was measured as $1.9 \times 10^{-6}\ \Omega^{-1}\ cm^{-1}$, *vide infra*, section 5.1.1), and removing the Ag component will significantly increase the resistance of the electrode. In fact, the Ag in the sensor acts mainly as an electrical conductor. To improve the conductivity of the electrode, the AgCl was mixed with graphite, to make a homogeneous ink.
2. Silver – silver chloride electrodes loaded with KCl. In the previous chapter, we observed that once the electrode is placed in solution, a decrease or increase in potential is recorded. Due to this drift, it takes the electrode approximately 60 seconds (depending on the concentration of chloride) to reach equilibrium. Solid KCl was added to the counter-reference-electrode to increase the concentration of Cl^- in the sample and so equilibrate the electrode faster.

5.1. Electrochemical behaviour of AgCl

Before starting with the reference electrode, we should study the behaviour of AgCl particles, and their electrochemistry. The first experiment performed was to look at the AgCl particles (Gwent Electrode Materials, UK) in the microscope. A thin layer of AgCl particles was placed on a microscope sample holder. In our case, we rubbed the sample holder against a polishing pad loaded with AgCl particles.

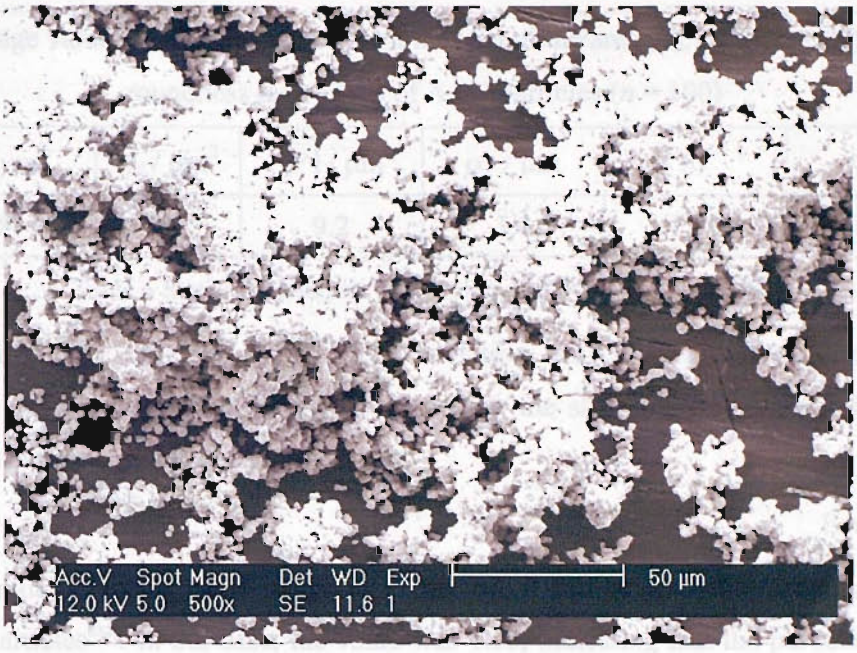

Figure 67: SEM image of AgCl particles deposited on a microscope sample holder.

In the SEM image in Figure 67, it can be seen that these AgCl particles are angular-spherical in shape with a large dispersion of sizes. In this picture it can be seen also that the particles tend to aggregate. Statistical analysis of the sizes of the particles was made with the AnalySIS software. For the analysis, several areas of the sample holder with a sparse coverage of particles were selected, and the analysis was performed choosing those isolated particles, as can be seen in Figure 68. The results obtained are summarised in Table 6.

Figure 68 Statistical analysis of the size and area of Gwent's AgCl particles.

Average values ($\bar{x}$) and standard deviation (σ) of the area (a), perimeter (P) and roundness factor (R_F) of AgCl particles (n = 100)					
$\overline{(a)}$ / μm^2	σ_a / μm^2	$\overline{(P)}$ / μm	σ_P / μm	R_F	σ_{R_F}
6.8	3.4	9.2	3.0	1.05	0.26

Table 6 Statistical analysis of sampled AgCl particles (n = 100).

From the values of the standard deviation, we can see that the size of the particles is highly variable. A way of measuring the shape of the particles is by the roundness factor. This factor is defined as[110]:

$$R_F = \frac{4\pi a}{P^2}$$ Equation 34

This formula states that for a circle the roundness factor is one, and near one for circular shaped particles[xxii]. In our case, the value was 1.05, indicating that the particles are, on average, circular. The large standard deviation (0.26) suggests that the shape is quite irregular. More important that the average of the area of the particles is their size distribution.

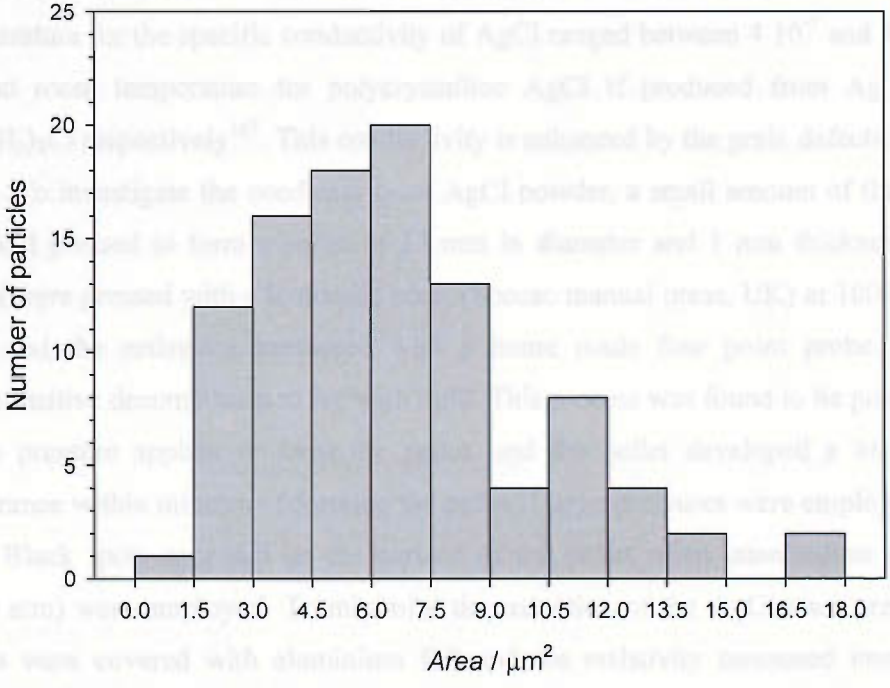

Figure 69 Histogram of the distribution of AgCl particles according to their areas (n = 100).

[xxii] The roundness calculation gives a value between 0 and 1. Note that because the perimeter and area are not computed precisely, it is quite unusual to get a roundess of 1, and eventually, values above 1 can be obtained. The roundness is useful, not as an exact measure, but rather as an approximation.

From the histogram in Figure 69, we can see that the most frequent size is between 6 and 7.5 μm^2. Considering a circular shape, and an estimate area of 6.75 μm^2, we conclude that the most usual particle geometry is a circle of 1.5 μm radius.

We have to be really careful when considering this image analysis. The first limitation is that the particles are considered as flat 2D objects. Thus, the area analysed is not the real geometric area, but the area they occupy in the direction normal to the electron beam. We suppose that the particles arrange in random orientations on the sample holder, and that there is no preferential arrangement of the particles in any particular direction. In this way, we can then assume that our analysis can be extrapolated to 3D by considering that the third dimension shows the same distribution mode as the analysed 2D. Thus, we consider the AgCl particles as roughly angular spheroids of 1.5 μm radius.

5.1.1. Conductivity of AgCl

AgCl is a conductor with low conductivity or large resistivity. Values found in the literature for the specific conductivity of AgCl ranged between 4 10^{-7} and 8 10^{-7} Ω^{-1} cm^{-1} at room temperature for polycrystalline AgCl if produced from Ag or from $Ag(NH_3)_2Cl$ respectively[165]. This conductivity is enhanced by the grain defects.

To investigate the conductivity of AgCl powder, a small amount of the powder was cold pressed to form a pellet of 13 mm in diameter and 1 mm thickness. These pellets were pressed with a hydraulic press (Specac manual press, UK) at 1000 kg (730 atm), and the resistance measured with a home made four point probe. AgCl is photosensitive decomposing to Ag with light. This process was found to be proportional to the pressure applied to form the pellet, and the pellet developed a black shiny appearance within minutes of forming the pellet if large pressures were employed (7300 atm). Black spots appeared on the surface of the pellet when intermediate pressures (3650 atm) were employed. To minimise the reduction of the AgCl once pressed, the pellets were covered with aluminium foil and the resistivity measured immediately afterwards.

The four point probe consists of four equally spaced contacts (numbered from one to four), all of them in contact with the substance to be measured. A current is passed through the 1st and 4th contacts, creating a potential drop across the resistive

substance to be analysed. The difference in voltage between the 2nd and 3rd contact is measured, and the resistivity obtained through[166]:

$$\rho = \frac{V}{i} Th \times k \times k' \qquad \text{Equation 35}$$

where ρ is the resistivity (in Ω cm), i the applied current between the 1st and 4th probes, V the voltage measured between the 2nd and 3rd probe, Th the thickness of the pellet, k is a correction factor that depends on the ratio of the spacing between the probes and the wafer diameter and k' is another factor that depends on the ratio between probe separation and wafer thickness. Considering that the spacing between the probes in our setup is approximately 0.9 mm and the diameter of the pellet is 13 mm, k equals 4.3646.[167] The ratio of the thickness of the pellet to the spacing of the probes was approximately 1, so k' is 0.9214.[167]

The resistivity (inverse of the conductivity) was measured at room temperature passing 1 μA across three pellets that were 13 mm in diameter and approximately 1 mm thick. Three measurements were made per pellet, rotating the pellet around between each measurement to probe different areas of the pellet each time. The conductivity obtained was 1.9×10^{-6} Ω^{-1} cm^{-1} and the standard deviation was 0.5×10^{-6} (n = 3 pellets). This value is larger than the values found in the literature[165] (between 4×10^{-7} and 8×10^{-7} Ω^{-1} cm^{-1}), but no evidence of how the measurements were made appears in that article. We can assume that although the AgCl pellet remained shiny-white after pressure, it could be possible that a thin layer of Ag (highly conductive) or small patches are formed on the surface of the pellet due to the pressure and the light, increasing the conductivity. Nevertheless, the obtained value means that the AgCl particles are poorly conductive.

5.1.2. Electrochemistry of the AgCl particles

The first problem to be solved before studying the electrochemical behaviour of AgCl particles is how to bring a solid compound into an electric field to study its electrochemical reactions. An excellent chapter from Fritz Scholz and Birgit Meyer explains several approaches for the attachment of solid particles to an electrode[111].

Two approaches for attaching the AgCl particles to the electrode were tried: rubbing a Glassy Carbon electrode (GCE) on the particles or mixing AgCl particles with carbon paste. Other approaches proposed by Scholz include the use of a packed electrode of the material to be studied (in this case AgCl) or electroanalysis of discrete particles by holding the particles between two electrodes[168]. The first one permits only

the analysis of conductive particles, meanwhile the last technique will not be representative, since it will only study the interface of the particle with the electrode, and not the interface between particles[168]. This limitation can be solved by using larger electrodes and holding a larger amount of material between the electrodes, but it was not tried in this work.

5.1.3. Glassy carbon electrodes

In this case, a GCE with an approximate diameter of around 4 mm was thoroughly polished with 1 and 0.3 μm Al_2O_3. Some AgCl was then transferred to the electrode by rubbing the electrode against a polishing pad covered with AgCl particles. Due to the ease in which AgCl is affected by light and air, the AgCl on the pad was removed and discarded every time.

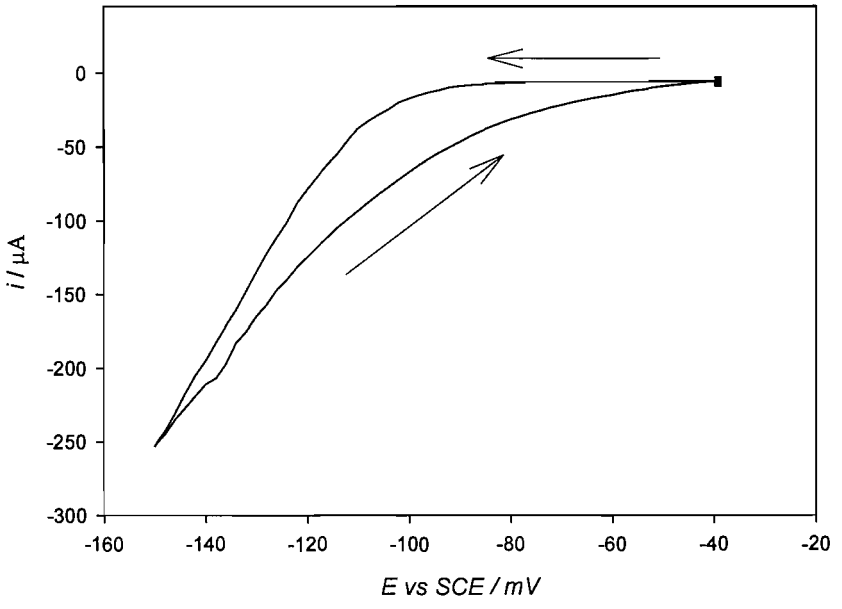

Figure 70 Cyclic voltammogram of AgCl particles on a GCE. Scan performed in 2 M KCl, at 20 mV/s.

The first important feature seen in this scan (Figure 70) is the appearance of a nucleation loop, very similar to the loop shown in Figure 34 for the SPE. On the forward scan, there is no current flowing until the scan reaches -100 mV (vs. SCE). The similarities between Figure 70 and Figure 34 supports our idea that the change in the nucleation loop shown in Figure 31 is due to the presence of two kinds of particles in the screen printed electrode that are reduced at different overpotentials, or at least, that

the process in region B in Figure 31 is due to the reduction of AgCl to Ag through a nucleation mechanism.

Some slow scans (at 1 mV / s) were also performed, and they are compared in Figure 71 with similar scans of screen printed electrodes (from Figure 17). In this case, and since a limited amount of AgCl is present in the sample, all of it was reduced on the forward scan. Then, an oxidative scan could be performed.

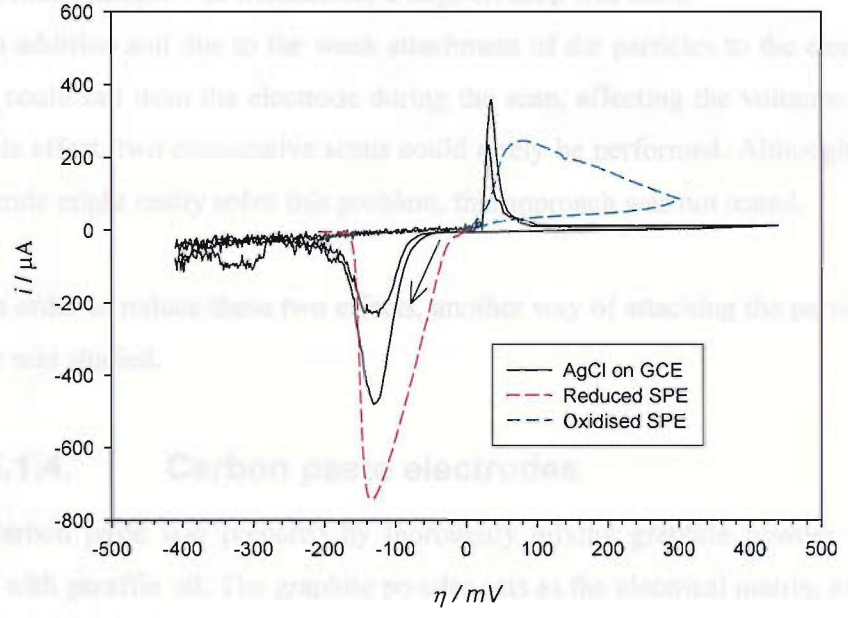

Figure 71 Solid lines, first scan of AgCl particles on a GCE (two repetitions). Scan started from OCP in 2 M KCl, at 1 mV/s. Dashed lines, reducing (blue) and oxidising (red) cyclic voltammogram of a screen printed electrode (SPE) performed under the same conditions.

In these scans we can see that an overpotential of around 60 mV is necessary to start to reduce the AgCl particles. Comparing these scans with those performed in the same conditions for screen printed electrodes, a separation of the peaks can be seen. The AgCl particles on a GCE need a larger overpotential to start the reduction than the AgCl particles in the SPE. At the beginning of the scan, there is only AgCl on the electrode, so a new interface (Ag/AgCl) should be formed. The creation of this new interface requires additional energy, in the form of potential.

On the first scan, since there is no silver, an overpotential of around -60 mV should be applied to create the new interface (Ag/AgCl) and start the nucleation of Ag on the AgCl particles. In the SPE, and since there are both Ag and AgCl particles present, this Ag/AgCl interface is already present and so there is no need to apply any extra overpotential. This is consistent with the model previously presented (section 3.9.1).

It is important to note that after the AgCl is reduced to Ag, there is still some Ag/AgCl interface remaining, and no extra overpotential is needed to start the oxidation. Consequently, the oxidation in the SPE and of the AgCl particles after reduction to Ag on the GCE occurs at a similar overpotential.

The major drawback of this technique (AgCl attached to a GCE) is that there is no control of the amount of material transferred to the electrode, and in some occasions when too much sample was transferred, a large *IR* drop was seen.

In addition and due to the weak attachment of the particles to the electrode, the particles could fall from the electrode during the scan, affecting the voltammetry. Also due to this effect, two consecutive scans could rarely be performed. Although inverting the electrode might easily solve this problem, this approach was not tested.

In order to reduce these two effects, another way of attaching the particles to the electrode was studied.

5.1.4. Carbon paste electrodes

Carbon paste was prepared by thoroughly mixing graphite powder and AgCl particles with paraffin oil. The graphite powder acts as the electrical matrix, as well as a diluent for the silver chloride. The paraffin oil was used in order to give the paste a sticky texture. Since this oil is immiscible in water the paste will remain stuck to the electrode. To this paste, we added AgCl and mixed it all with a mortar and pestle. The resultant paste was spread over the GCE (used as an electrical contact) with a spatula, covering it all with a thin layer. The paste was composed of 1 gram of solids per 0.37 ml of paraffin oil[119, 120] and contained a weight ratio of AgCl to graphite of 1 to 5 (12.6 % wt of AgCl, 62.9 % wt graphite and 24.6 % paraffin oil in the final mix[xxiii]).

Mixing the silver chloride with graphite forming the carbon paste has several advantages with respect to the previous technique (rubbing a GCE on a pad with AgCl) as:

- There is no need for the sample to have high electrical conductance since the conduction is mainly accomplished by the graphite.
- The currents can be kept within the desired range by altering the AgCl to graphite ratio. This means that signal resolution is improved.

[xxiii] The density of the paraffin oil is 0.88 kg l^{-1}

- In this case, AgCl particles, instead of being mechanically attached to the electrode, were embedded in a hydrophobic matrix, thus improving the mechanical properties. No detachment of the sample has been observed; several consecutive scans could be performed.
- The electrochemical reactions occur at the surface of the paste electrode, at this location, ion transfer between the solid sample and the electrolyte is possible.

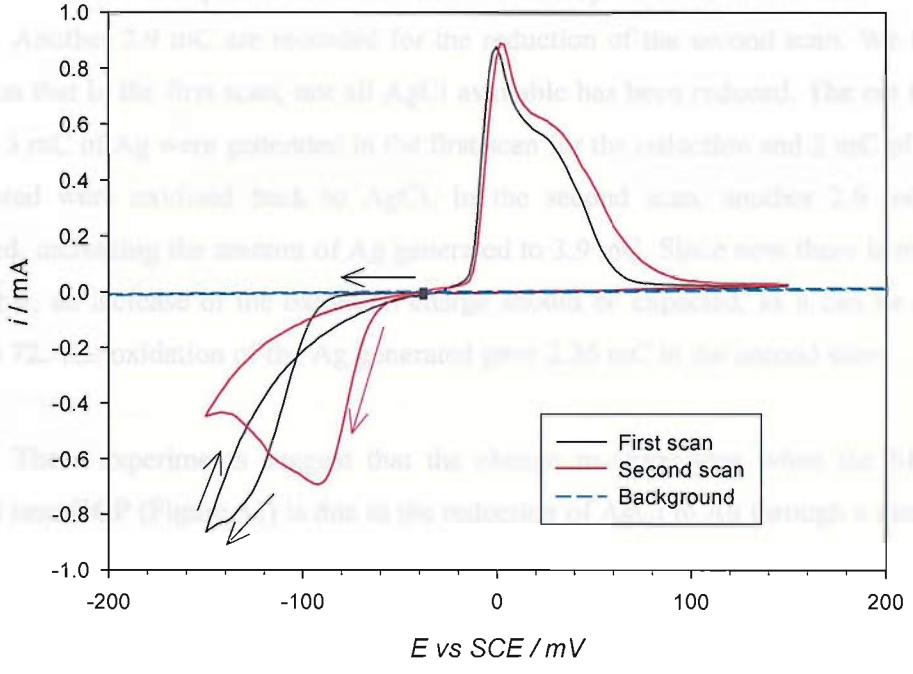

Figure 72 Two consecutive scans of a GCE covered with carbon paste loaded with 12.6 % in weight of AgCl particles on a GCE. Scan performed from OCP (black dot) in 2 M KCl, at 20 mV/s. In blue, a scan of carbon paste without any AgCl on the GCE.

Figure 72 shows, two consecutives scans of carbon paste loaded with AgCl. This scan features a nucleation loop. It is important to notice the shift in the starting potential of the reduction peak between the first and second scan, due to the need of an extra overpotential for the nucleation of Ag in the first scan. As we asserted before, this can be explained by means of the presence or absence of the Ag/AgCl interface on the electrode. We can also see in Figure 72 that the blank carbon paste (graphite and paraffin without added AgCl) is electroinactive in the potential range studied.

On the first scan, since there is no silver present, a potential of around -50 mV (vs. SCE) should be applied to create the new interface (Ag/AgCl) and start the

nucleation of Ag. In the second scan, this Ag/AgCl interface is already present and the reduction can start at smaller overpotentials (-20 mV). The charges obtained for the reduction of AgCl to Ag did not match the charges obtained in the oxidation scan (3 mC for the reduction and ~2 mC for the oxidation in the first scan), so not all the Ag formed during the reduction in the first scan is converted back to AgCl during the oxidation. This means that there is still 1/3 of the Ag remaining, so the reduction in the second scan can take place at smaller overpotentials. If this was not the case, and all the Ag was oxidised, we should expect to see a new nucleation loop for every new scan.

Another 2.9 mC are recorded for the reduction of the second scan. We have to mention that in the first scan, not all AgCl available has been reduced. The net balance is that 3 mC of Ag were generated in the first scan for the reduction and 2 mC of the Ag generated were oxidised back to AgCl. In the second scan, another 2.9 mC were reduced, increasing the amount of Ag generated to 3.9 mC. Since now there is more Ag available, an increase of the oxidation charge should be expected, as it can be seen in Figure 72. The oxidation of the Ag generated gave 2.36 mC in the second scan.

These experiments suggest that the change in slope seen when the SPE was cycled near OCP (Figure 31) is due to the reduction of AgCl to Ag through a nucleation mechanism. Also these experiments showed that embedding AgCl into the carbon paste is a suitable tool to study the Ag/AgCl system.

We can also see in figures 71 and 72 that the oxidation peaks feature some ill resolved shoulders at potentials slightly more oxidating than that of the oxidation of Ag to AgCl. Since the intensity, position and presence of this shoulder was quite random, we believe that this shoulder is due to some kind of impurity or contamination of the AgCl.

5.2. Graphite-AgCl counter reference electrodes. Preliminary studies.

As stated previously, there are several desired characteristics that a counter-reference electrode (CRE) should meet. The potential of the reference electrode system should be maintained over a wide range of conditions (*e.g.* temperature, sample

concentration), needing short equilibration times, constant and invariant performance with changes in solution composition and with low susceptibility to junction contamination or leaking that could contaminate the sample[91, 164]. All these characteristics should not be accepted faithfully without considering the particular characteristics of the system under study.

In our particular case (the screen printed electrode for glucose monitoring), we have mentioned that the Ag/AgCl electrode works at the same time as the reference and the counter electrode. At the working electrode oxidation takes place, while at the Ag/AgCl electrode reduction occurs. Since this is the case, both systems ($Ag + Cl^- \rightarrow AgCl + e^-$ and $AgCl + e^- \rightarrow Ag + Cl^-$) will not be necessary; actually in operation, only the reduction (silver chloride reducing to silver) will take place at the reference-counter electrode.

AgCl electrodes were tested as possible candidates to replace the Ag/AgCl ink. As we have mentioned in the introduction of this chapter, the AgCl was embedded in carbon paste to improve the conductivity of the electrode. A PTFE electrode with a stainless steel electrical contact in one end was constructed in such a way that it leaves a cavity in the other end. The size of this cavity was approximately a circle of 3 mm in diameter and a typical depth of 0.3 mm. The paste was packed inside the cavity. This paste had the same composition as the paste used in previous section (12.6 % of AgCl, 62.9 % graphite and 24.6 % paraffin oil, all percentages in weight).

The chronopotentiometric response at -5 μA of these electrodes was tested in 0.125 M KCl, and compared with the commercial Ag/AgCl SPE. This experiment is a good indication of the performance of the counter-reference electrode, as -5 μA is the current usually passed through this system in the device when low glucose levels are being oxidised at the working electrode[140].

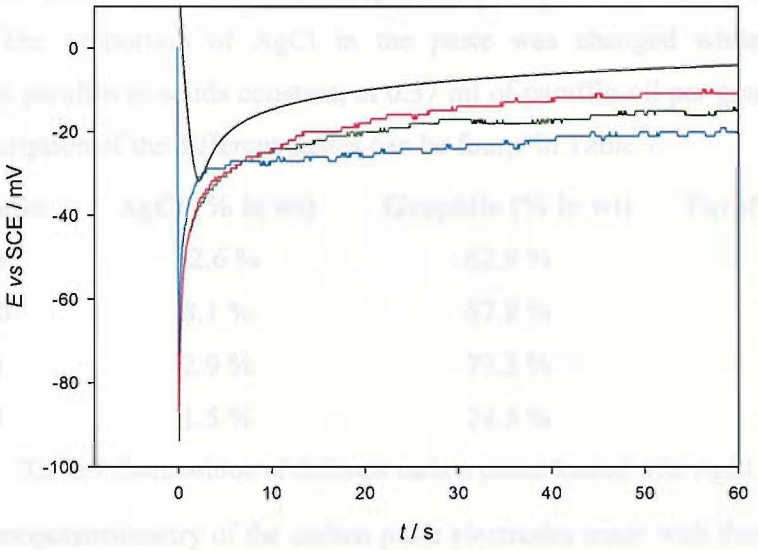

Figure 73 Chronopotentiometry at -5 μA of an Ag/AgCl screen printed electrode (in black) and three different AgCl loaded carbon paste electrodes in 0.125 KCl. The transients for the carbon paste and the SPE were recorded using instruments with different resolutions.

The low reproducibility of the carbon paste electrodes could be ascribed to the fact that the electrodes were hand made, pressing at different pressures different amounts of paste in the electrode. This amount of paste ranged between 12.5 and 15.5 mg. This will mean that the compactness of the paste varies from one electrode to another, forcing different amounts of AgCl to the surface of the electrode, and giving different active electrode areas.

The shape of the carbon paste curves is very similar to that of the screen printed electrode, but the potentials shown in the carbon paste experiments are higher than that of the Ag/AgCl electrode. Considering a fixed current density for this system, we could adjust the potential through a change in the area of the electrode. At a fixed current density, the larger the area, the more current can be driven through the system at similar overpotentials. In the same way, passing a fixed current will require smaller overpotentials the larger the area. This area can be increased by enlarging the geometrical area of the electrode, or by increasing the amount of AgCl in the surface of the electrode (increasing the concentration of AgCl in the paste). The reproducibility could be improved by using an automated manufacturing procedure

This experiment could be reproduced with a screen printable graphite ink previously loaded with AgCl. The electrodes build this way should offer a first alternative to the currently used screen printed Ag/AgCl electrode.

Carbon pastes with different compositions were studied as counter-reference electrodes. The proportion of AgCl in the paste was changed while keeping the proportion of paraffin to solids constant, at 0.37 ml of paraffin oil per gram of solids. A detailed description of the different pastes can be found in Table 7:

AgCl:C ratio	AgCl (% in wt)	Graphite (% in wt)	Paraffin (% in wt)
20: 100	12.6 %	62.9 %	24.1 %
12 : 100	8.1 %	67.8 %	24.1 %
4 : 100	2.9 %	73.3 %	24.1 %
2 : 100	1.5 %	74.5 %	24.1 %

Table 7 Composition of different carbon pastes loaded with AgCl.

Chronopotentiometry of the carbon paste electrodes made with these pastes were recorded *versus* SMSE in 0.5 M KNO_3 containing 30 mM KCl. Results appear in figures 74 and 75.

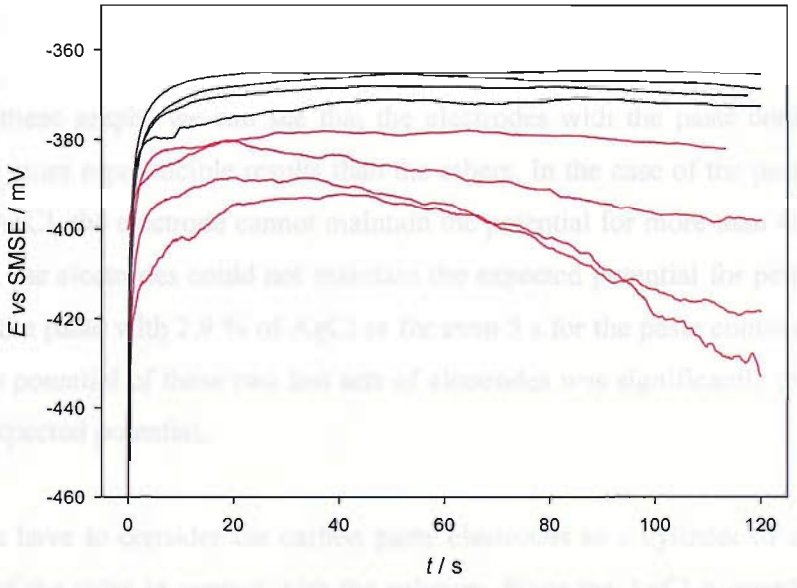

Figure 74 Chronopotentiometry at -5 μA of several carbon paste electrodes in a solution containing 0.5 M KNO_3 and 30 mM KCl. Black curves for electrodes with 12.6 % in weight of AgCl. Red curves for electrodes with 8.1 % in weight of AgCl.

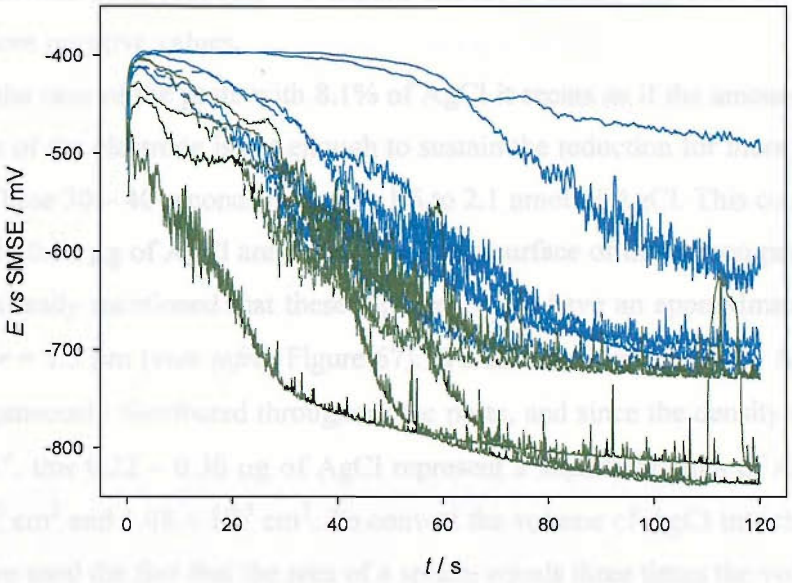

Figure 75 Chronopotentiometry at -5 μA of several carbon paste electrodes in a solution containing 0.5 M KNO_3 and 30 mM KCl. Blue curves for electrodes with 2.9 % in weight of AgCl. Green curves for electrodes with 1.5 % in weight of AgCl.

In these graphs we can see that the electrodes with the paste containing more AgCl give more reproducible results than the others. In the case of the paste containing 8.1 % of AgCl, the electrode cannot maintain the potential for more than 40 seconds. In Figure 75, the electrodes could not maintain the expected potential for periods as small as 20 s in the paste with 2.9 % of AgCl or for even 5 s for the paste containing 1.5 % of AgCl. The potential of these two last sets of electrodes was significantly more negative than the expected potential.

We have to consider the carbon paste electrodes as a cylinder of carbon paste, with one of the sides in contact with the solution. Since the AgCl is evenly distributed throughout the paste, we should then differentiate between that AgCl that is exposed on the surface, in contact with the solution, and that AgCl inside the cylinder, embedded in graphite and paraffin.

Only the AgCl at the surface (in contact with the solution) will be responsible for the electrochemistry of the system[111]. Once all the AgCl in contact with the solution is depleted, the AgCl inside the paste will be reduced. Since this AgCl is away from the solution and inside a hydrophobic matrix, it will require a larger overpotential to reduce, due to the additional resistance imposed by the paraffin oil. According to this model, we will expect, at the beginning a steady potential, and once all the AgCl in contact with

the solution has been reduced, we should expect a steady increase of the potential towards more negative values.

In the case of the paste with 8.1% of AgCl it seems as if the amount of AgCl on the surface of the electrode is not enough to sustain the reduction for more than 30 – 40 seconds. These 30 – 40 seconds represent 1.6 to 2.1 nmol of AgCl. This could mean that only 0.22 to 0.30 μg of AgCl are accessible in the surface of the carbon paste electrode. We have already mentioned that these AgCl particles have an approximately spherical size, with r = 1.5 μm (*vide infra*, Figure 67). We can consider that if the AgCl particles are homogeneously distributed throughout the paste, and since the density of AgCl[131] is 5.56 g cm^{-3}, this 0.22 – 0.30 μg of AgCl represent a superficial area of AgCl between 0.79 × 10^{-3} cm^2 and 1.08 × 10^{-3} cm^2. To convert the volume of AgCl into the area of the particles we used the fact that the area of a sphere equals three times the volume divided by the radius. Considering that each AgCl occupies a fraction of the surface of the electrode equal to πr^2, the area of the electrode occupied by the AgCl is between 0.2 × 10^{-3} cm^2 and 0.27 × 10^{-3} cm^2; approximately between 0.25 and 0.4 % of the surface of the electrode. We can also consider that since the silver chloride particles have a radius of 1.5 μm, we can see that only the particles that are at 1.5 μm or less from the surface are in contact with the solution, as can be seen in the scheme in Figure 76

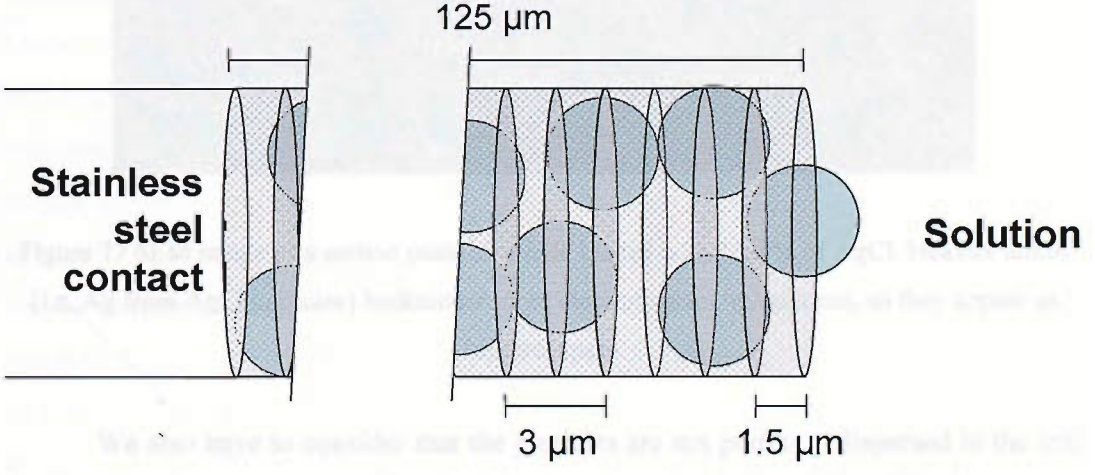

Figure 76 Schematic representation of a carbon paste electrode loaded with AgCl particles (blue dots). Dimensions are not proportionate.

The electrodes tested here had a typical thickness of 125 μm (Figure 77) and typically 3 mg of paste on average, so we can approximate that this 1.5 μm thick layer contains 36 μg of paste. For the carbon paste electrodes loaded with 8.1 % of AgCl, this represents approximately 2.9 μg of AgCl in the surface of the electrode. This value (2.9

μg of AgCl in the surface of the electrode) is approximately 10 times larger than the value obtained in the chronopotentiogram (between 0.22 and 0.3 μg of AgCl reduced, *vide supra*) giving us an idea that only around the 10 % of the AgCl in this first 1.5 μm thick section is reduced at the expected potential. This could be explained considering that the paraffin isolates the surface of the electrode from the solution, so part of the particles in the surface will be covered by paraffin, and hence will not be reduced at the same overpotential as particles not covered with paraffin. The potential at which those particles will be reduced will be affected by the resistance of the paraffin film on the surface of the electrode ($E_{app} = E_{AgCl/Ag} + iR$).

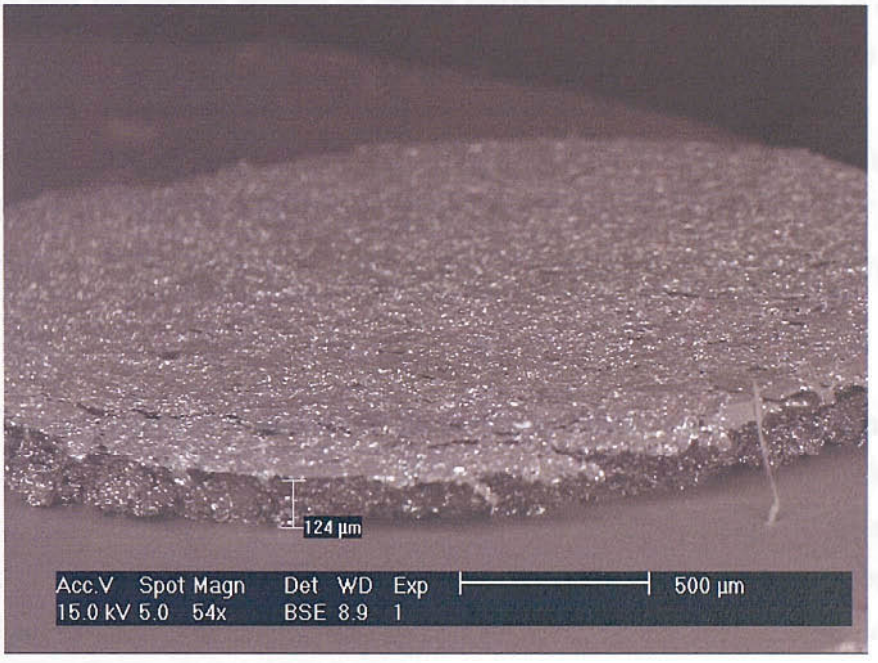

Figure 77 SEM image of a carbon paste electrode loaded with 12.6 % of AgCl. Heavier atoms (i.e. Ag from AgCl particles) backscatter more electrons than lighter ones, so they appear as brighter spots.

We also have to consider that the particles are not perfectly dispersed in the ink, but that there is some aggregation. In this case, the distribution of particles throughout the ink may be not as homogeneous as we calculated according to Figure 76. Also the aggregation of particles leads to a decrease of the area of AgCl in contact with the solution; the superficial areas of an aggregated cluster of particles is smaller than the sum of the superficial area of the constituting particles, leaving a smaller surface of AgCl in contact with the solution.

Another feature is apparent in Figure 75. Once the potential of the electrode drops below about -550 mV (*vs.* SMSE) the potential becomes extremely noisy.

Several other electrodes were prepared with these pastes but increasing the thickness of the electrodes, up to 4 times. The response of the electrodes was similar to that shown here. This is consistent with the model that states that the first part of the transient (the stable part) is due to the reduction of the AgCl in contact with the solution[111]. According to this model, the maximum charge that this kind of electrodes can pass is not related to the thickness of the carbon paste layer, but is controlled by the amount of AgCl present in contact with the solution. Electrodes could be constructed that could pass the desired amount of charge considering the concentration of AgCl in the mix and the area of the electrode, by altering the amount of AgCl in the surface and/or the area of the electrode.

In this sense, a carbon paste with a low concentration of AgCl can be used, provided that the area of the electrode is increased. The main advantage of using a carbon paste with low amount of AgCl will be the reduction of the resistivity of the paste.

The chronoamperometry at -5 μA is a significant test since it mimics the behaviour of the AgCl electrode during the glucose measurement in the overall sensor. Under these conditions, the potential of the reference electrode should be as stable as possible. The electrodes with a concentration of AgCl of 12.6% exhibit the most stable response under these conditions, and were compared against the MediSense screen printed electrode, as seen in Figure 78. In this figure we can see that the new electrodes exhibit a faster stabilisation of the potential than the commercial ones. In this case, the carbon paste electrodes present a stable behaviour after approximately 30 s (or less) whereas the commercial electrode will not reach a stable potential in the two min of the experiment. The faster equilibration could be due to a faster wetting of the electrode, or more precisely, that the electroactive available area of the electrode does not change during the chronopotentiometry.

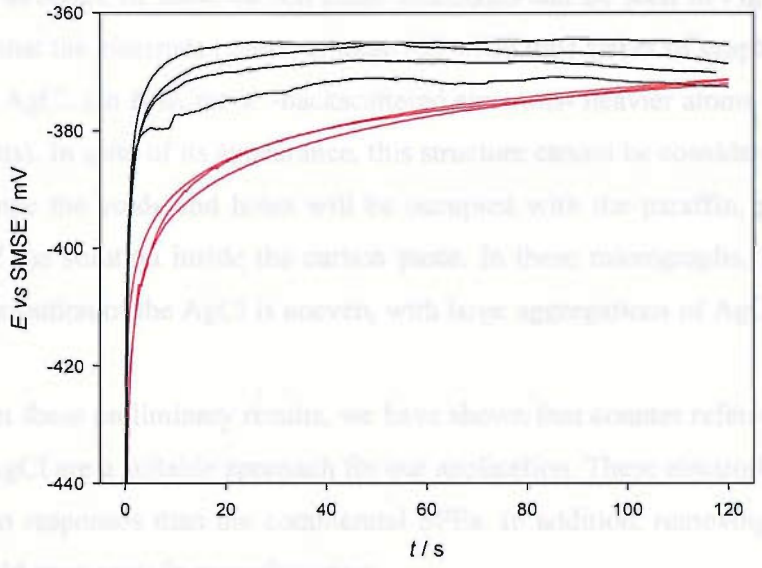

Figure 78 Chronopotentiometry at -5 μA in a solution containing 0.5 M KNO_3 and 30 mM KCl. Black curves, CPE loaded with 12.6 % of AgCl. Red curves for commercial Ag/AgCl SPE.

This result is very promising, both to reduce the duration of the experiment and to improve the overall performance of the sensor. Since the measurement of glucose could take place not during the transient part of the curve, but in a stable zone, using a reference electrode with a faster equilibration will increase the reliability of the overall sensor as well.

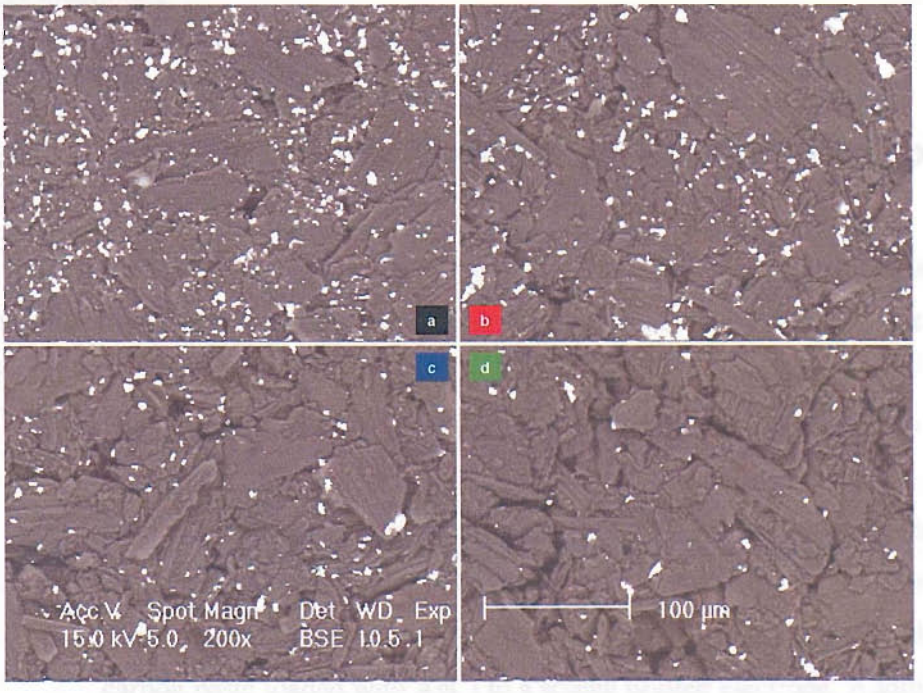

Figure 79 SEM images of four different carbon paste electrodes. a) Carbon paste with 12.6 % AgCl; b) With 8.1 % AgCl; c) 2.9 %; d) 1.5 %. All percentages refer to the weight of solids.

The structure of these carbon paste electrodes can be seen in Figure 79, where we can see that the electrodes presents large (60 - 100 μm) flakes of graphite with small particles of AgCl. (In BSE mode -backscattered electrons- heavier atoms will appear as brighter spots). In spite of its appearance, this structure cannot be considered as a porous structure since the voids and holes will be occupied with the paraffin, preventing the diffusion of the solution inside the carbon paste. In these micrographs, it can be seen that the distribution of the AgCl is uneven, with large aggregations of AgCl.

From these preliminary results, we have shown that counter reference electrodes with only AgCl are a suitable approach for our application. These electrodes show faster equilibration responses than the commercial SPEs. In addition, removing the Ag from the ink would save costs in manufacturing.

One important feature of these carbon paste electrodes is the high variation and irreproducibility. This lack of reproducibility could be ascribed to the manual manufacturing procedure. It is crucial to obtain a similar amount of AgCl at the surface of every electrode, with the same paste compactness, and this could not be achieved with the manual process employed. Furthermore, the goal of this project is to build a new reference electrode that could be used in screen printed glucose sensors, so the next step was to extend these results to build graphite – silver chloride screen printed counter reference electrodes.

5.3. Screen printed counter reference electrodes

Two different approaches were proposed to alter the screen printed counter – reference electrode; graphite electrodes loaded with AgCl, and Ag/AgCl electrodes loaded with KCl. These two approaches were chosen for the following reasons:

A. Graphite ink loaded with AgCl: In this case, the main advantage is the simplicity of the composition. Since we have stated that the AgCl particles behave differently if they are in contact with Ag or not, removing the Ag will simplify the reactions occurring at the electrode. This approach tries to extrapolate the good results obtained with the carbon paste loaded with AgCl to a screen printed electrode. Additionally, this approach offers a potential cost saving which, for productions of almost 100 million sensors per month, could be considerable.

B. DuPont's ink with added KCl: This approach uses the same ink as the commercial Ag/AgCl reference electrode, but adding the KCl will improve the performance, due to the improved wettability of the ink. In addition, including some source of soluble Cl^- in the ink could help us to understand the wetting of the electrode, monitoring the increase of the open circuit potential due to the diffusion of chloride from the ink. The processes that need Cl^- (formation of the double layer, adsorption of Cl^- on the Ag) will occur consequently faster (since the Cl^- is already in the ink) and if these processes control the equilibration of the potential, adding Cl^- in the ink will lead to the equilibration of the electrode at shorter times.

C.

All electrodes were printed on PVC boards, using G3 artwork. The change from G2b (used thoroughly in the earlier chapter) to G3 electrodes was motivated by MediSense's decision in the near future, to take G2b meters and electrodes out of the market. Apart from differences in the disposition of the electrodes, G3 electrodes are printed on Mylar boards (polyethylene terephthalate (polyester) film); meanwhile G2b electrodes are printed on PVC (polyvinylchloride) boards. In our trials, we chose PVC boards because they produce cleaner cross section cuts, important if we wish to study the distribution of components within the printed layers.

In the case of the Ag/AgCl ink loaded with KCl, a carbon track was printed under the Ag/AgCl layer to promote the adhesion of the Ag/AgCl ink to the PVC and to produce a good electrical contact. The enzyme layer was not printed.

5.4. Screen printed graphite loaded with AgCl

We have demonstrated in a previous section (5.2) that this kind of electrodes could be a good alternative to the actual Ag/AgCl electrodes, specifically when the secondary electrode is working as a cathodic counter - reference electrode. Electrodes were prepared with Gwent graphite ink with 0 %, 1 %, 2.91 %, 6.54 % and 9.09 % weight of AgCl.

5.4.1. Preparation and composition of the electrodes.

5.4.1.1. Rheology

Rheology is the study of the deformation and flow of matter in terms of stress, strain, temperature, and time. In screen printable inks this parameter is very important since it gives an idea of how a particular ink will flow through the screen. The way the ink flows though the screen will determine the shape and thickness of the final print. Very viscous inks will not flow evenly through the screen, giving non uniform prints and even clogging the screen. On the other hand, if the ink has very low viscosity, it could spread after the print, rendering the print thinner in the periphery of the electrode, or even, in extreme cases were the ink is too thin, the ink could drip though the mask.

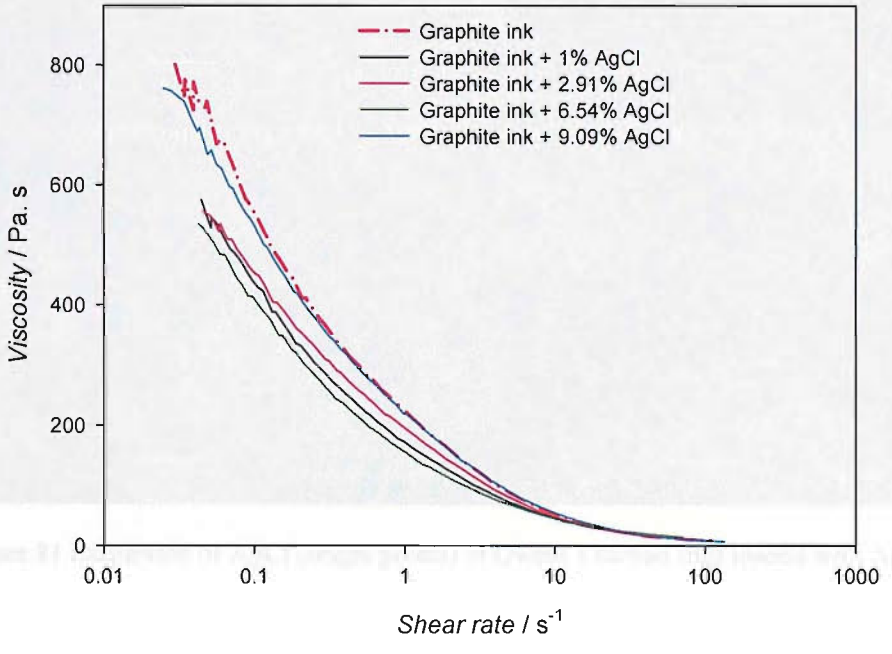

Figure 80 Viscosity of various carbon inks loaded with AgCl (at 25 °C).

In this case we can see in Figure 80, that adding only AgCl does not change the viscosity of the ink significantly, and hence these inks will flow through the screen in a similar way to the "control ink" (graphite ink). There is a small decrease of the viscosity for the inks containing 1, 2.91 and 6.54 % of AgCl. This decrease of the viscosity could be due to the mixing step. The AgCl is dispersed in the graphite ink using a Dispermat. The Dispermat is a mixing device analogue to a food blender and consists on a serrated disc spinning at a controlled rate. This rotation breaks up the structure of the ink.

5.4.1.2. SEM images of the SPE

After printing and drying several screen printed electrodes manufactured with these inks, micrographs of the SPEs were taken. This allows us to study the distribution of AgCl. The SEM images in Figure 81 show a homogeneous distribution of AgCl on the surface of the SPE, with a very low amount of AgCl on the surface of the ink containing only 1 % of AgCl.

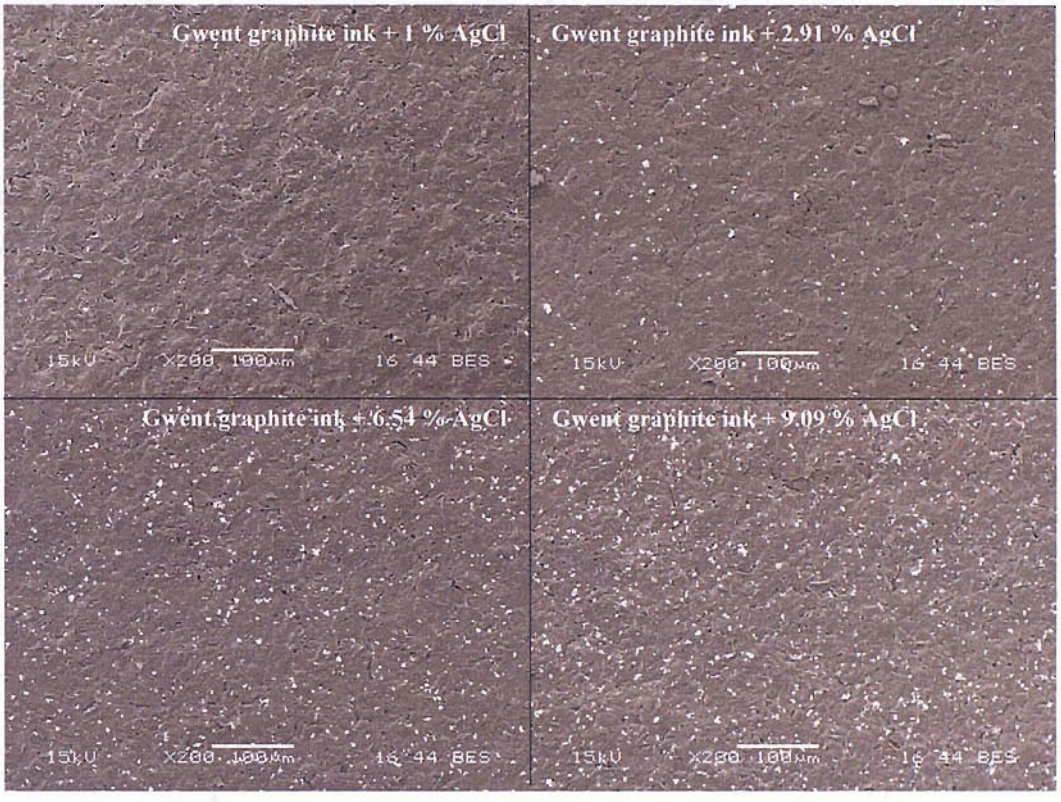

Figure 81 Dispersion of AgCl (bright points) in Gwent's carbon inks loaded with AgCl.

The distribution of AgCl in the surface is more homogeneous than that seen for carbon paste electrodes (Figure 79). For the SPE, the graphite flakes appear smaller, and the AgCl is less aggregated. The AgCl used for both the SPE and the carbon paste electrodes was of the same specifications. The difference in dispersion is probably related to a better mixing step in the SPE case, due to a better mixing using the Dispermat instead of a mortar and pestle, and to the fact that the graphite is already mixed in the carbon screen printable ink used here.

5.4.2. Behaviour of the carbon paste loaded with AgCl counter-reference electrodes.

The behaviour of these new screen printed electrodes was evaluated. The first test performed showed the potential transients when some current is driven through the electrode. As we have done with the carbon paste loaded with AgCl electrodes, this test consisted in passing the usual current that passes through the electrode during the measurement of glucose. This current is in the range between -5 μA (for low concentrations of glucose) to -50 μA (high concentrations of glucose).

These new type of electrodes (carbon loaded with AgCl) were compared with a standard electrode printed with DuPont's Ag/AgCl ink. The results appear in Figure 82 for -5 μA and Figure 83 for -50 μA.

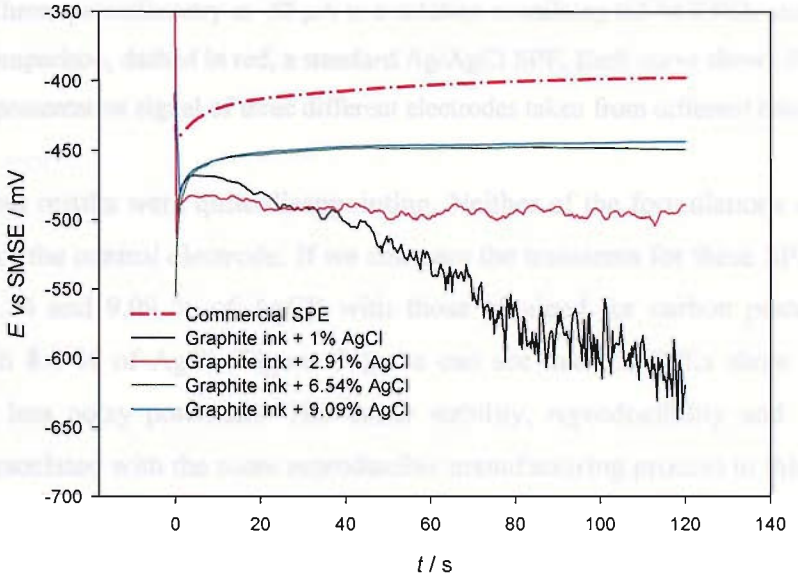

Figure 82 Chronopotentiometry at -5 μA in a solution containing 0.3 M KNO_3 and 0.3 M KCl. For comparison, dashed in red, a standard Ag/AgCl SPE. Each curve shows the most representative signal of three different electrodes taken from different boards.

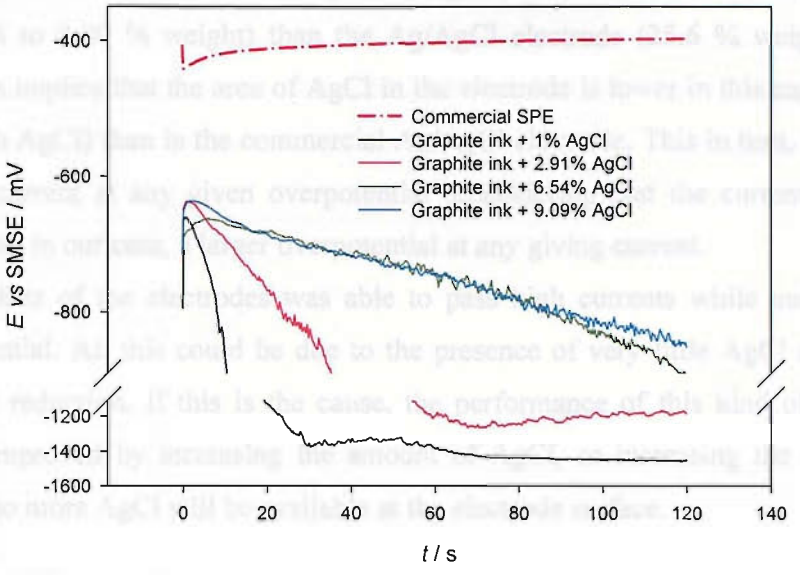

Figure 83 Chronopotentiometry at -50 μA in a solution containing 0.3 M KNO_3 and 0.3 M KCl. For comparison, dashed in red, a standard Ag/AgCl SPE. Each curve shows the most representative signal of three different electrodes taken from different boards.

These results were quite disappointing. Neither of the formulations matched the behaviour of the control electrode. If we compare the transients for these SPEs (graphite ink plus 6.54 and 9.09 % of AgCl) with those obtained for carbon paste electrodes loaded with 8.1 % of AgCl (Figure 74), we can see that the SPEs show much more stable and less noisy potentials. The better stability, reproducibility and lower noise could be associated with the more reproducible manufacturing process in this case.

If we now compare the graphite SPEs loaded with AgCl and the control electrode (commercial Ag/AgCl SPE), we can see, as a good result, that at low currents, the electrodes with a higher addition of AgCl (above 6.54 %) showed stable potentials 30 seconds after immersing the electrode in the solution, meanwhile the control electrode needs more than 2 min to achieve an stable potential. At low currents, this potential is approximately 50 mV more negative than that for the control electrode and approximately 200 mV at larger current. This shift of the potential could be due to the fact that the AgCl loaded graphite electrode is less conductive than the Ag/AgCl electrode. The electrode tracks with 6.54 and 9.09 % of AgCl had a resistance of 4.2 and 4.4 kΩ, for only 0.240 kΩ for the commercial screen printed Ag/AgCl electrodes. This increase of the resistance of approximately 4 kΩ will result in an *IR* drop of 20 mV for the lower current (-5 μA), and 200 mV for the larger one (-50 μA).

In addition, the carbon loaded with AgCl electrode has a smaller amount of AgCl (6.54 to 9.09 % weight) than the Ag/AgCl electrode (25.6 % weight, section 3.1.2). This implies that the area of AgCl in the electrode is lower in this case (graphite loaded with AgCl) than in the commercial Ag/AgCl electrode. This in turn, will lead to a smaller current at any given overpotential (considering that the current density is constant), or, in our case, a larger overpotential at any giving current.

Neither of the electrodes was able to pass high currents while maintaining a stable potential. All this could be due to the presence of very little AgCl available to sustain the reduction. If this is the cause, the performance of this kind of electrodes could be improved by increasing the amount of AgCl, or increasing the area of the electrode, so more AgCl will be available at the electrode surface.

Increasing the amount of AgCl could improve the performance of the electrode, but this also increases the resistivity. Two additional ink compositions were tried. These compositions had an increased amount of AgCl and, to compensate the increase of resistivity, more graphite was added to the ink. Adding such a large amount of solids made the ink too thick and viscous. 40 ml of cyclohexanone per kg of ink was added to thin the ink.

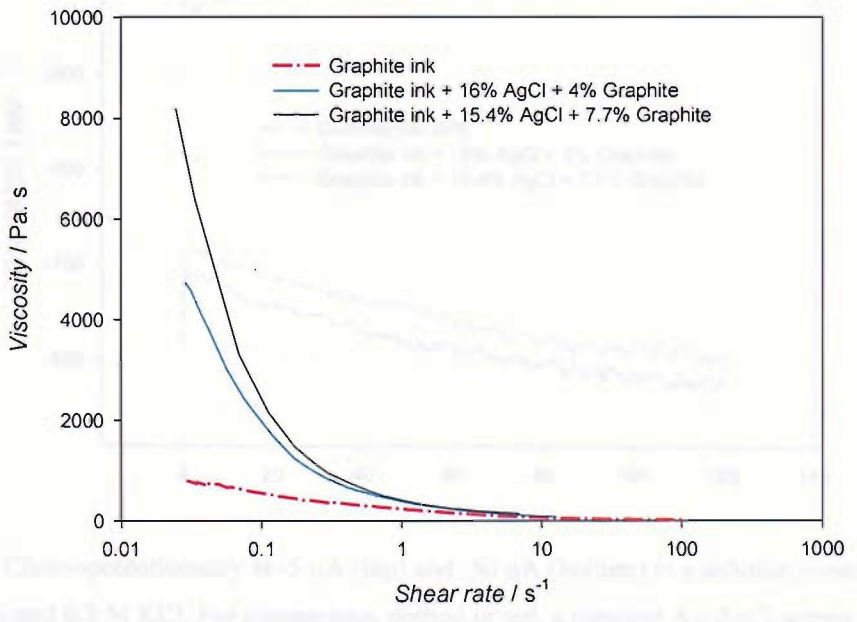

Figure 84 Viscosity of various carbon inks loaded with AgCl and graphite (at 25 °C).

The first effect observed was a very significant increase of the viscosity of the ink, as can be seen in Figure 86. These inks with additional graphite contain a very large

proportion of solids (16 % AgCl plus 4 % of graphite, and 15.38 % of AgCl plus 7.69 % of graphite) and showed a viscosity 6 and 10 times larger than the control ink (Gwent's carbon ink), and flowed badly through the screen during the printing step. The resistance of the SPEs made with these inks was 5.4 kΩ and 4.6 kΩ respectively.

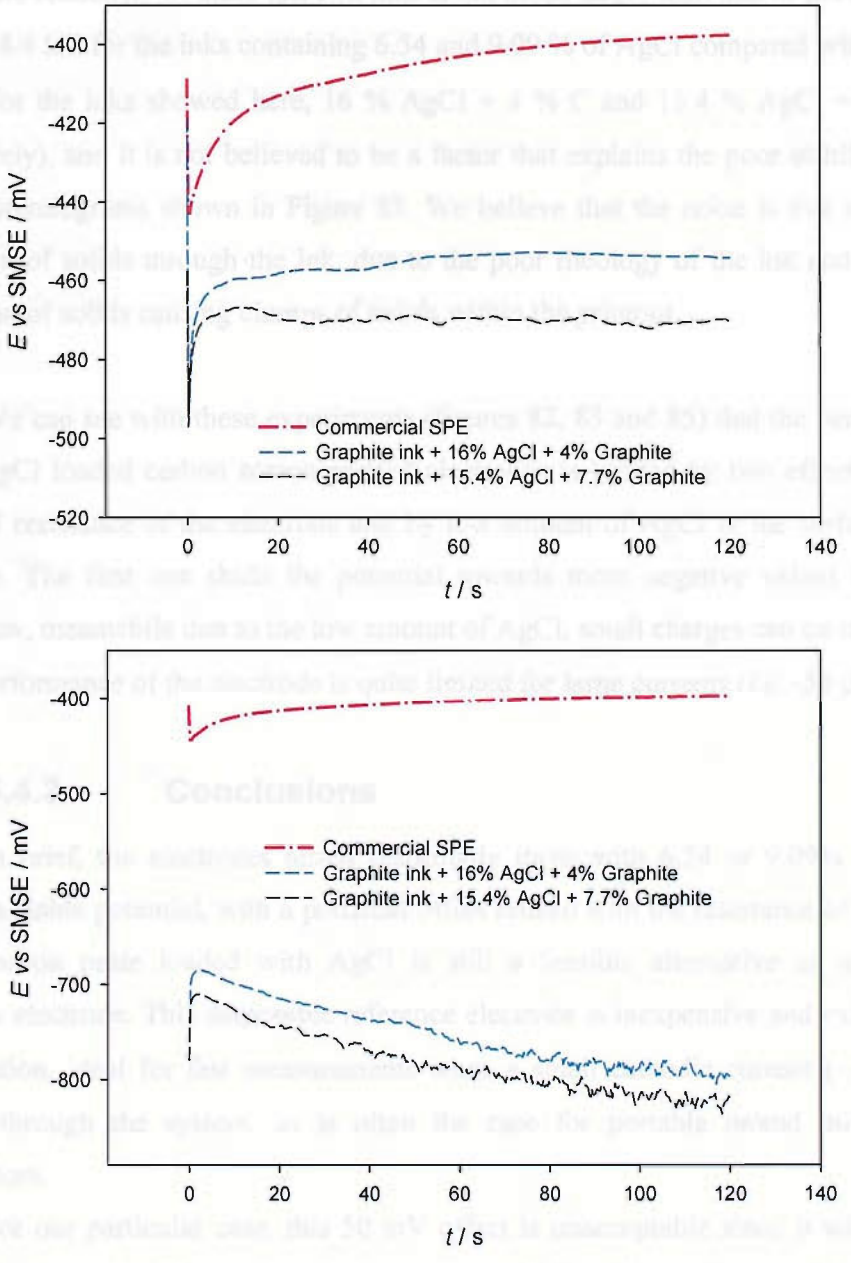

Figure 85 Chronopotentiometry at -5 μA (top) and -50 μA (bottom) in a solution containing 0.3 M KNO_3 and 0.3 M KCl. For comparison, dashed in red, a standard Ag/AgCl screen printed reference electrode. Each curve shows the most representative signal of three different electrodes taken from different boards

In Figure 85, it can be seen that the performance of these inks was worse than the graphite inks loaded with 6.54 and 9.09 % of AgCl shown in Figure 82 and Figure

83, so no improvement was achieved by increasing the amount of AgCl. The chronoamperometry at -5 μA is much noisier, meanwhile the chronoamperometry at -50 μA looks the same as those performed with graphite inks loaded with 6.54 and 9.09 % of AgCl.

The resistivity of these last two inks is not much larger than that of previous inks (4.2 and 4.4 kΩ for the inks containing 6.54 and 9.09 % of AgCl compared with 5.4 and 4.6 kΩ for the inks showed here, 16 % AgCl + 4 % C and 15.4 % AgCl + 7.7 % C respectively), and it is not believed to be a factor that explains the poor stability of the chronopotentiograms shown in Figure 85. We believe that the noise is due to the bad dispersion of solids through the ink, due to the poor rheology of the ink and the large proportion of solids causing clumps of solids within the printout.

We can see with these experiments (figures 82, 83 and 85) that the performance of the AgCl loaded carbon screen printed electrodes is limited by two effects, *i.e.* the electrical resistance of the electrode and by low amount of AgCl in the surface of the electrode. The first one shifts the potential towards more negative values following Ohm's law, meanwhile due to the low amount of AgCl, small charges can be transferred, so the performance of the electrode is quite limited for large currents (*i.e.* -50 μA).

5.4.3. Conclusions

In brief, the electrodes tested (especially those with 6.54 or 9.09% of AgCl) showed a stable potential, with a potential offset related with the resistance of the track. Using carbon paste loaded with AgCl is still a feasible alternative as a cathodic reference electrode. This disposable reference electrode is inexpensive and exhibits fast equilibration, ideal for fast measurements when a small cathodic current (~-5 μA) is passing through the system, as is often the case for portable or/and miniaturised (bio)sensors.

For our particular case, this 50 mV offset is unacceptable since it will mean a change in the potential applied by the meter which will require an obligatory re-approval by the Health authorities. In addition, at high concentrations of glucose and hence higher currents (50 μA), the reference electrode is not capable of maintaining a stable and acceptable potential.

We have tried to improve the performance of the electrode by increasing the amount of C (to decrease the resistance of the track) while increasing the amount of

AgCl, but the result obtained (Figure 85) was discouraging, since the viscosity of the ink and the electrical resistance of the track increased, but we could not improve the amount of charge that could be transferred with minimal potential shift.

In this sense, we could increase the performance of the electrode by reducing the electrical resistance of the track by other means. This resistance comes both from the whole electrode (the part in contact with the solution and also the conducting part of the track). A feasible idea that could be tested could be maintaining the same paste in the electrode (graphite loaded with AgCl), but decreasing the resistance of the conducting track, *e.g.* by printing a highly conductive ink (*e.g.* Ag ink). This could reduce the overall resistance of the track, but will increase the cost per electrode since there will be an additional printing step and an increase in the cost of the printing materials.

Other ways of possibly enhancing the performance of the electrode could be through enlarging its surface area. A larger surface (and hence larger amount of ink) could expose enough AgCl to perform the reduction at the required current density. However no experiments modifying the shape or the dimensions of the electrode were performed. The area of the electrode is restricted in the overall sensor by the drop of blood needed for the measurement; increasing the size of the electrode will eventually require a larger blood droplet to cover the electrode, thus making the analysis more painful for the user, as we have already mentioned (section 1.5.3).

5.5. Ag/AgCl pastes loaded with KCl as counter reference electrodes.

This experiment was performed in order to investigate if the diffusion of chloride from and/or towards the electrode (and through the ink) has some effect on the potential of the reference electrode. In this case the electrodes were printed with a large and known amount of chloride, so the diffusion of Cl^- could be predicted. Since there is going to be some soluble Cl^- embedded in the ink, we expect that once the electrode is dipped in the sample, the solution will dissolve this Cl^- locally increasing the amount of chloride. This Cl^- will then diffuse from the electrode towards the solution. According to this model, we expect to see a shift in the potential of the electrode towards less negative values as the Cl^- diffuses from the electrode to the bulk. Additionally, the

dissolution of the Cl^- salt will increase the porosity of the printed ink facilitating the wetting of the electrode.

Electrodes were screen printed with inks produced by mixing Ag/AgCl screen printable commercial ink (DuPont plc.) with increasing amounts of KCl (0 %, 1.96 %, 4.76 %, 6.98 %, and 9.09 % weight of KCl). To test whether the presence of other salts (non-chloride salts) affect the properties of the electrodes, two additional inks were prepared with DuPont's Ag/AgCl ink and $NaNO_3$, a highly soluble salt in one case (92.1 g can be dissolved in 100 ml of water[131] at 20 °C) and Na_2SO_4, a less soluble salt in the other (only 4.76 grams can be dissolved in 100 ml of water[131] at 0 °C). 1.96 % weight of these salts were incorporated in the ink.

5.5.1. Preparation and composition of the electrodes.

5.5.1.1. Rheology

As we have already done with the carbon inks loaded with AgCl, the first test with these inks loaded with KCl was to evaluate the viscosity. This will also help us to predict how these inks will flow in the screen.

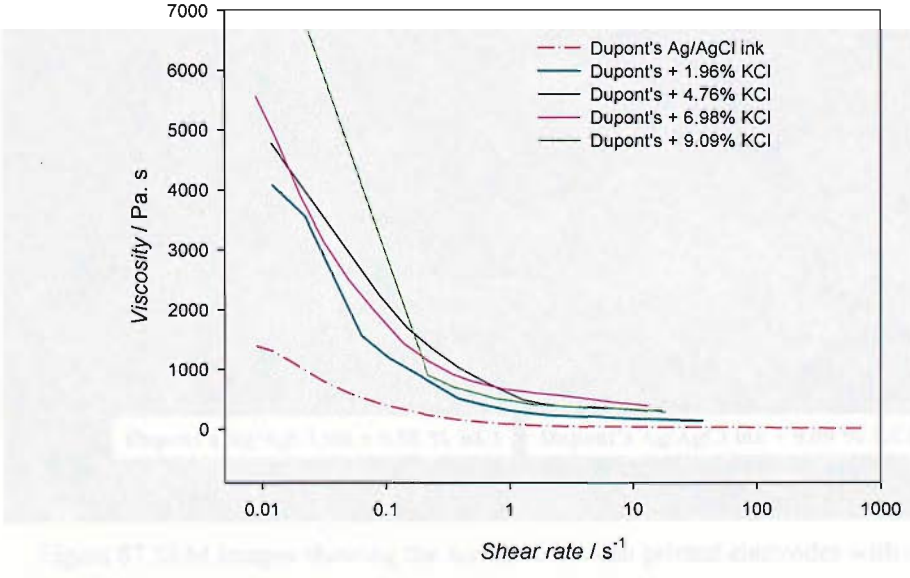

Figure 86 Viscosity of various Ag/AgCl inks loaded with KCl (at 25 °C).

In the case of these inks, the addition of ions dried the ink significantly producing an increase of the viscosity. At low shear rates (low rotation rates of the disk) the ink is too viscous to allow the disk to rotate smoothly. As a result, at low shear rates, the measurement of viscosity values was discontinuous, as can be seen in the low

resolution of Figure 86. The viscosity of the ink increases significantly with increasing amounts of salt. Inks with larger concentration of salt were too thick, and could not be printed uniformly. This set of inks gave proper prints, but the surface of the electrode was not smooth, especially for the ink with 9.09 % of KCl, which showed mounds and valleys. This can be explained with a real life example as spreading butter on a toast. If the butter is lukewarm (fluid), it can be spread on the toast uniformly; but if it is cold (and hence harder), once you try to spread it, it will spread out in chunks.

5.5.1.2. SEM images of the SPE

Apart from the non-uniformity of the prints, the electrodes manufactured with Ag/AgCl ink loaded with KCl showed larger porosity with larger concentrations of KCl. The porosity of the tracks can be seen in Figure 87).

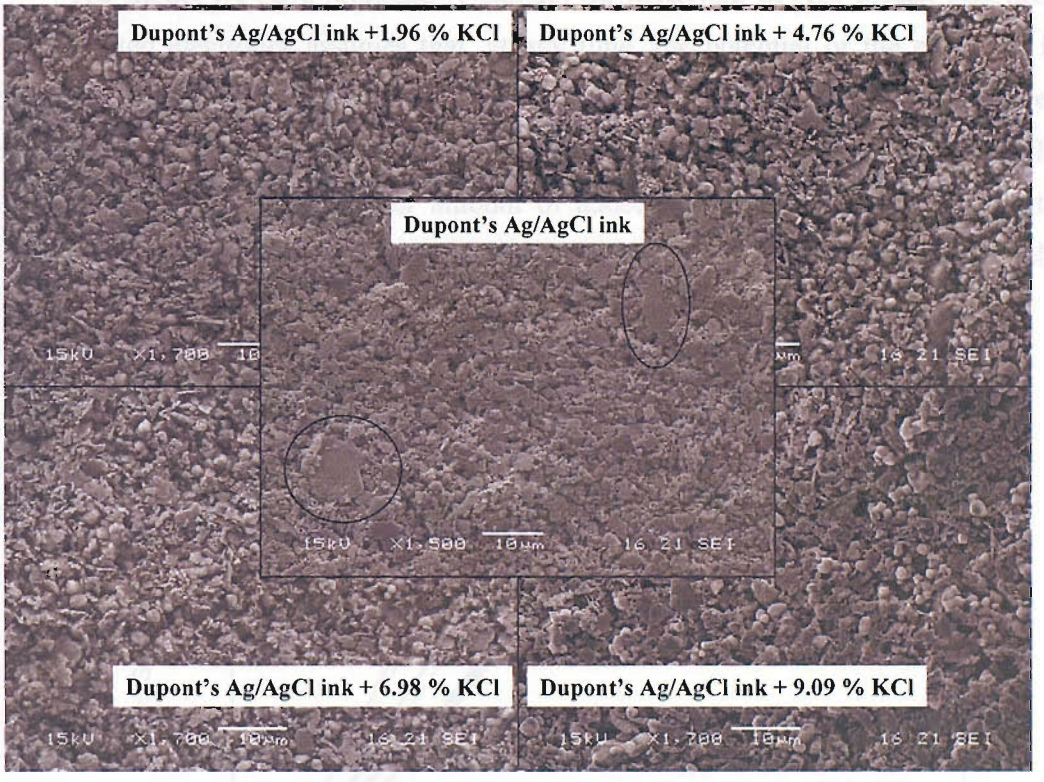

Figure 87 SEM images showing the surface of screen printed electrodes with different concentrations of KCl. All the pictures were taken at the same conditions and magnification (The scale bars at the bottom and middle of the figure represents 10 μm).

As we can see in Figure 87, increasing the amount of KCl in the Ag/AgCl ink increases the porosity and the roughness of the screen printed electrode. The electrodes with larger content of KCl show more voids and a more grainy structure, meanwhile the electrode without KCl, shows a smoother and more uniform surface, with even some

flat areas (marked with ellipses in the SEM image). This is probably due to the increased viscosity of the ink, and its reluctance to flow. The increased porosity will have consequences for the wettability and also on the ability of the electrode to pass current, since the increased roughness will increase the specific area of the electrode.

5.5.2. Behaviour of the Ag/AgCl electrodes loaded with KCl.

As we have done previously with the AgCl loaded graphite SPEs, several tests were performed with the KCl loaded Ag/AgCl SPEs to evaluate their performance.

5.5.2.1. *Chronopotentiometry at OCP.*

The model we have proposed to explain the behaviour of KCl loaded Ag/AgCl screen printed electrodes assumes that, at any time, the potential of the electrode is determined by the activity of chloride at the electrode, and that this activity changes with time as the KCl embedded in the electrode dissolves and diffuses to the bulk. In this case, electrodes with a larger amount of added KCl should take more time to stabilise the potential, since more Cl^- has to diffuse from the electrode. In order to study this effect, chronopotentiometry at open circuit potential was performed.

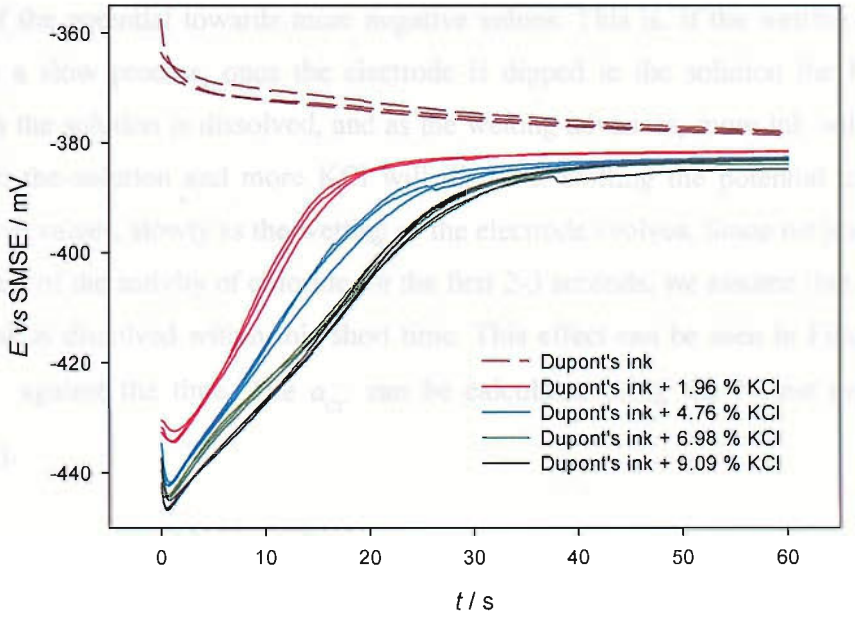

Figure 88 Variation of the chronopotentiometry at open circuit potential for different electrode compositions (3 electrodes of each type) in 0.3 M KNO_3 and 0.3 M KCl

In Figure 88, we can see that the response of the SPE loaded with KCl is very different to the control SPE. The control SPE shows open circuit transients similar to those shown previously (Figure 30); meanwhile the electrodes loaded with KCl show a linear increase of the potential with time.

This behaviour is believed to be due to the presence and dissolution of the KCl inside the electrode and agrees with our expectations. Once the solution penetrates in the porous structure of the electrode, it will dissolve the KCl embedded in the ink, increasing locally the amount of Cl^- in the electrode. As a result, at the beginning of the experiment, the potential of the Ag/AgCl shifts sharply to more negative values, as expected from the Nernst equation. This local increase of the concentration will create a concentration gradient, and the Cl^- will then diffuse to the bulk until the concentration at the electrode is equal to that of the solution. During the diffusion of Cl^-, the local concentration of Cl^- at the electrode will decrease and thus the potential of the electrode will shift to less negative potentials.

We can also see in Figure 88 that the potential of the SPE loaded with KCl shifts slightly to more negative values within the first 2-3 seconds after placing it in solution. This indicates that the wetting of the electrode occurs within the first 2-3 seconds after the electrode is dipped in the solution. If the wetting of the electrode was a slow process, we should see in these transients an increase of the concentration of Cl^- at the electrode as a shift of the potential towards more negative values. This is, if the wetting of the electrode is a slow process, once the electrode is dipped in the solution the KCl in contact with the solution is dissolved, and as the wetting advances, more ink will be in contact with the solution and more KCl will dissolve, shifting the potential towards more negative values, slowly as the wetting of the electrode evolves. Since we just see a small increase of the activity of chloride for the first 2-3 seconds, we assume that all the Cl^- in the ink is dissolved within this short time. This effect can be seen in Figure 89, plotting a_{Cl^-} against the time. The a_{Cl^-} can be calculated using the Nernst equation (Equation 6).

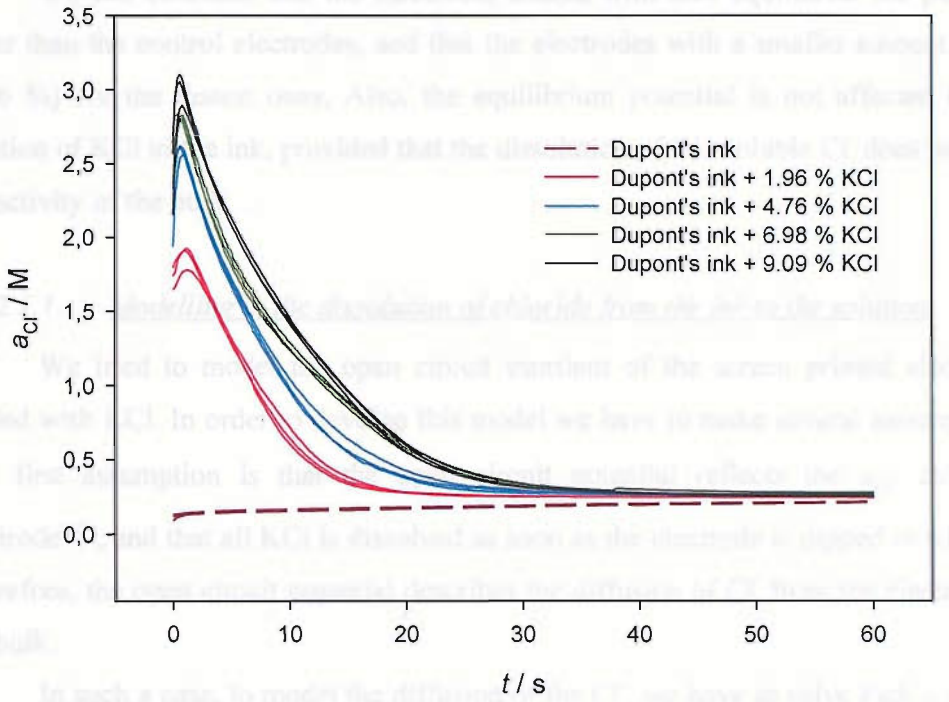

Figure 89 Variation of the activity of chloride at the electrode when different SPEs with different compositions (3 electrodes of each type) are placed in a solution containing 0.3 M KNO_3 and 0.3 M KCl. The activity has been calculated from the open circuit potential measured in Figure 88 using the Nernst equation.

We can see in Figure 88 that the SPE loaded with larger amounts of KCl show a more negative starting potential, related with the larger amount of Cl^- dissolved from the ink. Also, these electrodes loaded with larger amounts of Cl^- need more time to stabilise the potential, indicating that more time is needed to equilibrate the a_{Cl^-} at the electrode with that of the bulk, also indicating that more Cl^- has to diffuse from the electrode to the bulk. Both these affirmations can be obtained from Figure 89. The SPE printed with larger concentrations of Cl^- show larger a_{Cl^-} right after the electrode is dipped in the solution, and these electrodes need longer times to equilibrate the a_{Cl^-} at the electrode with that of the bulk than electrodes loaded with less KCl.

We can also see in Figure 88 that the SPE loaded with KCl reach the thermodynamic potential expected from the Nernst equation within 30 s after dipping them in solution. Figure 89 shows that within this time span, the a_{Cl^-} at the electrode equals that of the bulk solution (0.3 M).

We can conclude that the electrodes loaded with KCl equilibrate the potential faster than the control electrodes, and that the electrodes with a smaller amount of Cl^- (1.96 %) are the fastest ones. Also, the equilibrium potential is not affected by the addition of KCl to the ink, provided that the dissolution of this soluble Cl^- does not alter the activity of the bulk.

5.5.2.1.1. Modelling of the dissolution of chloride from the ink to the solution

We tried to model the open circuit transient of the screen printed electrodes loaded with KCl. In order to develop this model we have to make several assumptions. The first assumption is that the open circuit potential reflects the a_{Cl^-} at/in the electrode[xxiv], and that all KCl is dissolved as soon as the electrode is dipped in solution. Therefore, the open circuit potential describes the diffusion of Cl^- from the electrode to the bulk.

In such a case, to model the diffusion of the Cl^-, we have to solve Fick's second law:

$$\frac{\partial C}{\partial t} = D\left(\frac{\partial^2 C}{\partial x^2} + \frac{\partial^2 C}{\partial y^2} + \frac{\partial^2 C}{\partial z^2}\right) \qquad \text{Equation 36}$$

where C is the concentration of the diffusing species and D is the diffusion coefficient.

To simplify, we have assumed that the diffusion occurs only in one direction, from the electrode to the bulk and that the activity coefficient for Cl^- does not change significantly, so $C_{Cl^-} \approx a_{Cl^-}$.

We also need to define some boundary conditions, *i.e.* that the concentration of chloride at any point at $t = \infty$ equals the concentration in the bulk ($C^*_{Cl^-}$) and that at $t = 0$, the concentration of Cl^- equals the bulk everywhere except at the electrode, where it is an amount A larger than in the bulk due to the dissolution of the KCl. This value A depends on the amount of Cl^- added in the ink, and the volume of solution in which it is dissolved, so we can interpret this amount of Cl^- dissolved as a concentration value added ($C^0_{Cl^-}$) to the concentration of the bulk (Equation 40).

[xxiv] We will define what "a_{Cl^-} at the electrode" refers to for every model proposed. The simplest model we propose describes the electrode as a 2D layer with no thickness, meanwhile other model describe the electrode as a 3D porous layer, and the a_{Cl^-} is then referred as the average activity within the film thickness.

$$\frac{\partial C_{Cl^-}(x,t)}{\partial t} = D_{Cl^-}\left[\frac{\partial^2 C_{Cl^-}(x,t)}{\partial x^2}\right] \quad \text{Equation 37}$$

$$x \to \infty\,(\forall t) \Rightarrow C_{Cl^-}(\infty,t) = C^*_{Cl^-} \quad \text{Equation 38}$$

$$t \to \infty\,(\forall x) \Rightarrow C_{Cl^-}(x,\infty) = C^*_{Cl^-} \quad \text{Equation 39}$$

$$t=0 \quad \begin{cases} x=0 \Rightarrow C_{Cl^-}(0,0) = C^*_{Cl^-} + C^0_{Cl^-} \\ x \neq 0 \Rightarrow C_{Cl^-}(x,0) = C^*_{Cl^-} \end{cases} \quad \text{Equation 40}$$

To solve the diffusion of Cl^- from the electrode to the solution, three approaches were used.

5.5.2.1.2. Assuming that the electrode is a 2D structure with no thickness, and hence the Cl^- is initially confined in a plane:

This model describes the spreading by diffusion of an amount of substance (M) deposited at time $t = 0$ in the plane $x = 0$. If all the diffusion occurs in the direction of positive x, the expression of $C(x,t)$ has the form[169]:

$$C_{Cl^-}(x,t) = \frac{M}{\sqrt{\pi D t}} \exp\left(\frac{-x^2}{4Dt}\right) + C^*_{Cl^-} \quad \text{Equation 41}$$

To evaluate how the concentration changes with time, the concentration was evaluated at $x = 0$, that is, at the surface of the electrode, and was compared with the experimental data from Figure 89 above.

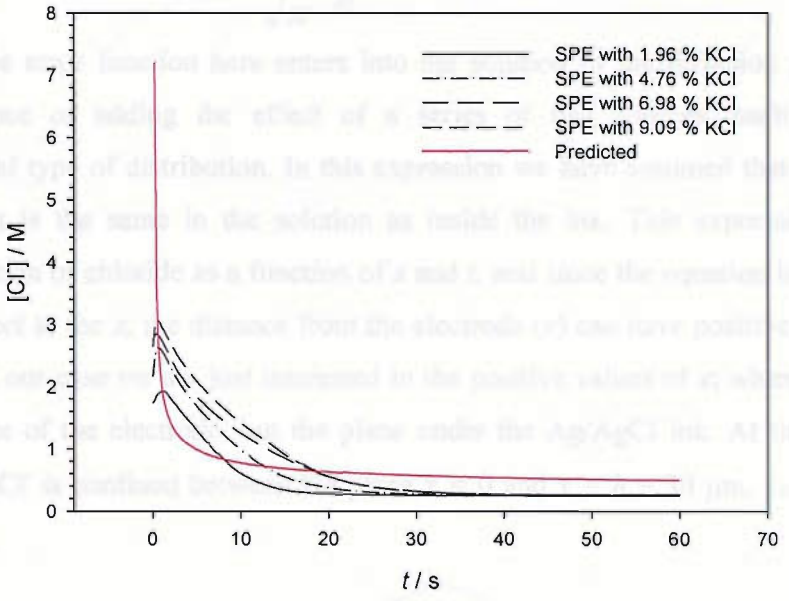

Figure 90 Variation of the [Cl^-] with time at the electrode when a SPE loaded with KCl is placed in a solution containing 0.3 M KNO_3 and 0.3 M KCl, compared with the model proposed in Equation 41 (red line). To solve the equation, M was chosen as 0.4 mmol cm^{-2} and D was, at 20 °C[114], 1.5×10^{-9} m^2 s^{-1}.

We can see in Figure 90 that the predicted model does not fit the data. The concentration profile for the predicted diffusion decreases very rapidly as compared with the experimental one, until it reaches 0.6 M, after 10 seconds. From there on, the decrease of the concentration is steadier. The concentration of Cl^- at $x = 0$ and long times ($t > 60$ s) is significantly larger than that of the bulk, indicating that the equation proposed does not adequately describe the experimental data.

5.5.2.1.3. *Assuming that the Cl^- is diffusing out of a layer of thickness h at the electrode:*

In this case, the diffusing substance is initially confined in a layer of thickness h (in our case, the thickness of the electrode, *i.e.* 30 μm). The expression that describes how the concentration of Cl^- changes with time is[169]:

$$C_{Cl^-}(x,t) = \frac{C^0_{Cl^-}}{2}\left[\operatorname{erf}\frac{x+h}{2\sqrt{Dt}} - \operatorname{erf}\frac{x-h}{2\sqrt{Dt}}\right] + C^*_{Cl^-} \qquad \text{Equation 42}$$

where erf(y) is the error function, defined by Equation 43:

$$\mathrm{erf}(y) = \frac{2}{\sqrt{\pi}} \int_0^y e^{-x^2} dx \qquad \text{Equation 43}$$

The error function here enters into the solution of the diffusion problem as a consequence of adding the effect of a series of line sources, each yielding an exponential type of distribution. In this expression we have assumed that the diffusion coefficient is the same in the solution as inside the ink. This expression gives the concentration of chloride as a function of x and t, and since the equation is symmetrical with respect to the x, the distance from the electrode (x) can have positive and negative values. In our case we are just interested in the positive values of x; where $x = 0$ is not the surface of the electrode, but the plane under the Ag/AgCl ink. At time $t = 0$, the diffusing Cl^- is confined between the plane $x = 0$ and $x = h = 30$ μm, *i.e.* the layer of Ag/AgCl.

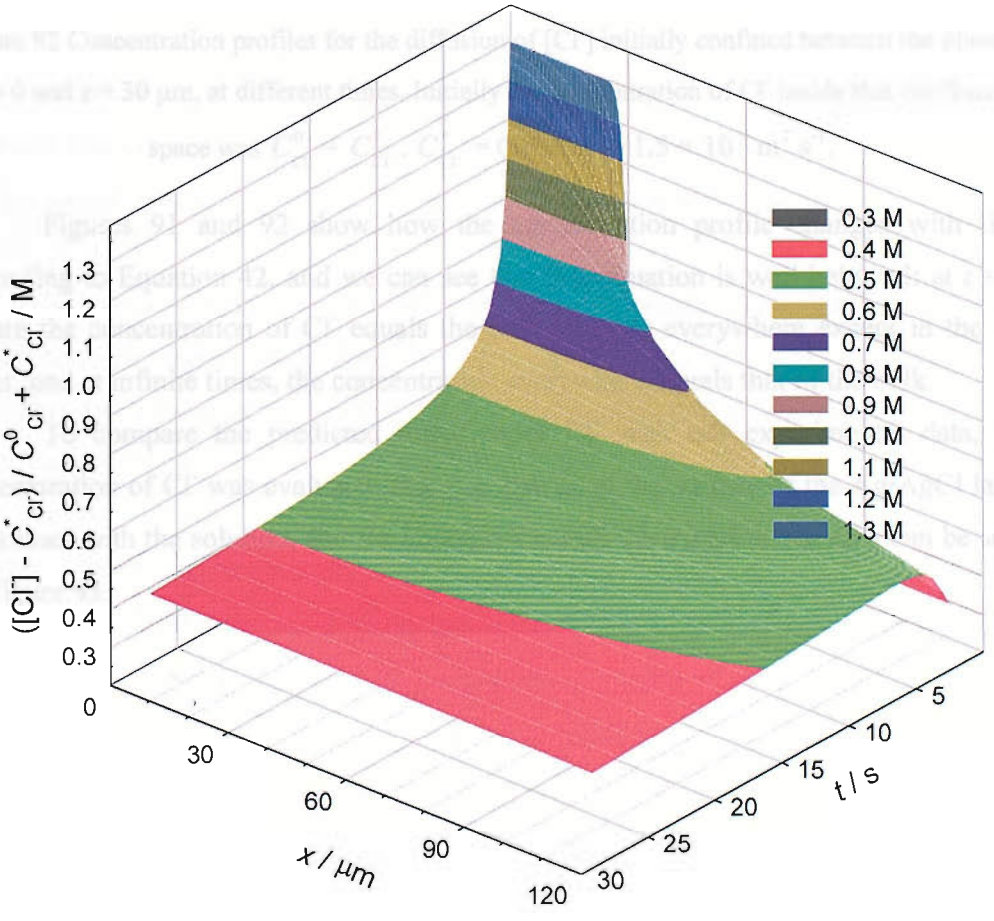

Figure 91 Predicted diffusion with time (t) and distance (x) of a defined [Cl^-] initially confined between the planes $x = 0$ and $x = 30$ μm. Initially the concentration of Cl^- inside that confined space was $C^0_{Cl^-} + C^*_{Cl^-}$. $C^*_{Cl^-} = 0.3$ M, $D = 1.5 \times 10^{-9}$ m^2 s^{-1}.

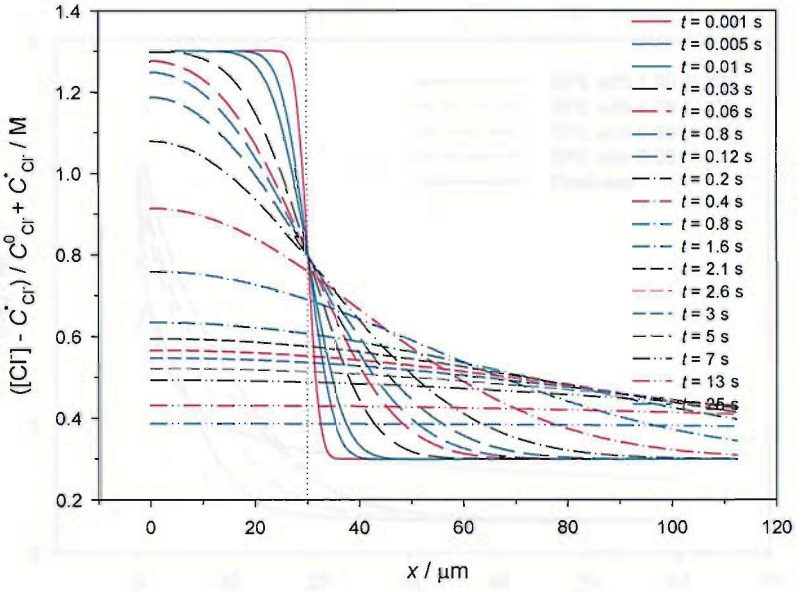

Figure 92 Concentration profiles for the diffusion of [Cl^-] initially confined between the planes $x = 0$ and $x = 30$ μm, at different times. Initially the concentration of Cl^- inside that confined space was $C^0_{Cl^-} + C^*_{Cl^-}$. $C^*_{Cl^-} = 0.3$ M, $D = 1.5 \times 10^{-9}$ m^2 s^{-1}.

Figures 91 and 92 show how the concentration profile changes with time according to Equation 42, and we can see that this equation is well behaved: at $t = 0$, where the concentration of Cl^- equals the bulk (0.3 M) everywhere except in the ink layer, and at infinite times, the concentration everywhere equals that of the bulk.

To compare the predicted diffusion of Cl^- with our experimental data, the concentration of Cl^- was evaluated at $x = h$, that is, at the surface of the Ag/AgCl layer in contact with the solution, and the comparison with the experimental data can be seen in Figure 93.

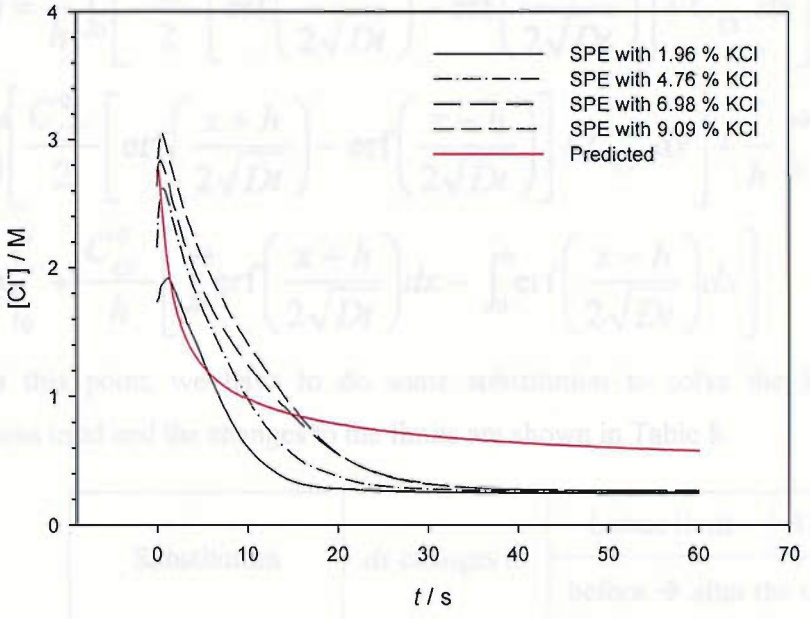

Figure 93 Variation of the [Cl^-] with t at the electrode surface (*i.e.* $x = h$) when a SPE loaded with KCl is placed in a 0.3 M KNO_3 and 0.3 M KCl solution, compared with model proposed in Equation 41 (red line). To solve the equation, $C^0_{Cl^-}$ was 4 M and D was 1.5×10^{-9} m^2 s^{-1}.

As in previous case, the concentration of Cl^- decreases very fast at the beginning, faster than the experimental data, but after the first 10-15 s, the decrease of the concentration is steadier. At $t = 60$ s, the predicted concentration is much larger that that of the bulk (0.3 M).

5.5.2.1.4. *Averaging the concentration in the whole layer of ink*

The concentration of Cl^- in the last equation (Equation 42) was evaluated at only one plane of x ($x = h$). This point may not be representative of the whole layer of AgCl, so a better way of evaluating the concentration of Cl^- measured at the electrode is by dividing the electrode layer in sections of infinitesimal thickness, and integrating across the whole layer of the electrode (from 0 to h). In this case, the expression takes the form of:

$$\overline{C}_{Cl^-}(t) = \frac{1}{h}\int_0^h C_{Cl^-}(x,t)dx \qquad \text{Equation 44}$$

and since we know the expression for the concentration of Cl^- (Equation 42):

$$\overline{C}_{Cl^-}(t) = \frac{1}{h}\int_0^h \left[\frac{C^0_{Cl^-}}{2}\left[\operatorname{erf}\left(\frac{x+h}{2\sqrt{Dt}}\right) - \operatorname{erf}\left(\frac{x-h}{2\sqrt{Dt}}\right)\right] + C^*_{Cl^-}\,dx \right] =$$

$$\frac{C^0_{Cl^-}}{h}\int_0^h \left[\frac{C^0_{Cl^-}}{2}\left[\operatorname{erf}\left(\frac{x+h}{2\sqrt{Dt}}\right) - \operatorname{erf}\left(\frac{x-h}{2\sqrt{Dt}}\right)\right] + C^*_{Cl^-}\,dx \right] + \frac{1}{h}\int_0^h C^*_{Cl^-}\,dx =$$

$$\frac{1}{h}C^*_{Cl^-}\,x\Big|_0^h + \frac{C^0_{Cl^-}}{h}\left[\int_0^h \operatorname{erf}\left(\frac{x+h}{2\sqrt{Dt}}\right)dx - \int_0^h \operatorname{erf}\left(\frac{x-h}{2\sqrt{Dt}}\right)dx \right]$$

At this point, we have to do some substitution to solve the integral. The substitutions used and the changes to the limits are shown in Table 8.

	Substitution	*dx* changes to	Lower limit	Upper limit
			before → after the substitution	
1st integral	$z = {(x+h)}/{2\sqrt{Dt}}$	$dx = 2\sqrt{Dt}\,dz$	$0 \rightarrow {h}/{2\sqrt{Dt}}$	$h \rightarrow {h}/{\sqrt{Dt}}$
2nd integral	$z' = {(x-h)}/{2\sqrt{Dt}}$	$dx = 2\sqrt{Dt}\,dz$	$0 \rightarrow -{h}/{2\sqrt{Dt}}$	$h \rightarrow 0$

Table 8 Substitutions performed to solve the integrals.

$$\overline{C}_{Cl^-}(t) = C^*_{Cl^-} + \frac{2C^0_{Cl^-}\sqrt{Dt}}{h}\left[\int_{h/2\sqrt{Dt}}^{h/\sqrt{Dt}} \operatorname{erf}(z)dz - \int_{h/2\sqrt{Dt}}^{0} \operatorname{erf}(z')dz' \right]$$

and knowing that[170]:

$$\int_a^b \operatorname{erf}(z)dz = z\operatorname{erf}(z) + \frac{e^{-z^2}}{\sqrt{\pi}}\Big|_a^b$$

we can conclude, after operating, that:

$$\overline{C}_{Cl^-}(t) = C^*_{Cl^-} + C^0_{Cl^-}\operatorname{erf}\left(\frac{h}{\sqrt{Dt}}\right) + \frac{C^0_{Cl^-}\sqrt{Dt}}{h}\left[\frac{e^{-\frac{h^2}{Dt}} - 1}{\sqrt{\pi}} \right] \qquad \text{Equation 44}$$

Equation 44 describes how the average chloride concentration in the ink varies with time, considering that initially all the chloride was confined in the region $-h < x < h$. Equation 44 was compared against the experimental data in Figure 95.

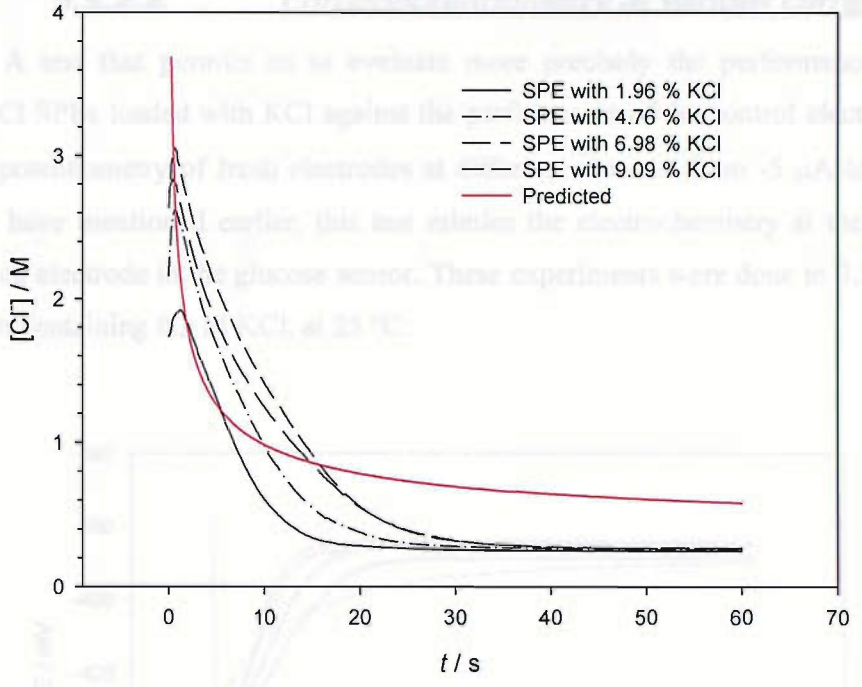

Figure 94 Variation of the average [Cl^-] within the Ag/AgCl layer with t (model proposed in Equation 44), compared with when a SPE loaded with KCl is placed in a 0.3 M KNO_3 and 0.3 M KCl solution. To solve the equation, $C^0_{Cl^-}$ was chosen as 4 M and D was 1.5×10^{-9} m^2 s^{-1}.

Again, the predicted model does not match the experimental data. As with the other two models, the concentration decreased sharply at the beginning, and after 10-15 seconds the concentration started to decrease more slowly. In the 30 seconds of the experiment, the concentration did not drop to the expected value of the bulk solution.

The experimental data differs from the three models that we have tried in that the concentration of chloride gets down to the value of the bulk within 30-40 seconds, meanwhile the models require much more time to equilibrate. Therefore we conclude that there is some other effect that is helping in the equilibration of the concentration of Cl^- at the electrode, and it is probably the natural convection. Although the solution is not stirred, the fact that the electrode is immersed in the solution to start the measurement, this movement will create some perturbation in the solution that could favour convection, and hence assisting in transport of Cl^- away from the electrode.

5.5.2.2. Chronopotentiometry at various currents.

A test that permits us to evaluate more precisely the performance of these Ag/AgCl SPEs loaded with KCl against the performance of the control electrode is the chronopotentiometry of fresh electrodes at different currents, from -5 μA to -100 μA. As we have mentioned earlier, this test mimics the electrochemistry at the counter – reference electrode in the glucose sensor. These experiments were done in 0.5 M KNO_3 solution containing 0.3 M KCl, at 25 °C.

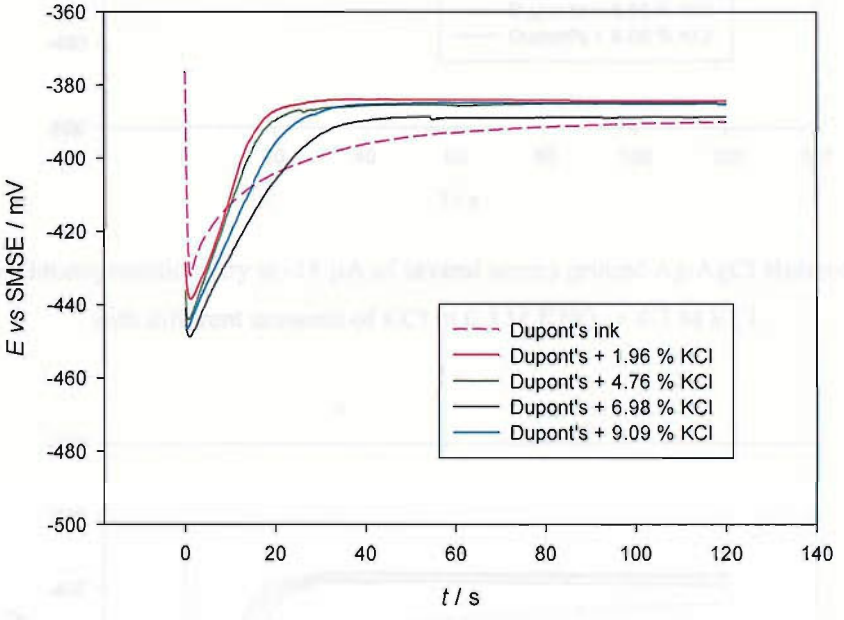

Figure 95 Chronopotentiometry at -5 μA of several screen printed Ag/AgCl electrodes loaded with different amounts of KCl in 0.3 M KNO_3 + 0.3 M KCl.

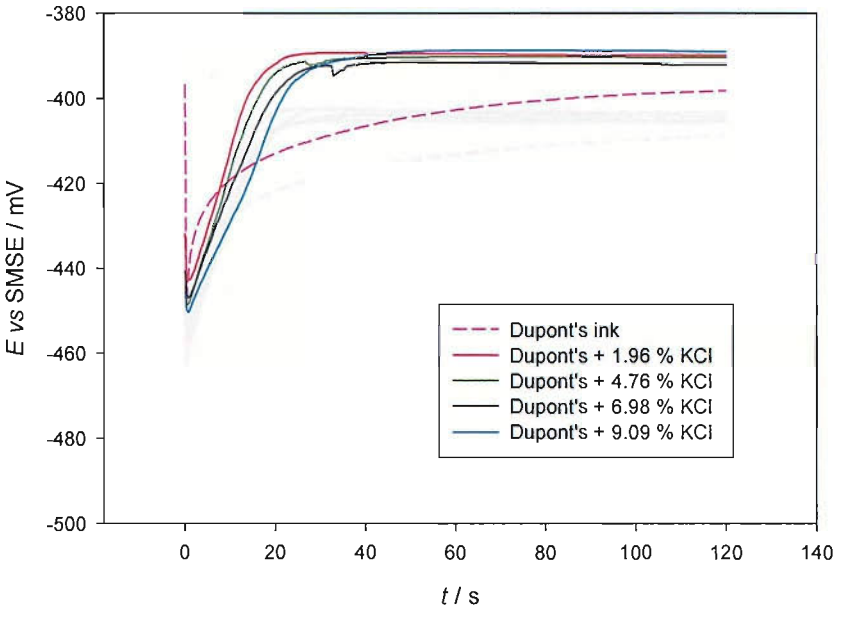

Figure 96 Chronopotentiometry at -15 μA of several screen printed Ag/AgCl electrodes loaded with different amounts of KCl in 0.3 M KNO_3 + 0.3 M KCl.

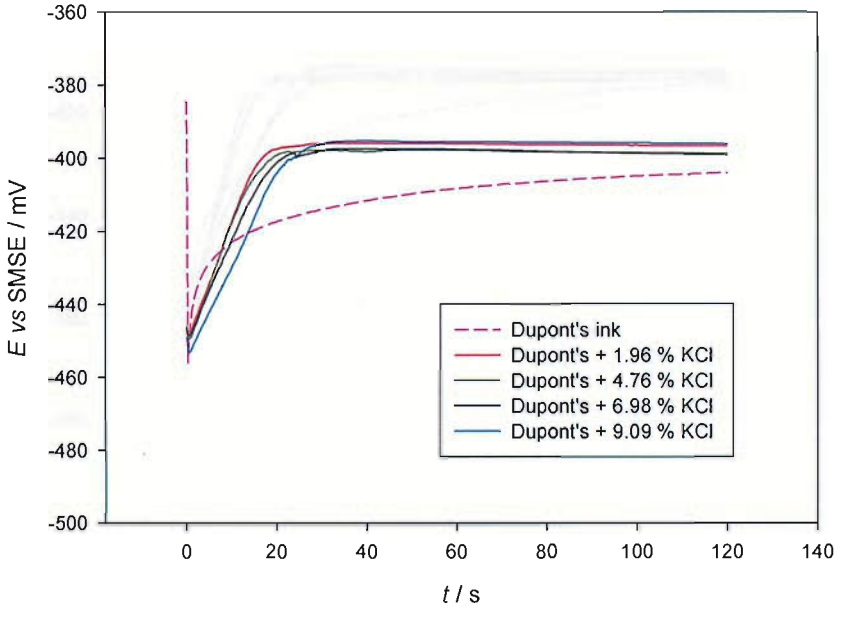

Figure 97 Chronopotentiometry at -30 μA of several screen printed Ag/AgCl electrodes loaded with different amounts of KCl in 0.3 M KNO_3 + 0.3 M KCl

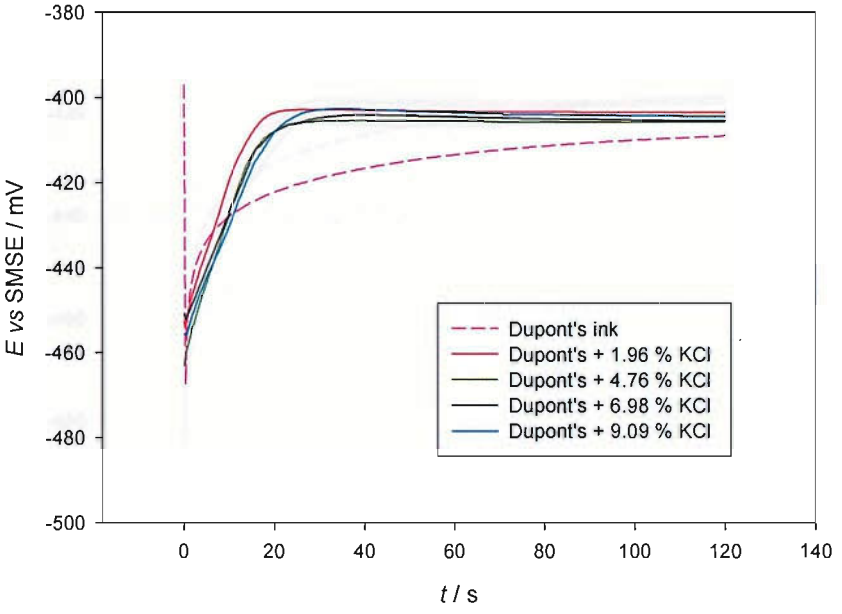

Figure 98 Chronopotentiometry at -50 μA of several screen printed Ag/AgCl electrodes loaded with different amounts of KCl in 0.3 M KNO_3 + 0.3 M KCl.

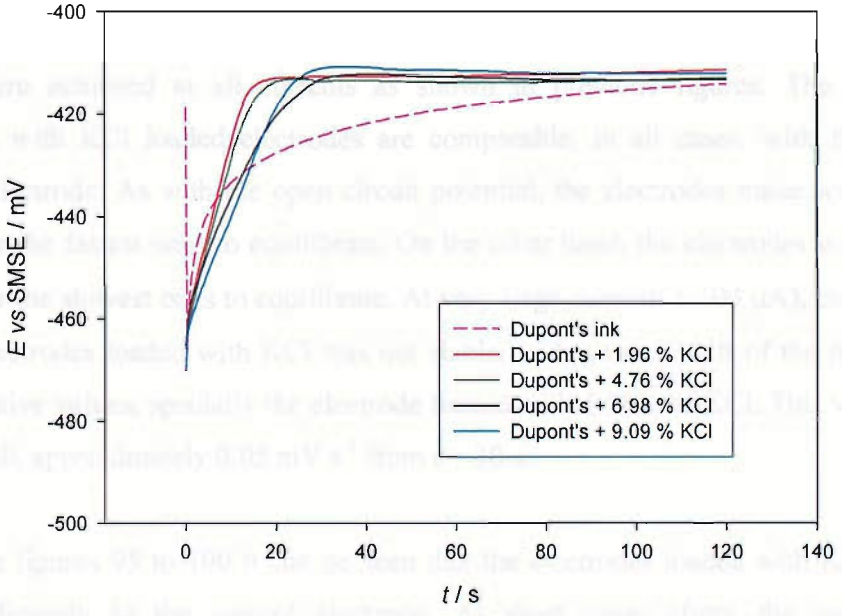

Figure 99 Chronopotentiometry at -75 μA of several screen printed Ag/AgCl electrodes loaded with different amounts of KCl in 0.3 M KNO_3 + 0.3 M KCl.

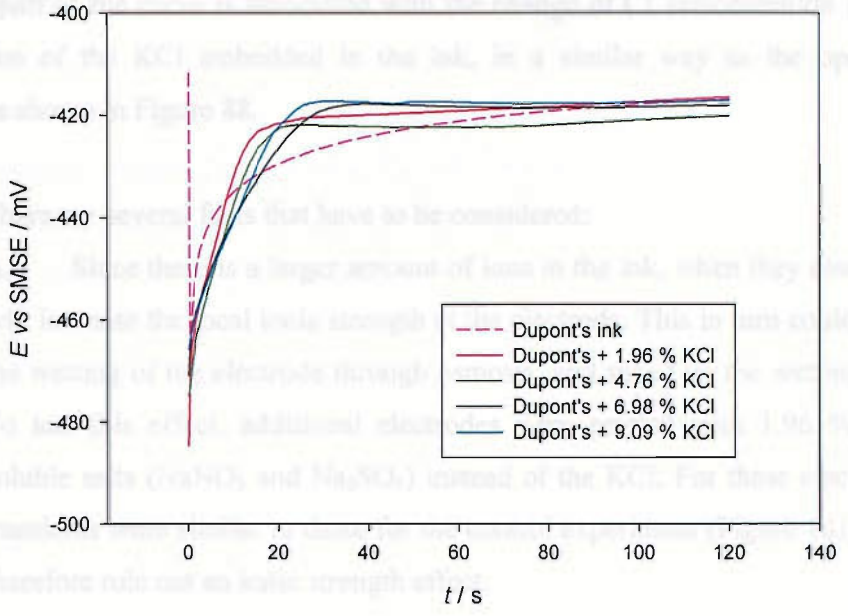

Figure 100 Chronopotentiometry at -100 μA of several screen printed Ag/AgCl electrodes loaded with different amounts of KCl in 0.3 M KNO_3 + 0.3 M KCl.

As we have seen in previous section (Figure 88) the performance of the electrodes loaded with KCl was better than the commercial ones. Faster equilibration times were achieved at all currents as shown in previous figures. The potentials achieved with KCl loaded electrodes are comparable, in all cases, with that of the control electrode. As with the open circuit potential, the electrodes made with 1.96 % KCl were the fastest ones to equilibrate. On the other hand, the electrodes with 6.98 % KCl were the slowest ones to equilibrate. At very large currents (-100 μA), the potential of the electrodes loaded with KCl was not stable, with a small shift of the potential to less negative values, specially the electrode loaded with 1.96% of KCl. This variation is very small, approximately 0.05 mV s^{-1} from t = 30 s.

In figures 95 to 100 it can be seen that the electrodes loaded with KCl behave very differently to the control electrode. At short times (from the start of the measurement till approximately 20-30 seconds) the slope is constant, and at long times (after approximately 30 s) the potential is equilibrated. At short times, the mechanism that controls the potential is different for the electrode loaded with KCl and for the control electrode.

In the case of the electrode loaded with KCl, we have mentioned that the wetting of the whole electrode occurs rapidly, within 2-3 seconds after the electrode is placed in

solution (Figure 88 and its interpretation). In this case, the variation of the potential in the first part of the curve is associated with the change of Cl^- concentration due to the dissolution of the KCl embedded in the ink, in a similar way as the open circuit transients shown in Figure 88.

There are several facts that have to be considered:

A. Since there is a larger amount of ions in the ink, when they dissolve they will increase the local ionic strength at the electrode. This in turn could facilitate the wetting of the electrode through osmosis, and speed up the wetting process. To test this effect, additional electrodes were printed with 1.96 % of other soluble salts ($NaNO_3$ and Na_2SO_4) instead of the KCl. For these electrodes the transients were similar to those for the control experiment (Figure 101). We can therefore rule out an ionic strength effect.

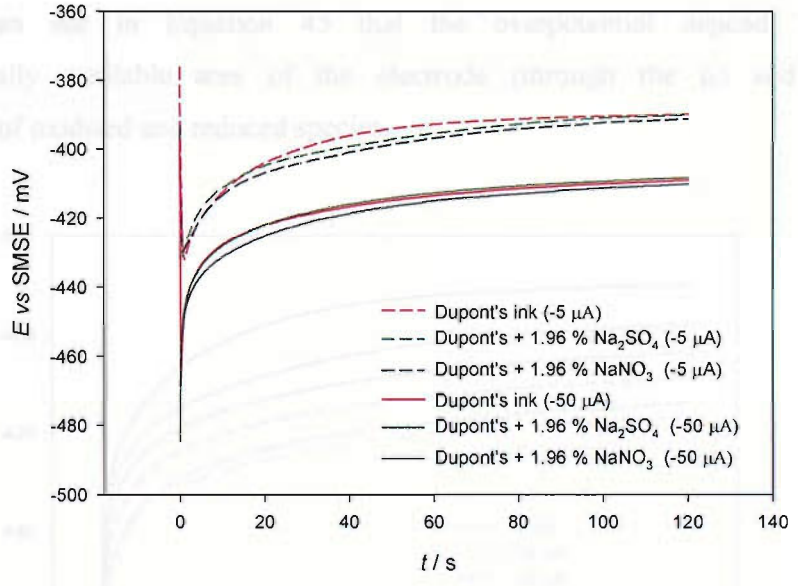

Figure 101 Comparison of the chronopotentiometry at -5 µA (dashed lines) and -50 µA (solid lines) of SPEs loaded with non-chloride salts against control SPEs (red lines). Experiment was carried at 25 °C in 0.3 M KNO_3 + 0.3 M KCl.

B. The increase in porosity of the electrode could also favour a better wetting of the electrode. Additionally, when the KCl is dissolved, it could create channels and additional pores, increasing the specific area of the electrode. If this was the case, other salts like $NaNO_3$ and Na_2SO_4 should exhibit the same effect, (biased considering their relative solubilities), but, *idem quod ante*, these electrodes with $NaNO_3$ and Na_2SO_4 exhibit the same transients as the control

electrodes. *A fortiori*, electrodes with larger amounts of KCl should show an enhanced effect, but this was not the case.

Another interesting observation is that the electrodes loaded with KCl show the same behaviour at open circuit Figure 88 and when a current is applied (*i.e.* at -5μA, Figure 95), meanwhile, for the control SPE the potential transient is significantly different at open circuit and when a current is applied to the electrode. The open circuit potential is established by the relative concentrations of the species through the Nernst equation, meanwhile the potential at any given current is controlled by the Butler-Volmer equation shown previously in Equation 11, included here again as Equation 45.

$$i = i_0 \left[\frac{c_R(0,t)}{c_R^*} e^{\frac{(1-\alpha)nF\eta}{RT}} - \frac{c_O(0,t)}{c_O^*} e^{\frac{-\alpha nF\eta}{RT}} \right] \qquad \text{Equation 45}$$

We can see in Equation 45 that the overpotential depends on the electrochemically available area of the electrode (through the i_0) and in the concentration of oxidised and reduced species.

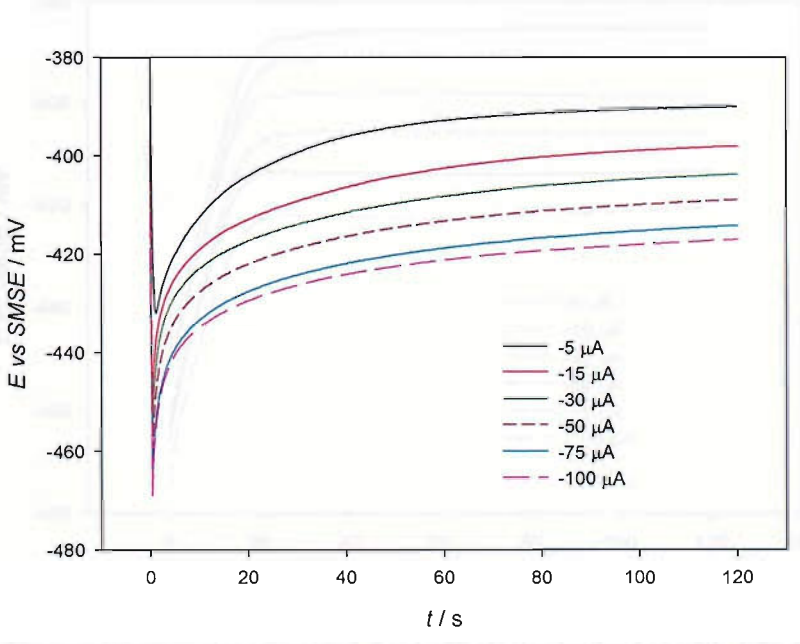

Figure 102 Chronopotentiometry of several Ag/AgCl electrodes without added KCl held at the specified current in 0.3 M KNO_3 + 0.3 M KCl.

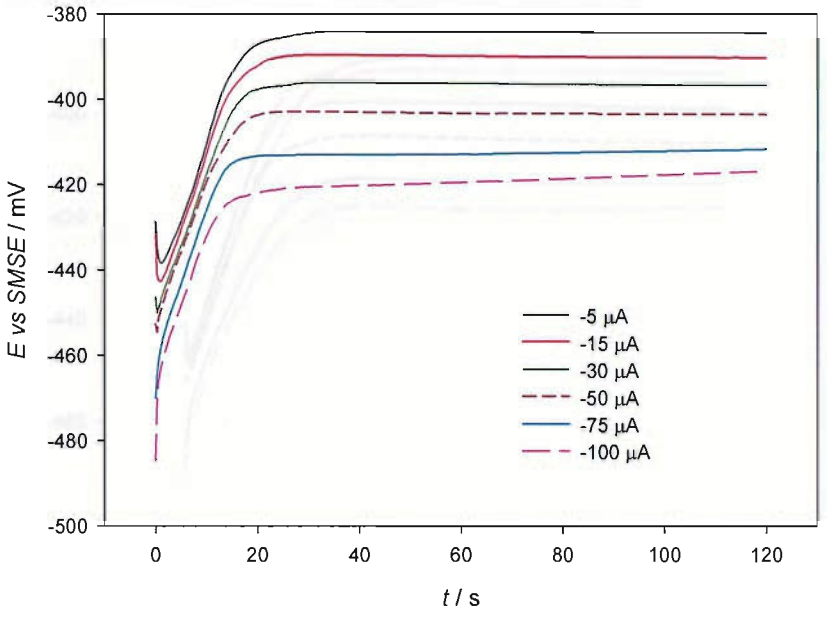

Figure 103 Chronopotentiometry of several Ag/AgCl electrodes loaded with 1.96 % KCl held at the specified current in 0.3 M KNO_3 + 0.3 M KCl.

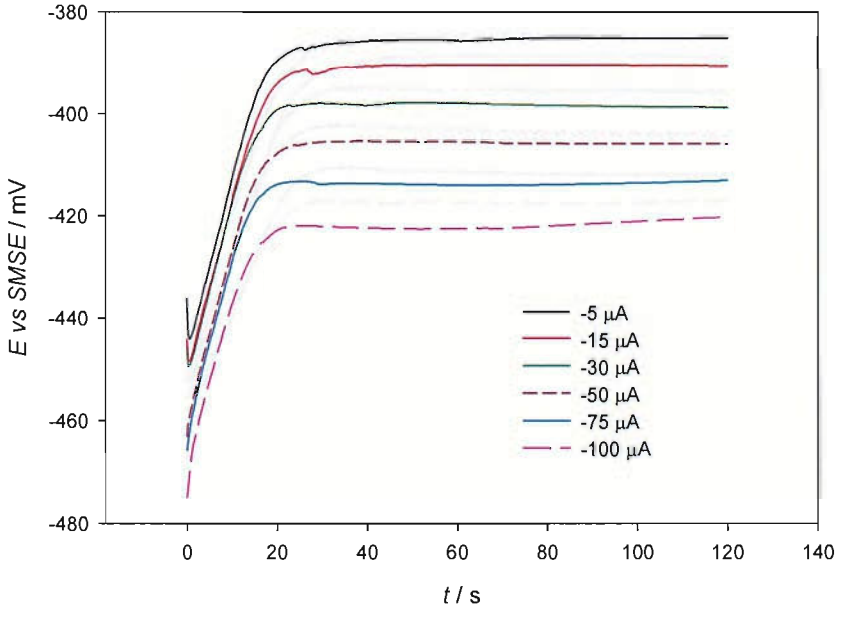

Figure 104 Chronopotentiometry of several Ag/AgCl electrodes loaded with 4.76 % KCl held at the specified current in 0.3 M KNO_3 + 0.3 M KCl.

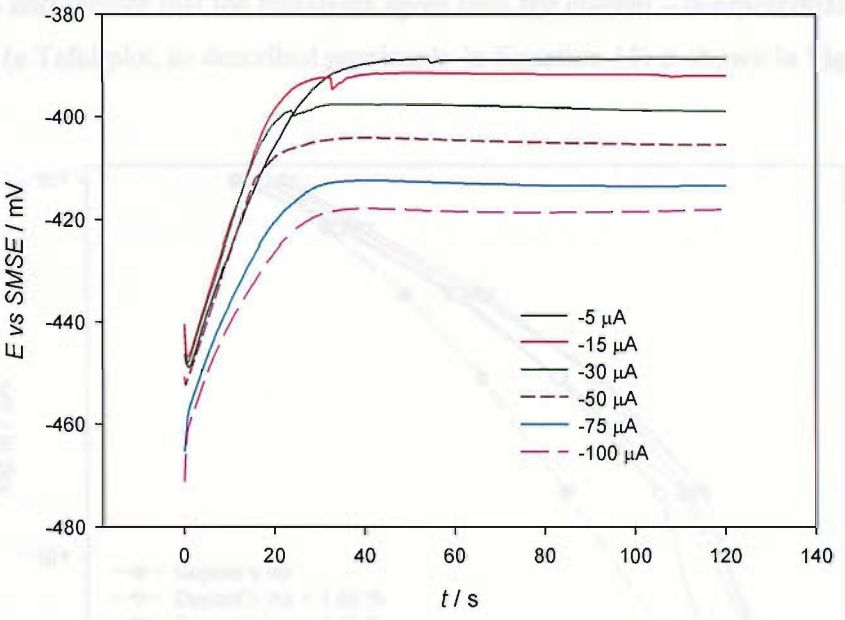

Figure 105 Chronopotentiometry of several Ag/AgCl electrodes loaded with 6.98 % KCl held at the specified current in 0.3 M KNO_3 + 0.3 M KCl.

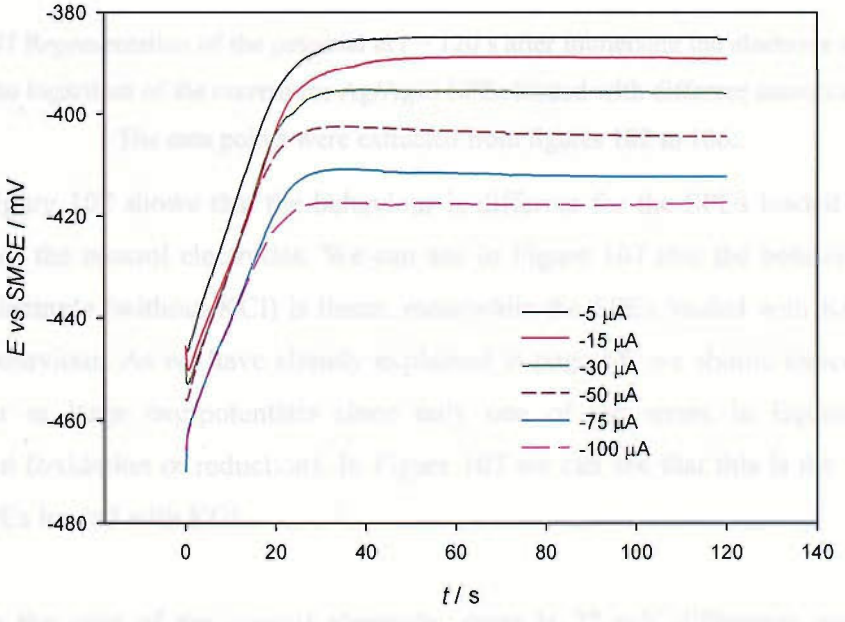

Figure 106 Chronopotentiometry of several Ag/AgCl electrodes loaded with 9.09 % KCl held at the specified current in 0.3 M KNO_3 + 0.3 M KCl.

The potential of the electrode at longer times is established by the current overpotential equation (Equation 11, page 58) where the current is a function of the potential and the concentration of chloride at the electrode. We can represent the

potential at t = 120 s for each electrode against the logarithm of the current (in absolute value), to corroborate that the transients agree with the current – overpotential equation. This plot (a Tafel plot, as described previously in Equation 13) is shown in Figure 107.

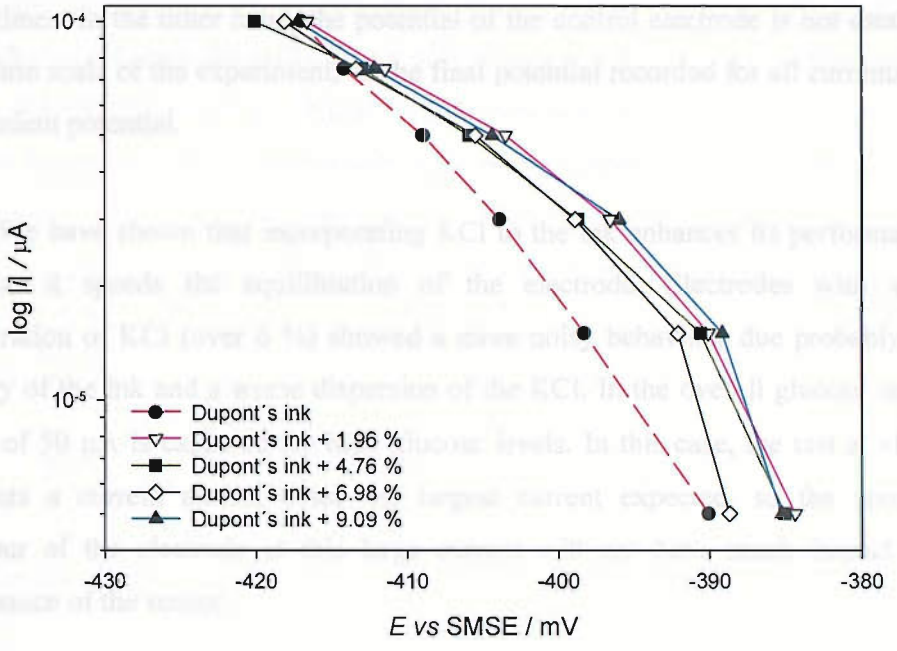

Figure 107 Representation of the potential at t = 120 s after immersing the electrode in solution against the logarithm of the current for Ag/AgCl SPEs loaded with different amounts of AgCl. The data points were extracted from figures 102 to 106.

Figure 107 shows that the behaviour is different for the SPEs loaded with KCl and that of the control electrodes. We can see in Figure 107 that the behaviour of the control electrode (without KCl) is linear, meanwhile the SPEs loaded **with KCl** show a curved behaviour. As we have already explained in page 58, we should expect a linear behaviour at large overpotentials since only one of the terms in Equation 11 is significant (oxidation or reduction). In Figure 107 we can see that this is the behaviour of the SPEs loaded with KCl.

In the case of the control electrode, there is 27 mV difference between the potentials at -5 µA and -100 µA. This difference is 32 mV for the electrodes with 1.96 % wt of KCl, 35 mV, 29 mV and 32 mV for the electrodes with 4.76 %, 6.98 % and 9.09 % respectively. According to these values, the difference in the potential at different currents is slightly larger for the electrodes loaded with KCl than control SPE. This slight difference can be associated with the fact that, in the case of SPEs loaded with KCl, the potential is equilibrated for low currents, but it is still shifting towards

less negative potentials at the larger current measured, so the final potentials at -5 μA and -100 μA were not recorded under the same circumstances (at -5 μA the value is a steady state value, meanwhile at -100 μA the potential is not well equilibrated). It is expected that less negative potentials will be recorded if the experiment is carried over longer times. In the other hand, the potential of the control electrode is not established in the time scale of the experiment, so the final potential recorded for all currents tested is a transient potential.

We have shown that incorporating KCl to the ink enhances its performance, in particular it speeds the equilibration of the electrode. Electrodes with a large concentration of KCl (over 6 %) showed a more noisy behaviour due probably to the rheology of the ink and a worse dispersion of the KCl. In the overall glucose sensor, a current of 50 μA is expected for high glucose levels. In this case, the test at -100 μA represents a current almost twice the largest current expected, so the anomalous behaviour of the electrode at this large current will not have much impact in the performance of the sensor.

5.5.2.3. Chronoamperometry of a reversible redox couple using the screen printed electrode as reference-counter electrode.

Ag/AgCl electrodes loaded with KCl seem, based in the experiments presented so far, a suitable alternative as a screen printed counter-reference electrode. In order to test these electrodes further, they were used as counter reference electrodes in an electrochemical characterization of a redox couple. The electrochemical system was composed of a 4 mm diameter glassy carbon electrode (GCE) as the working electrode and KCl loaded Ag/AgCl SPE as the counter-reference electrode in a two electrode configuration. The area of the WE was 3.14 times larger than the size of the Ag/AgCl counter-reference electrode.

The redox system tested was 1,1'-ferrocenedicarboxylic acid [$Fe(C_5H_4$-$COOH)_2$]. For this compound, the Fe(II) centre can be oxidised reversibly at a glassy carbon electrode. In this case, when the Fe(II) is oxidised at the GCE, an equivalent reduction current must flow at the counter- reference electrode. This mimics the behaviour of the glucose sensor as described in the introduction. The 1,1'-ferrocenedicarboxylic acid was dissolved in an alkaline solution (pH ~ 11.3) in order to

deprotonate the carboxylic group and increase its solubility. This increase of the pH is not expected to affect the electrochemistry of the counter-reference electrode, so these results can be extrapolated to the case of the glucose sensor. Additionally, the electrochemistry of the $Fe(C_5H_4\text{-}COOH)_2$ is very similar to that of the ferrocene used in the working electrode of the glucose sensor as the mediator of the GOx, so this setup mimics reasonably well the performance of the overall sensor. A concentration of 5 mM of $Fe(C_5H_4COOH)_2$, was used because this concentration, for this setup and under mass transport control at large overpotentials, generates a current of approximately 100 μA. This current is comparable with the currents tested in previous section, and is twice as large as the maximum current expected in the glucose sensor.

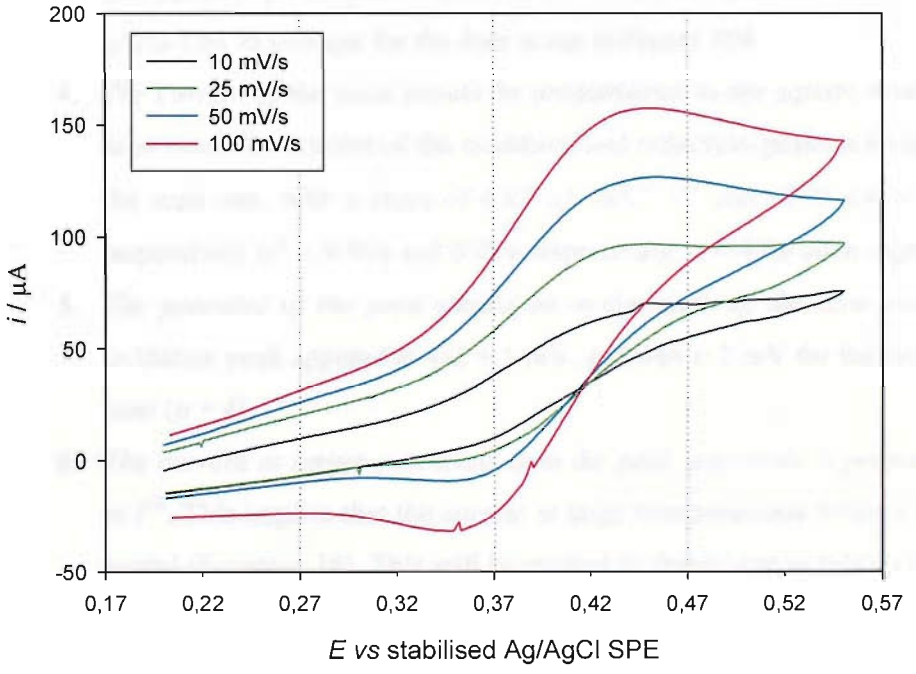

Figure 108 Cyclic voltammetry at different scan rates of 5 mM $Fe(C_5H_4COOH)_2$ in 0.3 M KNO_3 and 0.3 M KCl (pH 11.3) at a GCE ($\phi = 4$ mm). A previously stabilised Ag/AgCl SPE was used as the counter-reference electrode.

The electrochemistry of the $Fe(C_5H_4COOH)_2$ is shown in Figure 108. We can see that the potential of the oxidising and reducing peaks does not change with the scan rate, suggesting that the system is reversible under these experimental conditions. We can also see that there is some *iR* drop in the scan, due to the resistance of the track. Tis *iR* is evidenced in the slope of the baseline, with currents recorded even at lower overpotentials than the oxidation process (-0.2 to -0.3 V *vs* Ag/AgCl). In addition, we have to consider that we are using a two electrode system (the Ag/AgCl SPE acts both

as counter and reference electrode), so the potential applied depends on the resistance of the cell and the current flowing across the system.

To test the reversibility of the system, several other tests of reversibility[90] were performed, and the results appear in next points:

1. *The difference between the potential of the oxidation and reduction peaks should be 59/n mV.* This difference is 67.5 ± 2.65 mV for the average of the four scans in Figure 108.
2. *The difference between the peak potential and the half peak potential should be 59/n mV.* It is 54.2 ± 1.35 mV for the eight peaks (4 oxidation, 4 reduction) in Figure 108.
3. *The current of both peaks (oxidation and reduction) should be the same.* i_a/i_c is 1.01 in average for the four scans in Figure 108.
4. *The current of the peak should be proportional to the square root of the scan rate.* The current of the oxidation and reduction peaks is linear with the scan rate, with a slope of 6.82 μA $mV^{½}$ $s^{-½}$ and -6.73 μA $mV^{½}$ $s^{-½}$ respectively (r^2 = 0.996 and 0.999 respectively, n = 4 for each regresion)
5. *The potential of the peak should be independent of the scan rate.* The oxidation peak appears at 432 ± 1 mV, and 364 ± 2 mV for the reduction scan (n = 4).
6. *The current at larger potentials than the peak potentials is proportional to* $t^{-½}$. This implies that the current at large overpotentials follows Cotrell model (Equation 16). This will be studied in detail later in this section.

These results show that the $Fe(C_5H_4COOH)_2$ behaves almost as a perfectly reversible system. An implication of this is that the kinetics of the electron transfer are significantly faster than the rate of mass transport, and hence the system is under Nernstian equilibrium at any given potential. The current will therefore be limited by the amount of redox species at the electrode, and by the diffusion of these species to and from the bulk solution.

The new counter-reference electrode was evaluated at two different potentials; +370 mV and +550 mV. These potentials were chosen as the half peak potential ($E_{P/2}$), and a potential larger than the peak potential ($E > E_P$). Under these experimental conditions, fluctuations of the potential of the reference electrode will force variations in the potential applied for the oxidation at the working electrode. At potentials before

the peak potential, and especially at the $E_{P/2}$, small variations in the potential applied will cause significant variations of the concentration of the species at the electrode so different currents will be recorded. At potentials after the peak potential, the potential is large enough to oxidise all the Fe^{2+} at the electrode, so the concentration of species at the electrode is effectively zero, so small variations of the potential will have no effect in the concentration of the species at the electrode and little effect in the measured current.

Special attention was paid to the response immediately following immersion of the SPE in the solution. Two different sets of experiments were therefore performed. One set, with fresh, new, dried electrodes, to study the incidence of the potential evolution in the current. In the second set, the electrode was left in solution until the potential of the reference electrode was equilibrated (at least 4 minutes) and afterwards, another transient was recorded. Although this last setup is not representative for the glucose sensor (for measuring glucose, the sensor will not be equilibrated for such a long time and it will be discarded after use), it allows us to identify differences in the behaviour of the counter-reference electrode right when it is placed in solution, with the behaviour once it has already been equilibrated. Any differences between both set of experiments will be due to the wetting and equilibration of the potential of the counter-reference electrode.

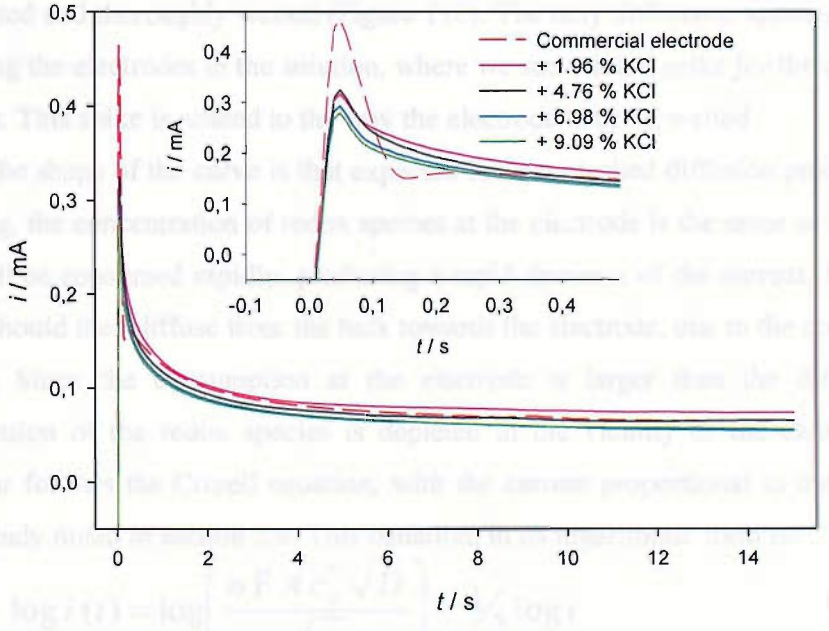

Figure 109 Chronoamperometry at 550 mV of 5 mM $Fe(C_5H_4COOH)_2$ in 0.3 M KNO_3 and 0.3 M KCl at a GCE ($\phi = 4$ mm) with fresh Ag/AgCl SPE as the counter-reference electrode.

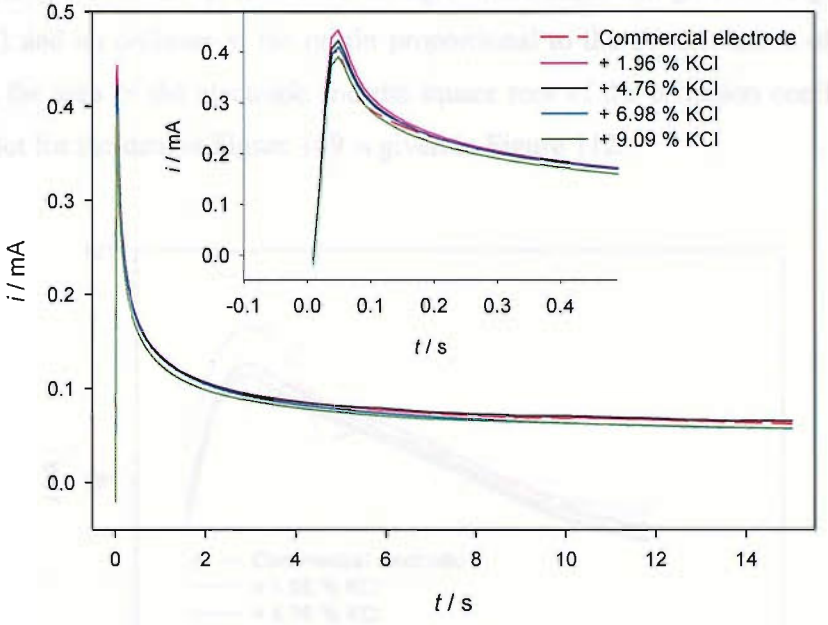

Figure 110 Chronoamperometry at 550 mV of 5 mM $Fe(C_5H_4COOH)_2$ in 0.3 M KNO_3 and 0.3 M KCl at a GCE (ϕ = 4 mm) with stabilised Ag/AgCl SPE as the CR electrode.

Each of the transients shown in figures 109 and 110 (and also for the following figures 113 and 114) represents the most characteristic signal obtained from three different electrodes from different printed boards.

At 550 mV, all the electrodes performed similarly once the electrode has been equilibrated and thoroughly wetted (Figure 110). The only difference appears right after immersing the electrodes in the solution, where we see a small spike for the commercial electrode. This spike is related to the way the electrode is being wetted.

The shape of the curve is that expected for a controlled diffusion process. At the beginning, the concentration of redox species at the electrode is the same as in the bulk, but it will be consumed rapidly, producing a rapid decrease of the current. More redox species should then diffuse from the bulk towards the electrode, due to the concentration gradient. Since the consumption at the electrode is larger than the diffusion, the concentration of the redox species is depleted in the vicinity of the electrode. This behaviour follows the Cotrell equation, with the current proportional to the $t^{-1/2}$ as we have already noted in section 3.4. This equation, in its logarithmic form is:

$$\log i\,(t) = \log\left(\frac{n\,\mathrm{F}\,A\,c_0^*\sqrt{D}}{\sqrt{\pi}}\right) - \tfrac{1}{2}\log t \qquad \text{Equation 46}$$

The *i-t* transient representation in logarithmic scale will give a straight line with slope -1/2 and an ordinate at the origin proportional to the concentration of species in the bulk, the area of the electrode and the square root of the diffusion coefficient. The Cotrell plot for the data in Figure 109 is given in Figure 112.

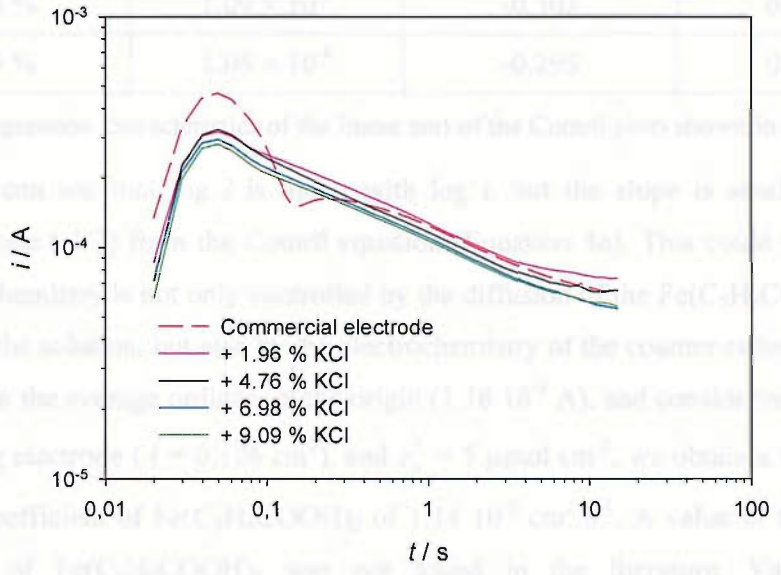

Figure 111 Cotrell plot for data in Figure 109.

In Figure 111 we can see that although all the electrodes loaded with KCl show similar Cotrell plots, the response for the commercial electrode presents a strange behaviour at very short times ($t < 1$ s). After this first second, all the electrodes show similar plots.

At longer times ($10 < t < 15$), those loaded with concentrations of KCl under 5 % exhibit a non linear relationship of the log *i* with the log *t*. This deviation from the linearity indicates that the current has reached a plateau and no longer varies with time. When the chronoamperometry is taking place, we are depleting the species from the electrode, creating a diffusion layer in the vicinity of the electrode. This diffusion layer does not grow indefinitely, and it is limited by natural convection in the solution.

An analysis of the linearity of this data can be found in Table 9.

% of KCl in ink	Ordinate / A	Slope	*r*
0 %	1.22×10^{-4}	-0.289	0.9984
1.96 %	1.27×10^{-4}	-0.300	0.9988
4.76 %	1.16×10^{-4}	-0.296	0.9973
6.98 %	1.09×10^{-4}	-0.302	0.9988
9.09 %	1.06×10^{-4}	-0.295	0.9986

Table 9 Regression characteristics of the linear part of the Cotrell plots shown in Figure 112.

We can see that log *i* is linear with log *t*, but the slope is smaller than the expected slope (-1/2) from the Cotrell equation (Equation 46). This could indicate that the electrochemistry is not only controlled by the diffusion of the $Fe(C_5H_4COOH)_2$ from the bulk to the solution, but also by the electrochemistry of the counter-reference.

From the average ordinate at the origin ($1.16\ 10^{-4}$ A), and considering the area of the working electrode ($A = 0.126$ cm^2), and $c_o^* = 5$ μmol cm^{-3}, we obtain a value for the diffusion coefficient of $Fe(C_5H_4COOH)_2$ of $1.14\ 10^{-5}$ cm^2 s^{-1}. A value of the diffusion coefficient of $Fe(C_5H_4COOH)_2$ was not found in the literature. Values for 1-ferrocenecarboxylate in water have been reported ($0.48\ 10^{-5}$ cm^2 s^{-1})[171]. According to White *et al.*, the diffusion coefficient of $Fe(C_5H_4COOH)_2$ is significantly larger than that of the 1-ferrocenecarboxylate[172], since $Fe(C_5H_4COO^-)_2$ produces a larger limiting current at a submicrometer electrode than a similar solution of 1-ferrocenecarboxylate. In this work they did not include the value of the diffusion coefficient for these species; neither did they state the radius of the electrode.

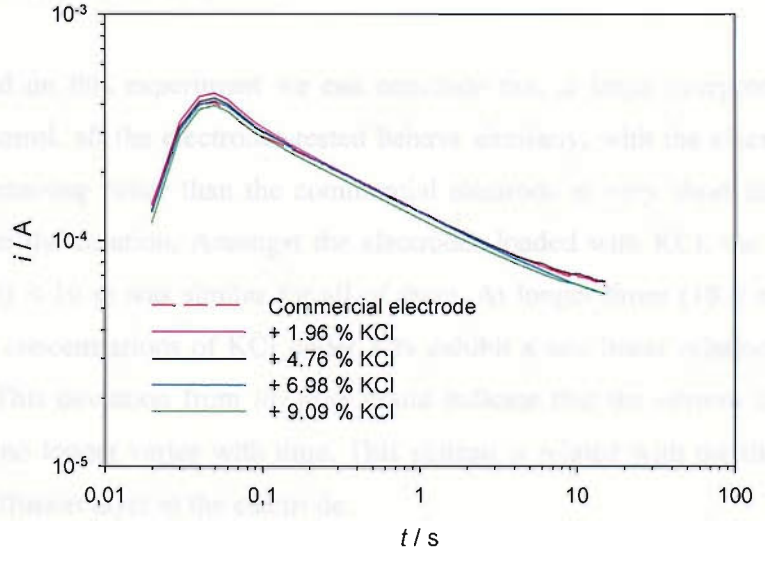

Figure 112 Cotrell plot for data in Figure 110.

The Cotrell plot for the transients recorded with equilibrated counter-reference SPEs is presented in Figure 112. In this case we have obtained very similar Cotrell plots for every electrode composition. In Figure 112 we can see that at long times ($t > 10$ s), the log i of the electrodes with less than 5 % of KCl is, again, not linear against log t. An analysis of the linearity of this data can be found in Table 10.

% of KCl in ink	Ordinate / a.u.	Slope / a.u.	r
0 %	1.35×10^{-4}	-0.3365	0.9998
1.96 %	1.36×10^{-4}	-0.3475	0.9994
4.76 %	1.34×10^{-4}	-0.3423	0.9996
6.98 %	1.34×10^{-4}	-0.3496	0.99996
9.09 %	1.26×10^{-4}	-0.3474	0.9997

Table 10 Regression characteristics of the linear part of the Cotrell plots shown in Figure 112.

The slope of these linear segments is slightly larger than that shown in Table 9, but still smaller than the expected -1/2 shown in Equation 46. The ordinate at the origin is very similar in all cases (except 9.09 %), and again, slightly larger than that shown in Table 9. From the average ordinate at the origin (without considering the value for 9.09% KCl), and considering $A = 0.126$ cm^2, and $c_o^* = 5$ μmol cm^{-3}, in this case, the calculated value for the diffusion coefficient of $Fe(C_5H_4COOH)_2$ is 1.58 10^{-5} cm^2 s^{-1}. Also in this case, the electrodes with less than 5 % of KCl appear to reach a plateau at long times ($t > 10$ s), meanwhile electrodes with larger amount of KCl still show the predicted behaviour at longer times.

Based on this experiment we can conclude that at large overpotentials, under diffusion control, all the electrodes tested behave similarly, with the electrodes loaded with KCl behaving better than the commercial electrode at very short times after the immersion in the solution. Amongst the electrodes loaded with KCl, the behaviour at short times ($t < 10$ s) was similar for all of them. At longer times ($10 < t < 15$), those loaded with concentrations of KCl under 5 % exhibit a non linear relationship of log i with log t. This deviation from linearity could indicate that the current has reached a plateau and no longer varies with time. This plateau is related with the time needed to create the diffusion layer at the electrode.

Electrodes were also poised at 370 mV against the SP Ag/AgCl electrode. This potential was chosen as a potential at the half peak ($E_{P/2}$). At this potential, since the potential difference between the counter-reference and working electrodes is fixed, small variations of the potential of the counter-reference electrode will cause the largest possible variation in the current at the working electrode.

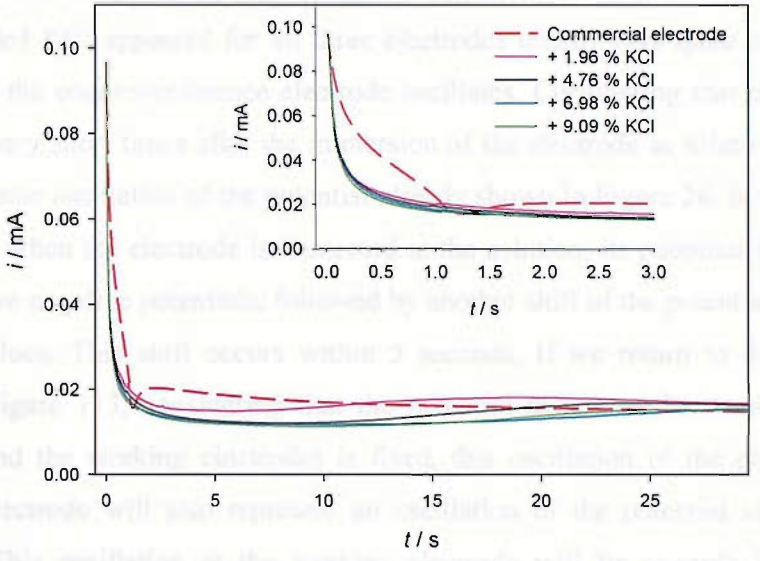

Figure 113 Chronoamperometry at 370 mV of 5 mM $Fe(C_5H_4COOH)_2$ in 0.3 M KNO_3 and 0.3 M KCl at a GCE (ϕ = 4 mm) with fresh Ag/AgCl SPE as the counter-reference electrode.

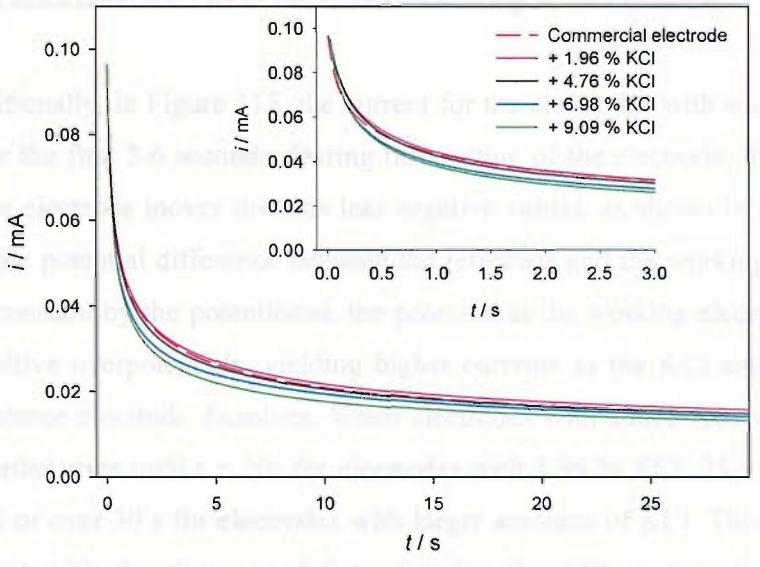

Figure 114 Chronoamperometry at 370 mV of 5 mM $Fe(C_5H_4COOH)_2$ in 0.3 M KNO_3 and 0.3 M KCl at a GCE (ϕ = 4 mm) with stabilised Ag/AgCl SPE as the CR electrode.

In the figures 113 and 114, the same experiment was performed, but at a much smaller overpotential. The results are similar to those obtained at +550 mV. Once the

electrodes are stabilised, the response is exactly the same for all the electrodes, independent of the concentration of chloride added in the ink. The differences appear when the experiment is performed with dried electrodes. In this case, all the electrodes with added Cl^- perform in a very similar way at short times (less than 3 seconds), following a Cotrell decay, meanwhile the commercial electrode shows a strange transient. The spike present at short times (t = 1 s) in the transient for the electrode without added KCl appeared for all three electrodes tested. This spike means that the potential of the counter-reference electrode oscillates. Considering that this oscillation appears at very short times after the immersion of the electrode in solution, we believe that is the same oscillation of the potential already shown in Figure 26. In that figure we can see that when the electrode is immersed in the solution, its potential shifts abruptly towards more negative potentials, followed by another shift of the potential towards less negative values. This shift occurs within 5 seconds. If we return to the experiment shown in Figure 113, considering that the potential difference between the counter-reference and the working electrodes is fixed, this oscillation of the potential of the Ag/AgCl electrode will also represent an oscillation of the potential at the working electrode. This oscillation at the working electrode will be towards less oxidizing potentials, with a consequent sharp decrease of the current as shown in Figure 113. This oscillation was the topic of the previous chapter (chapter 4) and we have proposed that this effect is associated with some nucleation occurring at the electrode.

Additionally, in Figure 113, the current for the electrodes with added KCl starts to raise after the first 3-6 seconds. During the wetting of the electrode, the potential of the reference electrode moves towards less negative values, as shown in figures 103 to 106. Since the potential difference between the reference and the working electrodes is being held constant by the potentiostat, the potential at the working electrode is shifted to more positive overpotentials, yielding higher currents as the KCl embedded in the counter-reference electrode dissolves. When electrodes with added KCl were used, the current recorded rises until t = 20s for electrodes with 1.96 % KCl, 25 s for electrodes with 4.76 % or over 30 s for electrodes with larger amounts of KCl. These time values are consistent with the times needed to dissolve the KCl in the electrode and to equilibrate the concentration of Cl^- (and hence to equilibrate the potential) shown previously in Figure 88. Once the current stabilises, the value of the current matched the values recorded with stabilised electrodes.

5.5.3. Conclusions

In this section we have shown that the electrodes loaded with KCl exhibit faster and more stable responses right after immersion in the sample than the commercial electrodes. The dissolution of the Cl^- embedded in the ink facilitates the equilibration of the electrode as seen in the open circuit potential and in the galvanostatic transients.

A ferrocene derivative ($Fe(C_5H_4COOH)_2$) was used in a model reaction to evaluate further the performance of the new SPE in a system that mimics the operation of the glucose sensor. The electrodes loaded with KCl behaved as expected from the theory, meanwhile the commercial SPE showed strange transients, specially at very short times (t < 3 s). We believe that these differences are due to the way the commercial electrode is wetted.

5.6. Conclusions

In this chapter, screen printed counter-reference electrodes with new compositions were evaluated. Two different approaches were tried: AgCl loaded graphite electrodes, and KCl loaded Ag/AgCl electrodes.

Graphite electrodes loaded with 6.54 or 9.09 % of AgCl exhibit stable potentials, with shorter (than the commercial SPE) equilibration times, but with a 50 mV offset (at -5 μA). The main drawback of this approach is that these electrodes can only pass a limited amount of current and charge without dramatically changing the potential. The amount of charge that these electrodes can drive without changing the potential was found to be related with the amount of AgCl present at the surface of the electrode. Electrodes with even larger amount of AgCl had a very large resistivity, and adding additional graphite to decrease the resistance and improve the performance was fruitless, mainly due to the high viscosity of the inks prepared in this way. Even with this limitations, we have to consider also that this disposable reference electrode is more economic and exhibits fast equilibration times, making it a possible alternative for fast measurements when small current densities are passing through the system, as is often the case for portable and/or miniaturised (bio) sensors.

The best results were achieved with KCl loaded Ag/AgCl electrodes. In this case, we have proposed an electrode with faster equilibration times (approximately 20

seconds). The most interesting feature is that the potential of these electrodes is established by the diffusion of Cl^- from the electrode. Screen printed electrodes loaded with KCl were evaluated as counter-reference electrodes with a reversible redox couple, and the performance was better than the standard AgCl SPE.

The overall aim of this project is to build a counter-reference electrode capable of working at very short times (even down to 3 seconds after dipping in the sample). At this short time, the potential of the counter-reference electrode that we have proposed is established by the sudden increase of the concentration of Cl^-, followed by its subsequent diffusion towards the bulk. This sudden increase in Cl^- concentration, and hence the behaviour of the counter-reference electrode could be easily predicted independently of the current passing through the SPE. Electrodes with 1.96 % KCl equilibrates in only 20 seconds, compared with the more than 120 seconds needed by the commercial counter–reference electrode. Actual glucose meters measure the glucose level at times between 30 to 40 seconds. At this time, the proposed counter-reference electrode exhibit a stable potential, meanwhile the potential of the commercial electrode is still decreasing.

The main goal of this work is to produce a counter reference electrode that can be used to measure glucose at very short times (*i.e.* 3 s). On this time scale, the potential of the commercial Ag/AgCl SPE is affected by the amount of Ag/AgCl in contact with the solution available to carry on the reduction. This amount increases with time as the electrode is wetted. It is easy to understand that different manufacturing lots of sensors could have different wetting properties, and thus show different transients at very short times that in turn will make the measurement at very short times impractical due to the irreproducibility of the counter-reference electrode.

On the other hand, the reference electrodes loaded with KCl that we have proposed here show faster wetting times, and the potential is not limited by the specific surface area in contact with the solution. At short times, the potential is established by the local concentration of Cl^- at the electrode, and more specifically to the way the Cl^- in the ink diffuses to the solution. In this case, the potential of the counter-reference electrode at very short times can be predicted and reproduced by knowing the amount of Cl^- added to the ink.

Due to these characteristics, we believe that these Ag/AgCl electrodes loaded with KCl can be used to perform the glucose measurement at very short times.

6 Effect of aging and oxidation on the performance of the SPEs

6.1. Introduction

Another characteristic that we should consider in the design of a reference electrode is its stability over time. We can define stability as the capability of the electrode to maintain its properties over time with minimal incidence from external variations within a specified range (*e.g.* temperature, incidence of light, possible oxidation), or any factor that could alter the properties of the reference electrode.

As we have already discussed in the first chapter, bulk reference electrodes with internal electrolyte are kept in a known solution and its stability is measured by measuring the open circuit potential against another reference electrode over a long period of time. In our case, we are more interested in the electrode maintaining its properties during the period of time that it is stored in its dried state before the measurement is performed, rather than in the capability of the screen printed reference electrode to maintain a fixed potential in solution over long periods of time. In other words, we should consider what could happen to the electrode from the moment it is manufactured until the moment it is used, and if these factors have any influence on the performance of the counter-reference electrode; if the electrode has the same behaviour upon immersion in the solution regardless of the time since the electrode was manufactured, and regardless the environmental conditions during storage.

MediSense's SPEs are sealed in a dried state in aluminium foil immediately after manufacturing, and they are kept in this sealed condition until the exact moment the sensor is used. This packaging excludes light and moisture, and preserves the enzyme layer by keeping it in sterile conditions. The expected lifetime of the electrodes is 18 months.

The factors that we have considered that could have an influence on the performance of the screen printed reference electrode are the amount of time the electrode has been kept sealed, the amount of time it has been kept unsealed, out of the package in air, and since AgCl is photo sensitive, the effect of light on the electrode.

6.2. Silver oxides

One of the first effects that we studied was the oxidation of the screen printed electrodes and whether this oxidation has any adverse influence on the performance of the SPE. Reports from MediSense[139, 140] suggested that the action of light and air adversely affect the potential of the screen printed reference electrode. Electrodes treated under these conditions showed anomalous potential transients such as those shown in Figure 115, where the potential of the transient shifts towards less negative values. They suggested that the formation of a layer of Ag_2O caused by exposure to light and air caused the shift in the potential of the electrode towards that of the Ag/Ag_2O couple (+0.342 V *vs.* SHE[93]).

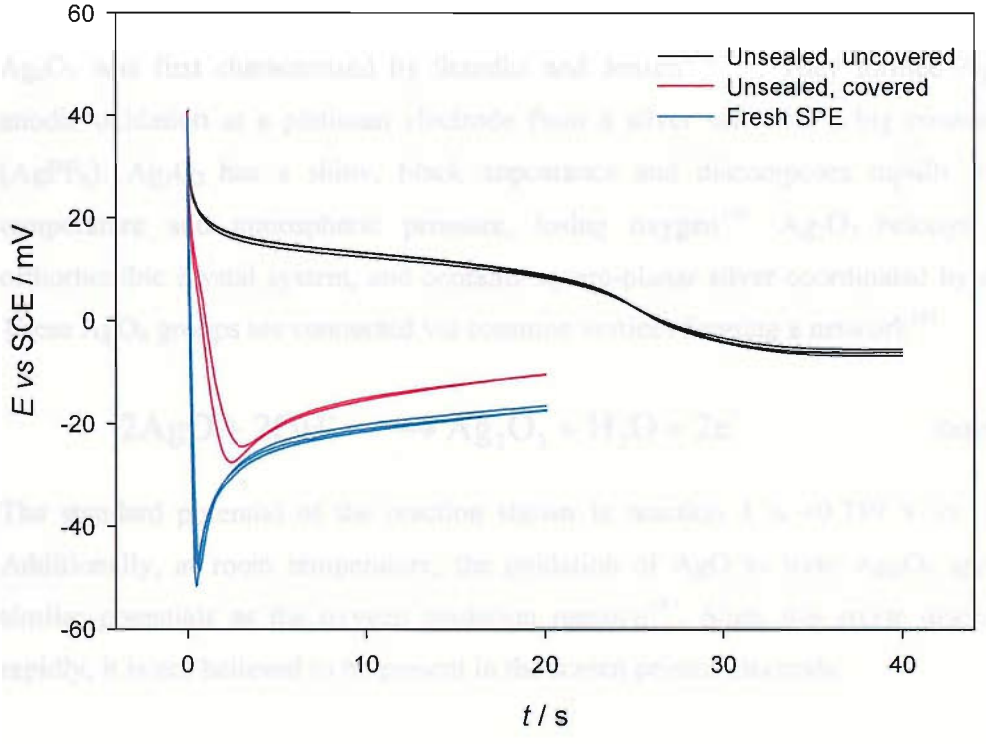

Figure 115 Effect of light and air in the chronopotentiometry at -5 μA of Ag/AgCl SPEs in 10 mM phosphate buffer. Black lines represent electrodes left for a month unsealed and uncovered, red lines for the transient of SPEs left for one month unsealed, and stored in the dark and blue lines for fresh electrodes.

Silver can appear in three different oxidised forms; Ag_2O, AgO and Ag_2O_3. Silver oxide (Ag_2O) is a grey-black powder with a large resistivity (~10^8 Ω cm[173]), and is a photoconductor[174]. Ag_2O has a face centered cubic lattice arrangement of Ag^+ ions with O^{2-} in the tetrahedral coordination holes forming a body-centered cubic pattern[175].

The standard potential for its reaction in water to form Ag_2O according to reaction1 is +0.342 V *vs.* SHE[93]. The potential of this redox pair (Ag/Ag_2O) has been proposed as a stable reference electrode[176].

$$2Ag + 2OH^- \longrightarrow Ag_2O + H_2O + 2e^- \qquad \text{Reaction 1}$$

The structure of AgO contains two types of silver ions, one with two collinear oxygen neighbours and the other with square-planar coordination[147] (some authors refer to this oxide as a $Ag(I)Ag(III)O_2$ mixture[177, 178]) crystallising in a body-centered tetragonal lattice[179]. The standard potential for the formation of AgO, according to reaction 2 is +0.604 V *vs.* SHE[93].

$$Ag_2O + 2OH^- \longrightarrow 2AgO + H_2O + 2e^- \qquad \text{Reaction 2}$$

Ag_2O_3 was first characterised by Standke and Jensen[180, 181]. They formed Ag_2O_3 by anodic oxidation at a platinum electrode from a silver salt with a big counter-anion ($AgPF_6$). Ag_2O_3 has a shiny, black appearance and discomposes rapidly at room temperature and atmospheric pressure, losing oxygen[180]. Ag_2O_3 belongs to the orthorhombic crystal system, and contains square-planar silver coordinated by oxygen. These AgO_4 groups are connected via common vertices forming a network[181].

$$2AgO + 2OH^- \longrightarrow Ag_2O_3 + H_2O + 2e^- \qquad \text{Reaction 3}$$

The standard potential of the reaction shown in reaction 3 is +0.739 V *vs.* SHE[182]. Additionally, at room temperature, the oxidation of AgO to form Ag_2O_3 appears at similar potentials as the oxygen evolution reaction[183]. Since this oxide discomposes rapidly, it is not believed to be present in the screen printed electrode.

6.2.1. Electrochemistry of silver - silver oxide

In this section, we will discuss the electrochemistry of the silver oxides with bulk and SPEs and compare it with the literature. Silver oxides can be formed easily in alkaline pH[136] and the electrochemistry of these oxides in alkaline solutions has been studied thoroughly in the literature[182, 184].

In our case (blood solution) we are more interested in the electrochemistry at neutral pH, so afterwards, we will extrapolate the behaviour at alkaline to neutral pH. Also, studying the behaviour in alkaline solutions will allow us to determine suitable

conditions to oxidise the SPE, and which silver oxide is formed predominantly under any given conditions.

The system Ag/Ag_2O was studied first on a silver macro electrode. A previously polished silver electrode (3.1 mm in diameter) was placed on a 1M KOH solution and a cyclic voltammogram was performed.

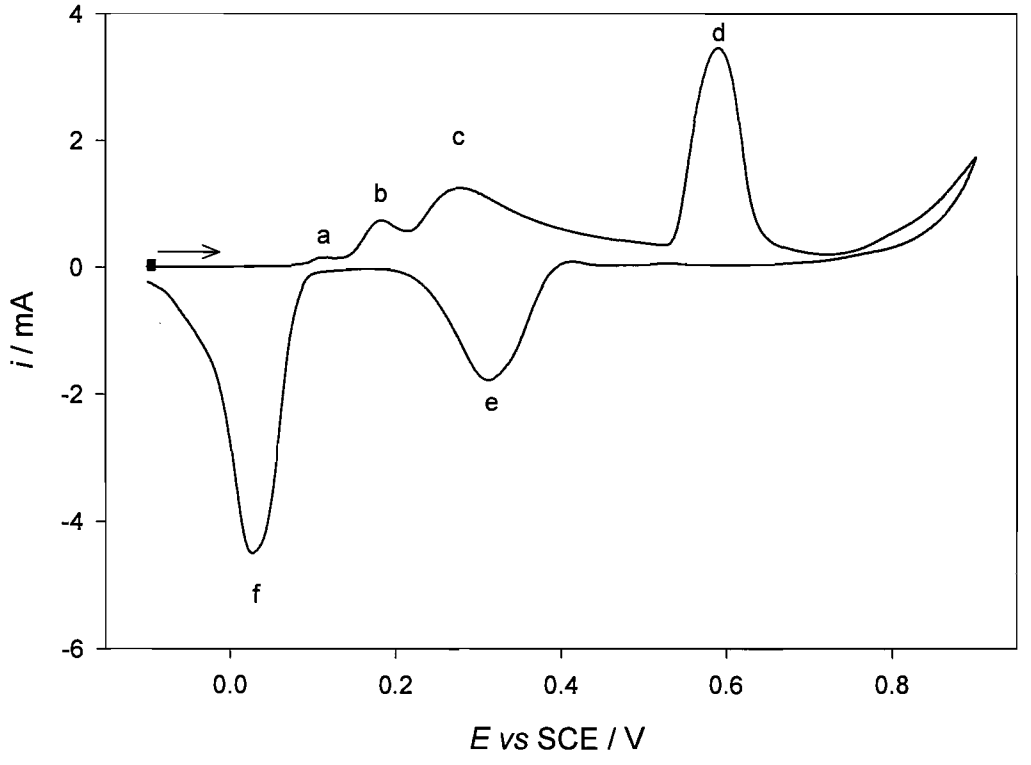

Figure 116 Oxidation of a silver electrode (diameter 3.1 mm) in 1M KOH. Scan started at -100 mV at 20 mV/s

There are four oxidation peaks (a, b, c and d) in the voltammogram, and two cathodic peaks (e and f). All these peaks are consistent with the results found in the literature[178, 182-191]. In the reviewed literature, the first two peaks (a, b) are not well studied and different authors give different explanations for their nature and formation mechanism. Table 11 shows different explanations for the origin of peaks a and b found in the literature.

Table 11 Different explanations for the electrochemical processes present for the oxidation of Ag in alkaline solutions suggested in the literature.

Reference	Peak (a)	Peak (b)
Tilak[183]	Carbonate impurities	Redissolution of Ag as: $Ag + 2OH^- \rightarrow [Ag(OH)_2]^- + 2e^-$ Non consolidated film maybe inhibited by the formation of a monolayer of Ag_2O.
Ambrose[185]	Maybe monolayer formation of AgOH (*sic*)	$Ag + 2OH^- \rightarrow [Ag(OH)_2]^- + e^-$
Burnstein[186]	Monolayer of AgOH at $E < E_a$ ($Ag + OH^- \rightarrow Ag(OH)_{ads} + e^-$)	Multilayer growth of Ag_2O and/or dissolution of $Ag(OH)_2^-$
	At $E = E_a$ ($Ag + Ag(OH)_{ads} + OH^- \rightarrow Ag_2O_{ads} + H_2O + e^-$)	
Arvía[187, 188, 192]	$Ag + OH^- \rightarrow Ag(OH)_{ads} + e^-$ (simultaneous formation of a few monolayers and soluble Ag(I) species)	$\lvert Ag_x\rvert Ag(OH)_{ads} + 2OH^- + y\,H_2O \rightarrow \lvert Ag_{x-2}\rvert Ag(OH)_{ads}/Ag_2O\,(y+1)\,H_2O$ (Peak b) Peak c follows a similar pattern as peak b, but the second oxide layer is less hydrated than the first one.
Chen[189]	Could be monolayer of Ag_2O. $i \propto t^{-1/2}$. Not related with the diffusion of OH^-	Dissolution of some species
Savinova[190, 191]	Adsorption of OH^-, followed by their incorporation in the Ag network	Not studied
Burke[182]	Monolayer oxide formation	Not studied

Several authors suggest that the first peak represents the adsorption of OH^- on the electrode and the reduction of Ag to form a layer of AgOH. Depending on the author, this layer is a monolayer or several layers thick. Meanwhile some others suggest the formation of a monolayer of Ag_2O at this potential (E_a).

Peak (b) has also been widely studied, but a consistent explanation has not been found. Several authors suggest that this peak represents the formation of a soluble species (namely $[Ag(OH)_2]^-$). The formation of this soluble species is inhibited by the formation of a monolayer of Ag_2O at (E_b), following the thickening of this monolayer at potentials more positive that (E_a). The main point of controversy is that if a soluble species is formed, the ratio of the anodic and cathodic charges for peak b should be smaller than 1, and dependant on the scan rate. At large scan rates, the ratio should approach 1 since there is not enough time for the species to diffuse away from the electrode. The presence of this soluble species is somewhat controversial since some authors report dependence of $Q_{b,anodic}/ Q_{b,cathodic}$ with the scan rate[183], meanwhile others report that this ratio is almost 1 at low scan rates[193]. EQCM (Electrochemical Quartz Crystal Microbalance) data suggest that there is a diminution of the mass on the electrode with time at this potential[189]. Also rotating ring disk experiments show the presence of soluble species at those potentials[185].

We believe that the first peak (a) represents the oxidation of the silver electrode to AgOH or Ag_2O. Bearing in mind the charges involved in Figure 116, the first peak accounts for 56.4 μC; this represents approximately 750 μC cm^{-2}. To deposit a monolayer of AgOH, 150 μC cm^{-2} are required[186] or 250 μC cm^{-2} for a monolayer of Ag_2O [considering the density of the Ag_2O (7.22 g/cm^3)[131], the length of Ag-O covalent bond (2.015 Å) and that a uniform and a compact layer is obtained]. In our case, we could estimate that we deposited 3 monolayers of Ag_2O or 5 monolayers of AgOH, if the geometrical area of the electrode matches the surface area (*i.e.* the electrode is perfectly flat and polished, and the roughness factor equals 1). Our Ag electrode was thoroughly polished with sand paper and alumina slurries down to 0.3 μm, so we can expect that the roughness factor will be between 1 and at most 2, so the number of monolayers could be half those quoted previously.

According to the literature, two processes could be occurring simultaneously at the potential of the peak b; the oxidation of silver to $[Ag(OH)_2]^-$ and the oxidation of Ag to a monolayer of hydrated Ag_2O that could prevent any further dissolution of

$[Ag(OH)_2]^-$. In our case, the anodic and cathodic charges were similar, so we do not believe that a soluble species is formed at this potential. This agrees with the results shown by Arvía[187, 188, 192], but contradicts the data presented by Tilak[183]. It seems that our data fits better the explanation of Arvía, where a highly hydrated layer of Ag_2O is formed at the potentials of peak b. At more positive potentials (peak c), a less hydrated layer of Ag_2O is formed. The charge transferred for peak b was 894 μC.

The third and larger peak (c) is attributed to the thickening of the completed basal monolayer[182, 184], *i.e.* the electroformation of a multilayer of Ag_2O as shown in reaction 1. Considering the charge for peaks a+b+c (9.5 mC, integrated between 0.085 V and 0.513 V), and assuming that the surface is compact, we conclude that a layer of approximately 120 nm of Ag_2O had been deposited on the electrode by the end of peak c, at +0.55 V *vs.* SCE.

The fourth sharp peak (d) is ascribed to the formation of AgO from Ag_2O as shown in reaction 2[182, 184]. Calculating the area under the peak, we find that all of the Ag_2O formed (9.5 mC for a+b+c) is oxidised to form AgO (10.2 mC for peak d, between 0.513 V and 0.727 V). The slightly larger charge for peak d as compared with a+b+c indicates that some Ag is still being reduced to Ag_2O at the potential of peak d[184].

The increase of the current at potentials over 0.75 V *vs.* SCE is due to the evolution of O_2 at the electrode from the oxidation of OH^- ($2\ OH^- - 2\ e^- \rightarrow ½\ O_2 + H_2O$).

The reduction peaks are associated with the reduction of AgO (peak e) and the reduction of Ag_2O (f) according to reaction 4 and 5 respectively.

$$2AgO + H_2O + 2e^- \longrightarrow Ag_2O + 2OH^- \qquad \text{Reaction 4}$$

$$Ag_2O + H_2O + 2e^- \longrightarrow 2Ag + 2OH^- \qquad \text{Reaction 5}$$

The charge transferred for peaks e and f was 8.2 mC and 15.5 mC respectively. These values are slightly different than those obtained for the oxidation peaks (9.5 mC and 10.2 mC for a+b+c and d respectively), suggesting that the charges in the oxidation scan were not properly assigned. In the first place, there is more charge for the reduction of Ag_2O to Ag in peak f (14.9 mC), than the sum of the oxidation peaks a+b+c. The integration of the area under the curve a+b+c has been done with a linear baseline between 0.085 V and 0.513 V, as shown in Figure 117 by the blue line.

In addition, the oxidation charge for the formation of AgO (peak d, 10.5 mC) is larger than the charge obtained in the reduction of this species (peak e, 8.2 mC). The charge of peak d does not account exclusively for the oxidation of Ag_2O to AgO, but also for some oxidation of Ag to Ag_2O.

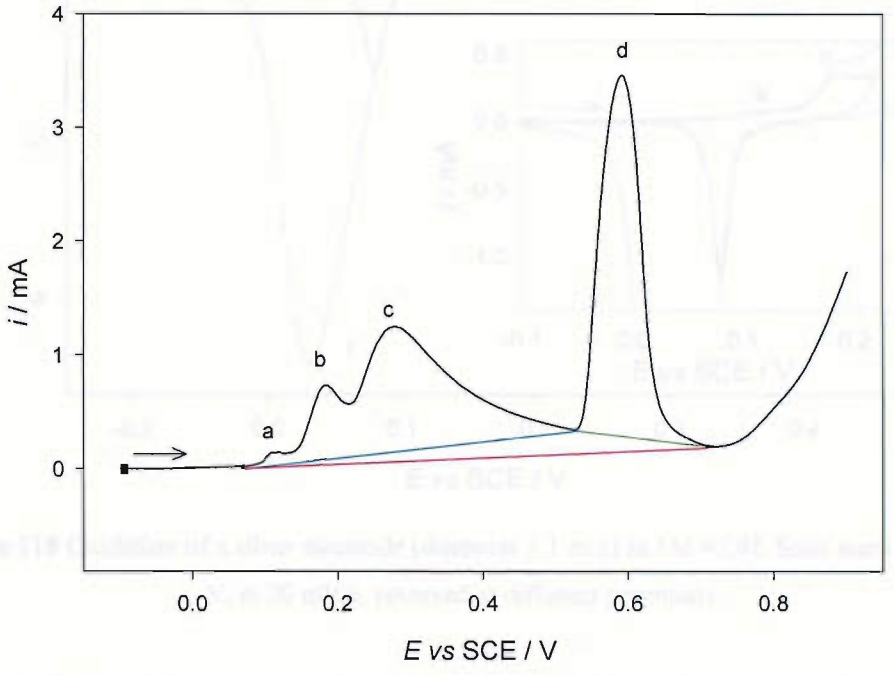

Figure 117 Oxidation of a silver electrode (diameter 3.1 mm) in 1M KOH. Scan started at -100 mV at 20 mV/s

It is evident from Figure 117 that to estimate the charge for the oxidation of Ag to Ag_2O (peaks a+b+c) by the area between the black and the blue lines in Figure 117 is not appropriate. The integration should have been made using the red line as the baseline. In this case, the total charge for all the oxidation processes (area between the black and the red lines in Figure 117) is 22.8 mC, and this matches the charge for the reduction processes (e + f), 23.7 mC.

In order to match unequivocally each oxidation and reduction peak, other scans were performed (Figure 118). In these scans, the scan was reversed at different potentials, +0.21 and +0.45 V.

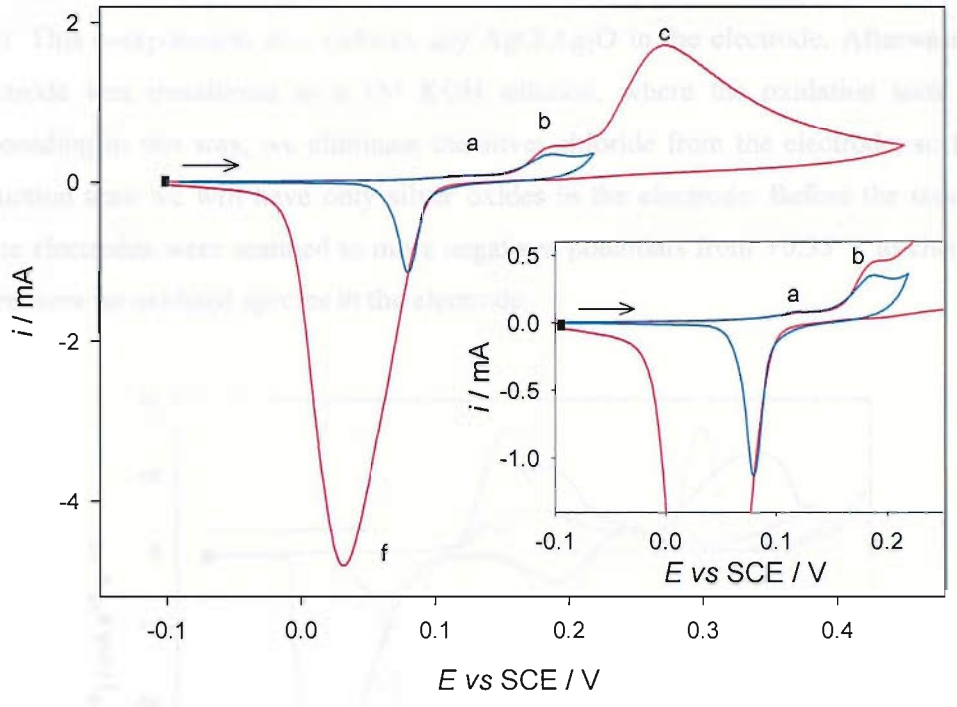

Figure 118 Oxidation of a silver electrode (diameter 3.1 mm) in 1M KOH. Scan started at -0.1 V, at 20 mV/s, reversed at different potentials.

In Figure 118, we can see that the oxidation peaks a b and c are all related with the formation of Ag_2O. The reduction of Ag_2O to Ag starts at approximately 100 mV regardless of the formation mechanism. The areas involved in the scan performed between -0.1 and 0.45 are 12.8 mC for the oxidation and 14.1 mC for the reduction. Meanwhile, the charges for the scan between -0.1 and -0.21 V are 0.98 mC and 1.16 mC respectively

6.2.2. Silver oxide on the screen printed electrodes

In order to know exactly how our system (the Ag/AgCl screen printed electrode) behaves with silver oxide, the oxidation of the SPE was studied under the same conditions as the Ag bulk electrode.

On the SPE we have both AgCl and Ag. In this solution (1 M KOH with no added Cl^-), the equilibrium (Nernst) potential of the Ag/AgCl system is 0.510 V *vs.* SHE (0.27 vs. SCE), as we have already shown in section 3.5. This value is very similar to the potential at which the reduction of AgO to Ag_2O occurs, so the reduction of AgCl and Ag_2O will therefore appear at similar potentials. In order to overcome this limitation

the SPE was first reduced at η = -150 mV in 0.5 M KNO_3 until the current dropped to zero. This overpotential also reduces any AgO/Ag_2O in the electrode. Afterwards, the electrode was transferred to a 1M KOH solution, where the oxidation took place. Proceeding in this way, we eliminate the silver chloride from the electrode, so for the reduction scan we will have only silver oxides in the electrode. Before the oxidation, some electrodes were scanned to more negatives potentials from +0.35 V to check that there were no oxidised species in the electrode.

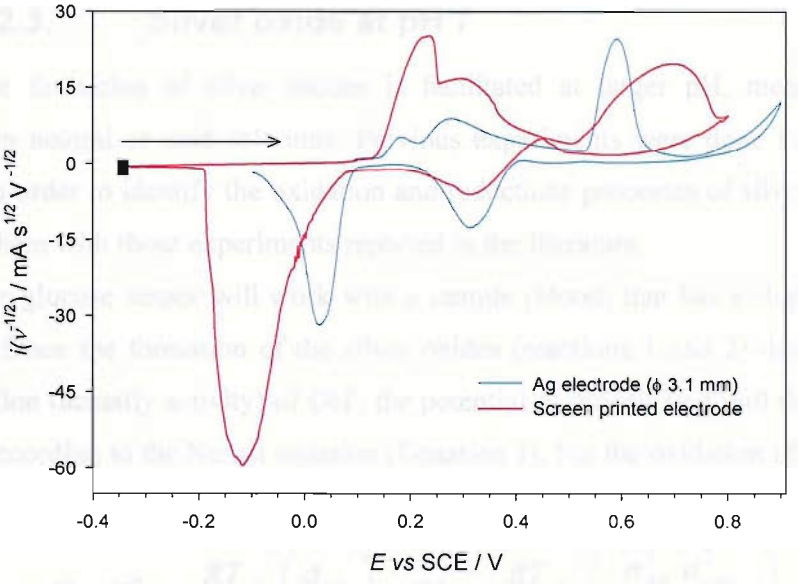

Figure 119 Comparison of the cyclic voltammograms in 1M KOH solution for a screen printed electrode and a silver electrode (diameter 3.1 mm). The SPE was previously reduced at η = -150 mV in 0.5 M KNO_3 until the current dropped to zero. Then the electrode was transferred to a fresh 1M KOH solution and the scan shown was performed at 0.3 mV/s. Silver electrode oxidising scan performed from -0.1 V, at 20 mV/s. Currents were normalised with the scan rate (ν in V/s) for comparison purposes.

In Figure 119, we can see that the peaks for the SPE correspond with those for the bulk silver electrode. The peak a (formation of AgOH) is not appreciable in the SPE, and the monolayer oxidation and the multilayer growth of Ag_2O are not as well resolved as before. The scan was performed at very low scan rates (ν = 0.5 mV s^{-1}), because doing it at this speed resolved the peaks reasonably well; larger scan rates merged all the peaks in a large lump.

Also seen on the scan is the IR drop present on the screen printed electrode, evidenced in the shift of the potentials and the poor resolution of the peaks. This IR drop was related with the resistivity of the screen printed conductive track. Since the

reduction peak at -120 mV has a current of 1.33 mA and the resistance of the screen printed track is approximately 135 Ω (section 3.3), we could expect a shift of the potential due to this resistance of ~180 mV ($V = IR$). In this case, correcting the expected shift of the potential, this peak should have appeared at about + 60 mV, approximately the value of the potential of the reduction peak of Ag_2O shown for the Ag bulk electrode (Figure 119). We can conclude that the IR drop present in the SPE's scan comes from the resistance of the track.

6.2.3. Silver oxide at pH 7

The formation of silver oxides is facilitated at larger pH, meanwhile it is hindered in neutral or acid solutions. Previous experiments were done in an alkaline medium in order to identify the oxidation and reductions processes of silver oxides and compare them with those experiments reported in the literature.

The glucose sensor will work with a sample (blood) that has a slightly alkaline pH (7.2). Since the formation of the silver oxides (reactions 1 and 2) depends on the concentration (actually activity) of OH^-, the potential of the reaction will therefore shift with pH according to the Nernst equation (Equation 3). For the oxidation of Ag to Ag_2O, we have:

$$E = E^0 - \frac{RT}{nF}\ln\left(\frac{a_{red}}{a_{ox}}\right) = E^0 - \frac{RT}{nF}\ln\left(\frac{a_{Ag}^2\, a_{OH^-}^2}{a_{Ag_2O}\, a_{H_2O}}\right)$$

$$E = E^0 - \frac{RT}{nF}\ln\left(\frac{a_{Ag}^2}{a_{Ag_2O}\, a_{H_2O}}\right) - \frac{RT}{nF}\ln a_{OH^-}^2$$

The second term of the equation is constant since the activities of solids (Ag, Ag_2O) equal 1 and the activity of water, being in large excess, does not change appreciably with the change of pH, so:

$$E = A - \frac{2RT}{nF}\ln a_{OH^-}$$

where A is a constant including the standard potential E^0_{Ag/Ag_2O}. Since n = 2, and considering that T = 298 K and that pH + pOH = 14

$$E = A - \frac{RT}{F}\ln a_{OH^-} = A + 0.059\ \text{pOH} = A + 0.059\ (14 - \text{pH})$$

$$E = A + 0.828 - 0.059\ \text{pH} \qquad \text{Equation 47}$$

So the potential for this reaction is pH dependant, and it will shift to less negative potentials the larger the pH. Consequently, and according to these thermodynamic calculations, a shift of -59 mV per pH unit should be expected.

Assuming that the kinetics for the oxidation and reduction reactions do not change by altering the pH, we can approximate the shift of the peaks with the variation of the pH. The oxidations of silver to Ag_2O and from this later species to AgO should appear, at pH 7, at +0.694 V and +1.005 V *vs.* SCE respectively (they appear at +0.281 V and +0.592 V *vs.* SCE at pH 14). For the reduction, the peaks should appear at +0.726 V and +0.441 V respectively (they appear at +0.313 V and +0.028 V vs. SCE at pH 14). Several attempts were made to study this displacement, in both Tris and PBS buffers at different pH, but neither expected nor reproducible behaviour were found.

According to the Pourbaix diagram[194], at pH lower than 10, Ag will not be oxidised to Ag_2O or AgO, but to Ag^+ (or AgCl in the presence of Cl^-). That means that if there are silver oxides (Ag_2O and/or AgO) on the screen printed electrode, these species will be unstable in contact with the solution at neutral pH. In the case of the Ag_2O, the solubility product is 2×10^{-8} M^3; at pH 7, we can expect that Ag_2O will be dissolved (in a solution where $[OH^-] = 10^{-7}$ M, up to 0.45 M of Ag^+ can be dissolved) or converted into AgCl if there is chloride present in the solution due to its larger insolubility ($K_s = 1.77 \times 10^{-10}$ M^2)[93].

Resuming, we have seen that there could be silver oxides present in the Ag/AgCl SPE, and that these species will be reduced, at pH 7, at potentials less negative than the reduction of AgCl. Thus, in a cathodic galvanostatic experiment, the potential should be established first by the Ag/Ag_2O system, and once all the Ag_2O has been consumed, the potential should change to that of the Ag/AgCl pair. In addition, at this pH, once the electrode is dipped in solution, the Ag_2O should be dissolved, so the potential should also shift with time from the Ag/Ag_2O system, and once all the Ag_2O has been dissolved, the potential should change to that of the Ag/AgCl system.

These two features are consistent with Figure 115, but the results are not yet conclusive. The oxidation of the electrode in Figure 115 was not done in a controlled way; we do not have information about how much oxide was present in the oxidised electrodes, or even which species are present, so further tests were performed.

6.3. Incidence of silver oxide on the performance of the SPE

MediSense's reports mentioned earlier showed an anomalous behaviour of the silver/silver chloride electrode when an unwrapped electrode was exposed to light for a month. This behaviour was believed to be due to the oxidation of silver to silver oxides (Ag_2O and/or AgO).

The influence of the oxidation of silver to Ag_2O on the performance of the screen printed electrodes was studied. Since the oxidation could not be performed at pH 7 (due to the low stability of the Ag_2O and AgO at pH more acidic than 10, *vide supra*), the electrodes were oxidised in an alkaline medium and then transferred to a cell at neutral pH. Since we have already studied the electrochemistry of silver oxides at pH 14, we performed the oxidation in the same medium.

Several SPE were oxidised by applying an oxidation current (+20 μA) in 1 M KOH for a fixed time. Considering Figure 119, we expect that the only species formed during this oxidation is Ag_2O, and we can control the amount of Ag_2O deposited by controlling the time of oxidation. Once the oxidation was performed the electrode was dried with tissue paper and transferred to a cell containing 0.125 M KCl, where the potential transient at -5 μA was recorded.

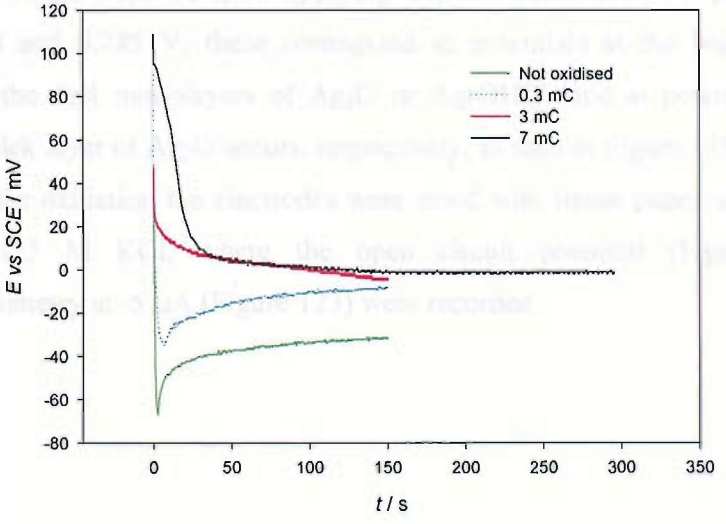

Figure 120: Effect of the presence of Ag_2O on the chronopotentiometry of four SPEs at -5 μA. Each electrode was oxidised at 20 μA in 1M KOH until a predetermined amount of charge had been transferred. The SPE was then transferred to a 0.125 M KCl solution where chronopotentiometry at -5 μA took place.

Figure 120 shows the difference in behaviour when more than 0.3 mC of Ag_2O were deposited with respect to the behaviour of the non-oxidised electrode. The time needed to achieve a stable potential is longer for the more oxidised electrodes. It can also be seen in this figure that the potential at long times is shifted to more positive values by the oxidation treatment.

In this system, when the electrode was not oxidised, the AgCl reaction is solely responsible of the electrochemistry. As soon as we generate some Ag_2O, larger potentials are obtained in the chronopotentiometry as a result of different species in the electrode, obtaining a mixed potential.

According to our model, the electrode should exhibit a less negative potential while there is Ag_2O in the electrode. Accordingly the potential of the electrode should shift to similar values as those shown for the control electrode (non oxidised SPE) once all the Ag_2O has been reduced. In this case, the electrode with 0.3 mC of Ag_2O deposited should switch back to "normal" values after 60 s at -5 μA ($Q = it$ = -5 μA × 60 s = -0.3 mC). In addition and as we have mentioned in earlier section, the Ag_2O is unstable at low pH, so we should expect that the Ag_2O layer dissolves in solution, even at open circuit potential, thus shifting the potential to "normal" values. These two observations contradict the model.

In order to have a better control over the oxidised species that we form on the electrode, the SPEs were oxidised applying a fixed potential. Two potentials were chosen, 0.135 and 0.285 V; these correspond to potentials at the beginning of the formation of the first monolayers of Ag_2O or $Ag(OH)_2^-$, and at potentials were the growth of a thick layer of Ag_2O occurs, respectively, as seen in Figure 119.

After the oxidation the electrodes were dried with tissue paper and placed in a cell with 0.125 M KCl, where the open circuit potential (Figure 121) and chronopotentiometry at -5 μA (Figure 123) were recorded.

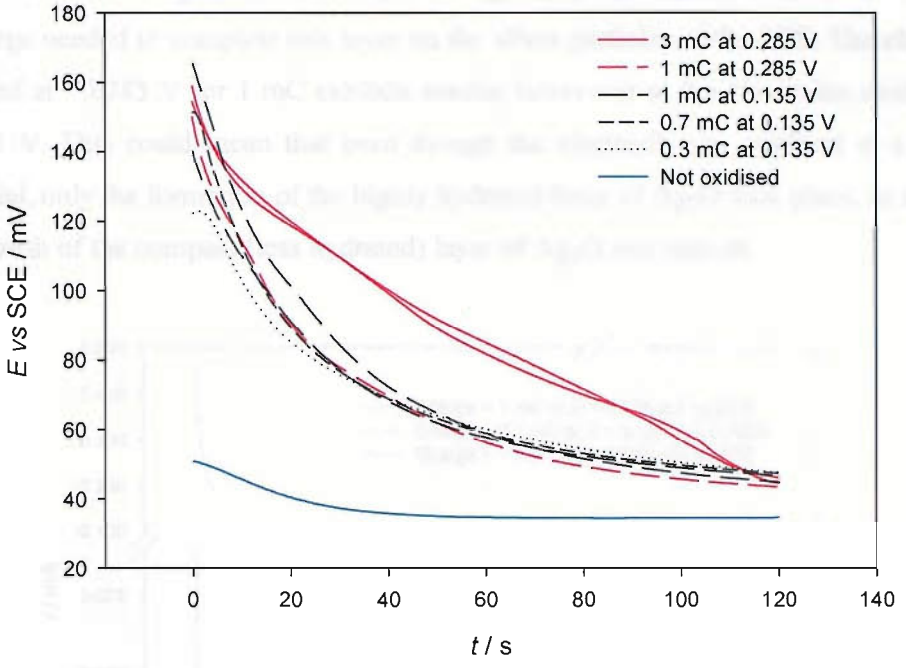

Figure 121 Effect of the oxidation of the Ag/AgCl SPE on the open circuit potential (OCP) in 0.125 M KCl. Each electrode was oxidised at 0.135 V (black lines) or 0.285 V (red lines) in 1M KOH until a predetermined amount of charge had been transferred. A control electrode (not oxidised, in blue) was also tested. The electrodes were oxidised to different degrees; 3 mC (red, solid line), 1 mC (long dashed lines, black oxidised at +0.135 V and red at +0.285 V), 0.7 mC (short dashed line) and 0.3 mC (dotted line). After oxidation, the screen printed electrode was transferred to a 0.125 M KCl solution where the OCP was recorded.

In Figure 121 we can see that the different types of oxidised species show different effects on the behaviour of the open circuit potential. The OCP represents the potential of the system when no current is flowing externally; that is the potential in which both oxidation and reduction reactions are taking place at the same rate.

First of all, we have to mention that the final potential (at t = 120 s), is more positive in the case of the oxidised electrodes than the control electrode. Also, the electrodes oxidised show different behaviours depending on the amount of Ag_2O deposited, and we can split them into two groups, electrodes oxidised for 1 mC[xxv] or less, and electrodes oxidised for more than 1 mC. It is important to mention that the electrodes oxidised at 0.135 mV could not be oxidised for more than 1 mC, with currents approaching zero at longer times, as is shown in Figure 122. Based on the cyclic voltammetry shown in Figure 119, this potential is in the range of peak b, where

[xxv] 1 mC represents less than 1% of the total Ag in the electrode.

the formation of a highly hydrated layer of Ag_2O occurs, and thus 1 mC is the amount of charge needed to complete this layer on the silver particles of the SPE. The electrode oxidised at +0.285 V for 1 mC exhibits similar behaviour to the electrodes oxidised at +0.135 V. This could mean that even though the electrode was oxidised at a higher potential, only the formation of the highly hydrated layer of Ag_2O took place, or at least, the growth of the compact (less hydrated) layer of Ag_2O was minute.

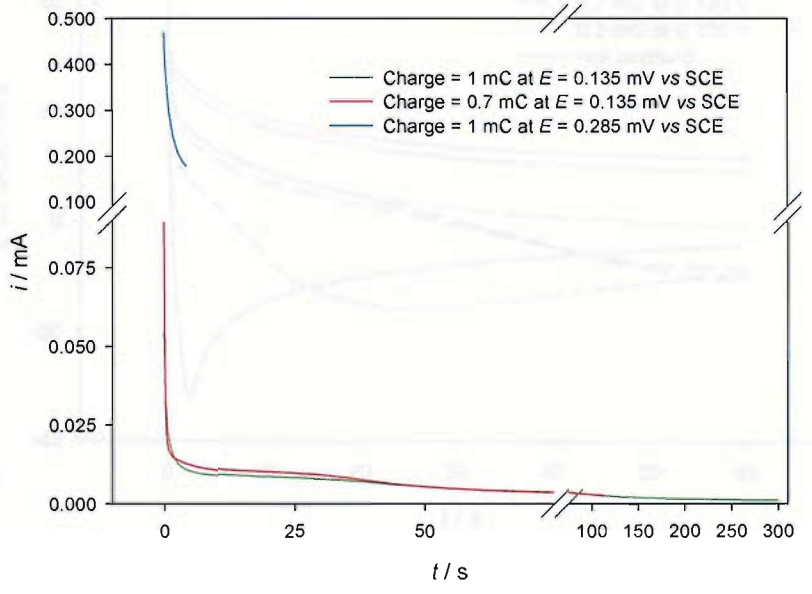

Figure 122 Chronoamperometry of the oxidation of three SPE in 1 M KOH, at +0.135 V (green and red), and at +0.285 V (blue) *vs.* SCE. The charges recorded are shown in the legend.

The first thing that we should consider when the oxidised electrode is placed in solution is that the Ag_2O is soluble in neutral solutions (*vide supra*, section 6.2.3). According to the Pourbaix diagram (on page 398 of the reference[194]) at this pH (an unbuffered solution of KCl 0.125 M will have a pH of approximately 6.5) and a concentration of Ag^+ of approximately 1.5×10^{-9} M, Ag_2O is very soluble in the form of Ag^+, which, in presence of chlorine, will precipitate in the form AgCl. In this case, we can expect that a layer of AgCl will be deposited on top of the Ag particles, or in the case that not all the Ag_2O is redissolved, a layer of AgCl will be deposited on top of the Ag_2O film already deposited on top of the Ag particles.

The different behaviour observed between the electrodes poised at 0.135 and 0.285 mV could be due to the characteristics of the oxide film formed. At the more positive potential, the oxide film is more compact and it could require more time to dissolve the oxide film and replace it with a AgCl film.

The difference in the final potential could be due to the fact that in the oxidised electrodes we have replaced the Ag particles with Ag particles covered with a film of AgCl over an Ag_2O layer, with a mixed potential established by the different interfaces present, *i.e.* Ag/AgCl and Ag/Ag_2O.

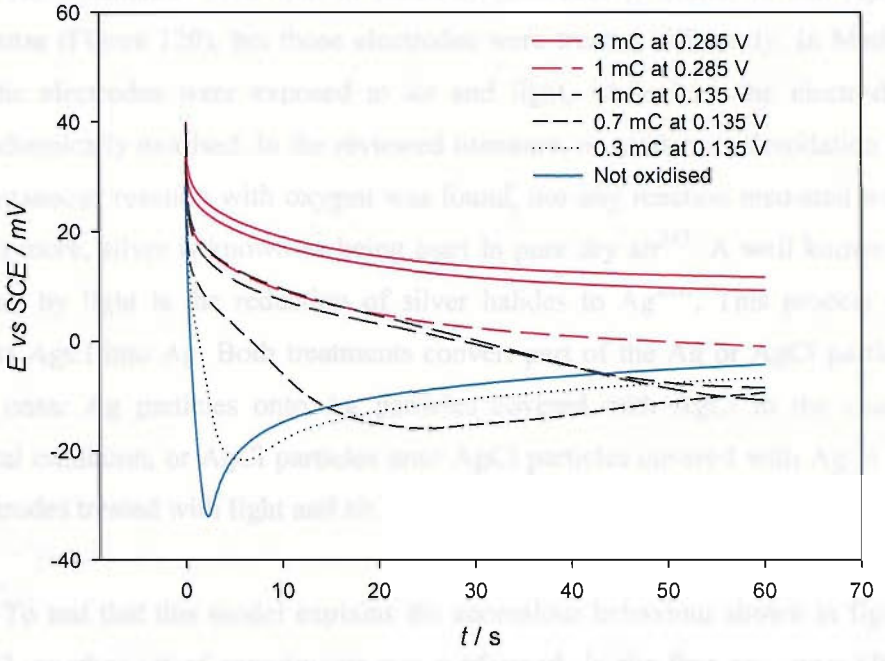

Figure 123 Effect of the oxidation of the Ag/AgCl SPE on the chronopotentiometry at -5 µA in 0.125 M KCl. Each electrode was oxidised at 0.135 V (black lines) or 0.285 V (red lines) in 1M KOH until a predetermined amount of charge had been transferred. A control electrode (not oxidised, in blue) was also tested. The electrodes were oxidised to different degrees; 3 mC (red, solid line), 1 mC (long dashed lines, black oxidised at +0.135 V and red at +0.285 V), 0.7 mC (short dashed line) and 0.3 mC (dotted line). After oxidation, the screen printed electrode was transferred to a 0.125 M KCl solution where the chronopotentiometry at -5 µA was recorded.

The effect of the oxidation of the electrodes on the chronopotentiometry at -5µA is shown in Figure 123. Again, the results can be split into two groups. In the case of the electrodes oxidised for 1 mC or less, the electrodes tend to the normal value of potential (as determined for the unoxidised electrode) on the time scale of the experiment, meanwhile the potential of the electrodes oxidised for more than 1 mC shows a less negative potential than the unoxidised electrode (approximately 20 mV less negative). The largest deviations occur in the first 30 seconds. In this part of the transient, the unoxidised electrodes exhibit a large negative potential, meanwhile for the other electrodes this sudden shift of the potential is less pronounced, and it is less pronounced the larger the oxidation charge passed. At longer times, the potential of the intermediate

oxidized electrodes converge with the value of the control electrode. In the cases where the oxidation took place for more than 1 mC, the electrodes did not converge with the non-oxidised electrode over the time of the experiment, maintaining a stable difference of 15 mV.

The anomalous behaviour of oxidised electrodes is similar to that reported by MediSense (Figure 120), but those electrodes were treated differently. In MediSense's case, the electrodes were exposed to air and light, while here the electrodes were electrochemically oxidised. In the reviewed literature, no evidence of oxidation of silver by spontaneous reaction with oxygen was found, nor any reaction mediated with light. What is more, silver is known as being inert in pure dry air[147]. A well known process mediated by light is the reduction of silver halides to Ag[xxvi]. This process partially converts AgCl into Ag. Both treatments convert part of the Ag or AgCl particles into mixed ones: Ag particles onto Ag particles covered with AgCl in the case of the chemical oxidation, or AgCl particles onto AgCl particles covered with Ag in the case of electrodes treated with light and air.

To test that this model explains the anomalous behaviour shown in figures 115 and 123, another set of experiments was performed. In the first one, new SPEs were slightly oxidised in a solution containing 0.5 M KNO_3, 0.3 M KCl and saturated AgCl, thus converting part of the Ag onto AgCl. The oxidation was performed by applying an overpotential of +150 mV, meanwhile the current was recorded (the transients recorded are similar to those previously shown in Figure 20, where a SPE was oxidised at several overpotentials). Before the oxidation, the electrode was left at OCP in the solution for one minute. The extent of the oxidation was calculated from the area under the chronoamperogram. After this oxidation, the electrode was left for a minute to stabilise at OCP, and the chronopotentiometry at -5 μA was recorded. For comparison purposes, the chronopotentiometry was also recorded for unoxidised electrodes. In this latter case, the electrode was left at OCP for approximately 2 minutes before recording the chronopotentiometry. This 2 min delay ensures that all electrodes have been in solution similar amounts of time before the chronopotentiometry. The effect of this pre-treatment on the chronopotentiometry at -5 μA is shown in Figure 124.

[xxvi] This process is the base of conventional photography

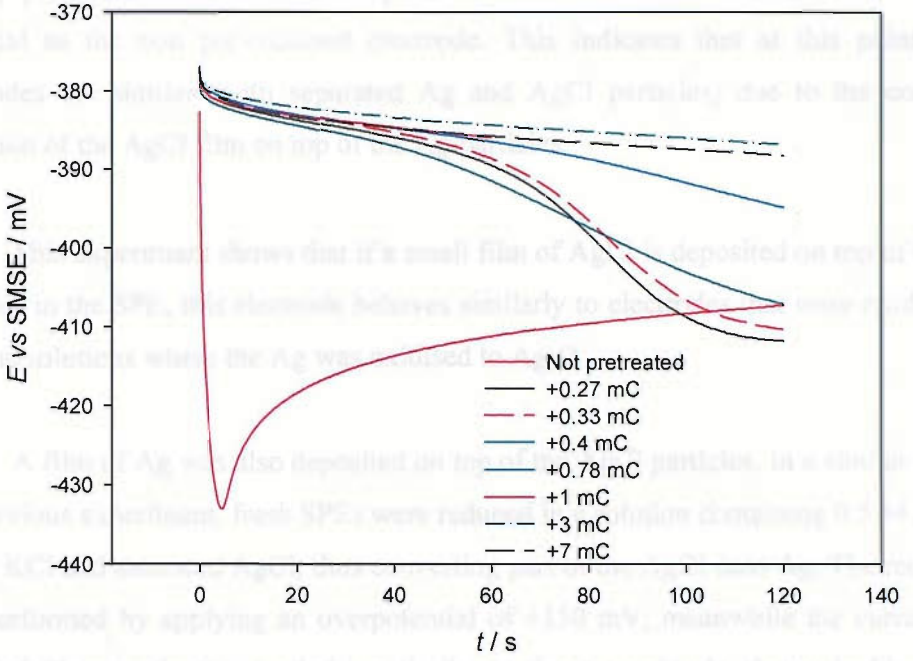

Figure 124 Effect of the length of the oxidation pretreatment on the chronopotentiometry at -5 μA of new SPEs in 0.5 M KNO_3, 0.3 M KCl and saturated AgCl. The pre-oxidation was performed in the same solution at η = +150 mV for different amounts of time. Each SPE was discarded after the measurement. For other conditions, see text.

We can see in Figure 124 that the behaviour of the electrode is significantly different after the electrode was treated, even for small oxidation charges. This behaviour is very similar to that shown in Figure 123, and especially to that shown in Figure 115. The pre-treated electrodes show, at short times, potentials 50 mV less negative that the electrode that has not been treated. For small charges, the potential of the electrodes shifted slowly towards that of the non pre-treated electrode in the time scale of the experiments. The charge needed for this change, 0.4 mC (a current of -5 μA for t ~80 s), is similar to the charge transferred when the electrode was pre-treated, suggesting that we are reversing the pre-treatment. The potential of the electrodes that were oxidised for longer times did not converge with that of the control electrode in the time scale of the experiments. We are left to assume that given enough time, the potential of these electrodes would converge as well, but this was not tested.

A possible explanation for this behaviour is that the AgCl film formed on the Ag particles can be reduced more easily than the AgCl particles. The transients show that the overpotential required to pass -5 μA is smaller when a pre-oxidation step has been performed. In addition, once this AgCl film has been completely reduced (t ~80 s for

slightly pre-oxidised electrodes), the potential of the electrode shifts to a similar over-potential as the non pre-oxidised electrode. This indicates that at this point, both electrodes are similar (with separated Ag and AgCl particles) due to the complete reduction of the AgCl film on top of the Ag particles.

This experiment shows that if a small film of AgCl is deposited on top of the Ag particles in the SPE, this electrode behaves similarly to electrodes that were oxidised in alkaline solutions where the Ag was oxidised to Ag_2O.

A film of Ag was also deposited on top of the AgCl particles. In a similar way to the previous experiment, fresh SPEs were reduced in a solution containing 0.5 M KNO_3, 0.3 M KCl and saturated AgCl, thus converting part of the AgCl onto Ag. The reduction was performed by applying an overpotential of +150 mV, meanwhile the current was recorded (the transients recorded are similar to those previously shown in Figure 23, where a SPE was completely reduced at several overpotentials). Before the reduction, the electrode was left at OCP in the solution for one minute. The extent of the reduction was calculated from the area under the chronoamperogram. After this reduction, the electrode was left for a minute to stabilise at OCP, and the chronopotentiometry at -5 μA was recorded. For comparison purposes, the chronopotentiometry was also recorded for non pre-treated electrodes. In this later case, the electrode was left at OCP for approximately 2 minutes before recording the chronopotentiometry. This 2 min delay ensures that all electrodes have been in solution similar amounts of time before the chronopotentiometry. The effect of this pre-treatment on the chronopotentiometry at -5 μA is shown in Figure 125.

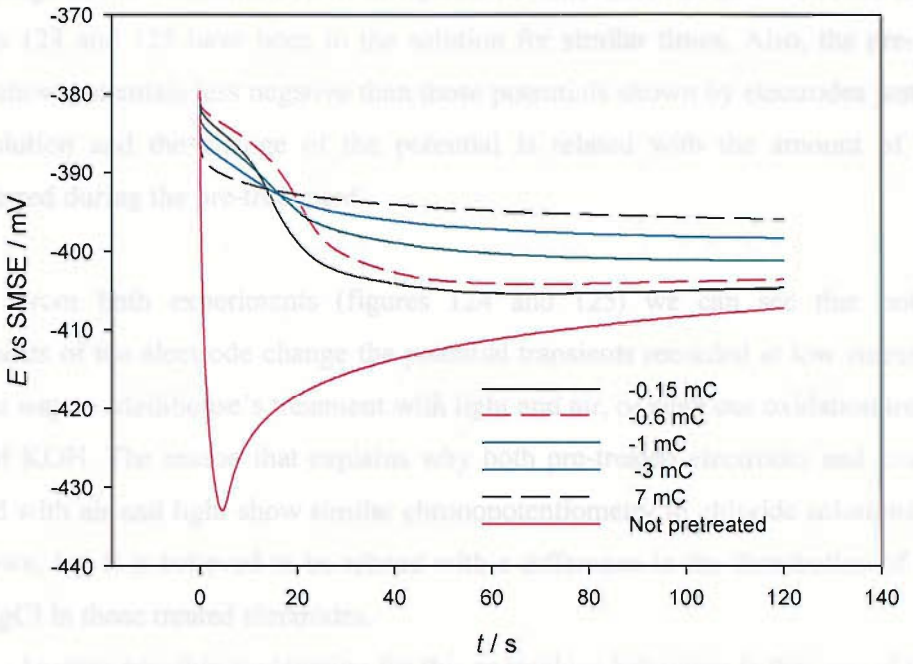

Figure 125 Effect of the length of the reduction pre-treatment on the chronopotentiometry at -5 μA of new SPEs in 0.5 M KNO_3, 0.3 M KCl and saturated AgCl. The reduction was performed in the same solution at η = -150 mV for different amounts of time. Each SPE was discarded after the measurement. For other conditions, see text.

The effect of the cathodic pre-treatment on the chronopotentiometry is similar to the previous experiment (Figure 124). In both cases, the potential of the electrode shifts to less negative values, suggesting that it is easier to pass the desired current with pre-treated electrodes than with non pre-treated SPEs. Again, electrodes pre-treated for shorter times converge quickly with the control one (not pre-reduced). The pre-treatment of these electrodes consisted on a small reduction of the electrode that converts some of the AgCl particles into Ag/AgCl mixed ones. Following the same reasoning as in the section 3.9.1, these mixed particles need a smaller over-potential to reduce. In this case, the pretreated electrodes converge with the control one not because we are undoing the pre-treatment, but because we could be consuming the mixed particles that can be reduced at a smaller overpotential.

Other possibility that could explain these transients (figures 124 and 125) is that there is a difference in the wetting of the SPE in the pre-treated electrodes and in the non pre-treated ones. From Figure 57 it is evident that the SPE evolves once it has been placed in the solution, even at OCP. We believe that this evolution is not the cause of

the change in the transients shown in figures 124 and 125. All the electrodes tested in figures 124 and 125 have been in the solution for similar times. Also, the pre-treated SPEs show potentials less negative than those potentials shown by electrodes just left in the solution and the change of the potential is related with the amount of charge transferred during the pre-treatment.

From both experiments (figures 124 and 125) we can see that both pre-treatments of the electrode change the potential transients recorded at low currents in a similar way to MediSense's treatment with light and air, or even our oxidation treatment in 1 M KOH. The reason that explains why both pre-treated electrodes and electrodes treated with air and light show similar chronopotentiometry in chloride solutions is still unknown, but it is believed to be related with a difference in the distribution of the Ag and AgCl in those treated electrodes.

Another possible explanation for this anomalous behaviour is that any of the pre-treatments tested (light and air, oxidation to Ag_2O or AgCl, partial pre-reduction) favours the nucleation of Ag and/or AgCl particles, so after the treatment, the reduction of AgCl is easier, *i.e.* it can be carried on at lower overpotentials.

6.4. Effect of oxidation on the performance of the proposed Ag/AgCl electrodes loaded with KCl

We have demonstrated that light and air affect the performance of the commercial SPE. In this section we present the results of a study of how this affects the SPEs loaded with KCl manufactured as described in section, 5.5.

Several SPEs manufactured with different compositions were stored for two months under different conditions. 1/3 of these electrodes were kept in opaque, sealed packages, another third were kept in the dark, but not sealed and the last third were left on the window sill uncovered. To store the electrodes in sealed packages, two boards (50 electrodes) were placed between sheets of plastic coated aluminium foil and the edges were sealed with heat, melting the plastic and hermetically sealing the contents. The sealing was done in air, so some amount of air was sealed inside the package. A proof that these packages are hermetically sealed is that when opening, there is a strong

smell to the organic solvents employed in the ink. If the packages leak gases and there is an exchange of gases during the storage of the electrodes, some of the solvent should have been evaporated and the smell to solvent should have faded away.

After 2 months (21st August till 21st September) the chronopotentiometry at -50 μA and the OCP of these electrodes were compared. The following results show the most representative curve of three identical electrodes, and in some cases, the transients for the three electrodes are shown, showing the high reproducibility of the behaviour between different electrodes. For comparison purposes, the scales of the figures are kept constant.

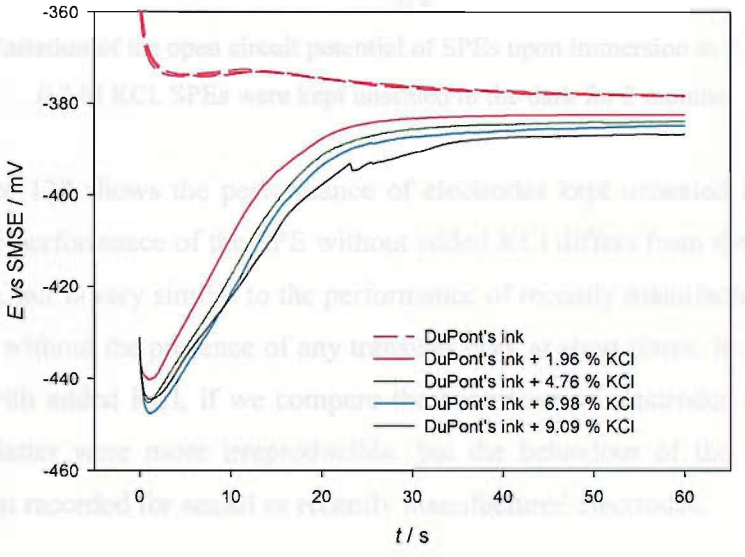

Figure 126 Variation of the open circuit potential of sealed SPEs upon immersion in 0.3 M KNO_3 and 0.3 M KCl. SPEs were kept in sealed packages for 2 months. The curve for the SPEs made with DuPont's ink shows three superposed transients from three different electrodes.

A very important feature can be seen in this first scan, and specially if we compare this figure with Figure 88. The transient for the electrode without added KCl shows a shoulder at 10 seconds, similar to those found for commercial SPEs in section 3.8. Electrodes recently manufactured (Figure 88) did not show this shoulder. In the case of the SPEs loaded with KCl, the transients do not show any remarkable difference with the storage time.

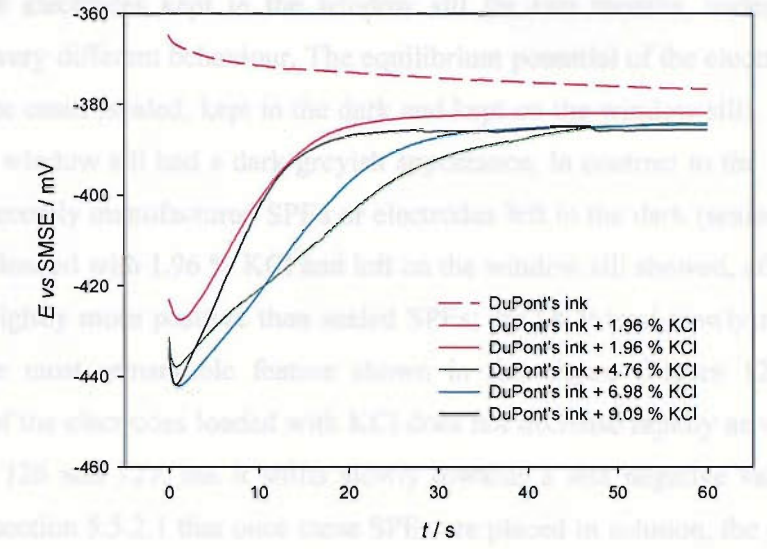

Figure 127 Variation of the open circuit potential of SPEs upon immersion in 0.3 M KNO_3 and 0.3 M KCl. SPEs were kept unsealed in the dark for 2 months.

Figure 127 shows the performance of electrodes kept unsealed in the dark. In this case, the performance of the SPE without added KCl differs from the previous case (Figure 126), but is very similar to the performance of recently manufactured electrodes (Figure 88), without the presence of any transient peak at short times. In the case of the electrodes with added KCl, if we compare the behaviour of electrodes sealed and not sealed, the latter were more irreproducible, but the behaviour of the transients was similar to that recorded for sealed or recently manufactured electrodes.

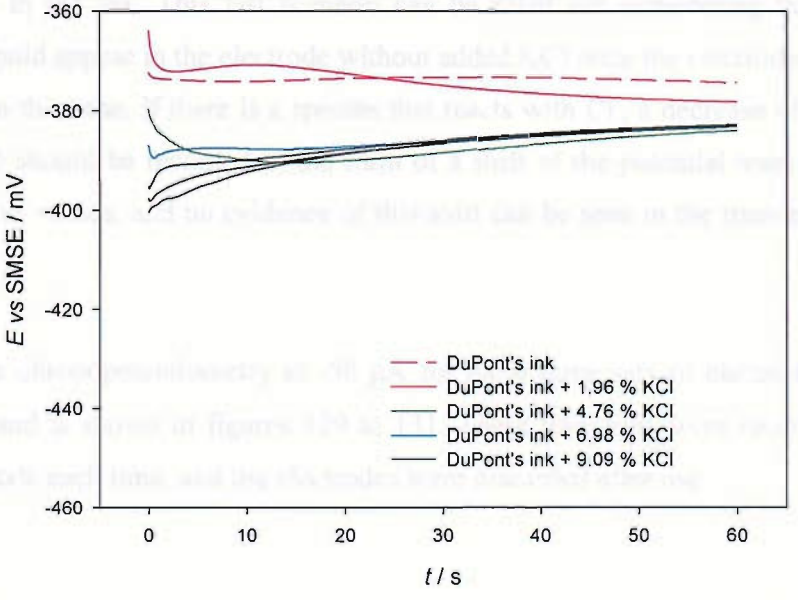

Figure 128 Variation of the open circuit potential of SPEs upon immersion in 0.3 M KNO_3 and 0.3 M KCl. SPEs were kept on the window sill for 2 months.

The electrodes kept in the window sill for two months, under light and air showed a very different behaviour. The equilibrium potential of the electrodes is similar for all three cases (sealed, kept in the dark and kept on the window sill). The electrodes left in the window sill had a dark greyish appearance, in contrast to the bright metallic finish of recently manufactured SPEs or electrodes left in the dark (sealed or unsealed). The SPEs loaded with 1.96 % KCl and left on the window sill showed, after 60 seconds, an OCP slightly more positive than sealed SPEs; the OCP tend slowly to the expected value. The most remarkable feature shown in this figure (Figure 128) is that the potential of the electrodes loaded with KCl does not decrease rapidly as we have shown in figures 126 and 127, but it shifts slowly towards a less negative values. We have shown in section 5.5.2.1 that once these SPEs are placed in solution, the potential shifts rapidly towards more negative values due to the dissolution of Cl^- embedded in the ink, and then the potential shifts towards the expected Nernst value as the Cl^- diffuses from the electrode towards the solution, reaching equilibrium within 30 seconds after immersing the electrode in solution. In the case of the electrodes loaded with KCl and left on the window sill, the potential recorded once the electrode is placed in solution is less negative than the expected one, suggesting either that the equilibrium is established between different species, or that the concentration of chloride at the electrode does not increase as much as in the case when the electrode has not been treated with light and air. In this later case, it could be due to a blocking by a passivation layer that prevents the dissolution of the KCl, or that some species at the electrode reacts with the Cl^- embedded in the ink. This last scenario can be ruled out considering that the same species should appear in the electrode without added KCl once the electrode is dipped in solution. In this case, if there is a species that reacts with Cl^-, a decrease of the activity of chloride should be recorded in the form of a shift of the potential transient towards less negative values, and no evidence of this shift can be seen in the transient in Figure 128.

The chronopotentiometry at -50 μA for these three sets of electrodes was also recorded, and is shown in figures 129 to 131. These transients were recorded using a new electrode each time, and the electrodes were discarded after use.

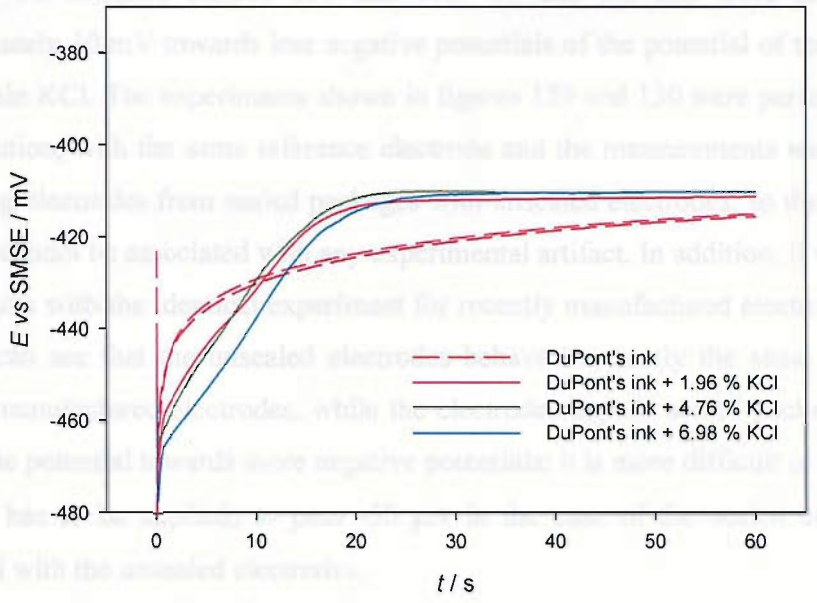

Figure 129 Variation of the potential transient at -50 μA for sealed SPEs upon immersion in 0.3 M KNO_3 and 0.3 M KCl. SPEs were kept in sealed packages for 2 months.

Figure 129 shows the behaviour of SPEs kept in sealed packages for two months. The chronoamperometry does not show any difference between these results and those recorded with recently manufactured SPEs (Figure 98). The chronopotentiometry of the SPEs kept unsealed, in the dark is shown in Figure 130:

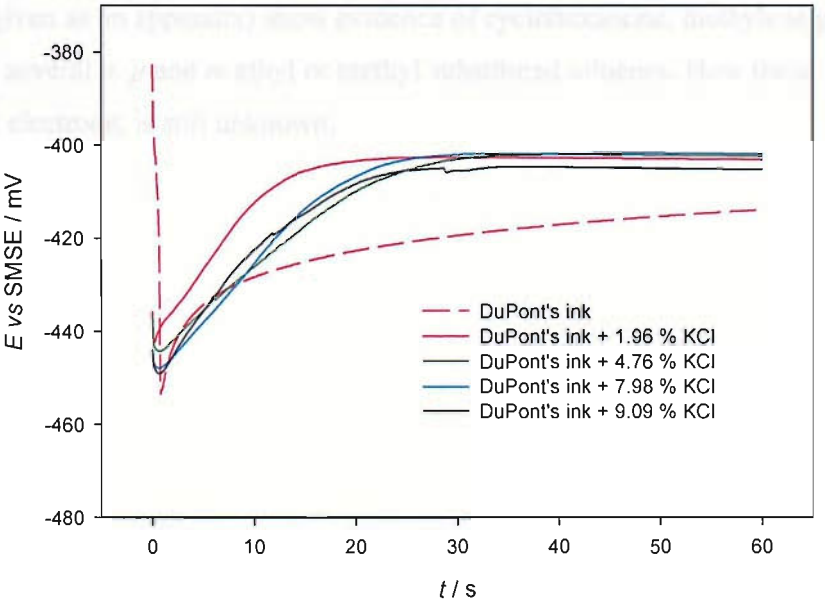

Figure 130 Variation of the potential transient at -50 μA for SPEs upon immersion in 0.3 M KNO_3 and 0.3 M KCl. SPEs were kept unsealed in the dark for 2 months.

If we compare figures 129 and 130, we can see that there is a shift of approximately 10 mV towards less negative potentials of the potential of the electrodes that contain KCl. The experiments shown in figures 129 and 130 were performed in the same solution, with the same reference electrode and the measurements were made by alternating electrodes from sealed packages with unsealed electrodes, so the shift in the potential cannot be associated with any experimental artifact. In addition, if we compare these results with the identical experiment for recently manufactured electrodes (Figure 98), we can see that the unsealed electrodes behave in exactly the same way as the recently manufactured electrodes, while the electrodes kept in sealed packages show a shift of the potential towards more negative potentials; it is more difficult (a larger over-potential has to be applied) to pass -50 μA in the case of the sealed electrodes as compared with the unsealed electrodes.

As we have said before (*vide supra*), the sealed electrodes smelt of organic solvent on opening. The smell was similar to that of cyclohexanone, but not as the fresh ink. The electrodes that we have manufactured were dried for approximately 20 mins at 55 °C in a continuous oven, in a similar way to the drying of commercial SPEs. Gas Chromatography coupled with Mass Spectroscopy (GC-MS) was used to analyse the volatile fraction in the package and identify the species responsible of the smell. To perform this analysis, a sealed screen printed electrode was opened and the package washed with H_2CCl_2 and a fraction of this washing was injected in the GC-MS. The spectra (given as an appendix) show evidence of cyclohexanone, diethylene glycol butyl ether and several *o, p* and *m* ethyl or methyl substituted toluenes. How these compounds affect the electrode, is still unknown.

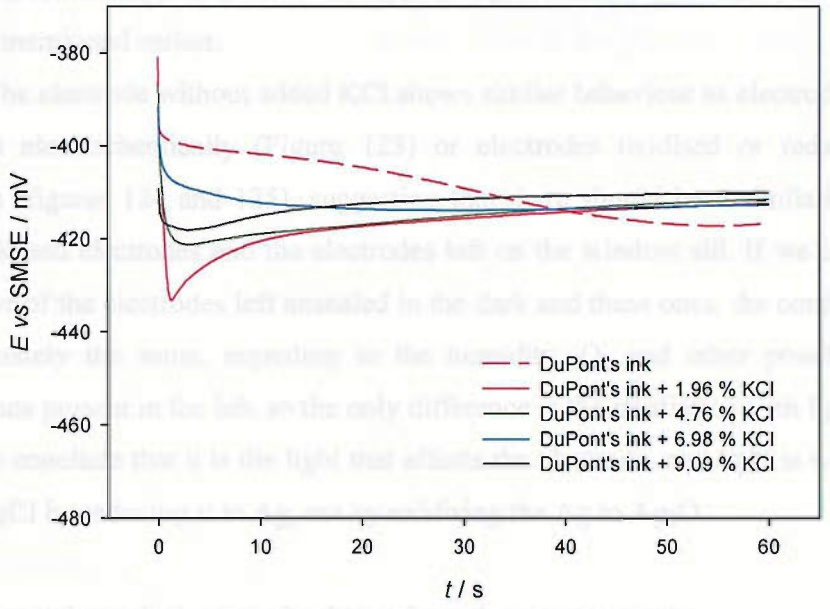

Figure 131 Variation of the potential transient at -50 μA for SPEs affected by light and air upon immersion in 0.3 M KNO_3 and 0.3 M KCl. SPEs were tarnished by leaving the electrodes on the window sill for 2 months.

Figure 131 shows the galvanostatic transient for electrodes left on the window sill for two months. In this case, the effect is more severe, and the behaviour of the electrodes is significantly different from that for the electrodes kept in the dark. The final potential for the electrodes loaded with KCl is similar to that of the sealed SPEs (Figure 129), and 10 mV more negative than the value for the recently manufactured electrodes (Figure 98). Meanwhile, the electrodes without added KCl show, once the steady state is achieved, an even more negative potential.

Apart from the final potential, the transients of the electrodes left on the window sill are also very different at short times to the ones recorded for electrodes kept in the dark (sealed or unsealed). As we have seen, the electrodes loaded with KCl show a very characteristic transient, with a sharp shift of the potential towards more negative potentials due to the dissolution of the KCl embedded in the ink, followed to a shift of the potential to less negative values as the Cl^- diffuses to the bulk. In this case (as well as for the open circuit potential shown in Figure 128), the transient does not show this characteristic sharp shift of the potential, suggesting that once the electrode is placed in solution, the concentration of chloride at the electrode does not increase as much as in the case when the electrode that has not been treated with light and air. This could be

due to the formation of a passivation layer that prevents the dissolution of the KCl, as we have mentioned earlier.

The electrode without added KCl shows similar behaviour as electrodes oxidised to Ag_2O electrochemically (Figure 123) or electrodes oxidised or reduced in Cl^- solutions (figures 124 and 125), suggesting that there should be a similarity between these oxidised electrodes and the electrodes left on the window sill. If we compare the behaviour of the electrodes left unsealed in the dark and these ones, the conditions were approximately the same, regarding to the humidity, O_2 and other possible volatile compounds present in the lab, so the only difference is the irradiation with light. We can therefore conclude that it is the light that affects the electrode, and light is well know to affect AgCl by reducing it to Ag, not by oxidising the Ag to Ag_2O.

Several conclusions can be drawn from these experiments:

- The final equilibrium potential of the SPEs loaded with KCl is not affected by the storage in any conditions tested. A slight variation of the equilibrium potential was recorded for SPEs without added KCl (+2 mV for unsealed electrodes and +4 mV for electrodes left in the light), but the transients were similar in all three cases.
- The electrodes loaded with KCl show a shift of the potential of the chronopotentiometry at -50 μA of around 10 mV if we compare them with recently manufactured electrodes and unsealed electrodes.
- Commercial screen printed electrodes (without added KCl) are affected by storage in the sealed package, developing a shoulder in the transient recorded at open circuit potential.
- The transients (at OCP and at -50 μA) are severely affected by light, especially in the case of the electrodes loaded with KCl. It is still unclear which is the mechanism that explains this behaviour.
- SPEs loaded with 1.96 % are the least affected by the light and air.

6.5. Conclusions

In this section we have studied how different storage conditions affect the SPEs. In general, the SPE is less altered if it is stored in unsealed packages, and kept in the

dark. This condition, although beneficial for the counter-reference screen printed electrode would not be ideal for the other electrodes in the glucose sensor, specially the working electrode, which contains ferrocene and GOx, both of which could be affected by air, moisture or biological degradation/contamination.

The mechanism that explains the alteration suffered by the Ag/AgCl electrode treated with light is still not clear; the most plausible mechanism is the conversion of AgCl to Ag mediated by light. These reduced electrodes show the same anomalous behaviour as electrodes oxidised in KOH at potentials where the formation of Ag_2O occurs. In this latter case, we believe that the Ag_2O formed can be converted to AgCl in the solution where the chronopotentiometry is taking place. Both treatments convert Ag or AgCl particles onto Ag/AgCl mixed particles, which can later be reduced at smaller over-potentials than AgCl particles. SPEs which have been subjected to a small reduction or oxidation in Cl^- solutions behave similarly to electrodes treated with light and air or oxidised electrodes, further supporting this model. In this sense, all of the pre-treatments tested (light and air, oxidation to Ag_2O or AgCl, partial pre-reduction) favour the nucleation of Ag and/or AgCl particles, so after the treatment, the reduction of AgCl is easier, *i.e.* it can be carried on at lower overpotentials.

Another effect shown in this chapter is that the OCP transient is affected by an aging effect when the electrodes are kept in sealed packages. In this case, no plausible explanation has been found. These sealed electrodes smelt of organic solvent on opening the package: the effect of storing the SPE without full removal of solvents from the ink has not been tested, but it could have some impact in the transients.

Of the different electrode compositions studied, SPEs loaded with 1.96 % KCl are the least affected by light and air. These electrodes show, after a severe aging treatment under light and air, similar OCP and galvanostatic transients to fresh SPEs without added KCl.

7 Overall conclusions

During this Thesis we have studied the performance of the Ag/AgCl electrode in MediSense G2b glucose sensor. We have shown that at long times, the behaviour of the electrode is similar to the theoretically expected one, with good reproducibility between electrodes of the same or different batches. We have found that the electrochemistry of the SPE is affected by the resistance of the track (approximately 120 Ω). The open circuit potential at long times (equilibrium potential) depends on the activity of Cl^- in the solution following the Nernst equation. The variation of the equilibrium potential with temperature was similar to that found in the literature for bulk Ag/AgCl electrodes[86].

We have found that all the AgCl in the electrode is electrochemically available. This is particularly interesting considering that in the glucose sensor a cathodic current has to pass through the Ag/AgCl counter-reference electrode (CRE). The oxidation of the Ag/AgCl electrode in Cl^- solutions was limited by the diffusion of a species with a small diffusion coefficient, probably due to the diffusion of the Cl^- through the ink or through the growing AgCl film.

We have found that the behaviour of the SPE at short times after the electrode was immersed in solution is more irreproducible. We have found that there is a change of the slope in the voltammetry performed with fresh SPE. This change of slope disappeared if the electrode was left in the solution for a short time before starting the measurement. Carbon paste electrodes loaded with AgCl showed similar behaviour. We believe that this behaviour is related to the nucleation of AgCl on Ag.

The potential transients recorded at OCP right after the SPEs were immersed in solution showed some strange oscillations. We have tried to find the experimental conditions that affected the transients (concentration of chloride in the solution, temperature, ionic strength, wetting of the SPE, effect of surfactants), but neither of the models proposed matched exactly all the experimental data. We believe that this feature is the sum of two distinct processes. The "*long time*" drift of the potential could be explained considering that the potential changes from a mixed, ill defined potential right after the electrode is dipped in the solution to the expected equilibrium potential from the Nernst equation. Superimposed to this drift, we have a "*short time*" feature that we have associated with a nucleation process occurring at the electrode.

The overall aim of this project was to build a counter-reference electrode with enhanced properties. This counter-reference electrode should be capable of working reproducibly at very short times (even down to 3 seconds after dipping in the sample).

We have proposed and tested two different screen printable approaches. These tests studied not only the proper electrochemical characteristics of the CRE, but also if these alternatives could be screen printed.

The first approach tested was carbon electrodes loaded with different amounts of AgCl. Since the CRE in the overall sensor carries out a reduction we can, in principle, eliminate the Ag from the electrode, hence giving a more economical electrode. These electrodes showed shorter equilibration times than the commercial Ag/AgCl SPE, but the decreased conductivity of the electrode (since the Ag was removed) shifted the potential towards more negative values following Ohm's law. In addition, the amount of AgCl at the electrode surface was too small to pass the required current densities. Increasing the proportion of AgCl in the ink affected both the conductivity and the viscosity of the ink, giving an even worse electrode. Still, this approach could be an appropriate alternative to Ag/AgCl SPEs for fast measurements with small current densities, as is often the case for portable or/and miniaturised (bio)sensors.

The second approach used the same ink that is currently being used, but with different amounts of KCl added. The electrodes built in this way showed a more stable response, with faster equilibration times than the commercial SPE. The main characteristic of these new electrodes is that the added KCl in the ink dissolves immediately once the electrode is placed in solution, thus increasing the a_{Cl^-} locally at the electrode and consequently shifting the potential towards more negative values. The potential of this CRE changes as this KCl dissolves in a reproducible way. This reproducibility means that this transient potential can be used as the reference potential in the system. We have not found anywhere in the literature the use of a transient potential established by the diffusion of some species as the reference potential of an electrochemical system. These electrodes were tested as the counter-reference electrodes in a model system with a glassy carbon electrode as working electrode and $Fe(C_5H_4COOH)_2$ as the electroactive species. More reproducible transients were obtained with the SPE loaded with KCl than with the commercial electrode.

MediSense has reported that SPEs treated with light and air showed an anomalous behaviour. We have found that this anomalous behaviour was similar to the behaviour of SPEs oxidised to Ag_2O. We are not sure of the mechanism that explains this anomalous behaviour, but we believe that it is related with the conversion of some of the Ag or AgCl particles into AgCl or Ag, since SPEs partially oxidised or reduced in Cl^- solutions showed similar behaviour.

We have also studied the effect of light and air and the storage conditions in the performance of the proposed Ag/AgCl SPEs loaded with KCl, finding that the electrodes loaded with 1.96 % of KCl were the least affected by the storage conditions.

In short, we have proposed an Ag/AgCl SPE loaded with KCl as a stable alternative to the commercial SPE. This electrode shows shorter equilibration times (*i.e.* 20-30 s), and reproducible behaviour within the first moments after the electrode is dipped in solution. We believe that this electrode could be applied in a reproducible and reliable way to a sensor operating at very short times (*e.g.* 3-5 s) after the immersion of the sensor in the solution.

The Ag/AgCl SPEs loaded with KCl had shown good characteristics, but a more in depth analysis should be carried. This analysis should mainly study the performance of the sensor build with this electrode in the real sample (whole blood) and also study the variation of the performance between different batches. We have found that adding large concentrations of chloride salts to the ink affect negatively the rheology and the characteristics of the print. A better way of dispersing the Cl^- in the ink should be investigated; KCl in smaller particle sizes could give more homogeneous inks, other chloride salts might alter the ink less than KCl. KCl yields 13.4 mmol of Cl^- per gram, meanwhile other chlorinated salts like LiCl or $MgCl_2$ can give 18 mmol or 21 mmol of Cl^- per gram of salt, thus requiring less mass of salt for the same amount of Cl^-.

CRE with only AgCl were not satisfactory for our application mainly due to their low conductivity. Ways of enhancing this conductivity could be tested, such as printing a conductive layer underneath or over the reference track or using a conductive polymer as the ink matrix.

We have not found a solid explanation for the anomalous behaviour of the electrode once the electrode has been treated with light and air or during its storage. Actually, it is still unclear if this effect is due to the light or to the light and air. Surface techniques like XPS could give an insight of the species present in the surface of the SPE after these treatments, and their oxidation status. After understanding this effect, strategies to minimise its incidence could be proposed.

8 Appendices

8.1. Penetration depth of electrons in the sample

When a specimen is irradiated with electrons, the penetration of these electrons in matter is a function of the energy of the electrons and the density of the specimen. The following empirical equation shows this relationship[195]:

$$Pr = \frac{4120}{\rho} E^{(1.265 - 0.0954 \operatorname{Ln} E)} \qquad \text{Equation 48}$$

where Pr is the penetration depth in μm; ρ the density of the material (in g/cm^3) and E the energy of the electrons (in eV). The detected X-rays will then provide information from this irradiated area. Considering the densities of AgCl (5.56 g/cm^3)[131] and Ag (10.5 g/cm^3)[131] and that the electron microscope's usual operating voltages is 15 kV, electrons will penetrate approximately 0.7 and 0.37 μm into each of the respective kinds of particles.

To calculate the density of the dried ink, the following calculation was made, starting from the total reduction charge of a Ag/AgCl SPE, ~55 mC (section 3.4). This charge corresponds to an AgCl content of approximately 8.17 μg per SPE, and considering the percentage of AgCl in the ink (27.48 %, as stated by DuPont), we calculate that there is approximately 0.3 mg of Ag/AgCl ink per electrode (only considering the part of the reference electrode in contact with the solution). The volume of this mass can be calculated from the area of the electrode (2.69 mm^2) and the thickness of the Ag/AgCl layer (approximately 30 μm). In the case of the Ag/AgCl printed layer, we have estimated a density of approximately 3.72 g/cm^3, so the electrons can penetrate approximately 1 μm.

It is important to note that this is an approximation, since several assumptions have been made. These were that the density of the electrode is uniform (and it is obviously not uniform, considering the presence of Ag and AgCl particles with large densities, as well as pores), that all the AgCl in the electrode is electroactive[129], and that the AgCl contents per gram of wet ink is the same as that of the cured ink (this last approximation is quite precarious).

Anyway, this approximation allows us to realise that the electrons penetrate only a small fraction of the top of the electrode, and that the X-ray analysis is not representative of the whole Ag/AgCl layer.

8.2. GC-MS analysis of the solvents enclosed with the SPE in the package

This analysis was performed at the Mass Spectrometry facilities at the University of Southampton. The sealed SPE was opened and the package washed with H_2CCl_2 and a fraction of this washing was injected in the GC-MS. The GC-MS used was a ThermoQuest TraceMS with an electroionization source and an AS800 autosampler. The sample was injected onto a Zebron ZB5 column (Phenomenex) of 30 m × 0.25 mm with 0.25 μm pore size. The column was placed in an oven, and the following temperature program was applied:

1. Initial temperature: 60 °C, for 10 mins.
2. Temperature rose till 150 °C at 10 °C min^{-1}.
3. Temperature rose till 320 °C at 40 °C min^{-1}, and kept constant at this temperature for 6 min to clean and purge the column.

The chromatogram obtained with the ionization detector is shown in Figure 132. This chromatogram shows each component of the injected mixture (the sample) as it is eluted from the column.

Each of the separated compounds was injected into the mass spectrometer, and its chemical composition analysed. In the following figures, we show the data for the most representative compounds analysed. We compared the obtained spectra of each compound for possible matches in the library of compounds included with the software of the instrument, and we included the spectrum of the best match in the library and the chemical structure with each spectrum.

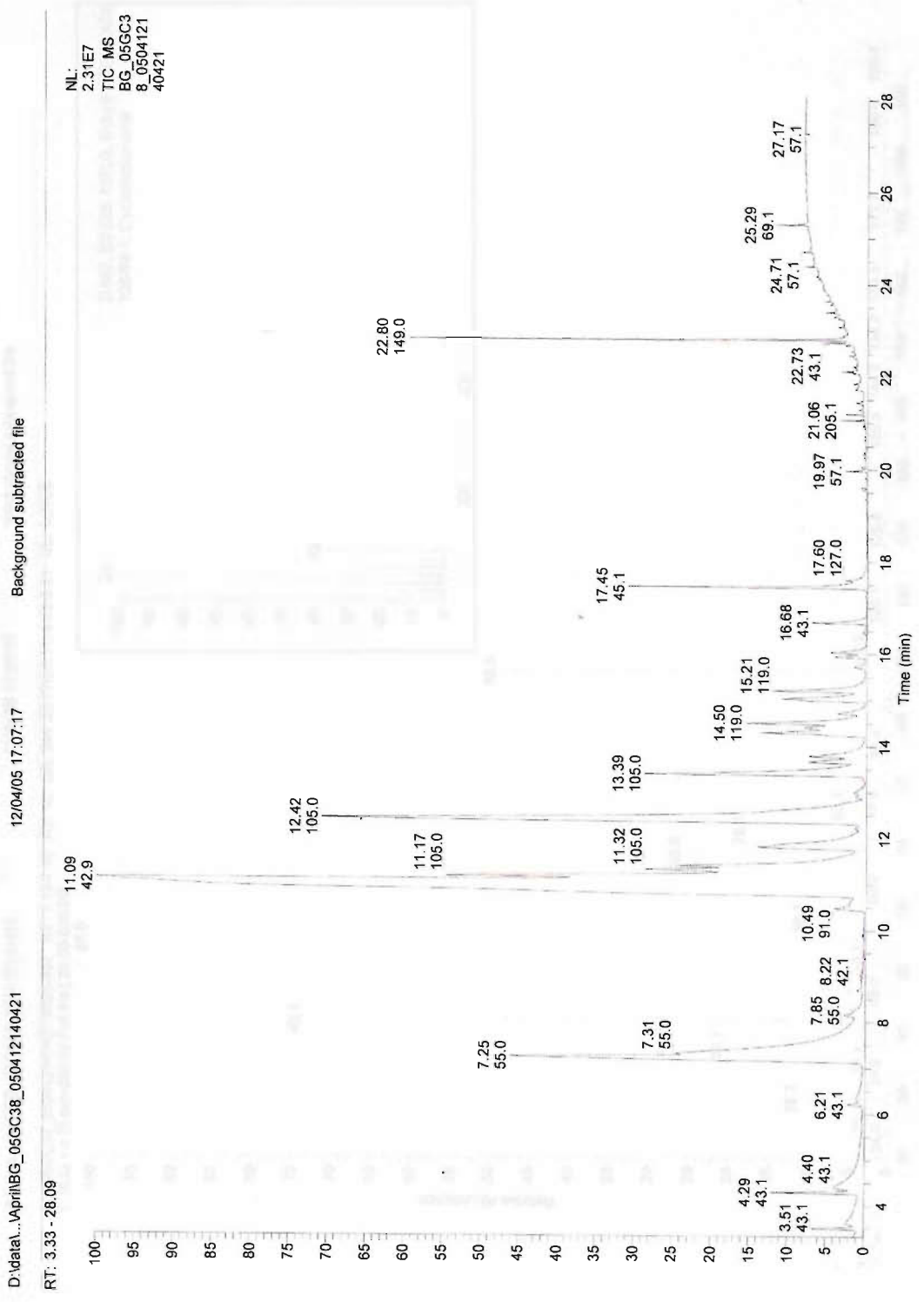

Figure 132 Gas chromatogram of the solvents entrapped with the SPE inside the sealed package.

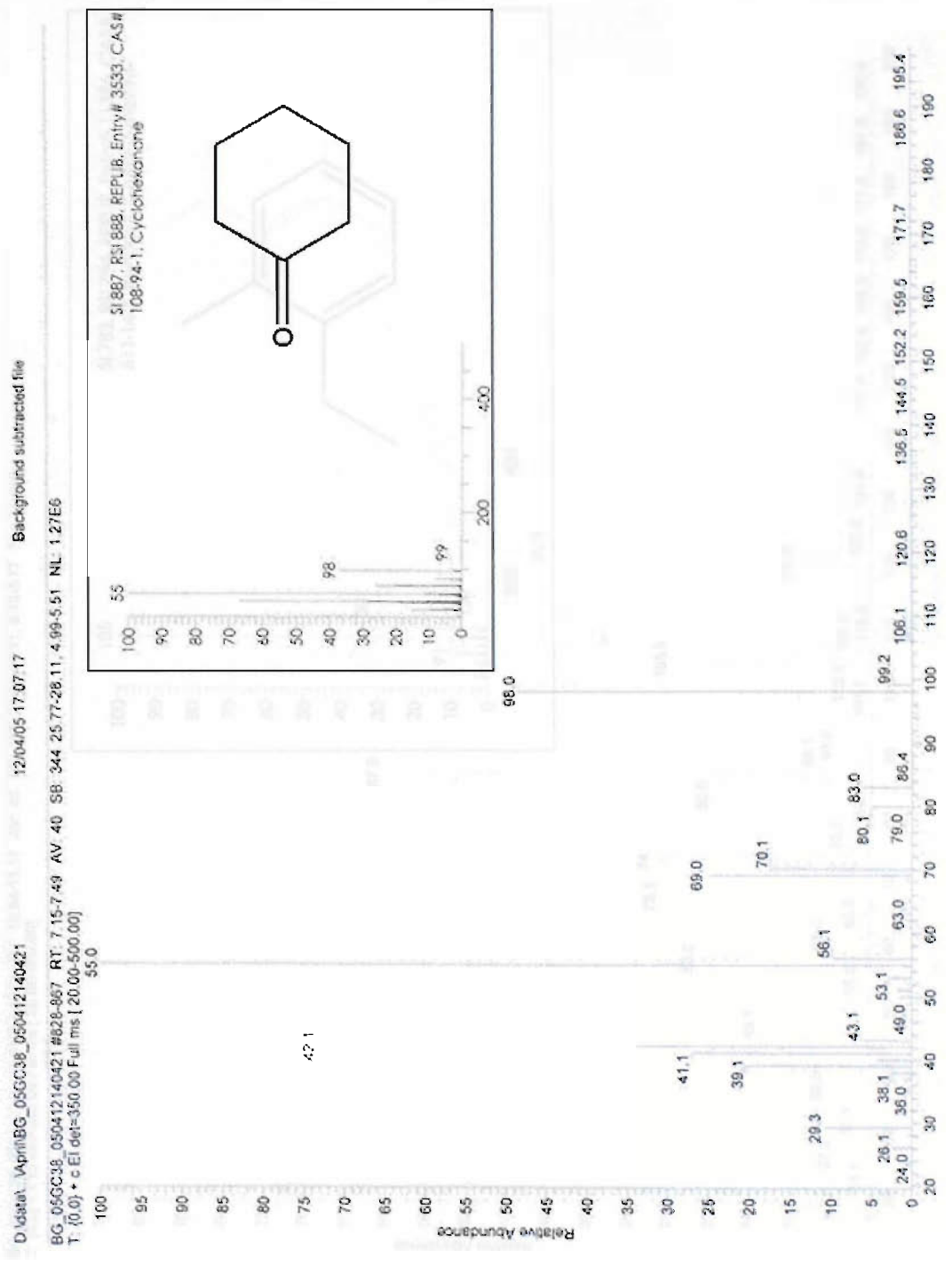

Figure 133 Mass spectra of the compound eluted at 7.15-7.49 min. The box shows the spectrum of cyclohexanone, the best match from the library for this component.

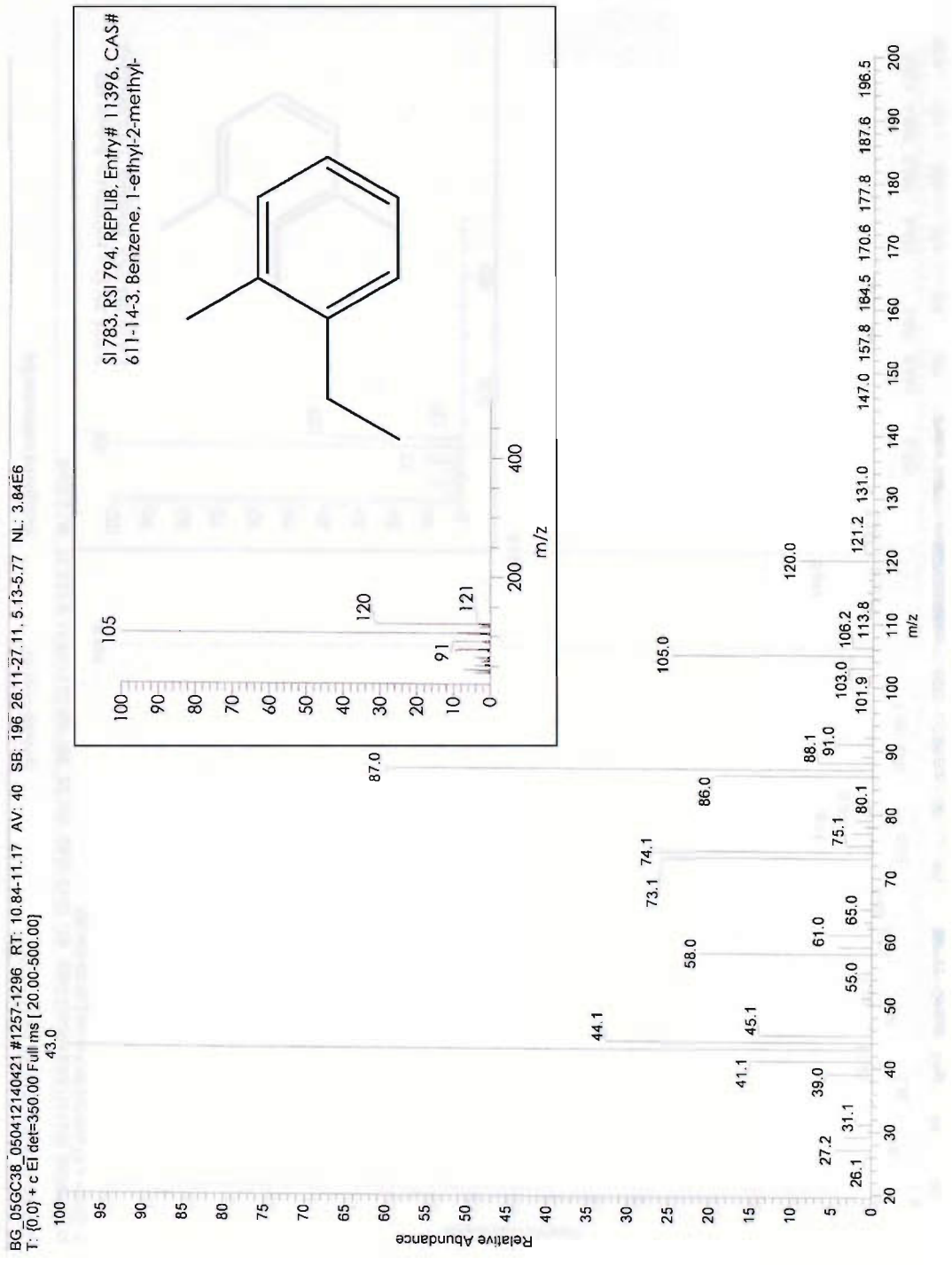

Figure 134 Mass spectra of the compound eluted at 10.84-11.17 min. The box shows the spectrum of 1-methyl-2-ethylbenzene, the best match from the library for this component.

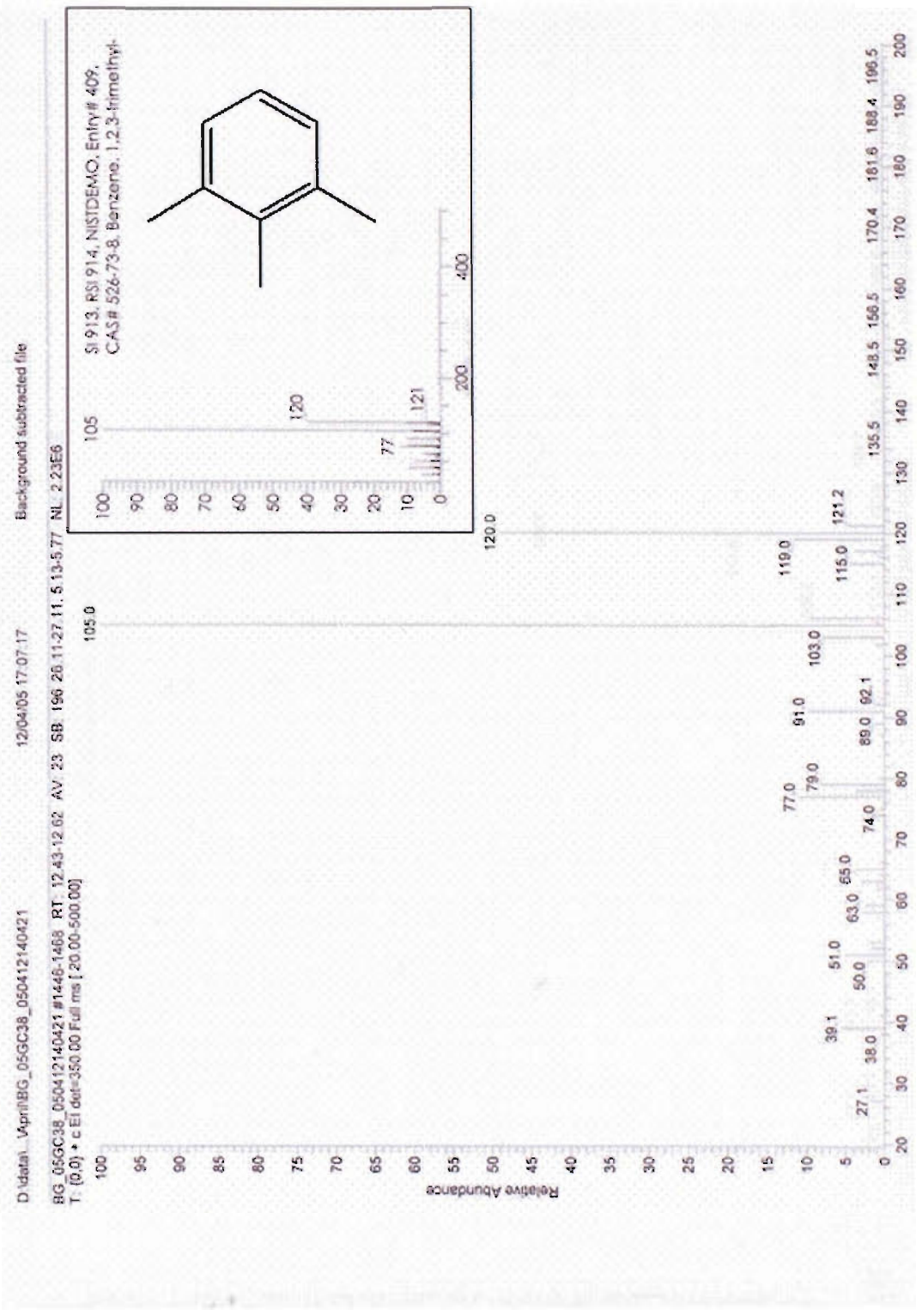

Figure 135 Mass spectra of the compound eluted at 12.43-12.62 min. The box shows the spectrum of 1,2,3-trimethylbenzene, the best match from the library for this component.

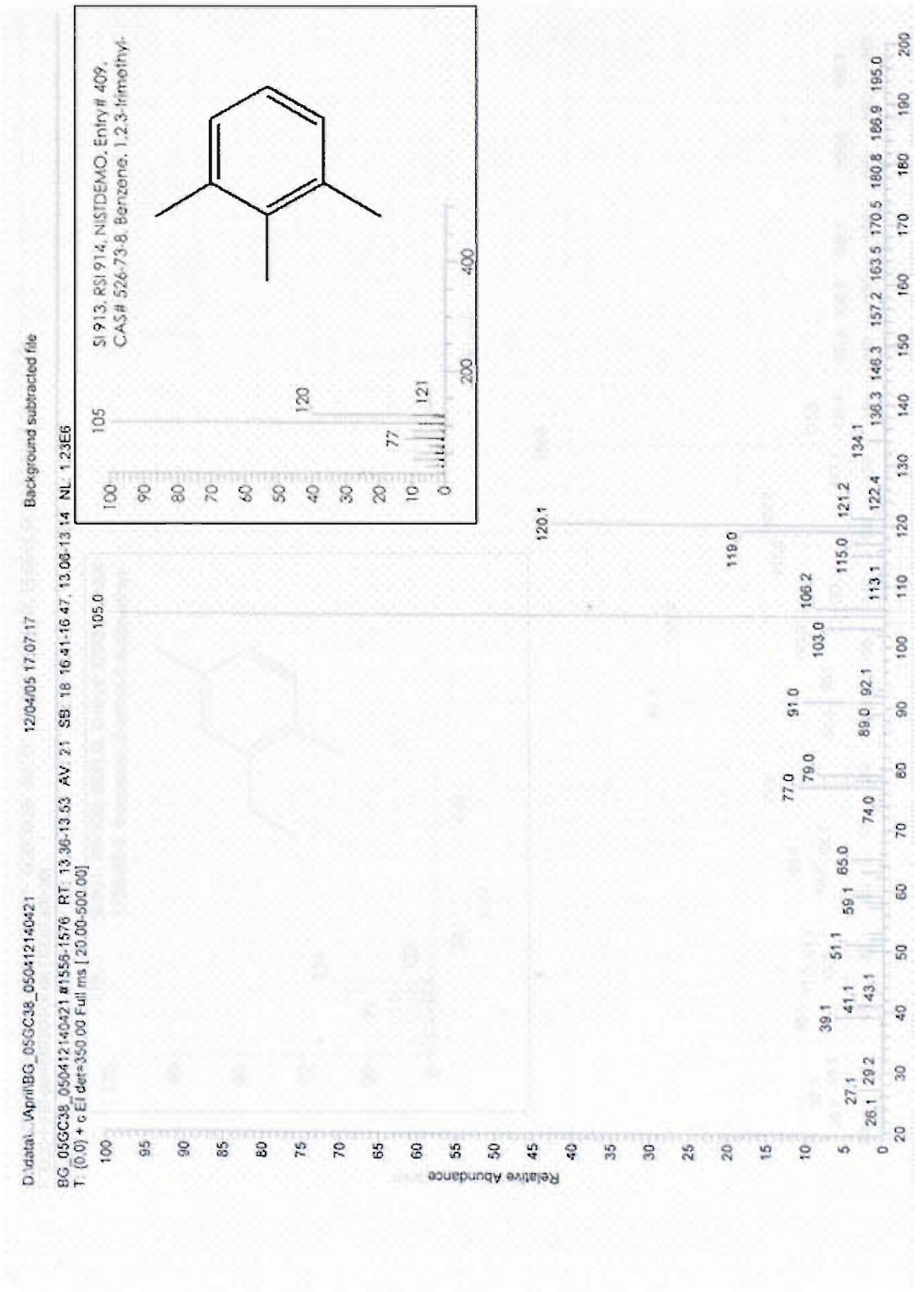

Figure 136 Mass spectra of the compound eluted at 13.36-13.53 min. The box shows the spectrum of 1,2,3-trimethylbenzene, the best match from the library for this component.

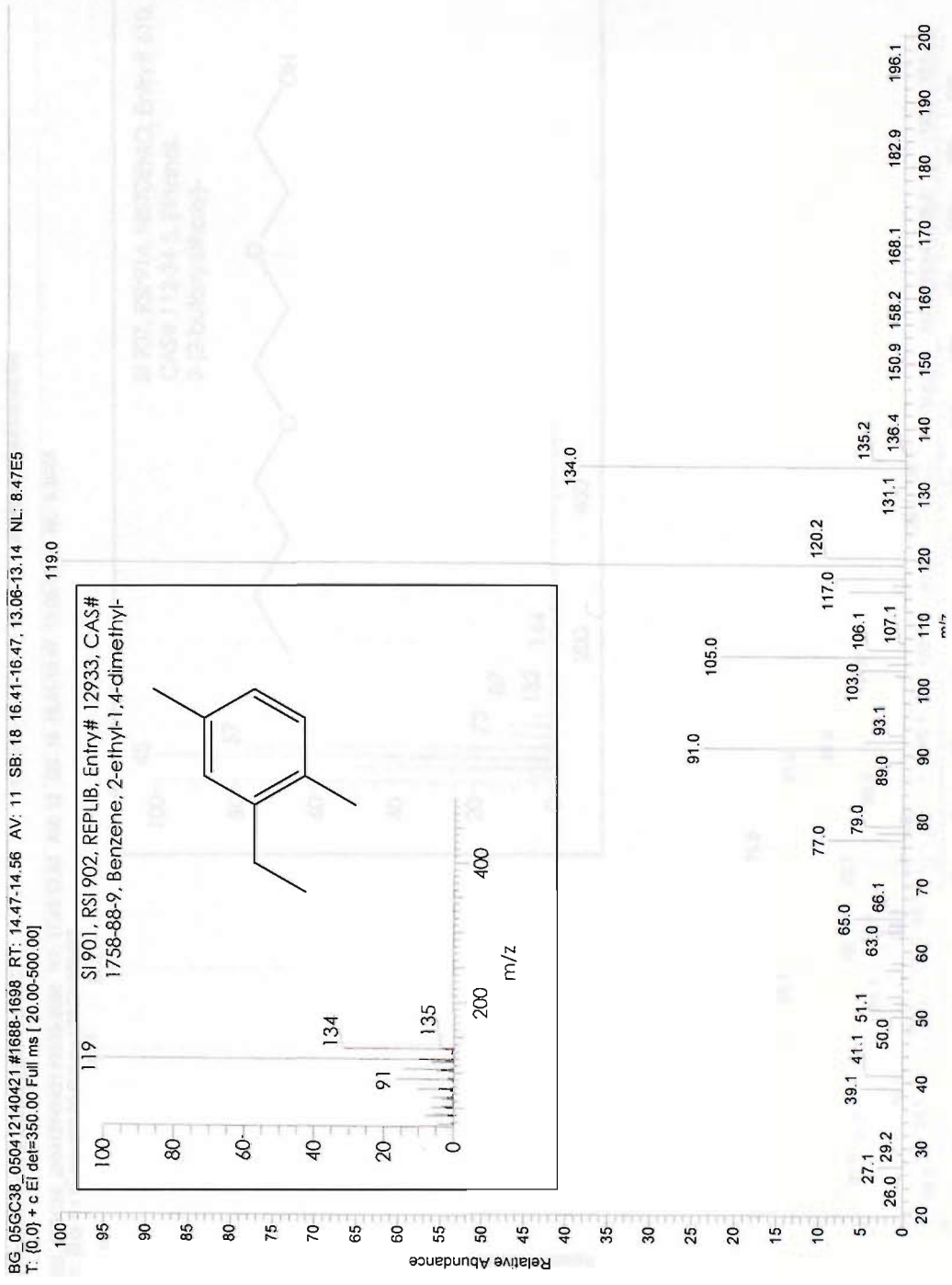

Figure 137 Mass spectra of the compound eluted at 14.47-14.56 min. The box shows the spectrum of 2-ethyl-1,4-dimethylbenzene, the best match from the library for this component.

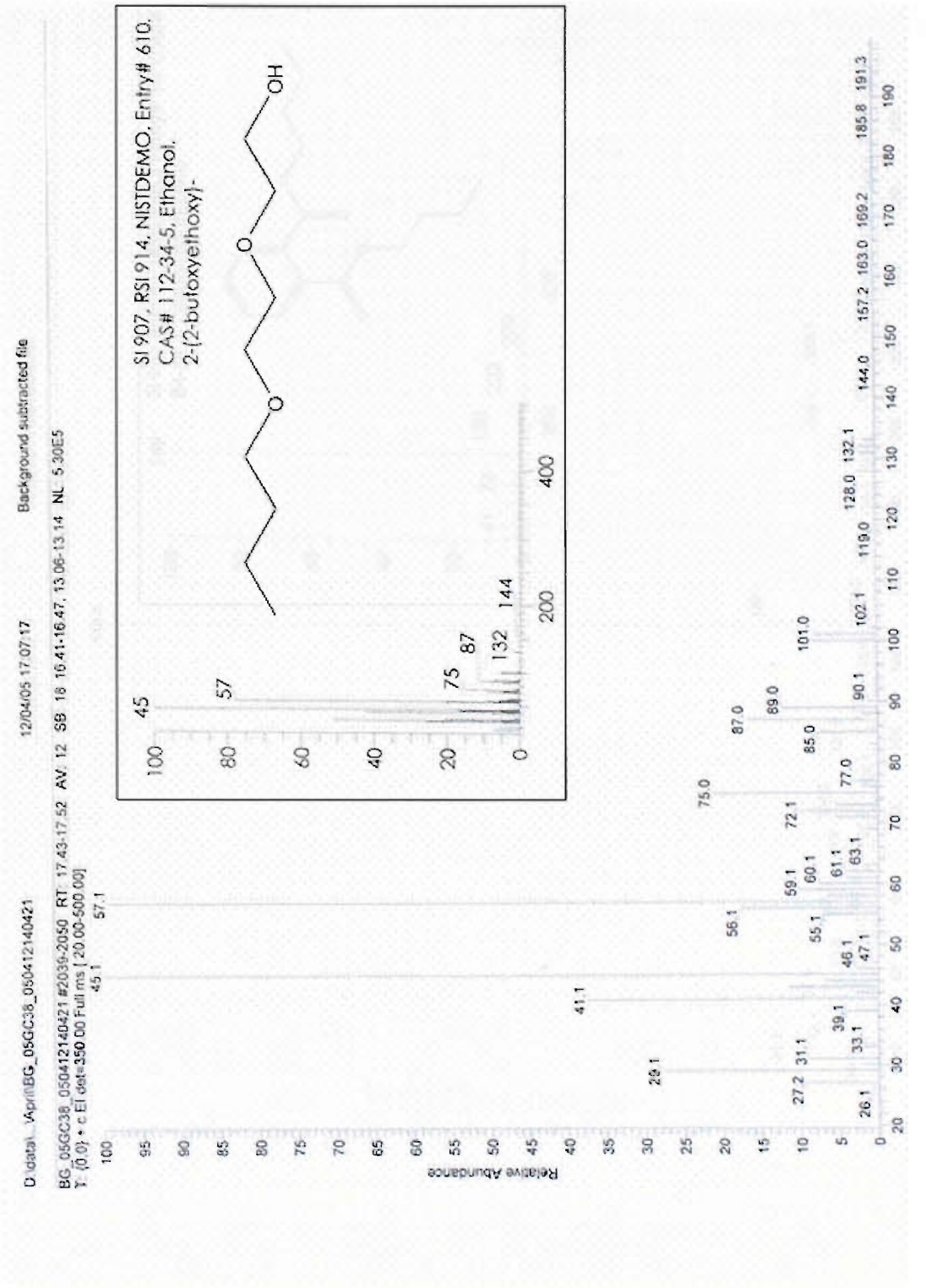

Figure 138 Mass spectra of the compound eluted at 17.43-17.52 min. The box shows the spectrum of 2-(2-butoxyethoxy)ethanol, the best match from the library for this component.

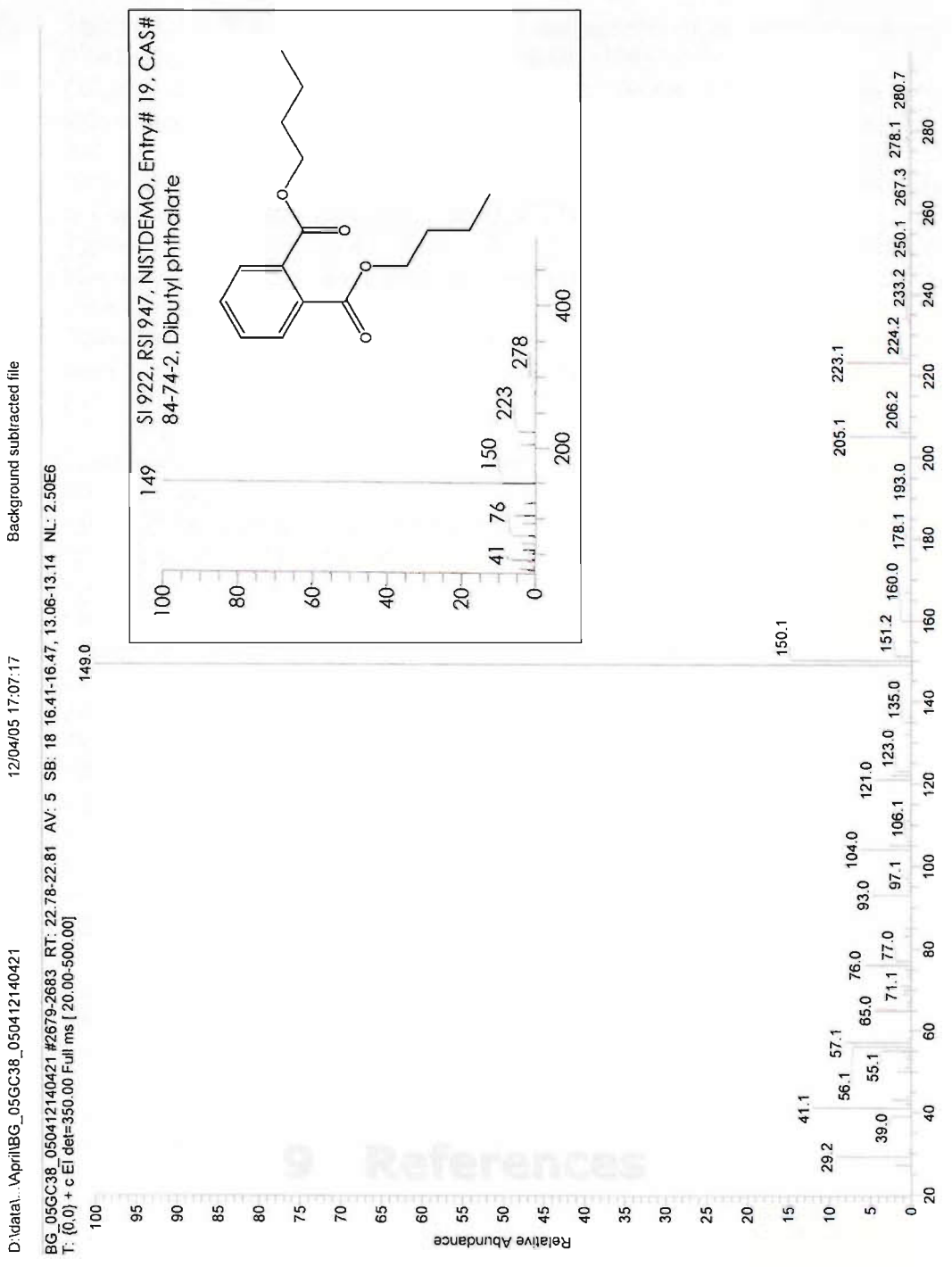

Figure 139 Mass spectra of the compound eluted at 22.78-22.81 mins. The box shows the spectrum of dibutylphtalate, the best match from the library for this component.

9 References

(1) Skoog, A. S.; West, D. M.; Holler, F. J. *Fundamentals of Analytical Chemistry*, 7th ed.; Harcourt College Publishers: Fort Worth, 1995.

(2) Galan-Vidal, C. A.; Munoz, J.; Dominguez, C.; Alegret, S. "Chemical sensors, biosensors and thick-film technology" *Trac-Trends Anal Chem* **1995**, *14*, 225-231.

(3) Gerard, M.; Chaubey, A.; Malhotra, B. D. "Application of conducting polymers to biosensors" *Biosens Bioelectron* **2002**, *17*, 345-359.

(4) Thévenot, D. R.; Toth, K.; Durst, R. A.; Wilson, G. S. "Electrochemical biosensors: Recommended definitions and classification - (Technical Report)" *Pure Appl Chem* **1999**, *71*, 2333-2348.

(5) Thévenot, D. R.; Toth, K.; Durst, R. A.; Wilson, G. S. "Electrochemical biosensors: Recommended definitions and classification" *Anal Lett* **2001**, *34*, 635-659.

(6) Thévenot, D. R.; Toth, K.; Durst, R. A.; Wilson, G. S. "Electrochemical biosensors: recommended definitions and classification" *Biosens Bioelectron* **2001**, *16*, 121-131.

(7) Mello, L. D.; Kubota, L. T. "Review of the use of biosensors as analytical tools in the food and drink industries" *Food Chem* **2002**, *77*, 237-256.

(8) Kröger, S.; Piletsky, S.; Turner, A. P. F. "Biosensors for marine pollution research, monitoring and control" *Mar Pollut Bull* **2002**, *45*, 24-34.

(9) Turner, A. P. F. "Biosensors - Sense and sensitivity" *Science* **2000**, *290*, 1315-1317.

(10) Alvarez-Icaza, M.; Bilitewski, U. "Mass-Production of Biosensors" *Anal Chem* **1993**, *65*, A525-A533.

(11) Albareda-Sirvent, M.; Merkoci, A.; Alegret, S. "Pesticide determination in tap water and juice samples using disposable amperometric biosensors made using thick-film technology" *Anal Chim Acta* **2001**, *442*, 35-44.

(12) Lindner, E.; Buck, R. P. "Microfabricated potentiometric electrodes and their in vivo applications" *Anal Chem* **2000**, *72*, 336A-345A.

(13) Clark, L. C., Jr.; Lyons, C. "Electrode systems for continuous monitoring in cardiovascular surgery" *Ann NY Acad Sci* **1962**, *102*, 29-45.

(14) Brainina, K. "Electroanalysis: From laboratory to field versions" *J Anal Chem* **2001**, *56*, 303-312.

(15) Lauks, I. R. "Microfabicated biosensors and microanalytical systems for blood analysis" *Acc Chem Res* **1998**, *31*, 317-324.

(16) Newman, J. D.; White, S. F.; Tothill, I. E.; Turner, A. P. F. "Catalytic Materials, Membranes, and Fabrication Technologies Suitable for the Construction of Amperometric Biosensors" *Anal Chem* **1995**, *67*, 4594-4599.

(17) Wang, J. "Glucose biosensors: 40 years of advances and challenges" *Electroanal* **2001**, *13*, 983-988.

(18) Hart, J. P.; Wring, S. A. "Screen-Printed Voltammetric and Amperometric Electrochemical Sensors for Decentralized Testing" *Electroanal* **1994**, *6*, 617-624.

(19) Hart, J.; Wring, S. "Recent Developments in the Design and Application of Screen-Printed Electrochemical Sensors for Biomedical, Environmental and Industrial Analyses" *Trac-Trends Anal Chem* **1997**, *16*, 89-103.

(20) Galan-Vidal, C.; Muñoz, J.; Dominguez, C.; Alegret, S. "Glucose biosensor strip in a three electrode configuration base on composite and biocomposite materials applied by planar thick film technology" *Sensor Actuat B-Chem* **1998**, *52*, 257-263.

(21) Liu, D.; Meruva, R. K.; Brown, R. B.; Meyerhoff, M. E. "Enhancing EMF stability of solid-state ion-selective sensors by incorporating lipophilic silver-ligand complexes within polymeric films" *Anal Chim Acta* **1996**, *321*, 173-183.

(22) Masawat, P.; Liawruangrath, S.; Slater, J. M. "Flow injection measurement of lead using mercury-free disposable gold-sputtered screen-printed carbon electrodes (SPCE)" *Sensor Actuat B-Chem* **2003**, *B91*, 52-59.

(23) Erlenkotter, A.; Kottbus, M.; Chemnitius, G. "Flexible amperometric transducers for biosensors based on a screen printed three electrode system" *J Electroanal Chem* **2000**, *481*, 82-94.

(24) http://www.g-e-m.com/info/hybrid/hybrid2.html

(25) Hart, J. P.; Abass, A. K.; Cowell, D. "Development of disposable amperometric sulfur dioxide biosensors based on screen printed electrodes" *Biosens Bioelectron* **2002**, *17*, 389-394.

(26) Shepherd, R. L.; Barisci, J. N.; Collier, W. A.; Hart, A. L.; Partridge, A. C.; Wallace, G. G. "Development of conducting polymer coated screen-printed sensors for measurement of volatile compounds" *Electroanal* **2002**, *14*, 575-582.

(27) Williams, E. W.; Keeling, A. G. "A low cost screen printed room temperature carbon monoxide tin oxide sensor" *J Mater Sci Lett* **1997**, *16*, 906-907.

(28) Maccà, C.; Soldà, L.; Voltan, R.; Calliari, I. "Stripping chronopotentiometry with dry-preservable supporting electrolyte" *Electroanal* **2004**, *16*, 1311-1317.

(29) Kadara, R. O.; Newman, J. D.; Tothill, I. E. "Stripping chronopotentiometric detection of copper using screen-printed three-electrode system-application to acetic-acid bioavailable fraction from soil samples" *Anal Chim Acta* **2003**, *493*, 95-104.

(30) Pötter, W.; Dumschat, C.; Cammann, K. "Miniaturized Reference Electrode Based on a Perchlorate-Selective Field Effect Transistor" *Anal Chem* **1995**, *67*, 4586-4588.

(31) Silber, A.; Bisenberger, M.; Braeuchle, C.; Hampp, N. "Thick-film multichannel biosensors for simultaneous amperometric and potentiometric measurements" *Sensor Actuat B-Chem* **1996**, *B30*, 127-132.

(32) Fanjul-Bolado, P.; Gonzalez-Garcia, M. B.; Costa-Garcia, A. "Voltammetric determination of alkaline phosphatase and horseradish peroxidase activity using 3-indoxyl phosphate as substrate application to enzyme immunoassay" *Talanta* **2004**, *64*, 452-457.

(33) Fanjul-Bolado, P.; Gonzalez-Garcia, M. B.; Costa-Garcia, A. "3-indoxyl phosphate as an electrochemical substrate for horseradish peroxidase" *Electroanal* **2004**, *16*, 988-993.

(34) Kataky, R.; Bryce, M. R.; Goldenberg, L.; Hayes, S.; Nowak, A. "A biosensor for monitoring formaldehyde using a new lipophilic tetrathiafulvalene-tetracyanoquinodimethane salt and a polyurethane membrane" *Talanta* **2002**, *56*, 451-458.

(35) Desmond, D.; Lane, B.; Alderman, J.; Glennon, J. D.; Diamond, D.; Arrigan, D. W. M. "Evaluation of miniaturised solid state reference electrodes on a silicon based component" *Sensor Actuat B-Chem* **1997**, *44*, 389-396.

(36) Simonis, A.; Lueth, H.; Wang, J.; Schoening, M. J. "Strategies of miniaturised reference electrodes integrated in a silicon based "one chip" pH sensor" *Sensors* **2003**, *3*, 330-339.

(37) Simonis, A.; Luth, H.; Wang, J.; Schoning, M. J. "New concepts of miniaturised reference electrodes in silicon technology for potentiometric sensor systems" *Sensor Actuat B-Chem* **2004**, *B103*, 429-435.

(38) Schumacher, J. T.; Munch, I.; Richter, T.; Rohm, I.; Bilitewski, U. "Investigations with respect to stabilization of screen-printed enzyme electrodes" *J Mol Catal B-Enzym* **1999**, *7*, 67-76.

(39) Wang, J.; Tian, B.; Nascimento, V.; Angnes, L. "Performance of Screen-Printed Carbon Electrodes Fabricated from Different Carbon Inks" *Electrochim Acta* **1998**, *43*, 3459-3465.

(40) Nagy, G.; Gyurcsanyi, R.; Cristalli, A.; Neuman, M.; Lindner, E. "Screen-Printed Amperometric Microcell for Proline Iminopeptidase Enzyme-Activity Assay" *Biosens Bioelectron* **2000**, *15*, 265-272.

(41) Sántha, H.; Dobay, R.; Harsányi, G. "Amperometric uric acid biosensors fabricated of various types of uricase enzymes" *IEEE Sens J* **2003**, *3*, 282-287.

(42) Lam, Y.-Z.; Atkinson, J. "Disposable screen-printed biosensor for transcutaneous oxygen measurement" *Meas Sci Technol* **2002**, *13*, 2074-2081.

(43) Sprules, S.; Hartley, I.; Wedge, R.; Hart, J.; Pittson, R. "A Disposable Reagentless Screen-Printed Amperometric Biosensor for the Measurement of Alcohol in Beverages" *Anal Chim Acta* **1996**, *329*, 215-221.

(44) Boujtita, M.; Hart, J.; Pittson, R. "Development of a Disposable Ethanol Biosensor Based on a Chemically-Modified Screen-Printed Electrode Coated with Alcohol Oxidase for the Analysis of Beer" *Biosens Bioelectron* **2000**, *15*, 257-263.

(45) Hu, T.; Zhang, X.; Zhang, Z.; Chen, L. "A Screen-Printed Disposable Enzyme Electrode System for Simultaneous Determination of Sucrose and Glucose" *Electroanal* **2000**, *12*, 868-870.

(46) Ge, F.; Zhang, X.-E.; Zhang, Z.-P.; Zhang, X.-M. "Simultaneous determination of maltose and glucose using a screen-printed electrode system" *Biosens Bioelectron* **1998**, *13*, 333-339.

(47) Kröger, S.; Turner, A. "Solvent-Resistant Carbon Electrodes Screen-Printed Onto Plastic for Use in Biosensors" *Anal Chim Acta* **1997**, *347*, 9-18.

(48) Collier, W. A.; Janssen, D.; Hart, A. L. "Measurement of soluble L-lactate in dairy products using screen-printed sensors in batch mode" *Biosens Bioelectron* **1996**, *11*, 1041-1049.

(49) Collier, W. A.; Lovejoy, P.; Hart, A. L. "Estimation of soluble L-lactate in dairy products using screen-printed sensors in a flow injection analyser" *Biosens Bioelectron* **1998**, *13*, 219-225.

(50) Hart, A.; Matthews, C.; Collier, W. "Estimation of Lactate in Meat Extracts by Screen-Printed Sensors" *Anal Chim Acta* **1999**, *386*, 7-12.

(51) Burns, I. W.; Nylander, C. I. "An evaluation of a novel type of solid state sensor" *Anal Proc* **1986**, *23*, 289-291.

(52) Hu, T.; Zhang, X.-E.; Zhang, Z.-P.; Ge, F.; Liu, M.-L. "Simultaneous determination of glucoamylase activity and glucose in fermentation process based on screen-printed disposable biosensor" *Anal Lett* **2001**, *34*, 79-90.

(53) Nagata, R.; Yokoyama, K.; Clark, S.; Karube, I. "A Glucose Sensor Fabricated by the Screen Printing Technique" *Biosens Bioelectron* **1995**, *10*, 261-267.

(54) Patel, N.; Meier, S.; Cammann, K.; Chemnitius, G. "Screen-Printed Biosensors Using Different Alcohol Oxidases" *Sensor Actuat B-Chem* **2001**, *75*, 101-110.

(55) Moody, A.; Setford, S.; Saini, S. "Peroxidase enzyme sensor for on-line monitoring of disinfection processes in the food industry" *Analyst* **2001**, *126*, 1733-1739.

(56) Cui, G.; Yoo, J.; Woo, B. "Disposable amperometric glucose sensor electrode with enzyme-immobilized nitrocellulose strip" *Talanta* **2001**, *54*, 1105-1111.

(57) Tymecki, L.; Zwierkowska, Z.; Koncki, R. "Screen-printed reference electrodes for potentiometric measurements" *Anal Chim Acta* **2004**, *526*, 3-11.

(58) Olschewski, H.; Erlenkotter, A.; Zaborosch, C.; Chemnitius, G. C. "Screen-printed enzyme sensors for l-lysine determination" *Enzyme Microb Tech* **2000**, *26*, 537-543.

(59) Cui, G.; Yoo, J. H.; Lee, J. S.; Yoo, J.; Uhm, J. H.; Cha, G. S.; Nam, H. "Effect of pre-treatment on the surface and electrochemical properties of screen-printed carbon paste electrodes" *Analyst* **2001**, *126*, 1399-1403.

(60) Zhang, C.; Gao, Q.; Aizawa, M. "Flow-Injection Analytical System for Glucose with Screen-Printed Enzyme Biosensor Incorporating Os-Complex Mediator" *Anal Chim Acta* **2001**, *426*, 33-41.

(61) Cui, G.; Kim, S.; Choi, S.; Nam, H.; Cha, G.; Paeng, K. "A Disposable Amperometric Sensor Screen-Printed on a Nitrocellulose Strip - A Glucose Biosensor Employing Lead-Oxide as an Interference-Removing Agent" *Anal Chem* **2000**, *72*, 1925-1929.

(62) Wang, J.; Chen, Q.; Pedrero, M.; Pingarron, J. "Screen-Printed Amperometric Biosensors for Glucose and Alcohols Based on Ruthenium-Dispersed Carbon Inks" *Anal Chim Acta* **1995**, *300*, 111-116.

(63) Schumacher, J. T.; Hecht, H. J.; Dengler, U.; Reichelt, J.; Bilitewski, U. "Direct electron transfer observed for peroxidase to screen- printed graphite electrodes" *Electroanal* **2001**, *13*, 779-785.

(64) Koncki, R.; Glab, S.; Dziwulska, J.; Palchetti, I.; Mascini, M. "Disposable Strip Potentiometric Electrodes with Solvent-Polymeric Ion-Selective Membranes Fabricated Using Screen-Printing Technology" *Anal Chim Acta* **1999**, *385*, 451-459.

(65) Silber, A.; Brauchle, C.; Hampp, N. "Electrocatalytic oxidation of reduced nicotinamide adenine dinucleotide (NADH) at thick-film gold electrodes" *J Electroanal Chem* **1995**, *390*, 83-89.

(66) Walcarius, A.; Rozanska, S.; Bessiere, J.; Wang, J. "Screen-Printed Zeolite-Modified Carbon Electrodes" *Analyst* **1999**, *124*, 1185-1190.

(67) Ricci, F.; Amine, A.; Tuta, C. S.; Ciucu, A. A.; Lucarelli, F.; Palleschi, G.; Moscone, D. "Prussian Blue and enzyme bulk-modified screen-printed electrodes for hydrogen peroxide and glucose determination with improved storage and operational stability" *Anal Chim Acta* **2003**, *485*, 111-120.

(68) Nunes, G. S.; Barcelo, D.; Grabaric, B. S.; Diaz-Cruz, J. M.; Ribeiro, M. L. "Evaluation of a highly sensitive amperometric biosensor with low cholinesterase charge immobilized on a chemically modified carbon paste electrode for trace determination of carbamates in fruit, vegetable and water samples" *Anal Chim Acta* **1999**, *399*, 37-49.

(69) Albareda-Sirvent, M.; Merkoci, A.; Alegret, S. "Configurations Used in the Design of Screen-Printed Enzymatic Biosensors - A Review" *Sensor Actuat B-Chem* **2000**, *69*, 153-163.

(70) Held, M.; Schuhmann, W.; Jahreis, K.; Schmidt, H.-L. "Microbial biosensor array with transport mutants of Escherichia coli K12 for the simultaneous determination of mono-and disaccharides" *Biosens Bioelectron* **2002**, *17*, 1089-1094.

(71) Andreescu, S.; Noguer, T.; Magearu, V.; Marty, J.-L. "Screen-printed electrode based on AChE for the detection of pesticides in presence of organic solvents" *Talanta* **2002**, *57*, 169-176.

(72) Andreescu, S.; Barthelmebs, L.; Marty, J.-L. "Immobilization of acetylcholinesterase on screen-printed electrodes: comparative study between three immobilization methods and applications to the detection of organophosphorus insecticides" *Anal Chim Acta* **2002**, *464*, 171-180.

(73) Galan-Vidal, C.; Munoz, J.; Dominguez, C.; Alegret, S. "Glucose Biosensor Based on a Reagentless Graphite-Epoxy Screen-Printable Biocomposite" *Sensor Actuat B-Chem* **1997**, *45*, 55-62.
(74) Koopal, C. G. J.; Bos, A. A. C. M.; Nolte, R. J. M. "Third-generation glucose biosensor incorporated in a conducting printing ink" *Sensor Actuat B-Chem* **1994**, *18*, 166-170.
(75) http://www.nlm.nih.gov/medlineplus/ency/article/001214.htm
(76) Gale, E. A. M. "The discovery of type 1 diabetes" *Diabetes* **2001**, *50*, 217-226.
(77) Guilbault, G. G.; Lubrano, G. J. "An enzyme electrode for the amperometric determination of glucose" *Anal Chim Acta* **1973**, *64*, 439-455.
(78) Wang, J. *Analytical Electrochemistry*, 2nd ed.; Wiley-VCH: New York, 2000.
(79) Willner, I.; Katz, E. "Integration of Layered Redox Proteins and Conductive Supports for Bioelectronic Applications" *Angew Chem Int Ed* **2000**, *39*, 1180-1218.
(80) http://www.therasense.com/FreeStyleFlash/index.aspx
(81) Koschinsky, T.; Heinemann, L. "Sensors for glucose monitoring: Technical and clinical aspects" *Diabetes-Metab Res* **2001**, *17*, 113-123.
(82) Bode, B. W.; Gross, T. M.; Thornton, K. R.; Mastrototaro, J. J. "Continuous glucose monitoring used to adjust diabetes therapy improves glycosylated hemoglobin: a pilot study" *Diabetes Res Clin Pract* **1999**, *46*, 183-190.
(83) http://www.americandiabetes.com/diasensor.htm
(84) Tierney, M. J.; Tamada, J. A.; Potts, R. O.; Jovanovic, L.; Garg, S. "Clinical evaluation of the GlucoWatch (R) biographer: a continual, non-invasive glucose monitor for patients with diabetes" *Biosens Bioelectron* **2001**, *16*, 621-629.
(85) Bode, B. W.; Gross, T. M.; Thornton, K. R.; Mastrototaro, J. J. "Continuous glucose monitoring used to adjust diabetes therapy improves glycosylated hemoglobin: a pilot study (vol 46, pg 183, 1999)" *Diabetes Res Clin Pract* **2000**, *47*, 225-225.
(86) Ives, D. J. G.; Janz, G. J. *Reference electrodes. Theory and Practice*, 1st ed.; Academic Press: New York, 1961.
(87) Atkins, P. W. *Physical Chemistry*, 3rd ed.; Oxford University Press: Oxford, 1986.
(88) Inczedy, J.; Lengyel, T.; Ure., A. M. *Compendium of analytical nomenclature. Definitive rules 1997*, 3rd ed.; Blackwell Science: Oxford, 1998.
(89) Bard, A.; Faulkner *Electrochemical Methods*, 1st ed.; John Wiley & Sons, Inc.: New York, 1980.
(90) Southampton Electrochemistry Group *Instrumental Methods in Electrochemistry*, 1st ed.; Ellis Horwood Limited: Chichister, 1985.
(91) Ciobanu, M.; Wilburn, J. R.; Buss, N. L.; Ditavong, P.; Lowy, D. A. "Miniaturized reference electrodes based on Ag/Ag$_i$X internal reference elements. I. Manufacturing and performance" *Electroanal* **2002**, *14*, 989-997.
(92) Will, F. G. "A self-contained miniature hydrogen reference electrode" *J Electrochem Soc* **1986**, *133*, 454-455.
(93) Bard, A.; Parsons, R.; Jordan, J. *Standard potentials in aqueous solution*, 1st ed.; Marcel Dekker, Inc.: New York, 1985.
(94) Suzuki, H.; Hiratsuka, A.; Sasaki, S.; Karube, I. "Problems associated with the thin-film Ag/AgCl reference electrode and a novel structure with improved durability" *Sensor Actuat B-Chem* **1998**, *46*, 104-113.
(95) Tu, Y.; Fu, Z.; Chen, H. "The fabrication and optimization of the disposable amperometric biosensor" *Sensor Actuat B-Chem* **2001**, *80*, 101-105.
(96) Cranny, A. W. J.; Atkinson, J. K. "Thick film silver silver chloride reference electrodes" *Meas Sci Technol* **1998**, *9*, 1557-1565.

(97) Vaireanu, D.-I.; Simion, A.; Colesa, M. "A disposable screen printed silver/silver chloride electrode array for pollution monitoring systems" *Sci Technol Env Prot* **2002**, *9*, 17-22.

(98) Desmond, D.; Lane, B.; Alderman, J.; Hill, M.; Arrigan, D. W. M.; Glennon, J. D. "An environmental monitoring system for trace metals using stripping voltammetry" *Sensor Actuat B-Chem* **1998**, *48*, 409-414.

(99) Suzuki, H.; Shiroishi, H.; Sasaki, S.; Karube, I. "Microfabricated Liquid Junction Ag/AgCl Reference Electrode and Its Application to a One-Chip Potentiometric Sensor" *Anal Chem* **1999**, *71*, 5069-5075.

(100) Suzuki, H.; Ozawa, H.; Sasaki, S.; Karube, I. "A novel thin-film Ag/AgCl anode structure for microfabricated Clark-type oxygen electrodes" *Sensor Actuat B-Chem* **1998**, *53*, 140-146.

(101) Cosofret, V. V.; Erdosy, M.; Johnson, T. A.; Buck, R. P.; Ash, R. B.; Neuman, M. R. "Microfabricated Sensor Arrays Sensitive to pH and K+ for Ionic Distribution Measurements in the Beating Heart" *Anal Chem* **1995**, *67*, 1647-1653.

(102) Huang, I. Y.; Huang, R.-S. "Fabrication and characterization of a new planar solid-state reference electrode for ISFET sensors" *Thin Solid Films* **2002**, *406*, 255-261.

(103) Huang, I. Y.; Huang, R.-S.; Lo, L.-H. "Improvement of integrated Ag/AgCl thin-film electrodes by KCl-gel coating for ISFET applications" *Sensor Actuat B-Chem* **2003**, *B94*, 53-64.

(104) Lindner, E.; Cosofret, V. V.; Ufer, S.; Buck, R. P.; Kusy, R. P.; Ash, R. B.; Nagle, H. T. "Flexible (Kapton-Based) Microsensor Arrays of High-Stability for Cardiovascular Applications" *J Chem Soc-Faraday Trans* **1993**, *89*, 361-367.

(105) Yoon, H. J.; Shin, J. H.; Lee, S. D.; Nam, H.; Cha, G. S.; Strong, T. D.; Brown, R. B. "Solid-state ion sensors with a liquid junction-free polymer membrane-based reference electrode for blood analysis" *Sensor Actuat B-Chem* **2000**, *B64*, 8-14.

(106) Yang, S.; Lu, Y.; Atanossov, P.; Wilkins, E.; Long, X. "Microfabricated glucose biosensor with glucose oxidase entrapped in sol-gel matrix" *Talanta* **1998**, *47*, 735-743.

(107) Yalcinkaya, F.; Powner, E. T. "Ag/AgCl/Cl- coated silver-stripe reference electrode" *Med Eng Phys* **1997**, *19*, 299-301.

(108) Goodhew, P. J.; Humphereys, J.; Beanland, R. *Electron Microscopy and analysis*, 3rd ed.; Taylor and Francis: London, 2001.

(109) Goldstein, J. I.; Newbury, D. E.; Echlin, P.; Joy, D. C.; Romig, A. D.; Lyman, C. E.; Fiori, C.; Lifshin, E. *Scanning electron microscopy and X-ray analysis : a text for biologists, material scientists and geologists*, 2nd ed.; Plenum Press, 1992.

(110) Wilcox, C. D.; Dove, S. B.; McDavid, W. D.; Greer, D. B., *"Image Tool"* 3.0, Department of Dental Diagnostic Science at The University of Texas Health Science Center, San Antonio, Texas., 2002.

(111) Scholz, F.; Meyer, B. In *Electroanalytical Chemistry,* 1st ed.; Bard, A., Rubinstein, I., Eds.; Marcel Dekker, Inc.: New York, 1998; Vol. 10, pp 1-86.

(112) Birkin, P. R., PhD Thesis, Southampton University, 1994.

(113) Robinson, R. A.; Stokes, R. H. *Electrolyte Solutions*, 2nd ed.; Butterworths: Boston, 1959.

(114) Lobo, V. M. M. *Handbook of electrolyte solution. (Part A)*, 1st ed.; Elsevier: New York, 1989.

(115) Horvath, A. L. *Handbook of Aqueous Electrolyte Solutions*, 1st ed.; Ellis Horwood Ltd: Chichester, 1985.

(116) Bromley, L. A. "Thermodynamic properties of strong electrolytes in aqueous solutions" *AIChE J* **1973**, *19*, 313-320.
(117) Bartlett, P. In *Biosensors: A Practical Approach*, 1st ed.; Cass, A., Ed.; Oxford University Press: New York, 1990, pp 59-60.
(118) Katan, T.; Szpak, S.; Bennion, D. N. "Silver/Silver chloride electrode: Reaction paths on discharge" *J Electrochem Soc* **1973**, *120*, 883-888.
(119) Martinez-Montequin, S.; Fernandez-Sanchez, C.; Costa-Garcia, A. "Voltammetric monitoring of the interaction between streptavidin and biotinylated alkaline phosphatase through the enzymatic hydrolysis of 3-indoxyl phosphate" *Anal Chim Acta* **2000**, *417*, 57-65.
(120) Corujo-Antuña, J. L.; Martinez-Montequin, S.; Fernandez-Abedul, M. T.; Costa-Garcia, A. "Sensitive adsorptive stripping voltammetric methodologies for the determination of melatonin in biological fluids" *Electroanal* **2003**, *15*, 773-778.
(121) Bakker, E.; Pretsch, E.; Buhlmann, P. "Selectivity of potentiometric ion sensors" *Anal Chem* **2000**, *72*, 1127-1133.
(122) Sutherland, F.; MediSense: Abingdon, 1999.
(123) Flewitt, P. E. J.; Wild, R. K. *Physical methods for materials characterisation*, 1st ed.; Institute of Physics Publishing: London, 1994.
(124) Vogel, A. *A text book of quantitative inorganic analysis*, 3rd ed.; Longmans: London, 1961.
(125) Reid, T. A.; MediSense: Abingdon, 1999.
(126) Caglioti, E.; Coniglio, A.; Herrmann, H. J.; Loreto, V.; Nicodemi, M. "Segregation of granular mixtures in the presence of compaction" *Europhys. Lett.* **1998**, *43*, 591-597.
(127) Ciobanu, M.; Wilburn, J. P.; Lowy, D. A. "Miniaturized reference electrodes. II. Use in corrosive, biological, and organic media" *Electroanal* **2004**, *16*, 1351-1358.
(128) Macdonald, D. *Transient Techniques in Electrochemistry*; Plenum Pub Corp: New York, 1977.
(129) Reid, T. A. Personal Communication, Abbingdon, 2003.
(130) Band, D. M.; Treasure, T. In *Ion-Selective Electrode Methodology*, 1st ed.; Covington, A. K., Ed.; CRC Press, Inc.: Florida, 1979; Vol. II.
(131) *CRC Handbook of Chemistry and Physics*, 58th ed.; CRC Press: Cleveland, 1977.
(132) Jaya, S.; Rao, T. P.; Rao, G. P. "Mono- and multilayer formation studies of silver chloride on silver electrodes from chloride-containing solutions" *J Appl Electrochem* **1987**, *17*, 635-640.
(133) Birss, V. I.; Smith, C. K. "The anodic behavior of silver in chloride solutions - I. The formation and reduction of thin silver chloride films" *Electrochim Acta* **1987**, *32*, 259-268.
(134) Bates, R. G.; Macaskill, J. B. "Standard potential of the silver-silver chloride electrode" *Pure Appl Chem* **1978**, *50*, 1701-1706.
(135) Taniguchi, H.; Janz, G. J. "Preparation and reproducibility of the thermal-electrolytic silver-silver chloride electrode" *J Electrochem Soc* **1957**, *140*, 123-127.
(136) Djokic, S. S.; Burrell, R. E. "Behavior of silver in physiological solutions" *J Electrochem Soc* **1998**, *145*, 1426-1430.
(137) Temsamani, K. R.; Cheng, K. L. "Studies of chloride adsorption on the Ag/AgCl electrode" *Sensor Actuat B-Chem* **2001**, *B76*, 551-555.
(138) Cheng, K. L. "Recent development of non-faradaic potentiometry" *Microchem J* **2002**, *72*, 269-276.
(139) Peacock, M.; Medisense: Abbingdon, 2002.
(140) Davidson, G.; Peacock, M.; MediSense: Abingdon, 2002.

(141) Jovic, B. M.; Jovic, V. D.; Drazic, D. M. "Kinetics of chloride ion adsorption and the mechanism of AgCl layer formation on the (111), (100) and (110) faces of silver" *J Electroanal Chem* **1995**, *399*, 197-206.
(142) Kautek, W.; Gordon, J. G. "XPS Studies on Emersed Silver Electrodes - Coverage and Bonding State of Specifically Adsorbed Chloride" *J Electrochem Soc* **1990**, *137*, 3405-3409.
(143) Kautek, W.; Dieluweit, S.; Sahre, M. "Combined scanning force microscopy and electrochemical quartz microbalance in-situ investigation of specific adsorption and phase change processes at the silver/halogenide interface" *J Phys Chem B* **1997**, *101*, 2709-2715.
(144) Stevenson, K. J.; Gao, X. P.; Hatchett, D. W.; White, H. S. "Voltammetric measurement of anion adsorption on Ag(111)" *J Electroanal Chem* **1998**, *447*, 43-51.
(145) Salaita, G. N.; Lu, F.; Lagurendavidson, L.; Hubbard, A. T. "Structure and Composition of the Ag(111) Surface as a Function of Electrode Potential in Aqueous Halide Solutions" *J Electroanal Chem* **1987**, *229*, 1-17.
(146) Forrow, N. J.; Reid, T. A. Personal, Personal communication.
(147) Greenwood, N. N.; Earnshow, A. *Chemistry of the Elements*, 1st ed.; Pergamon Press plc.: Hong Kong, 1989.
(148) Fleischmann, M.; Thirsk, H. R. In *Advances in Electrochemistry and Electrochemical Engineering*; Delahay, P., Ed.; Interscience: New York, 1963; Vol. 3, pp 123-210.
(149) Deutscher, R. L.; Fletcher, S. "Nucleation on Active-Sites .5. The Theory of Nucleation Rate Dispersion" *J Electroanal Chem* **1990**, *277*, 1-18.
(150) Abyaneh, M. Y. "Extracting nucleation rates from current-time transients - Part I: the choice of growth models" *J Electroanal Chem* **2002**, *530*, 82-88.
(151) Abyaneh, M. Y.; Fleischmann, M. "Extracting nucleation rates from current-time transients - Part II: comparing the computer-fit and pre-pulse method" *J Electroanal Chem* **2002**, *530*, 89-95.
(152) Abyaneh, M. Y. "Extracting nucleation rates from current-time transients - Part III: nucleation kinetics following the application of a pre-pulse" *J Electroanal Chem* **2002**, *530*, 96-104.
(153) Fletcher, S. "Extracting nucleation rates from current-time transients. Comments on three papers by Abyaneh and Fleischmann published in this issue" *J Electroanal Chem* **2002**, *530*, 105-107.
(154) Abyaneh, M. Y.; Fleischmann, M. "Extracting nucleation rates from current-time transients: comments on the criticisms of Fletcher on three papers published in this issue" *J Electroanal Chem* **2002**, *530*, 108-118.
(155) Fletcher, S. "Extracting nucleation rates from current-time transients. Concluding remarks" *J Electroanal Chem* **2002**, *530*, 119-122.
(156) Abyaneh, M. Y.; Fleischmann, M. "Extracting nucleation rates from current-time transients: further comments" *J Electroanal Chem* **2002**, *530*, 123-125.
(157) Scharifker, B.; Hills, G. "Theoretical and Experimental Studies of Multiple Nucleation" *Electrochim Acta* **1983**, *28*, 879-889.
(158) Harrison, J. A.; Thirsk, H. R. In *Electroanlytical Chemistry*; Bard, A., Ed.; Marcel Dekker: New York, 1971; Vol. 5, pp 67-148.
(159) Armstrong, R. D.; Metcalfe, A. A. "Two-dimensional nucleation and growth. Potentiostatic case" *J Electroanal Chem Interf Electrochem* **1975**, *63*, 19-22.
(160) Clark, M. M.; Harrison, J. A.; Thirsk, H. R. "Two dimensional nucleation and growth and the electrocrystallization of metals" *Z Phys Chem* **1975**, *98*, 153-160.
(161) Mirkin, M. V.; Nilov, A. P. "3-Dimensional Nucleation and Growth under Controlled Potential" *J Electroanal Chem* **1990**, *283*, 35-51.

(162) Sluyters-Rehbach, M.; Wijenberg, J. H. O. J.; Bosco, E.; Sluyters, J. H. "The theory of chronoamperometry for the investigation of electrocrystallization. Mathematical description and analysis in the case of diffusion-controlled growth" *J Electroanal Chem Interf Electrochem* **1987**, *236*, 1-20.
(163) Palomar-Pardave, M.; Miranda-Hernandez, M.; Gonzalez, I.; Batina, N. "Detailed characterization of potentiostatic current transients with 2D-2D and 2D-3D nucleation transitions" *Surf Sci* **1998**, *399*, 80-95.
(164) Kaden, H.; Vonau, W. "Reference electrodes for electrochemical measurements" *J Prakt Chem-Chem Ztg* **1998**, *340*, 710-721.
(165) Maier, J. "Defect chemistry and conductivity effects in heterogeneous solid electrolytes" *J Electrochem Soc* **1987**, *134*, 1524-1535.
(166) Yeager, J.; Hrusch-Tupta, M. A., Eds. *Low level measurements.*
(167) Smits, F. M. "Measurements of Sheet Resistivity with the Four-Point Probe" *BSTJ* **1958**, *37*, 711-718.
(168) Perdicakis, M.; Grosselin, N.; Bessiere, J. "Voltammetric behavior of single particles of silver chalcogenides in the micrometric range. Comparison with measurements at modified carbon paste electrodes" *Electrochim Acta* **1997**, *42*, 3351-3358.
(169) Crank, J. *The mathematics of difussion*, 2nd ed.; Oxford University Press: Oxford, 1975.
(170) *CRC Standard Mathematical Tables and Formulae*, 30th ed.; CRC Press: Boca Raton, 1996.
(171) Hyk, W.; Nowicka, A.; Stojek, Z. "Direct determination of diffusion coefficients of substrate and product by chronoamperometric techniques at microelectrodes for any level of ionic support" *Anal Chem* **2002**, *74*, 149-157.
(172) Conyers, J. L., Jr.; White, H. S. "Electrochemical Characterization of Electrodes with Submicrometer Dimensions" *Anal Chem* **2000**, *72*, 4441-4446.
(173) Liu, H. T.; Xia, X.; Guo, Z. P. "A novel silver oxide electrode and its charge-discharge performance" *J Appl Electrochem* **2002**, *32*, 275-279.
(174) Hughes, A. L. In *International Critical Tables of Numerical Data, Physics, Chemistry and Technology,* 1st Electronic ed.; West, C., Dorsey, N., Eds.; National Research Council: Norwich, 2003; Vol. 6.
(175) Young, L. *Anodic oxide films*, 1st ed.; Academic Press: London, 1961.
(176) Hamer, W.; Craig, D. "A reproducible and stable Silver - Silver Oxide Electrode" *J Electrochem Soc* **1957**, *104*, 206-211.
(177) Perkins, R. S.; Tilak, B. V.; Conway, B. E.; Kozlowska, H. A. "Impedance and formation characteristics of electrolytically generated silver oxides--II. photo-effects" *Electrochim Acta* **1972**, *17*, 1471-1489.
(178) Miller, B. "Rotating ring-disk study of the silver electrode in alkaline solution" *J Electrochem Soc* **1970**, *117*, 491-499.
(179) Yvon, K.; Bezinge, A.; Tissot, P.; Fischer, P. "Structure and magnetic properties of tetragonal silver(I,III) oxide, AgO" *J Solid State Chem* **1986**, *65*, 225-230.
(180) Standke, B.; Jansen, M. "Ag_2O_3, a Novel Binary Silver-Oxide" *Angew Chem Int Ed* **1985**, *24*, 118-119.
(181) Standke, B.; Jansen, M. "Preparation and Crystal-Structure of Ag_2O_3" *Z Anorg Allg Chem* **1986**, *535*, 39-46.
(182) Nagle, L. C.; Ahern, A. J.; Burke, L. D. "Some unusual features of the electrochemistry of silver in aqueous base" *J Solid State Electrochem* **2002**, *6*, 320-330.
(183) Tilak, B. V.; Perkins, R. S.; Kozlowska, H. A.; Conway, B. E. "Impedance and formation characteristics of electrolytically generated silver oxides--I formation

and reduction of surface oxides and the role of dissolution processes" *Electrochim Acta* **1972**, *17*, 1447-1469.

(184) Abd El Rehim, S. S.; Hassan, H. H.; Ibrahim, M. A. M.; Amin, M. A. "Electrochemical behavior of a silver electrode in NaOH solutions" *Monatsh Chem* **1998**, *129*, 1103-1117.

(185) Ambrose, J.; Barradas, R. G. "The electrochemical formation of Ag_2O in KOH electrolyte" *Electrochim Acta* **1974**, *19*, 781-786.

(186) Burstein, G. T.; Newman, R. C. "Anodic behaviour of scratched silver electrodes in alkaline soluion" *Electrochim Acta* **1980**, *25*, 1009-1013.

(187) López Teijelo, M.; Vilche, J. R.; Arvía, A. J. "The Electroformation and Electroreduction of Anodic Films Formed on Silver in 0.1 M Sodium-Hydroxide in the Potential Range of the Ag/Ag_2O Couple" *J Electroanal Chem* **1984**, *162*, 207-224.

(188) López Teijelo, M.; Vilche, J. R.; Arvía, A. J. "Comparative Voltammetric Behavior of the Silver Silver-Oxide Electrode Prepared on Vitreous Carbon and Silver Substrates" *J Appl Electrochem* **1988**, *18*, 691-698.

(189) Chen, S. L.; Wu, B. L.; Cha, C. S. "The time-resolved EQCM and study of the kinetics of silver(I) oxide formation on a polycrystalline silver electrode in alkaline solution" *J Electroanal Chem* **1997**, *420*, 111-118.

(190) Savinova, E. R.; Zemlyanov, D.; Scheybal, A.; Schedel-Niedrig, T.; Doblhofer, K.; Schlögl, R. "Ex Situ X-ray Photoelectron Spectroscopy Study of the Interface between a Ag(111) Electrode and an Alkaline Electrolyte. 1. Influence of the Electrode Potential on the Adsorption of Oxygen Species" *Langmuir* **1999**, *15*, 6546-6551.

(191) Savinova, E. R.; Zemlyanov, D.; Pettinger, B.; Scheybal, A.; Schlögl, R.; Doblhofer, K. "On the mechanism of Ag(111) sub-monolayer oxidation: a combined electrochemical, in situ SERS and ex situ XPS study" *Electrochim Acta* **2000**, *46*, 175-183.

(192) Zerbino, J.; López Teijelo, M.; Vilche, J. R.; Arvía, A. J. "Electrochemical and Ellipsometric Data Related to the Formation of Soluble Silver (I) During the Potentiodynamic Polarization of Polycrystalline Silver in Basic Solutions" *Electrochim Acta* **1985**, *30*, 1521-1525.

(193) López Teijelo, M.; Vilche, J. R.; Arvía, A. J. "Complex Potentiodynamic Response of Silver in Alkaline Electrolytes in the Potential Range of the Ag/Ag_2O Couple" *J Electroanal Chem* **1982**, *131*, 331-339.

(194) Pourbaix, M. *Atlas of electrochemical equilibria in aqueous solutions*, 1st ed.; Pergamon Press: Oxford, 1966.

(195) EDAX instrument manual.